Deep Soil Mixing as a Slope Stabilization Technique in Northland Allochthon Residual Clay Soil

---

A thesis submitted in fulfilment of the requirements
for the Degree of Doctor of Philosophy in the
Department of Civil and Natural Resources
Engineering

by Catherine M. Tatarniuk

University of Canterbury

Christchurch, New Zealand

2014

Table of Contents

List of Figures

List of Tables

Acknowledgements

First and foremost, I would like to express deep gratitude to Dr. Elisabeth Bowman whose support and encouragement has been second to none. She always made time for me, and was supportive yet tactfully critical of my ideas, and for that I am very appreciative. I would also like to thank Dr. Cedric Lambert for his advice and support during the last year of my studies. I am grateful to Andy O'Sullivan of Hiway Geotechnical Ltd. for making the acquisition of the field data and soil samples used in this research possible, for financial support to attend conferences, and for valuable conversations about Northland Allochthon slopes, deep soil mixing, and Plaxis. Thank you to Muhamad Yusa for sharing the GDS triaxial apparatus and his knowledge of it with me. I would like to thank my mother Elaine, my sister Christina, my friend Kelly Robinson, and most especially, my husband Brad Harasymchuk, who provided me with unrelenting support throughout this research. I am also grateful to the New Zealand Commonwealth Scholarship plan and the National Science and Engineering Council of Canada. Thank you to all the kind people that have touched my life in the past four years, and impacted my journey to completing this thesis at the University of Canterbury in Christchurch, New Zealand. I have learned so much during this unforgettable experience, and I feel blessed to have had this opportunity.

Abstract

Road slips are common in Northland Allochthon residual clay soil, and are commonly mitigated using deep soil mixing (DSM). A deficiency in laboratory investigations on Northland Allochthon residual clay and a need for a better understanding of the numerical modelling of DSM columns used to mitigate unstable slopes in this soil type is evident in literature, and has been highlighted by practitioners. This research has aimed to fill aspects of these deficiencies.

Field testing and classification tests have provided insight into how the soil varies between sites and with depth, and how in situ testing methods compare to one another. Field testing has also demonstrated that soil property changes around DSM columns have been shown to exist through seismic flat plate dilatometer testing before and after column installation, which has not previously been proven using an in situ method. This is important for practitioners who use DSM to demonstrate the additional soil improvements provided by the columns.

The testing of reconstituted soil is fundamental in examining soil behaviour, and this study is the first to examine the triaxial behaviour of reconstituted specimens of Northland Allochthon soil. Laboratory triaxial testing and oedometer testing have allowed for a normalized comparison of the intact strength of Northland Allochthon residual clay soil to its reconstituted state. This work provides an answer to the important question regarding the role of soil structure in this soil type. It was revealed that soil structure results in increased shear strength of the soil, and that this increase is primarily cohesive in nature. The near coincidence of the post-rupture strength of intact specimens with the critical state angle of internal shearing resistance provides support for its use in examining first time slope failures in this soil type. This is an important finding for practitioners, as it demonstrates the value of testing reconstituted specimens, which are much easier to obtain than high quality intact specimens. In addition, relationships between the plasticity index (*PI*) of the soil and certain soil parameters (and soil behaviour) have been demonstrated to be relevant and useful for this soil type.

Soil properties acquired in this study were tabulated along with those from other field sites in Northland Allochthon soil. It was found that there is significant variation between field sites,

likely due to varying degrees of weathering, which is an important consideration for practitioners dealing with this soil type.

A brief examination of constitutive models for representation of Northland Allochthon residual clay soil have shown that several different models can sufficiently represent the behaviour of this soil. The Mohr-Coulomb model was selected for use in subsequent finite element numerical models. A case study of a road slip at a field site in Northland Allochthon residual clay soil, mitigated using DSM columns, revealed that the use of a pre-existing slip surface after first time failure leads to an improved match between observed field behaviour and the behaviour of the slope as exhibited in a numerical model. This type of failure mechanism has not been previously examined in this soil type, and this case study demonstrates it is a useful approach that should be considered when dealing with second time failure in Northland Allochthon slopes. This numerical model also introduces the replacement ratio method (RRM), a technique used to represent the three dimensional (3D) geometry of the DSM columns in the more commonly used two dimensional (2D) analysis.

Examination of laterally loaded DSM columns in plan view, which has not previously been performed in the context of DSM columns, has illustrated how installation effects and column shape influence load displacement curves, and demonstrates the effects of soil arching. This analysis provides practitioners with evidence that improved soil property changes, found to occur around DSM columns, lead to improved DSM column performance. A simplified 3D numerical model of laterally loaded DSM columns, which builds on the ideas developed in the previous two 2D models, has been compared to an identical 2D model. It is shown that the commonly used RRM results in an overestimation of the resisting force provided by the columns as compared to the 3D model. However, this does not necessarily imply that the use of the RRM in an analysis will always result in a safe slope. The degree to which its use will affect the results will depend on the slope geometry, location of the DSM columns, and the type of analysis performed (i.e. factor of safety or deformation based). A modification to the RRM has been proposed. It is recommended that when the DSM column diameter and soil properties are similar to those used in this study, the MRRM developed in this study should be utilized. In circumstances where they differ, it is recommended that practitioners perform a sensitivity analysis using the MRRM developed here as a basis for modifying the RRM in

order to determine the extent to which their results are influenced. If the influence is significant, the use of a 3D model should be considered.

List of Symbols

Greek Terms

γ	unit weight
γ_{dry}	dry unit weight
γ_w	unit weight of water
$\gamma_{0.7}$	shear strain level at which the secant shear modulus is reduced to 70% of G_0
δ	displacement
δ_p	displacement in plastic zone
Δ	change
ε_a	axial strain
ε^e	elastic strain
ε^p	plastic strain
ε_q	shear strain
ε_r	radial strain
ε_s	deviatoric strain
ε_{vol}	volumetric strain
η	stress ratio q/p'
Θ	$45° + \varphi'/2$
κ	gradient of a swelling line
λ	gradient of the normal compression and critical state line
ν	Poisson's ratio
ρ	bulk density
σ	total stress
σ'	effective stress
σ_a	axial stress
σ_p	pressure at interface of plastic and elastic zone
σ_r	radial stress
σ^*_{ve}	equivalent stress on the intrinsic one dimensional compression line corresponding to the void ratio of the soil
σ_{vy}'	yield stress in oedometer compression
σ_{v0}	total vertical stress
σ'_{v0}	effective vertical stress

σ_x	horizontal stress
σ_Θ	horizontal stress on a soil element
$\sigma_1, \sigma_2, \sigma_3$	principal stresses (total stress; effective stress is denoted by ‘, e.g. σ'_1)
τ	shear stress
τ_{max}	maximum value of shear stress for the case where the Mohr’s circle is expanded to touch the Coulomb failure envelope
τ_{rel}	relative shear stress
τ^*	the maximum value of shear stress (i.e. the radius of the Mohr’s circle)
φ	angle of internal shearing resistance
φ'	effective angle of internal shearing resistance
φ^b	unsaturated angle of internal shearing resistance
φ'_{crit}	effective critical state angle of internal shearing resistance
φ^*_{cs}	intrinsic critical state angle of internal shearing resistance
φ^*_e	Hvorslev true angle of internal shearing resistance
φ'_e	Hvorslev angle of internal shearing resistance for intact soil (effective)
φ_{int}	angle of internal shearing resistance of the interface (sheared zone)
φ_{peak}	peak angle of internal shearing resistance (effective denoted by ‘)
φ_{res}	residual angle of internal shearing resistance
$\varphi_{safe, DMT}$	lower bound value of angle of internal shearing resistance as determined from the DMT
χ	Hvorslev cohesion intercept
χ^*	intrinsic Hvorslev cohesion intercept
ψ	angle of dilation

Roman Terms

A, B, C	first, second, and third raw DMT pressure readings
A_o	initial area of soil specimen
A_c	corrected area of soil specimen
A_{col}	area of the DSM columns in the replacement ratio method
A_{soil}	area of the soil in the replacement ratio method
A_T	area of a rectangle encompassing soil between two columns and one DSM column in the replacement ratio method
c	cohesion
c'	effective cohesion

c_h	coefficient of consolidation
$c_{h,\mathrm{DMT}}$	coefficient of consolidation as determined through correlations from DMT results
c_{int}	cohesion of the interface (sheared zone)
c_u	undrained shear strength
$c_{u,\mathrm{DMT}}$	undrained shear strength as determined through correlations from DMT results
c_{ur}	remoulded undrained shear strength
C_c	compression index
C^*_c	intrinsic compression index
C_s	swelling index
d	diameter of pile or column
d_e	equivalent diameter
e	void ratio
e_c	y-intercept value of the interception point between the critical state line and the line defining a typical test on a soil sample in the Cam-clay model in e-lnp' space
e_L	void ratio at the liquid limit
e_κ	y-intercept value of the line defining a typical unload-reload line in e-lnp' space
$e_{\lambda c}$	intercept point of the critical state line along the vertical axis
$e_{\lambda v}$	y-intercept value of the spherical compression line in e-lnp' space
e_v	y-intercept value of the interception point between the spherical compression line and the line defining a typical unload-reload line in e-lnp' space
e^*_{100}	intrinsic void ratio at a vertical effective stress of 100 kPa
e_0	initial void ratio
E	Young's modulus
E_{col}	Young's modulus of columns (discerned from that of the soil)
E_D	dilatometer modulus
E_{oed}	tangent stiffness for primary oedometer loading
E_{oed}^{ref}	tangent stiffness for primary oedometer loading at a reference pressure (in Plaxis)
E^{ref}	Young's modulus at a reference pressure (in Plaxis)
E_{soil}	Young's modulus of soil (discerned from that of the DSM columns)
E_{tan}	tangent Young's modulus

E_{ur}	unloading/reloading stiffness
E_{ur}^{ref}	unloading/reloading stiffness at a reference pressure (in Plaxis)
E_{u0}	total stress Young's modulus at small strain
E_0	Young's modulus at small strain
E_1	Young's modulus of the soil in which the radius of the cavity due to DSM column installation has been previously computed from field measurements
E_{50}	secant stiffness in a standard drained triaxial test
E_{50}^{ref}	secant stiffness in a standard drained triaxial test at reference pressure (in Plaxis)
EA	axial stiffness of a pile
EI	flexural rigidity (bending stiffness)
f_s	sleeve friction
F_c, F_q	dimensionless spherical cavity factors
F_2, F_1	yield surface function
g	gravity
G	shear modulus
G_{max}	maximum secant shear modulus
G_s	specific gravity
G_{sec}	secant shear modulus
G_u	total stress shear modulus
G'	effective shear modulus
G_0	small strain shear modulus
G_0^{ref}	small strain shear modulus at reference pressure (in Plaxis)
G_2, G_1	plastic potential functions
H_u	thickness of the unstable soil layer
I_c	consistency index
I_D	material index from flat plate dilatometer test
I_r	rigidity index
I_v	void index
k_x	hydraulic conductivity in the horizontal direction
k_y	hydraulic conductivity in the vertical direction
K	bulk modulus
K_D	horizontal stress index from flat plate dilatometer test

K_0	coefficient of lateral earth pressure at rest
$K_{0,DMT}$	coefficient of lateral earth pressure at rest as determined through correlations from DMT results
K_0^{NC}	coefficient of lateral earth pressure at rest under normally consolidated conditions
L_e	distance from the top of the interface to the base of the stable soil
m	power for stress-level dependency of stiffness (in the Hardening Soil model)
M	gradient of critical state line
M	vertical drained constrained modulus
M_{DMT}	vertical drained constrained modulus as determined through correlations to DMT results
M_h	horizontal drained constrained modulus
N_k	empirical cone factor
o	displacement
o_c	displacement of the column
o_{ic}	inter-column ground displacement
p'	mean effective stress
p	mean total stress
p'_c	mean effective stress at critical state
p_c	mean total stress at critical state
p'_e	equivalent isotropic pressure on the intrinsic isotropic compression line corresponding to the void ratio of the soil
p_l	lateral pressure
p'_P	mean effective stress at the critical state for a water content equal to the plastic limit
p'_L	mean effective stress at the critical state for a water content equal to the liquid limit
p^{ref}	reference pressure
p'_v	effective stress preconsolidation pressure
p_v	total stress preconsolidation pressure
p'_0	initial mean effective stress
p_0	initial dilatometer reading deduced from raw DMT pressure readings
p_1	second dilatometer reading deduced from raw DMT pressure readings
p_2	third dilatometer reading deduced from raw DMT pressure readings
P_u	cavity pressure

q	deviatoric stress
q_a	deviatoric stress at the asymptote of the stress-strain curve
q_c	cone penetration resistance
q_{crit}	deviatoric stress at critical state
q_f	deviatoric stress at the failure line of the stress strain curve
r	distance from centre of DSM column to point where displacement is measured
r_{col}	replacement ratio of the columns in the replacement ratio method
r_{soil}	replacement ratio of the soil in the replacement ratio method
R_M, R_{M0}	variables used to determine M_{DMT}
R_p	radius of plastic zone
R_u	radius of cavity
R_{u0}	radius of cavity corresponding to a Young's modulus of E_1
s'	$(\sigma'_1 + \sigma'_2)/2$
s	column spacing from centre-to-centre
S_t	strength sensitivity (as defined by Cottechia & Chandler, 2000)
S_{tr}	soil sensitivity (ratio of c_u to c_{ur})
S_σ	stress sensitivity (as defined by Cottechia & Chandler, 2000)
S_u	peak c_u of intact samples in the natural state
S_u*	undrained strength at the same void ratio on the IS_uL
t	$(\sigma'_1 - \sigma'_3)/2$
t_{flex}	time at conflecture point in A-log (time) DMT-A decay curve
t_{100}	time intercept
T	ratio of the normalized strengths of intact to reconstituted soil at intrinsic critical strength
u	pore pressure
u_0	equilibrium/pre-insertion pore pressure
U_D	pore pressure index
v	specific volume
v_λ	specific volume equal to $1 + e_{\lambda c}$
V_s	shear wave velocity
w	water content
w_0	initial water content
W	specific weight (for structural elements in Plaxis)

x	vibration velocity
Z_M	DMT gauge reading when vented to atmosphere
2s	column spacing of two times column diameter from centre-to-centre
3s	column spacing of three times column diameter from centre-to-centre
4s	column spacing of four times column diameter from centre-to-centre

Acronyms

CD	consolidated drained
CPT	cone penetration test
CSD	constant sheared stress drained triaxial test
CSL	critical state line
CU	consolidated undrained
DMT	dilatometer Marchetti test (also called flat plate dilatometer test)
DSM	deep soil mixing
FoS	factor of safety
GUI	graphical user interface
HOC	highly overconsolidated
HS	Hardening Soil
HS small	Hardening Soil small
ICL	Intrinsic compression line
IsSR	in situ stress ratio which represents the ratio of the in situ vertical stress (σ'_{v0}) to the intrinsic compression stress (σ^*_{ve})
IS_uL	the intrinsic strength line in the undrained condition
LI	liquidity index
LL	liquid limit
LOC	lightly overconsolidated
LVDT	linearly variable differential transformer
mbgl	meters below ground level
MC	Mohr-Coulomb
MRRM	modified replacement ratio method
NC	normally consolidated
OCR	overconsolidation ratio
OCR_{DMT}	overconsolidation ratio as determined though correlations from DMT results

PI	plasticity index
PI'	modified plasticity index
PL	plastic limit
RF	resisting force
RF_{column}	resisting force provided by the DSM columns
RF_{FF}	free field resisting force
RRM	replacement ratio method
SBP	self-boring pressuremeter
SCC or SCL	sedimentation compression curve or sedimentation compression line
sDMT	seismic dilatometer Marchetti test
SPCL	spherical plastic compression line (also called isotropic normal compression line)
SSC	soft soil creep
UCS	unconfined compressive strength
YSR	yield stress ratio which represents the ratio of yield stress measured in the oedometer (σ_{vy}') to the in situ vertical stress
2D	two dimensions
3D	three dimensions

1.0 Introduction

1.1 Background of the Research

Road slips in Northland Allochthon residual clay soil in the Northland region of New Zealand are a common issue, and in the past several years Deep Soil Mixing (DSM) has been used as a successful method for mitigating them. In situ field testing results at road slip sites have become increasingly available to provide a basis for soil parameters, but few thorough laboratory testing studies have been completed that investigate the behaviour of this problematic soil type. Soil specimens in their reconstituted state provide the foundation from which to build a deeper understanding of soil behaviour, and testing on such specimens has not been performed previously. Soil structure has been thought to play a role in the behaviour of this soil, but this could only be verified through comparison of intact specimens with reconstituted ones. In addition, the extent to which Northland Allochthon residual clay soil properties differ between different formations, and from the same formation but at different field sites, has not been examined.

Finite element numerical modelling is a critical tool that is used by practitioners for examining the failure of slopes in Northland Allochthon residual clay soil, and mitigation of these failures using DSM. Examining constitutive models that represent the behaviour of the soil is an important first step that is often eliminated due to time constraints. Analysis of Northland Allochthon residual clay slope failures at certain field sites is lacking a comparison between observed numerical behaviour to that seen in the field, and a plausible physical explanation of the slope failure at these sites is needed. In addition, an investigation of how DSM columns function under lateral loading mechanisms in plan view has not been performed. Such an analysis is important for understanding how soil property changes around the columns affect the performance of the soil-column system, and how soil arching mechanisms play a role in the overall resistance to lateral load. Finally, another important aspect of numerical modelling of slope stabilizing DSM columns which needs to be examined is how well conventional 2D models compare to a more realistic 3D scenario.

1.2 Objectives

The aims of this research fall under the umbrella of two main goals:

1) To investigate the properties and behaviour of Northland Allochthon residual clay soil.

2) To examine how laterally loaded DSM columns behave in Northland Allochthon residual clay soil, and how to better use numerical modelling as a tool to examine this behaviour. Current numerical modelling approaches are missing a thorough comparison between the commonly used 2D modelling technique to a 3D model. Modelling of DSM columns in plan view has also not been performed, and is important for examining the group effect (effects of column spacing) amongst other aspects of design. In the context of DSM columns in this soil type, failure mechanisms need to be examined in order to acquire a numerical model that matches the observed failure in the field.

Within the first objective, the sub-objectives are:

a) To use field testing and classification tests to provide background information on the soil properties and to compare and empirically correlate these to soil parameters and soil behaviour.

b) Make comparisons between different field sites in the same formation.

c) Carry out triaxial testing of reconstituted and intact soil specimens to use as a framework for comparison.

d) Examine the influence of soil structure on the strength of the intact soil.

e) Investigate the underlying behaviour of Northland Allochthon residual clay soil and compare it with the behaviour of common sedimentary clay soils.

f) Examine the suitability of different constitutive models in representing triaxial behaviour of Northland Allochthon clay soil as a basis for the use of these models in more complex analyses.

Under the second objective are the following sub-objectives:

a) Examine a case study of a road embankment failure in 2D in order to compare observed behaviour in a numerical model to that seen in the field. Develop a realistic physical explanation of how second time failure may have occurred in the context of what has been proposed about this soil type and site conditions.

b) Examine column behaviour in plan view. Specifically, to look at soil arching and the effects of the soil property changes around DSM columns and column spacing using load-displacement curves.

c) Evaluate the effect of column shape on the load-displacement curves.

d) Compare a 2D model of DSM columns using the replacement ratio method (introduced in the case study), as used for the mitigation of road slips, to a 3D model.

e) Determine how the replacement ratio method (RRM) can be altered in order for the 2D model to better approximate the results of the 3D model in terms of the resisting force provided by the DSM columns.

1.3 Structure of the Thesis

This thesis consists of nine chapters. Following this introduction (Chapter 1), Chapter 2 provides a literature review on DSM, Northland Allochthon residual clay soil, and the laboratory testing, field testing and numerical modelling methods used in this thesis.

Chapter 3 introduces the three field sites discussed in this thesis, and provides an investigation into Atterberg limits which are compared between sites. Other soil classification tests are also presented. Chapter 3 also examines in situ field testing results in order to better understand the Northland Allochthon residual clay soil properties, and changes with depth. In addition, changes to the soil after installation of DSM columns are examined.

Chapter 4 outlines how triaxial testing and oedometer testing was performed, and presents the results and a comparison between intact and reconstituted specimens from the same field site. The influence of structure on the strength of the natural material is highlighted. Well-defined critical state soil parameters are also acquired and compared to other soil types. The relationship between the Atterberg limits presented in Chapter 3 and certain soil parameters

and soil behaviour are discussed. In addition, the properties of Northland Allochthon residual clay soil acquired from this study and other studies are summarized.

The suitability of several constitutive models for the conventional triaxial behaviour of the soil from two different sites in its intact state and reconstituted state (where available) is examined in Chapter 5.

The numerical modelling of road slips is commonly performed in 2D. As such, Chapter 6 examines a case study of a road slip in Northland Allochthon clay soil mitigated using DSM. In this chapter, the RRM used for modelling DSM columns in 2D is introduced. The use of a pre-defined slip surface along the initial slope failure plane is proposed. Material covered in Chapter 6 has previously been published in Tatarniuk & Bowman (2012a).

As conventional 2D models are unable to portray the movement of soil around DSM columns, Chapter 7 examines a 2D model of laterally loaded DSM columns in plan view. Soil arching and installation effects are investigated primarily through load-displacement curves. Some of the material presented in Chapter 7 has previously been published in Tatarniuk & Bowman (2012b).

Chapter 8 combines the principles outlined in Chapters 5 and 6 by comparing a 2D model using the replacement ratio method to a 3D model. The hybrid method for slope stabilizing piles (Kourkoulis et al., 2011) is used as a basis for simplifying the model geometry. Suggestions are made for modifying the RRM to acquire a better match between the resisting force provided by the DSM columns in 2D to the 3D results. Recommendations for practitioners using this technique are also given. Some of the material covered in Chapter 8 has previously been published in Tatarniuk & Bowman (2013).

Chapter 9 summarizes the conclusions made from this research and provides suggestions for future work.

2.0 Background and Literature Review

2.1 Introduction

A literature review was carried out that included research on DSM columns and their properties, as well as on the Northland Allochthon residual clay soil type. In addition, background information was collected on laboratory testing techniques, particularly triaxial testing and the methods used to examine the effects of soil structure on soil behaviour. In situ field testing techniques and different constitutive numerical models commonly used for clay soil are also discussed.

Deep Soil Mixing for Slope Failure Mitigation

Although DSM has been successfully used in stabilizing road slips for several years, challenges with design still exist. Field experience indicates that the effectiveness of the columns is dependent on several construction, design and site-specific variables. For slope failure mitigation, DSM columns are typically installed in a zig-zag pattern with soil in between them, rather than a wall of continuous column material. This is discussed further in Section 2.2. O'Sullivan & Quickfall (pers. comm., 2011) and Terzaghi et al. (2005) state that the biggest uncertainties that remain in the design of slope stabilizing DSM columns are the group interaction of the columns, and their behaviour (and failure mechanisms). Due to the fact that the zig-zag installation pattern of slope stabilizing DSM columns allows for soil movement around them, DSM companies often experience difficulties convincing clients about the efficacy of the design (O'Sullivan & Quickfall, pers. comm., 2011). The kinematic restraint of the soil, via soil arching and installation effects, is a key issue that requires further investigation in order to demonstrate how these mechanisms play a role in the effectiveness of the columns as used for slope stabilization (O'Sullivan & Quickfall, pers. comm., 2011).

Another major issue is the modelling of DSM columns in 2D, and representation of the behaviour seen in 3D and in the field. These issues exist for the use of DSM columns in several different applications, but are particularly important when DSM columns are being utilized as a method for road slip repair. This is because the columns are typically modelled in 2D using the replacement ratio method (RRM) (Leung et al., 2006; O'Sullivan et al., 2009), a method where the column properties are averaged with the soil properties in the out-

of-plane direction. This commonly used method does not account for soil arching or soil flow around the columns. The RRM is utilized in 2D as an alternative to 3D, but it may give results that are over or under conservative, and may result in uneconomical design. Further research is required to verify its effectiveness (Leung et al., 2006).

The interaction of DSM columns with the surrounding soil mass has not been extensively studied. In the past, many researchers have assumed that there were no property changes at all in the soil surrounding DSM columns (Bergado et al., 1996; Kamon & Bergado, 1991; Shen et al., 2003b). Recent research has indicated that physical and chemical changes do take place in the soil surrounding DSM columns in clay, which is discussed in Section 2.3 (Larsson & Kosche, 2005; Muntohar & Hung, 2007; Shen et al., 2008). This research has largely focussed on strength parameters. Changes to soil stiffness have not been studied, nor have the ways in which soil property changes around the columns influence the soil flow past the columns in a lateral loading scenario.

Northland Allochthon Residual Clay Soil Properties, Soil Structure and Slope Failure Mechanisms

Limited geotechnical engineering lab testing has been performed on Northland Allochthon soil. As a result, its behaviour and properties are not well characterized. Of significant interest is how much of the soil behaviour is related to soil structure (O'Sullivan, 2009). The effects of soil structure can be assessed by comparing reconstituted specimens to intact specimens- something which has not yet been performed for this soil type. Further research into soil properties and constitutive modelling of Northland Allochthon soil would notably contribute to the body of knowledge surrounding this problematic soil type. In addition, the comparison of soil properties between sites requires further investigation, and a summary of the soil properties acquired to date would be useful for practitioners.

O'Sullivan (2009) discusses the difficulties experienced in obtaining a reasonable agreement between field behaviour of second time failure in a Northland Allochthon slope (Ogles No. 3 site) to that shown in a finite element simulation. Even after the incorporation of transient groundwater flow into the numerical model, the slope failure as seen in the field could not be obtained. However, an investigation into the possibility of second time failure along a pre-

existing shear plane was not performed for this field site. This type of failure mechanism, which has proven useful in clay soils (Skempton, 1964) should be examined as a possibility in Northland Allochthon residual clay soil.

2.2 Deep Soil Mixing Overview

Deep soil mixing (DSM) is a soil improvement technology used to enhance foundation strength, stabilise large earthworks, construct cut-off or retaining walls, and to treat contaminated soils in situ. This is accomplished with a series of stabilized soil columns in which a binder, such as cement or lime, is added and mechanically mixed into the existing soil. Binders can be introduced in slurry form (wet mixing) or in dry form (dry mixing). This study focuses on the wet mixing method, as it is the most common method utilized by Hiway Stabilizers Ltd. which is presently the only company to use DSM in New Zealand. Hiway Stabilizers Ltd. primarily uses a cement binder with a small amount of lime added. Lime induces mineralogical changes that help stabilise the soil, especially in clay (Rogers & Glendinning, 1996). The binder is injected through hollow, rotated mixing shafts tipped with some type of cutting tool. The shaft above the tool may be equipped with discontinuous flight augers and/or mixing blades and paddles. Shafts are mounted vertically on a suitable carrier usually for crawler work on land. Individual column diameters range from 0.6 m to 1.5 m and up to 40 m in depth (Bruce & Bruce, 2003). There are several different types of mixing blades. This research focuses on the Colmix method and TurboJET method which are utilized by Hiway Stabilizers Ltd. The cutting tools for these methods are shown in Figure 2-1 and Figure 2-2. The binder is injected as the tool penetrates the soil. Mixing and compaction takes place as the tool is withdrawn. The mixing process is enhanced through high pressure injection via nozzles in the cutting tool. Colmix uses twin (side by side) auger cutting tools whereas TurboJET uses two sets of blades on a single auger and a higher pressure for injection.

Figure 2-1: Colmix mixing blades.

Figure 2-2: TurboJET mixing blade.

Generally, the cemented material has a higher strength, lower permeability and lower compressibility than the native ground, though total unit weight may be less. The exact properties obtained are dependent on the characteristics of the native soil, construction variables (primarily the mixing method), operational parameters, and the binder characteristics (Bruce & Bruce, 2003).

For road slips, the columns are normally arranged in rows (Figure 2-3). Between two and five rows may be required depending on the geometry and geology of the site.

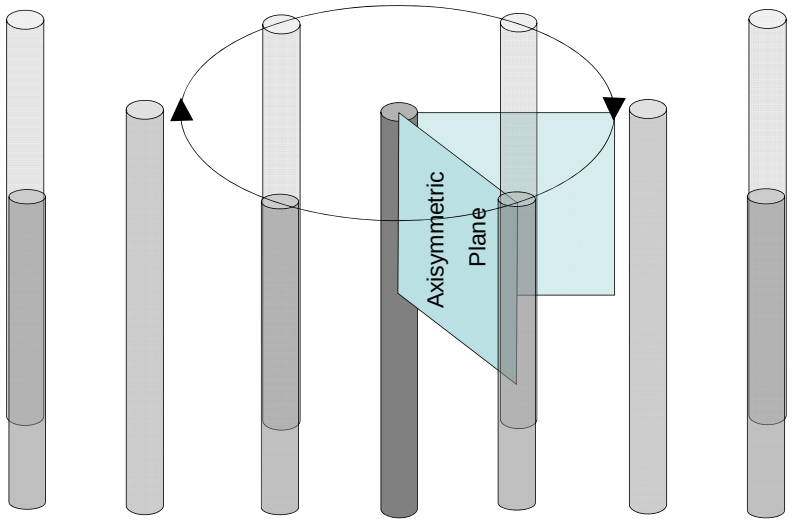

Figure 2-3: Typical column arrangement for road slip mitigation.

Column spacing varies, but it is usually a maximum of approximately 2.5 m (Terzaghi et al., 2005). The diameter of the columns is typically 0.6 m, but can be other sizes. If columns are too close there is no further gain in overall strength of the improved soil system. If they are too far apart, the columns begin behaving individually with no net benefits (Leung et al., 2006). Thus, column spacing is one of the main design parameters.

2.3 Deep Soil Mixing Properties

2.3.1 Mechanical Properties

Studies on mechanical properties of the clay soil surrounding DSM columns installed in the field have included cone penetration tests (CPT) (Muntohar & Hung, 2007; Shen et al., 2008; Shen, et al., 2003), laboratory unconfined compression tests, and vane shear tests (Shen et al., 2003b). Studies on the soil around DSM columns created in the laboratory have included undrained shear strength (Larsson & Kosche, 2005) and CPT (Muntohar & Hung, 2007, Shen

et al., 2003c). There appeared to be no difference between the mechanical properties of the soil surrounding dry-mixed and wet-mixed columns (Larsson & Kosche, 2005).

2.3.2 Chemical Changes in Soil Properties

A significant focus of previous studies on property changes of soil surrounding DSM columns has been on the migration of cations that occur due to the utilization of lime in the binder (Larsson & Kosche, 2005; Shen et al., 2008). It was found that the diffusion of cations away from the DSM columns was gradual with time, and that cation concentrations at relatively shallow depths were lower than those at greater depths. Diffused cations change the remoulded shear strength of the soil surrounding DSM columns because the readily exchangeable monovalent cations (such as K^+ and Na^+) initially adsorbed on the clay particle surface are replaced with trivalent cations (such as Fe^{3+}) and divalent cations (such as Ca^{2+} and Mg^{2+}) from the DSM columns. As a result, the thickness of the diffused double layer surrounding soil particles decreased, and the plastic limit increased. This leads to a decrease in the liquidity index (*LI*), which results in an increase in the remoulded shear strength (Shen, et al., 2008).

2.3.3 Physical Changes in Soil Properties

As mentioned, a decrease in *LI* towards the column periphery has been noted after DSM column installation (Larsson & Kosche, 2005; Shen et al., 2008). This change was not noticed immediately but took several days. Water content of the soil surrounding DSM lime columns has also been found to decrease after column installation (Muntohar & Hung, 2007).

2.3.4 Transition Zone

Laboratory test results from previous studies show that two to three zones exist outside the nominal diameter of the DSM blade (Larsson & Kosche, 2005; Shen et al., 2003a). These are the:

- Expanded zone
- Transition zone (also called Influential Zone)
- Boundary layer

These three zones are depicted in Figure 2-4. The transition zone is the largest of these and is enclosed by the boundary layer. It extends 1.5 to 2 times the column diameter from the column centre. The boundary layer is approximately 10-20 mm thick.

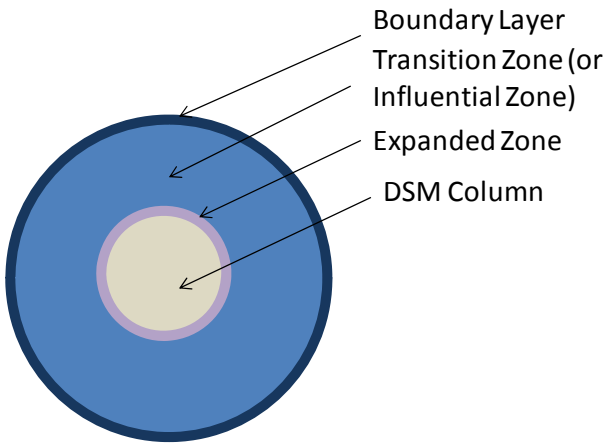

Figure 2-4: The expanded zone, transition zone, and boundary layer around a DSM column.

Soil property changes have been found to occur in these three zones located around DSM columns. In the transition zone, the migration of calcium ions increases the undrained shear strength of the soil. In the boundary layer, there is an increase in soil sensitivity (S_{tr}). These changes and other changes that have been found to occur in these zones are discussed further in Section 7.3.1. The expanded zone thickness is the difference between the actual column diameter and the diameter of the DSM mixing blade. The expanded zone may not exist, depending on the stiffness of the soil and the injection pressure of the DSM method. Higher injection pressures and softer soils are more likely to result in an expanded zone. The nature of the DSM columns as seen in the field during this study is discussed in Section 3.6.

2.3.5 Group Effects & Lateral Deformation due to Column Installation

One of the key issues with the design and performance of DSM columns used for slope failure mitigation is determining the extent to which the columns behave as group. A key component of group performance is soil arching. Soil arching is discussed further in Chapter 7.

Group effects of landslide stabilizing piles arranged in a similar fashion to Figure 2-3 have been studied fairly extensively (Bransby & Springman, 1999; Chen & Martin, 2002; Hsiung, 2003; Kourkoulis et al., 2011). Group interaction increases the efficiency of pile groups. For example, group interaction causes a 20% increase in the maximum bending moment in piles of groups with three diameter spacing in comparison to a single pile (Chandrasekaran et al., 2010). It is also evident that relative stiffness between the soil surrounding a pile and the pile itself play a key role in the pile's failure modes (Martin & Chen, 2005). This has not been studied extensively in a DSM context.

During DSM column installation, the cement slurry is injected into the ground under pressure, causing deformation and densification of the surrounding soil which enhances the group effect of the columns. Based on the theory of cylindrical cavity expansion (Vesic, 1972), a formula has been developed that estimates the amount of lateral displacement in the ground induced by DSM column installation (Chai et al., 2005). The effects of this on pressure- displacement curves and on the ability of the columns to resist lateral load are explored in Chapter 7.

2.3.6 Laboratory Testing on DSM Columns

Laboratory testing for research on the performance of DSM columns has largely been focussed on the columns themselves. Laboratory testing on the soil surrounding DSM columns has included CPT (Muntohar & Hung, 2007; Shen et al., 2008, Shen et al., 2003b), unconfined compressive strength (UCS) (Muntohar & Hung, 2007), undrained shear strength (Larsson et al., 2009; Shen et al., 2003b), and Atterberg limits (Larsson & Kosche, 2005; Larsson et al., 2009; Shen et al., 2008). Also, as discussed earlier, significant testing has been performed on the variation in cation concentrations in the soil surrounding DSM columns (Larsson & Kosche, 2005; Larsson et al., 2009; Shen et al., 2008; Shen et al., 2003c).

2.3.7 Deep Soil Mixing in New Zealand's Northland Allochthon Slopes

Many slopes within the Northland Allochthon geology in the Northland region of New Zealand are known to be vulnerable to instability and creep over time. This is partly due to the unique characteristics of the Northland Allochthon, which has a low strength and a highly sheared fabric (Winkler, 2003). Road instability due to slope failures is not uncommon. In some locations the slope problems have been compounded by inadequate drainage and inappropriate remedial work in the past such as placing additional fill on a subsiding road foundation (Gani, 2004). Deep soil mixing has been found to be an economical and effective option for addressing road slips in this material (Gani, 2004; Terzaghi et al., 2005; Terzhagi et al., 2004), and it has become a commonly implemented solution.

2.4 Northland Allochthon Geology, Formation and Properties

An Allochthon, by definition, is a body of rock which has been uplifted from its original site of formation through a low angle thrust fault. Although the Northland Allochthon was previously described as Onerahi chaos-breccia, this term is no longer used, as the displaced rocks of Northland are neither chaotic, nor breccias. The Northland Allochthon can be subdivided into four main complexes (Isaac et al., 1994):

- Tangihua (submarine basaltic volcanics)
- Tupou (strongly indurated, fractured, sheared conglomerate and sandstone only found in the far northern Whangaroa area)

- Mangakahia (variable calcareous clay shales and siliceous mudstones and sandstones)
    - Punakitere Sandstone- clastic flysch, interbedded fine to coarse sandstone and mudstone, fine medium sandstone with pebble conglomerates, micaceous and concretionary sandstone
    - Whangai Formation- siliceous and locally calcareous mudstone to fine sandy siltstone and muddy limestone
    - Hukerenui Mudstone- non-calcareous clay-rich mudstone
- Motatau (predominantly calcareous limestones, mudstones and sandstones)
    - Puriri Mudstone- calcareous mudstone (and sandstone)
    - Mahurangi Limestone- fine grained micritic limestone with fine to coarse sandstone interbeds

The Mangakahia Complex is the focus of this study. The Northland Allochthon rocks are thought to have been originally deposited in a sedimentary marine basin off what is now modern day northern and north-eastern Northland. The soils that develop above the Northland Allochthon are generally thin, with their thickness being a function of the permeability of the underlying parent rock (Winkler, 2003). They can be considered residual soils, developed in place from their underlying parent rocks. All three of the Northland Allochthon complexes pose some difficulties for geotechnical design. Road slips are often seen in the Mangakahia and Motatau Complexes. Northland Allochthon soils developed from Mangakahia clay shales are highly plastic with high shrink-swell potential. The liquid limit is highly variable and can be in excess of 80. The shrinkage limit is less than 15, indicating that the soil is highly reactive and susceptible to creep (Winkler, 2003). Soils developed from the Mangakahia clay shales typically comprise very soft to stiff, plastic, light coloured, clayey silts and silty clays with some sands or gravel-sized clasts (Lentfer, 2007).

The geological formations in Northland have also been fairly well mapped on a broad scale. The NZ Geological Survey Map 1:250,000, Sheet 2A Whangarei by Thompson (1961) and NZ Geological Survey Map 1:250,000, Sheet 1 North Cape by Kear and Hay (1961) are

widely used publications of geological information in the Northland area, but they are now more than 40 years old and have been superseded by Geology of the Whangarei Area Map 1:250,000 by Edbrooke and Brook (2009) and Geology of the Kaitaia Area Map 1:250,000 by Isaac (1996). The physical properties and classification of Northland Allochthon soils from the Mangakahia Complex have been defined in three theses: Lentfer (2007), O'Sullivan (2009) and Harris (2013). However, a significant amount of geotechnical laboratory testing remains to be done to determine how soil derived from the different complexes and formations varies, how much the soil from the same formation varies from site to site, and how much the soil behaviour is related to microstructure. The location of Northland Allochthon soil is depicted in Figure 2-5. Northland Allochthon soils, in their undrained condition, are usually stiff (Gani, 2004). In the Mangakahia Complex, the residual angle of internal shearing resistance of the soil is affected by the presence of shear zones and sheared fabrics and is typically in the range of just 10° to 15° (Winkler, 2003). Slopes that are underlain by Northland Allochthon geology typically reflect the strength of the underlying rockmass. Consequently, they are often only at gentle to moderate gradients due to the generally low to very low overall rockmass strength. For example, non-calcareous and non-siliceous mudstone lithologies (such as Hukerenui Mudstone from the Mangakahia Complex) tend to stand between 7° and 14°, calcareous and/ or siliceous mudstone lithologies usually stand between 14° and 30°, whilst limestones and marls naturally stand at gradients greater than 30° (Irwin & Rogers, 2006). The surface morphology of slopes underlain by Northland Allochthon lithologies is also typically (and distinctively) hummocky and undulating, mainly due to the susceptibility of the materials to slope instability. Localised "floaters" of harder Northland Allochthon lithologies incorporated within the sheared and crushed softer lithologies tend to stand out, also providing a hummocky surface morphology (Irwin & Rogers, 2006). Figure 2-6 shows the typical geomorphology of Northland Allochthon slopes. The photo is taken in an area where the underlying rock is of the Mangakahia Complex.

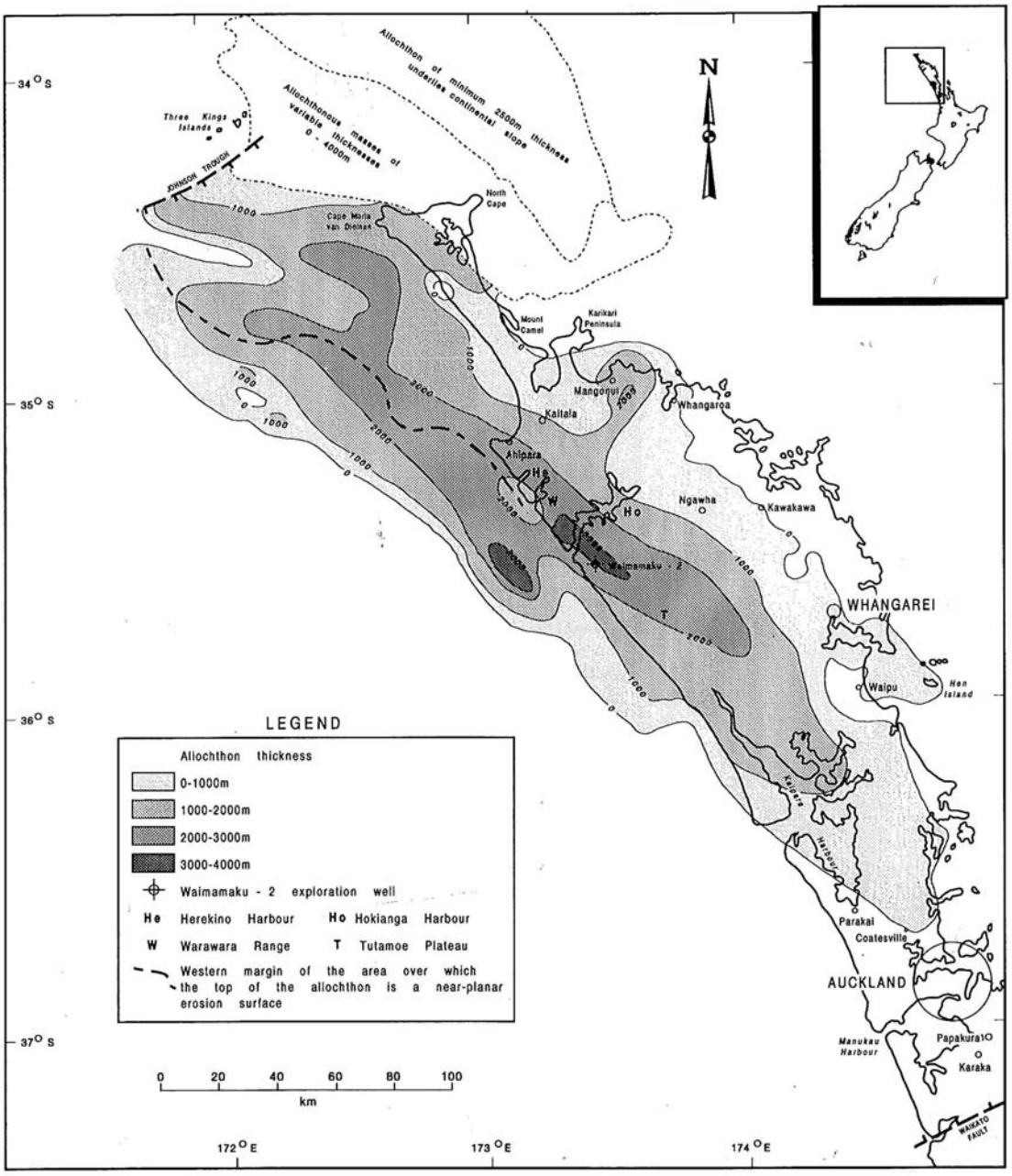

Figure 2-5: The present day extent of Northland Allochthon (Isaac et al., 1994).

Figure 2-6: Typical geomorphology of Northland Allochthon (Mangakahia Complex).

Two other theses delve into the behaviour and soil properties of Northland Allochthon residual clay soil. These are referred to throughout this thesis, and provide information about the soil parameters and behaviour. As such, a brief description of these studies is provided in this section.

O'Sullivan (2009): Ogles No.3 Site, Hukerenui Mudstone (Mangakahia Complex)

The focus of this study was on the suitability of advanced soil models, available in Plaxis finite element software, to simulate the behaviour of Northland Allochthon residual clay soil. Soil specimens from the Ogles No. 3 site were tested in triaxial compression in the consolidated drained (CD) and consolidated undrained (CU) conditions in order to acquire soil parameters. The location of the Ogles No. 3 site is discussed in Section 3.2. Other laboratory tests included Atterberg limits, ring shear, and oedometer testing. Several constitutive models were examined through numerical simulations of triaxial tests. In order to assess whether the use of advanced soil models are warranted in this soil type, the Hardening Soil model (discussed in Section 2.8.2) was selected for use in the analysis of a 2D infinite slope model of a "typical" Northland Allochthon slope. Triaxial testing results from O'Sullivan (2009) are discussed in Section 2.8.2 and strength parameters and oedometer results obtained by O'Sullivan (2009) are compared to laboratory testing performed in this thesis in Section 4.5 and 4.7.2, as well as Section 4.7.3. The main conclusions in O'Sullivan

(2009) pertain to proposed slope failure mechanisms, which are briefly discussed in Section 6.4.1.

Harris (2013): Silverdale Site, Whangai Formation (Mangakahia Complex)

In this study, a site-specific early warning system is developed for a rainfall induced landslide at a field site located in the town of Silverdale (located approximately 30 km north of Auckland) along State Highway 1. Laboratory tests were undertaken in order to better understand the characteristics of the soil which included determination of soil-water characteristic curves, falling head tests (permeability), consolidated drained (CD) triaxial tests, and constant shear stress drained (CSD) triaxial tests. In a CSD triaxial test, failure of the soil specimen is instigated through the development of pore pressures, while the shear stress remains constant throughout the test. This is in contrast to a conventional triaxial test (such as a CD test) where failure is brought on through an increase in shear stress. Atterberg limits and grain size distribution were also reported in Harris (2013) (performed by Melrose and Willis (2010)). Field monitoring included volumetric water content sensors and rainfall monitoring. The rainfall events were inputted into a numerical model of the slope and coupled with a slope stability analysis, incorporating the matrix suction and pore pressure profile. Field and numerical results were used to train an artificial neural network to predict slope failure at the field site.

The research by Harris (2013) revealed several characteristics of the slopes in Northland Allochthon residual clay soil. The water content probes showed that the site was subject to significant drying out during the summer periods. In addition, rainfall events captured at the site during the summer were more intense and of shorter duration then those experienced during the winter. Other conclusions about the behaviour of the soil and slope failures are discussed in Sections 3.5.4, 4.7.3, and 6.4.1. Section 3.4.4 compares the Atterberg limits in O'Sullivan (2009) and Melrose & Willis (2010) as cited in Harris (2013) to those of the soil specimens obtained from different field sites as part of the field testing portion of this thesis.

Neither O'Sullivan (2009) nor Harris (2013) includes the following points in relation to Northland Allochthon residual clay soil which are included in this thesis:

- In situ testing results

- Triaxial and oedometer testing of reconstituted specimens
- Evaluation of the effects of soil structure on the shear strength of the soil
- Comparison of soil properties between various field sites
- The use of a slip surface where the soil strength is reduced to residual strength when examining second time failure of a landslide in Northland Allochthon clay soil

2.5 Slope Failure Mechanisms

Northland Allochthon slopes are subject to creep and instability that tends to progress gradually with time. This is in part due to the fact that the Northland Allochthon lithologies are typically moderately to pervasively sheared and crushed (depending on the underlying rock type). The soil mantle is generally quite thin, especially in the Mangakahia Complex, and it often overlies a parent rock with very low permeability. This can cause water to perch within the soil mantle. Most slope instability is within the soil mantle (Winkler, 2003). Small changes in slope conditions can upset equilibrium, including changes in groundwater conditions. The shrink-swell potential of the soil likely also contributes to slope instability. Soils with a high shrink-swell potential tend to have weaker slope stability than those with a lower shrink-swell potential (EPA, 2011). These types of soils are prone to developing fissures during dry spells. These fissures allow rainfall to enter and saturate the soil, which causes swelling. Swelling reduces the soil density, which is not recoverable (EPA, 2011). This leads to further development of fissures during dry periods. Rainfall then delivers a load, and lubrication, which the weakened soil is unable to withstand, and slip-plane failure eventually results (EPA, 2011).

Deep seated failures also exist, but can be difficult to recognize due to re-grading of the headscarps and lateral scarps which results in loss of definition of the original feature (Winkler, 2003). Failure is often found to occur at the interface between the residual soil (which lies closest to the ground surface) and the "transition" zone soil (which overlies the parent rock), or at the interface between the transition zone and the parent rock itself (O'Sullivan, 2009).

2.5.1 Use of the Critical State Angle of Internal Shearing Resistance for First Time Failure

Skempton (1977) advised the use of the fully softened strength (by definition, equivalent to critical state strength) in association with the highest foreseeable pore water pressures, for design against long term first-time failure based on back analysis of several slope failures in London clay. Take and Bolton (2011) also demonstrate that the use of Skempton's 'fully softened' strength is appropriate in the design of clay slopes that will be subject to seasonal variations of groundwater conditions. Furthermore, Stark et al. (2005) suggest the use of fully softened strength in evaluating the stability of slopes in cohesive soils that have not undergone previous sliding. The critical state angle of internal shearing resistance (φ'_{crit}) is used in Chapter 6 in a case study where first time failure of slope in Northland Allochthon residual clay soil (followed by second time failure) is evaluated.

2.5.2 Shrink-Swell Potential

The shrink-swell potential of Northland Allochthon clay soil identified by Winkler (2003) is due to high content of montmorillonite (Lentfer, 2007) and other high swelling clay minerals. However, aspects of previous research involving Northland Allochthon residual clay soil suggest that the shrink-swell potential of the soil is not necessarily a critical factor in the investigation of slope failures in this soil type. These aspects are summarized below.

- O'Sullivan (2009) performed two oedometer tests to assess swelling of Northland Allochthon residual clay soil from the Ogles No. 3 site. These tests showed zero swelling pressure, suggesting that the shrink-swell potential of this soil is not significant.
- Harris (2013) excluded the shrink-swell potential effects due to high montmorillonite content from his study. Numerical modelling of a landslide event at a nearby field site (also in the Whangai Formation) was performed by Harris (2013) to verify the modelling process used in his study. The results of the simulation gave a factor of safety of unity for the stability of the slope, suggesting failure, and confirming that the process used (which did not account for the effects of shrink-swell potential) was reasonably accurate.
- Lentfer (2007) performed linear shrinkage testing on soil from the Hukerenui Mudstone and Whangai Formation in Silverdale. The expansive rating is "non-

critical" for soils with a linear shrinkage limit of 0-12%, "marginal" for soils between 12-17%, "critical" for soils between 17-22% and "very critical" for soils that are above 22% (Aniculaesi et al., 2013; Mills et al., 1980). Testing performed by Lentfer (2007) resulted in an average linear shrinkage limit of 11% (non-critical) in the Whangai Formation residual soil, 10% (non-critical) in the Hukerenui Mudstone transition zone soil, and 18% (critical, but at the lower end of this range) in the residual soil of the Hukerenui Mudstone.

Volume change potential due to shrinking and swelling of the soil is briefly examined for Northland Allochthon residual clay soil from several field sites in Section 3.5.3. Based on the results from this analysis (as well as the points listed above), for the field sites pertaining to the investigations in this thesis (Ogles No. 3 site and Mountain Road site), shrink-swell potential was not deemed to be important in the context of this thesis.

2.6 Laboratory Testing and Evaluation of Soil Structure

2.6.1 Triaxial Testing

Triaxial testing is widely used to investigate the stress-strain behaviour of soils. The framework developed by Burland (1990), which is chosen in this thesis for examining the effects of soil structure on soil strength, requires triaxial testing to be performed on both intact and reconstituted soil specimens. This is further discussed in Section 2.6.5. The following terms are used in this thesis:

$$q = \sigma'_1 - \sigma'_3 \qquad (2.1)$$

where q is the deviatoric stress and σ'_1 and σ'_3 are principal effective stresses. σ'_2 is also a principal effective stress. In a typical triaxial test, $\sigma'_2 = \sigma'_3$ = cell pressure (as effective stress, denoted by ') and σ'_1 is equal to the cell pressure plus the axial load (also as effective stress). In plane strain, the deviatoric stress is represented as t:

$$t = \frac{\sigma'_1 - \sigma'_3}{2} \qquad (2.2)$$

The mean effective stress, p' is defined as follows:

$$p' = \frac{\sigma_1' + \sigma_2' + \sigma_3'}{3} \quad (2.3)$$

In plane strain the mean effective stress is defined as *s'*:

$$s' = \frac{\sigma_1' + \sigma_3'}{2} \; or \; \frac{3*p' - \sigma_2'}{2} \quad (2.4)$$

2.6.2 LVDT Local Strain Transducers

LVDT (Linear Variable Differential Transformer) local strain transducers provide on-sample small strain measurements of axial and/or radial strain. Soil stiffness is difficult to measure accurately using conventional triaxial testing methods where strains are based on external measurements of displacement. The actual strains occurring within the soil specimen can be concealed by deflections occurring due to compliances of the loading system and load measuring system. To add to this, sample bedding effects can cause further apparent deformation. These issues lead to a less accurate determination of the stress-strain response of the soil especially at small strains. Most triaxial tests therefore tend to give apparent soil stiffnesses far lower than those inferred from field behaviour (Jardine et al., 1984).

It is widely believed that triaxial test specimens with a height to diameter ratio of two have end zones which are more or less restrained while the middle third is more or less unrestrained. Therefore, it is highly desirable that radial and axial deformations are measured locally in this region if realistic deformation moduli are to be found. LVDT local strain transducers allow for measurement of strains in this region, and thus can result in a more accurate determination of stress-strain behaviour and small strain stiffness. The use of LVDTs for local strain measurement is discussed further in Chapter 4.

2.6.3 Oedometer Testing

The oedometer test is used to investigate the stress-strain behaviour of low permeability soils in one dimensional compression and swelling. Oedometer testing of reconstituted soil is required in order to normalize triaxial testing results when using the framework developed by Burland (1990) for comparing the behaviour of reconstituted and intact specimens. This is further discussed in Section 2.6.5.

The conventional oedometer test has been found to have limited usefulness in testing of intact Auckland residual soils (Pender et al., 2003). The tests reported by Pender et al., (2003) have focussed on Auckland residual clay, but it is probable that the shortcomings they identified in the oedometer test will apply to any stiff (or very stiff) residual soil. They found that stiffness modulus values measured in the oedometer were less than those from conventional triaxial testing. One reason could be that the specimen height is quite small (19 mm), which would result in any bedding errors dominating the modulus value. Loading is not continuous so there are no closely spaced data points to correct bedding errors as with the triaxial test. Another reason is that there is no way to ensure saturation with the oedometer test (Pender et al., 2003). O'Sullivan (2009) performed some oedometer testing on intact Northland Allochthon residual clay and had considerable difficulty. He found the main limitation was that shape of the displacement versus log of time did not resemble the typical shape expected for a standard consolidation test and therefore the end of primary consolidation was difficult to interpret from the graph.

2.6.4 Soil Structure and Fabric

Soil "structure" is used to define the combination of "fabric", the arrangement of the component particles, and "bonding", the inter-particle forces that are not of a purely frictional nature (Lambe & Whitman, 1969). Clay particles are formed by a sequence of structural units consisting of hydrated layered silicates of magnesium and aluminium (Gasparre, 2005). The layers and the links between them define them as different minerals (i.e. kaolinite, illite and chlorite which all have stable structures). Smectite is a clay mineral that has an unstable structure because the links between it are provided by hydrated cations. Figure 2-7 depicts the structures of kaolinite, illite and smectite (which are the primary minerals in the Mangakahia lithofacies of Northland Allochthon (Lentfer, 2007)).

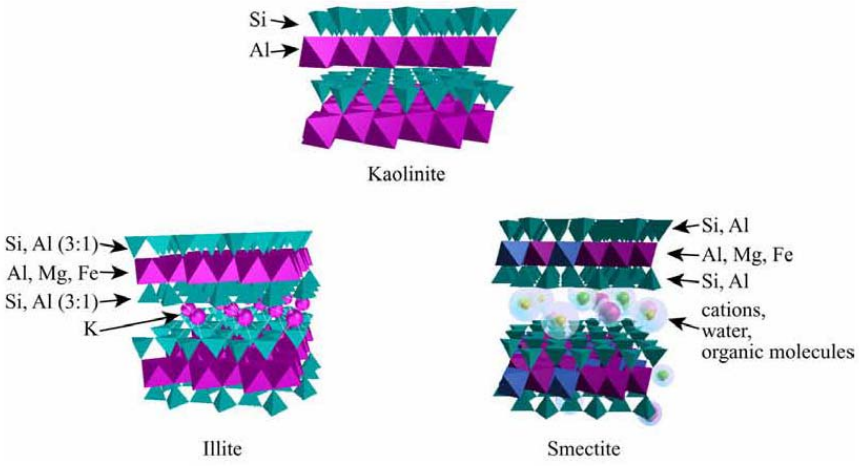

Figure 2-7: Structures of kaolinite, illite and smectite represented as layers of tetrahedral and octahedral (Berti, 2003).

The orientation and distribution of the clay particles define the fabric of the clay soil (Lambe & Whitman, 1969). The fabric includes inhomogeneities, layering, and any distinct distribution or orientation of the soil particles and fissures (Coop & Cotecchia, 1995). The four fundamental fabrics of clay are: dispersed (no face-to-face association of the clay particles), aggregated (face-to-face association of several clay particles), flocculated (edge-to-edge or face-to-face association of aggregates), deflocculated (no association between aggregates) (Mitchell & Soga, 2005). Fabric can be determined through Scanning Electron Microscope (SEM) analysis. However, analysis through SEM requires the soil specimen to be dried, a process which can alter clay properties. Residual soils seem to be especially sensitive to changes that can occur due to drying. Even partial drying at moderate temperatures can change the structure and behaviour of tropical residual soils. (Fookes, 1997). However, Gasparre (2005) states that in stiff clays (such as the London clay examined in his study), the shrinkage due to air drying does not dramatically affect the soil structure. She therefore adopted air drying for the SEM analysis in her study.

With residual soils, structure results from the in situ physical and chemical processes that have taken place, altering the parent rock to become a residual soil. With sedimentary soils, the picture appears more complicated as a variety of factors have been involved in the formation of the final structure, covering the loading and unloading history and the

depositional and post-depositional processes (Wesley, 1990). Two important factors generally lead to a degree of predictability and homogeneity with sedimentary soil that is absent in residual soil. These are (Wesley, 1990):

1. The sorting processes that take place during erosion, transportation and deposition of sedimentary soils tend to produce homogenous deposits.

2. Stress history is generally a dominant factor in influencing the behaviour of sedimentary soils, and leads to the well known division of these soils into normally consolidated and overconsolidated materials.

The absence of these factors with residual soils means that structural effects may be generally more complex and important with residual soils than with sedimentary soils (Wesley, 1990).

2.6.5 Destructuration and Determination of the Degree of Structure

The definition of structure used in this study agrees with what Leroueil et al. (1984) called the 'intact state' of structure. This is the state that occurs in natural soil deposits, and is a result of the natural geological history of the soil. Structure tends to impart added strength to a soil, which is described by Burland et al. (1996).

A fully "destructured" state is defined as the state of a clay that has been reconstituted at a water content equal to or greater than the liquid limit without air or oven drying and consolidated under one dimensional conditions (Burland, 1990). In a reconstituted state, the clay will still have some structure, but it is different to the structure of the soil in its intact state. The soil structure in the reconstituted state will be comprised of a fabric and bonding that are more stable than the fabric and bonding that occur in the intact state (Cotecchia, 1996). Since the state of reconstituted soils does not change with disturbance, these basic properties are inherent, and are considered to be "intrinsic" properties (Burland, 1990).

The testing of reconstituted specimens of Northland Allochthon residual soil has not been performed to date by any researchers. The importance of testing reconstituted samples of clay is that the results should give a well defined frame of reference against which to evaluate the results of undisturbed samples. In order to be able to compare undisturbed to reconstituted

soil specimens, the soil must somehow be placed on the same 'scale'. Some researchers have used the same one dimensional compression pressure to create the reconstituted soil specimens as the estimated preconsolidation pressure of the natural soil (Callisto & Calabresi, 1998; Scarpelli et al., 2003). However, preconsolidation pressure can be difficult to determine accurately. Another method involves using trial and error to determine the compaction effort required to achieve the same dry unit weight for the reconstituted samples as the undisturbed samples (Casagrande et al., 1963). It is also possible to compact the specimens by kneading or tamping each layer until the accumulative mass of the soil placed in the mould is compacted to a known volume (ASTM, 2004). Other researchers have attempted to consolidate the reconstituted soil specimens to the same void ratio as the undisturbed soil. All of the above stated methods can be difficult. The results of numerous test programmes on reconstituted clayey soils (Burland, 1990; Burland et al., 1996) show that, if the results are normalised by the equivalent pressure, a simple picture becomes apparent. This equivalent pressure is an equivalent isotropic mean effective stress defined as p'_e when working in *q-p'* space. In plane strain (*t-s'* space), the equivalent pressure is an equivalent one dimensional pressure defined as σ^*_{ve}.

Figure 2-8 shows the intrinsic compression line (ICL) for similar reconstituted clayey soils, and their sedimentation (natural) compression line (SCL). In this figure, *e* is the void ratio, e^*_{100} is the intrinsic (reconstituted) void ratio corresponding to a vertical stress of 100 kPa, C^*_c is the intrinsic compression index, and σ'_{v0} is the vertical effective stress. I_v is the void index, defined on the y-axis, which can be used to normalize the intrinsic compression curve. The equivalent isotropic mean effective stress p'_e (or equivalent one dimensional pressure σ^*_{ve}) is defined as the pressure on the intrinsic isotropic (or one dimensional) compression line corresponding to the void ratio of the soil (as originally defined by Hvorslev). If, in its normally consolidated state, samples of soil at various initial values of mean effective stress are sheared (either drained or undrained), their peak strengths often correspond closely to a critical state condition in which shearing continues at constant void ratio and mean effective stress (Burland, 1990). A critical state void ratio line can be determined from such tests. Figure 2-9 shows axes of t/σ^*_{ve} versus s'/σ^*_{ve}, where σ^*_{ve} is the equivalent stress on the intrinsic compression line corresponding to the void ratio of soil, and *t* and *s'* are as defined in Section 2.6.1. The 'state paths' followed by the drained and undrained tests on the

normally consolidated samples of the reconstituted clay lie on a 'state boundary surface' known as the Roscoe/Rendulic surface which intersects the s'/σ^*_{ve} axis at a value of unity, and terminates at a point where it meets the critical state line (CSL) which plots as a single point (approximately) on this normalised graph (point C in Figure 2-9). The Roscoe/Rendulic surfaces obtained from drained and undrained tests usually lie very close to each other. In very silty low plasticity soils they may not be unique, although the end points are (Burland, 1990).

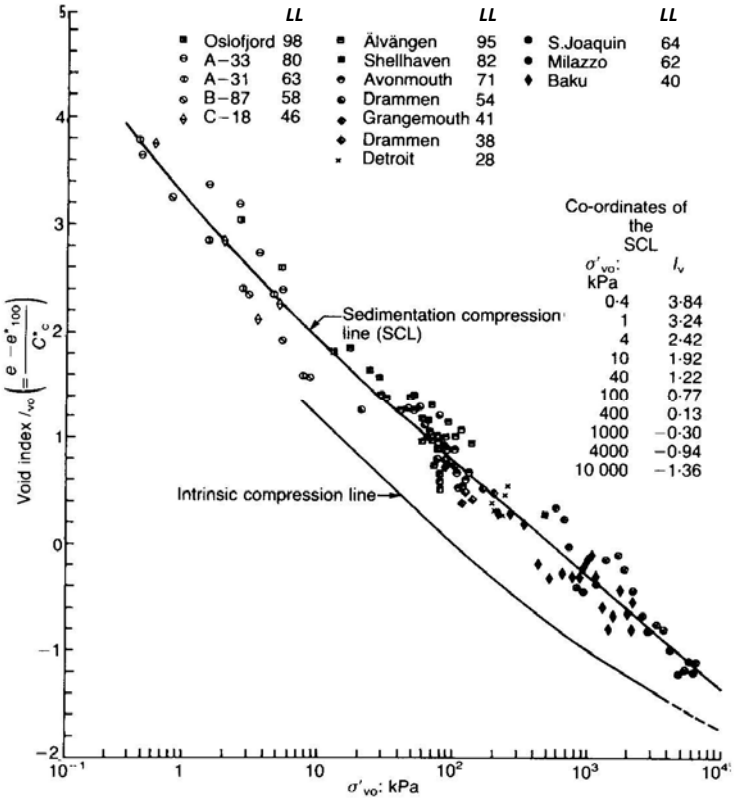

Figure 2-8: Intrinsic and sedimentation compression lines (modified after Burland, 1990).

For overconsolidated soils, a similar picture emerges. Figure 2-8 can be developed by isotropically consolidating several different samples to different values of *p'* (mean effective stress). If drained and undrained tests are carried out on a number of samples for different overconsolidation ratios and different preconsolidation pressures then it has been found that

the peak strengths lie on a well defined line in q/p'_e versus p'/p'_e space, where q and p' are as defined in Section 2.6.1. Results are normalized by either using equivalent isotropic mean effective stress (p'_e), or in *t-s'* space, an equivalent one dimensional effective stress (σ^*_{ve}) as discussed above. Figure 2-9 shows the Hvorslev failure surface and Roscoe-Rendulic surface for results in plane strain (*t-s'* space) normalized using σ^*_{ve} (rather than in *q-p'* space, where the results would be normalized by p'_e).

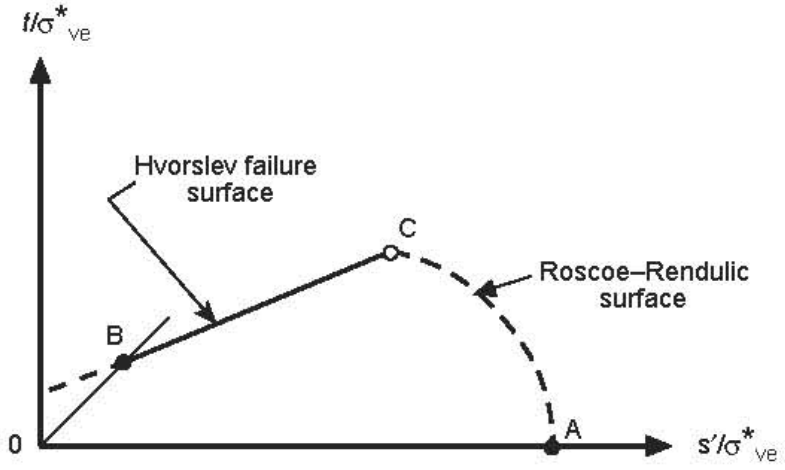

Figure 2-9: Critical state framework for reconstituted clays (Burland et al., 1996).

One of the most fundamental and important measures of the influence of microstructure on strength is the ratio of the normalized strengths at the intrinsic critical state (Burland et al., 1996). In Figure 2-10 this is given by DE/DF (=T). This can be thought of, in physical terms, as the ratio of the strength of the natural material to the critical state strength of the reconstituted material, normalized to the same void ratio at the same value of mean effective stress. Note that Figure 2-10 could be plotted as q/p'_e versus p'/p'_e, which would will yield the same T value as t/σ^*_{ve} versus s'/σ^*_{ve}. CSL is the critical state line.

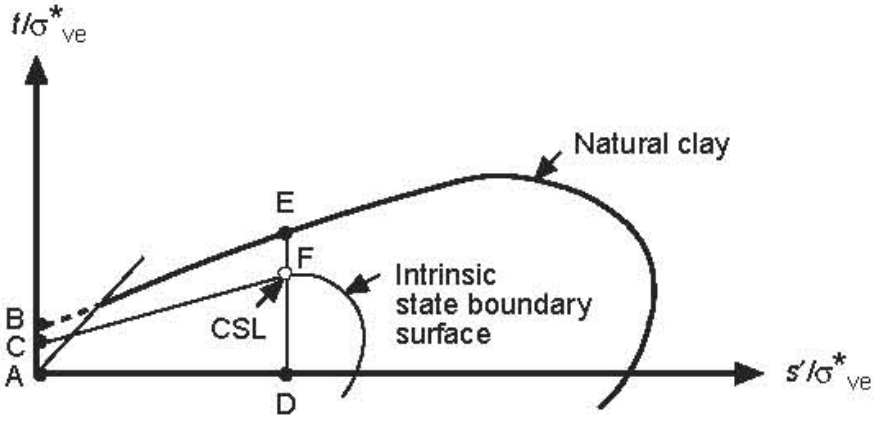

Figure 2-10: Comparison of natural and intrinsic state boundary surfaces showing increased resistance to compression and shearing (Burland et al., 1996).

Cottechia & Chandler (1997) developed the concept of "Strength Sensitivity" introduced by Skempton (1970) and defined a framework for clay behaviour based on the sensitivity of clays. The strength sensitivity (S_t) represents the ratio of the undrained strength after consolidation to gross yield to that of the reconstituted clay normally consolidated to the same water content as the natural clay at gross yield (Cotecchia & Chandler, 1997). The stress sensitivity (S_σ) is the distance between the yield stress of the material and the vertical stress on the intrinsic compression line (ICL) at the same void ratio. S_t and S_σ are represented graphically in Figure 2-11. Figure 2-11 shows the ICL and sedimentation compression curve (SCC) as well as the intrinsic strength line in undrained conditions (IS_uL). In Figure 2-11, the peak c_u of intact samples in the natural state is defined as S_u, S_u* is the undrained strength at the same void ratio on the IS_uL, SCC is the sedimentation compression curve, I_v is the void index, e is the void ratio, e_0 is the initial void ratio, w is the water content, and σ_{vy}' is the yield stress in oedometer compression. Note that σ^*_{ve} is represented as σ_{ve}* and σ'_{v0} is represented as σ_{v0}' in Figure 2-11. In addition, YSR is the yield stress ratio which represents the ratio of yield stress measured in the oedometer (σ_{vy}') to the in situ vertical stress (σ'_{v0}). IsSR is the in situ stress ratio which represents the ratio of the in situ vertical stress (σ'_{v0}) to the intrinsic compression stress (σ^*_{ve}).

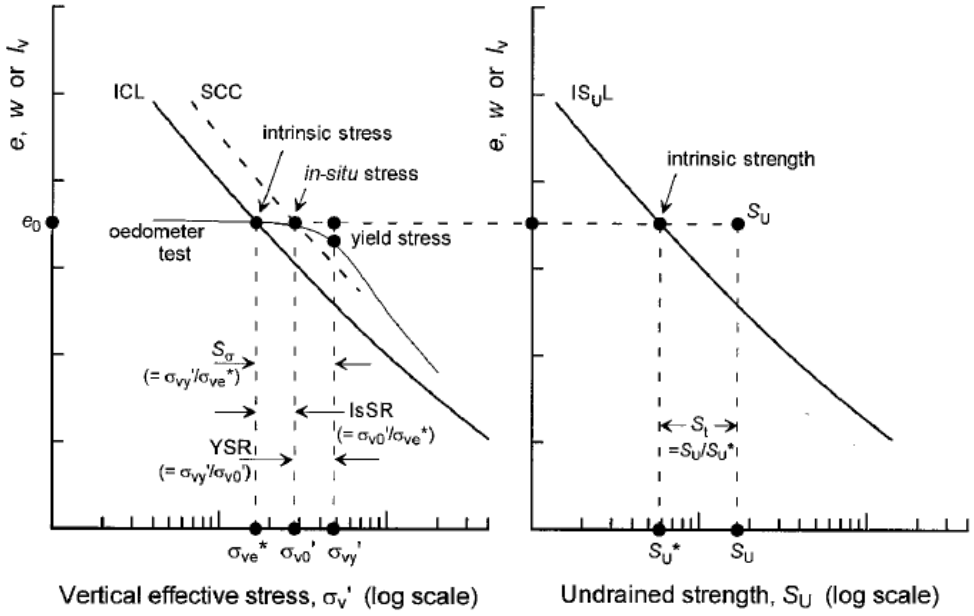

Figure 2-11: Intrinsic compression and intrinsic strength lines and other definitions (in situ stress state to the right of the ICL) (Chandler, 2000).

Reconstituted material has a S_t of exactly 1. For clays whose in situ state lies to the right of the ICL, S_t and S_σ are equal. Either stress or strength sensitivity uniquely defines the yield stresses of the clay, and provides a single parameter by which the clay structure may be represented (Cotecchia & Chandler, 2000). In order to use this type of analysis to determine the effect of structure on soil strength, both reconstituted and intact oedometer tests must be available. Oedometer tests on intact residual clay can be difficult and unreliable as discussed in Section 2.6.3. In addition, other difficulties can arise. For instance, Gasparre (2005) found the calculation of stress sensitivity for London clay quite difficult because the presumed post yield behaviour was still diverging from the corresponding intrinsic compression curve at the end of her tests. Due to the possibility of these foreseen difficulties, the sensitivity framework was not used in this study.

2.6.6 Yielding of Bonded Soils

'Yield' of soil has traditionally been described as a clear change in behaviour (Malandraki & Toll, 1996). Atkinson (1990) defined yield according to the classical meaning in soil mechanics - as the end of the elastic range. Natural soils are often considered to derive some

of their structure and strength from bonding. Smith et al. (1992) observed two kinematic sub-yield surfaces existing within an initial bounding surface during their research on Bothkennar clay. Malandraki and Toll (1994, 1996, 2000) defined yield for a weakly bonded artificial soil based on changes in the tangential stiffness (E_{tan}) versus axial strain plotted in log-log scale (Figure 2-12). They defined a 'first yield' as the first loss in stiffness. The final yield was defined by the point at which the bonded soil loses all of its stiffness from bonding. For their artificially bonded soil, Malandraki and Toll (1994, 1996) also identified an additional yield point, between the first and the final yield points, called 'second yield'. The term 'second yield' was used by Vaughan (1988) and Malandraki and Toll (1994, 1996). Since other researchers use the term "Y2", Malandraki and Toll (2000) introduced the term 'bond yield' to label the point where a major change in tangential stiffness occurs between the first and the final yield (Figure 2-12).

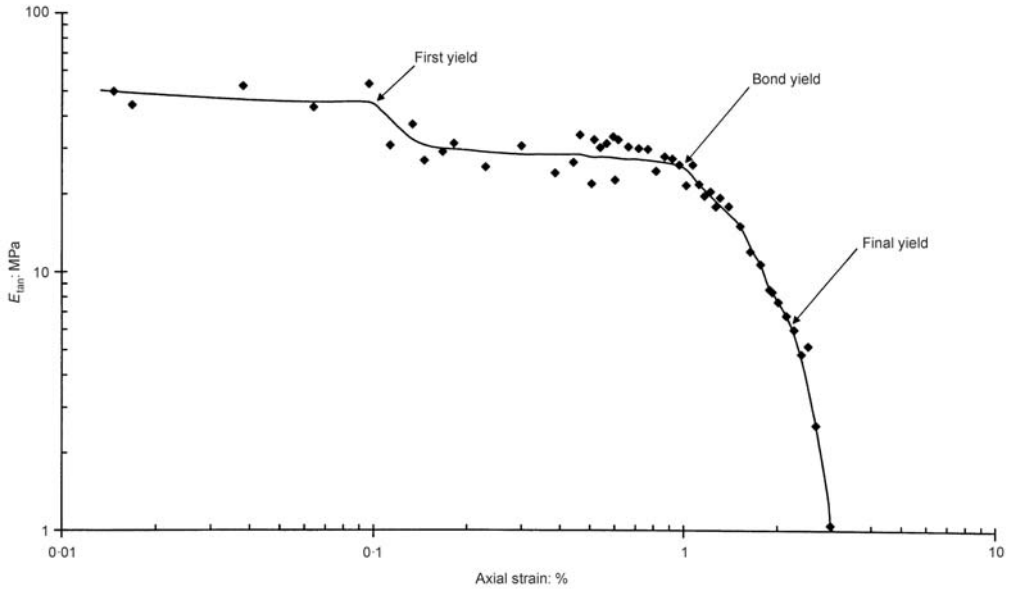

Figure 2-12: Definition of three yield conditions for bonded soil (Malandraki & Toll, 2000).

Hossain (2001) attempted to identify the first yield and bond yield points from several triaxial tests on intact specimens of residual tropical clay soil from Dhaka, Bangladesh. He found that there was no clear trend of yield points at confining stresses above 500 kPa, and even at

lower pressure ranges the identification of yield was sometimes tenuous. O'Sullivan (2009) alluded to the possibility of multiple yield points in Northland Allochthon residual clay soil. However, the work of Hossain (2001) highlights the difficulty of identifying them, and therefore the identification of these yield points was not attempted in this study. This study instead focuses on the mechanical behaviour of Northland Allochthon residual clay soil, and the use of Burland's technique discussed in Section 2.6.5 to determine the effects of structure on soil strength by comparing reconstituted and intact triaxial testing results.

2.7 Field Testing

2.7.1 Cone Penetration Testing

The cone penetration test (CPT) is a common in situ testing method in which a cone at the end of a series of rods is pushed into the ground at a constant rate. The sensors in the cone produce continuous analogue data of cone resistance (q_c), sleeve friction (f_s) and pore water pressure (u) that is converted to digital form at intervals of between 20 mm and 200 mm, depending on the equipment and test standard used. In soft clays and silts and in over water work, the measured q_c must be corrected for pore water pressures acting on the cone geometry to obtain the corrected cone resistance, which is discussed further in Lunne et al. (1997). CPT results can be used to estimate the undrained shear strength and overconsolidation ratio. CPT results from a Northland Allochthon field site are used to acquire these soil properties in Chapter 3, which are compared to flat plate dilatometer results.

2.7.2 Flat Plate Dilatometer Testing

The flat plate dilatometer test (DMT) is an in situ test device that utilizes an expanding membrane to measure in situ lateral stress and lateral soil stiffness. The DMT is presently not used as frequently as the CPT in engineering practice, but can be used for similar purposes and has some additional advantages in that it can measure horizontal stress and stiffness via a more direct method (i.e. the inflation of a diaphragm horizontally), and that the raw results can be correlated to obtain estimations for a larger number of soil parameters. It can also yield data similar to a pressuremeter test, such as the coefficient of lateral earth pressure at rest (K_0) and Young's modulus (E). However, they are empirically determined in the case of

the DMT, whereas they are obtained from theoretical considerations in the case of the pressuremeter. The DMT has been used fairly extensively in geotechnical site investigations over the past 20 years and its popularity appears to be continuing to grow (Campanella & Robertson, 1991; Chang, 1991; Finno, 1993; Monaco & Marchetti, 2004; Tong et al., 2004). Based on the literature review performed as part of this study, the DMT has had little use in the context of examining the soil property changes around DSM columns. However, an attempt is made in this study to use DMT results to examine these properties (Section 3.7).

The DMT is a stainless steel blade having a flat, circular steel membrane mounted flush on one side (Figure 2-13).

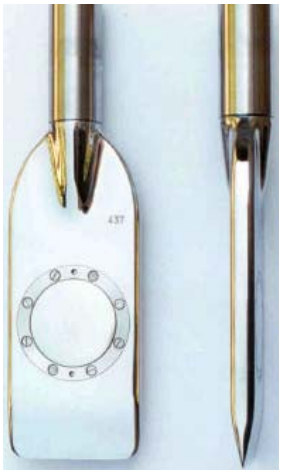

Figure 2-13: Flat plate dilatometer (Marchetti et al., 2001).

The blade is connected to a control unit at the ground surface by a pneumatic-electrical tube (transmitting gas pressure and electrical continuity). The blade is advanced into the ground using common field equipment (i.e. push rigs or drill rigs). Once at the desired depth, the membrane is inflated and two readings are acquired: an A-pressure (required to just begin to move the membrane against the soil) and a B-pressure (required to move the centre of the membrane 1.1 mm against the soil). A third reading (C-pressure) can optionally be taken by slowly deflating the membrane after B is reached. The pressure readings A and B are corrected by the values ΔA and ΔB (where Δ denotes "change", determined by calibration to

take into account membrane stiffness) and converted into parameters p_0 and p_1 which is described further in Marchetti (1980).

The first and second readings acquired from DMT results (p_0 and p_1) along with pre-insertion pore pressure (u_0) and pre-insertion overburden stress (σ'_{v0}), can be used to estimate a material index (I_D), a horizontal stress index (K_D) and a dilatometer modulus (E_D). These values can be used to interpret the overconsolidation ratio (OCR), coefficient of lateral earth pressure at rest (K_0), undrained shear strength (c_u) and the vertical drained constrained modulus (M). The coefficient of permeability and the horizontal coefficient of consolidation (c_h) can also be estimated, and the angle of internal shearing resistance (φ) can be estimated for sand (Marchetti et al., 2001). The basic DMT deduction formulae are presented in Table 2-1. The symbols in the first column are defined in the second column. Note that the angle of internal shearing resistance (φ) is defined as FF, and the coefficient of permeability in the horizontal direction (k_x) is defined as k_h. $K_{0,DMT}$, OCR_{DMT}, $c_{h,DMT}$, M_{DMT} and $c_{u,DMT}$ are values of K_0, OCR, c_h, M and c_u as estimated from DMT results. $\varphi_{safe,DMT}$ is a lower bound value (typically an underestimation of 2°-4°) of the angle of internal shearing resistance. Z_M and t_{flex} are defined in the left column (where time in Table 2-1 is denoted as t). M_h is the horizontal drained constrained modulus, and p_2 is determined as shown in the middle column of the last row in Table 2-1. R_M and R_{M0} are variables used to determine M_{DMT} and are defined in the second last row in the middle column in Table 2-1. γ_w is the unit weight of water. The pore pressure index (U_D) can be estimated from $(p_2-u_0)/(p_0-u_0)$. Note that p_2 is equal to u_0 in free draining soils, but p_2 is greater than p_0 in non free draining soils. U_D can aid in discerning between permeable layers (where $U_D = 0$), or non-permeable layers ($U_D > 0$), and can also indicate the location of the water table when the soil type is known to be relatively impermeable.

Table 2-1: Basic DMT reduction formulae (Marchetti et al., 2001).

SYMBOL	DESCRIPTION	BASIC DMT REDUCTION FORMULAE	
p_0	Corrected First Reading	$p_0 = 1.05\ (A - ZM + \Delta A) - 0.05\ (B - ZM - \Delta B)$	Z_M = Gage reading when vented to atm. If ΔA & ΔB are measured with the same gage used for current readings A & B, set $Z_M = 0$ (Z_M is compensated)
p_1	Corrected Second Reading	$p_1 = B - Z_M - \Delta B$	
I_D	Material Index	$I_D = (p_1 - p_0) / (p_0 - u_0)$	u_0 = pre-insertion pore pressure
K_D	Horizontal Stress Index	$K_D = (p_0 - u_0) / \sigma'_{v0}$	σ'_{v0} = pre-insertion overburden stress
E_D	Dilatometer Modulus	$E_D = 34.7\ (p_1 - p_0)$	E_D is NOT a Young's modulus E. E_D should be used only AFTER combining it with K_D (Stress History). First obtain $M_{DMT} = R_M E_D$, then e.g. $E = 0.8\ M_{DMT}$
K_0	Coeff. Earth Pressure in Situ	$K_{0,DMT} = (K_D / 1.5)0.47 - 0.6$	for $I_D < 1.2$
OCR	Overconsolidation Ratio	$OCR_{DMT} = (0.5\ K_D)1.56$	for $I_D < 1.2$
c_u	Undrained Shear Strength	$c_{u,DMT} = 0.22\ \sigma'_{v0}\ (0.5\ K_D)^{1.25}$	for $I_D < 1.2$
FF	Friction Angle	$\phi_{safe,DMT} = 28° + 14.6°\ \log K_D - 2.1°\ \log^2 K_D$	for $I_D > 1.8$
c_h	Coefficient of Consolidation	$c_{h,DMTA} \approx 7\ cm^2 / t_{flex}$	t_{flex} from A-log t DMT-A decay curve
k_h	Coefficient of Permeability	$k_h = c_h \gamma_w / M_h\ (M_h \approx K_0 M_{DMT})$	
γ	Unit Weight and Description	Acquired from chart (see Figure 16- Marchetti, Monaco, Totani, & Calabrese, 2001)	
M	Vertical Drained Constrained Modulus	$M_{DMT} = R_M E_D$ if $I_D \le 0.6$ $R_M = 0.14 + 2.36 \log K_D$ if $I_D \ge 3$ $R_M = 0.5 + 2 \log KD$ if $0.6 < I_D < 3$ $R_M = R_{M,0} + (2.5 - R_{M,0}) \log K_D$ with $R_{M,0} = 0.14 + 0.15\ (I_D - 0.6)$ if $K_D > 10$ $R_M = 0.32 + 2.18 \log K_D$ if $R_M < 0.85$ set $R_M = 0.85$	
u_0	Equilibrium Pore Pressure	$u_0 = p_2 = C - Z_M + \Delta A$	In free-draining soils

The pre-insertion pore pressure (u_0) and pre-insertion vertical effective stress (σ'_{v0}) must be known prior to blade insertion- at least approximately (Marchetti, 1980). DMT results can also be utilized to estimate the location of a slip surface in overconsolidated clays (Marchetti et al., 2001). The seismic dilatometer (sDMT) is a combination of the standard flat dilatometer (DMT) with a seismic module for measuring the shear wave velocity (V_s) which is discussed further below.

2.7.3 Shear Wave Velocity Testing (S-wave)

Seismic methods measure the wave propagation velocity in a material, from which the small-strain modulus can be calculated. Two types of body waves can be used for seismic tests: compression waves (P-waves) and shear waves (S-waves). The compression wave travels faster and arrives first at the observation point. The shear wave is slower but has the

important advantage that its propagation velocity is not affected by groundwater. Also, due to the lower propagation speed, the shear wave velocity can be measured with greater accuracy, as the time interval is larger than in the case of P-waves.

The objective of shear wave velocity testing is to determine the travel time of the polarized shear wave between different sensor levels. Shear waves propagate at very low strains, and the shear strain (ε_q) can be estimated from the following relationship:

$$\varepsilon_q = \frac{x}{V_s} \qquad (2.5)$$

where x is the vibration velocity amplitude and V_s is the S-wave velocity. The shear modulus at small strains (G_0) can be calculated from S-wave velocity (V_s) as follows (Hird & Chan, 2005; Massarsch, 2005):

$$G_0 = \rho V_s^2 \qquad (2.6)$$

where ρ is the bulk density of the medium.

The source geophone for the shear wave pulse is also located at ground surface. In the sDMT, the shear waves are recorded by the geophones in the seismic module located near the dilatometer blade. The geophone signals are sent back up to a computer located on the ground surface as seismographs. There are two geophones spaced 0.5 m apart. Re-phasing the seismographs leads to the calculation of the time interval between seismic wave arrivals. Then, knowing the distance and time interval, a shear wave velocity (V_s) can be determined.

2.7.4 Field Testing on Northland Allochthon Soil and DSM Columns

Northland Allochthon

As with lab testing, little published work on in situ field testing is available for Northland Allochthon soils. A thesis from the University of Auckland (Holtrigter, 2010) is the largest source of in situ testing results. This thesis provides correlations between sDMT and CPT test results at several sites, three of which are in Northland Allochthon soil.

DSM Columns

Apart from a few studies which included CPT testing, there has been very little in situ testing targeting the changes to the soil surrounding DSM columns in the field. However, actual DSM columns (rather than the soil around them) have been extensively studied in situ and in the laboratory by several researchers, and an overview of these studies is provided by Larsson (2005) (Deep Soil Mixing State of Practice Report). Testing using sDMT can aid in characterizing changes in stiffness, strength and stress state of the soil surrounding DSM columns, one of the objectives of this study.

2.8 Numerical Modelling

Through appropriate simplifications of reality, finite element and finite difference numerical modelling can allow geotechnical problems to be solved more efficiently and cost-effectively than physical modelling or by using numerous discrete calculations. However, the important aspects of the overall behaviour of the problem being modelled must be decided upon by the user in the early stages of model developement. If selected incorrectly, the model may not appropriately represent the situation to which it is being applied.

Numerical modelling is an important tool for understanding slope failures, and for the design of DSM columns used to mitigate these failures- particularly their spacing, depth and location. There is a need for understanding the group effect of the DSM columns, and how to model the effects of the change in stress distribution that can be seen in 3D models but not 2D ones (Leung et al., 2006). In addition, there is a need for a more thorough comparison between 2D results using the replacement ratio method and 3D results beyond simply examining the resulting factor of safety (FoS). This is because the post-column installation FoS tends to be for a slip surface that is below (downslope) of the columns, and it is influenced more by the slope geometry than the column strength. The FoS alone therefore does not give a good indication of the how the columns themselves are performing in 2D compared to 3D.

Plaxis finite element code is a commonly utilized program for modelling DSM columns, in New Zealand, and several authors discuss its use (Gani, 2004; Krenn & Karstunen, 2009; Leung et al., 2006; O'Sullivan et al., 2009; Terzaghi et al., 2005). Other authors from outside

of New Zealand also demonstrate the use of Plaxis for the numerical modelling of DSM columns (Baker et al., 1997; Karstunen, 1999; Krenn & Karstunen, 2009). Several types of constitutive models are available in Plaxis. It has been shown that the observed non-linear stress-strain behaviour of the DSM columns can be well represented by using the Hardening Soil model, which is based on the hyperbolic stress-strain relationship (Krenn & Karstunen, 2009). The other types of constitutive models are also discussed in the following sections.

2.8.1 Numerical Modelling Software Packages

Two numerical modelling software packages were considered for use: Plaxis and FLAC.

Plaxis

Plaxis is a finite element software package for the 2D analysis of deformation and stability in geotechnical engineering. The mesh is generated automatically but can be refined, and staged construction allows for the simulation of construction and excavation. Updated mesh analysis can be used to update the mesh during calculations when a small strain analysis may show a significant change in geometry. Plaxis has a graphical user interface (GUI).

FLAC

FLAC is a finite difference software package for the 2D analysis of soil, rock and other structures that may undergo plastic flow when they reach yield. FLAC can simulate large strains, and most features are user controlled, including the mesh size. FLAC uses a scripting language rather than a GUI.

Although there are differences in how finite element and finite difference solvers arrive at the final solution, both methods have comparable accuracy. Both Plaxis and FLAC were trialled as possible software programs for this study. Plaxis was selected because of its staged construction capabilities, GUI, because it contains all of the constitutive models desired, and because it is in more common use in New Zealand by practitioners.

2.8.2 Constitutive Models

Several constitutive models have been considered for representation of Northland Allochthon soil behaviour. These include Mohr-Coulomb model, Hardening Soil model and Hardening Soil small model, and the Cam-clay model.

Mohr-Coulomb Model

The Mohr-Coulomb (MC) model is a simple and commonly used elastic - perfectly plastic constitutive model with a fixed yield surface (Muir-Wood, 2004). The basic parameters of the MC model are: angle of internal shearing resistance (φ), cohesion (c), Poisson's ratio (v), and Young's modulus (E). A dilatancy angle (ψ) can also be implemented. Figure 2-14 shows the behaviour of the MC model in stress versus strain space. E is the slope of the initial part of the stress versus strain curve. At the bottom of the figure, ε denotes strain, and ε^p and ε^e indicate where plastic strain and elastic strain are occurring, respectively. The MC failure criterion are shown in Figure 2-15 where the effective angle of internal shearing resistance (φ') is the slope of the failure envelope which lies tangent to the Mohr circle at failure, and the effective cohesion (c') is the y-intercept. These parameters are further described in Chapter 5, Section 5.2.1. τ is the shear stress, and σ'_1 and σ'_3 are major and minor principal effective stresses, respectively.

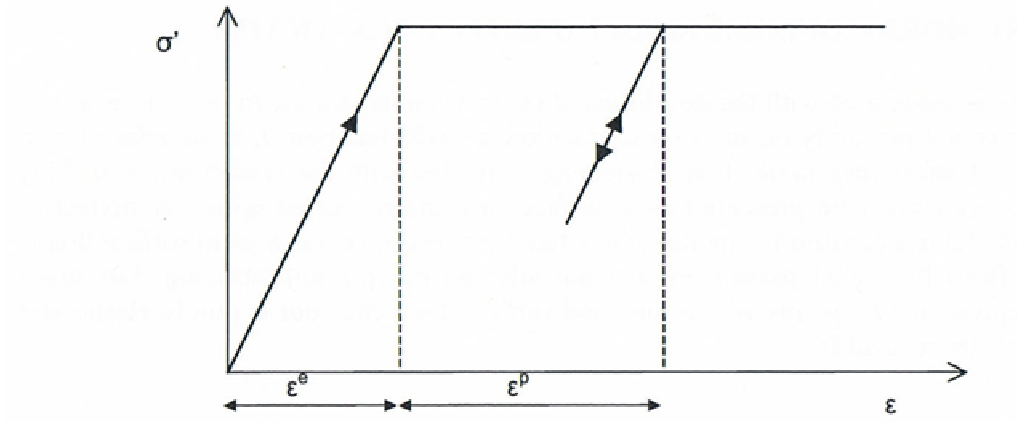

Figure 2-14: Basic idea of an elastic perfectly plastic model (Plaxis, 2008).

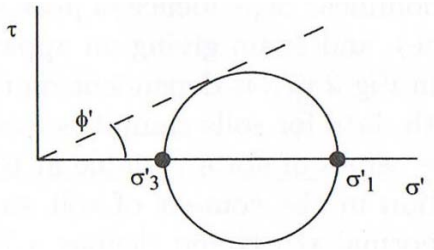

Figure 2-15: Mohr's circle and Mohr-Coulomb frictional failure criterion (Muir-Wood, 2004).

Hardening Soil Model & Hardening Soil Small Model

The Hardening Soil model is a constitutive model available in the Plaxis software package. It is available in two forms: 1) the Hardening Soil model with isotropic hardening (HS) and 2) the Hardening Soil model with small strain stiffness (HS small). The HS and HS small models consider non-recoverable plastic strains, both shear and volumetric, prior to failure. The theory of plasticity, rather than the elasticity is used, and the models include soil dilatancy and a yield cap (Brinkgreve et al., 2008). In the Hardening soil model, several parameters are used instead of E and v. These include E_{50} (secant stiffness at 50% strength in a standard drained triaxial test), E_{oed} (tangent stiffness for primary oedometer loading), E_{ur} (unload/reload stiffness) and m (power for stress level dependency of stiffness). Figure 2-16 depicts the hyperbolic stress-strain relationship. In Figure 2-16 q_a is the deviatoric stress at the asymptote of the stress-strain curve, q_f is the deviatoric stress at the failure line of the stress-strain curve, and σ_1 and σ_3 are major and minor principal stresses, respectively, as total stress.

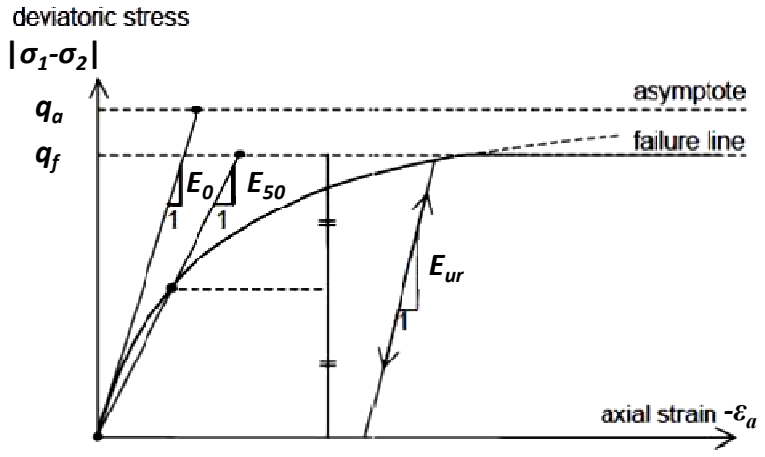

Figure 2-16: Hyperbolic stress-strain relation in primary loading for a standard drained triaxial test (modified after Plaxis, 2008).

O'Sullivan (2009) ran several triaxial tests in Plaxis using the HS small model, MC model and another Plaxis-specific model called Soft Soil Creep (SSC) for comparison to laboratory testing results. The SSC model has been developed for clays, clayey silts, and peats that are normally consolidated and have a high compressibility. Northland Allochthon soil does not fall into this category and it has therefore not been selected as a constitutive model to be used in this study. The SSC model was used by O'Sullivan (2009) because it incorporates a time dependant function which allows for secondary consolidation. However, a poor correlation was obtained for both the shear and volumetric behaviour (O'Sullivan, 2009).

O'Sullivan (2009) found that although there were several limitations to the HS small model and the model results did not perfectly mimic the laboratory results, the difference could be explained, or minimized with alterations to model parameters to result in good correlation with laboratory results. In Chapter 5, the 40 kPa consolidated drained test from O'Sullivan (2009) is re-examined for the HS, HS small and MC constitutive models with minor changes in soil parameters.

Cam-Clay

The Cam-clay model is a constitutive model developed for clays (Schofield & Wroth, 1968), depicted graphically in Figure 2-17. The Cam-clay model comprises the yield locus, the isotropic normal compression line and the critical state line. The void ratio (e) is an important parameter for the Cam-clay model and it is related to the specific volume (v) through the relationship e= 1+v. The Cam-clay model is fully defined by the soil properties v_λ, λ, κ and M. M is the slope of deviatoric stress (q) versus the effective pressure at critical state (p'_c). λ and κ are the slopes of the spherical plastic compression line (isotropic normal compression line) and a "typical line" (i.e. unload-reload line, respectively) which are shown in the bottom right graph in Figure 2-17. On this same graph, $e_{\lambda c}$ is the intercept point of the critical state line along the vertical axis. Note that v_λ is the specific volume corresponding $e_{\lambda c}$ ($v_\lambda = 1 + e_{\lambda c}$). In Figure 2-17, p'_v is the previous effective stress preconsolidation pressure. In the bottom right plot in Figure 2-17, $e_{\lambda v}$ is the y-intercept of the spherical plastic compression line (SPCL), e_κ is the y-intercept of the line defining a typical unload-reload line, e_c is the y-intercept of the interception point between the typical line and the critical state line, and e_v is the y-intercept of the interception point between the typical line and the spherical plastic compression line. The yield surface of the original Cam-clay model has been altered to be described as an ellipse (Roscoe & Burland, 1968) rather than the less symmetrical yield surface seen in Figure 2-17. When this change was originally described it was called the "Modified Cam-clay" model. However, the "modified" has been dropped throughout this document because it is presently more widely used than the "original" Cam-clay model.

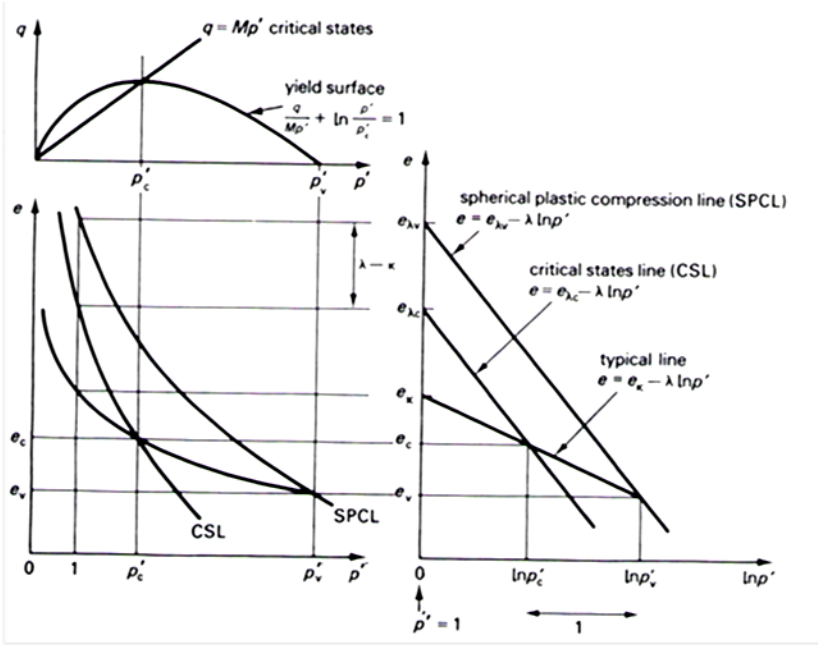

Figure 2-17: Cam-clay's prediction of (*q*, *p'*, *e*) space (Bolton, 1991).

Typical stress paths for drained and undrained conventional triaxial compression tests which demonstrate the behaviour of the Cam-clay model are shown in Figure 2-18. Note that in Figure 2-18, LOC is lightly overconsolidated, HOC is highly overconsolidated. In addition, p'_v is the previous effective stress preconsolidation pressure and p'_0 is the initial confining pressure.

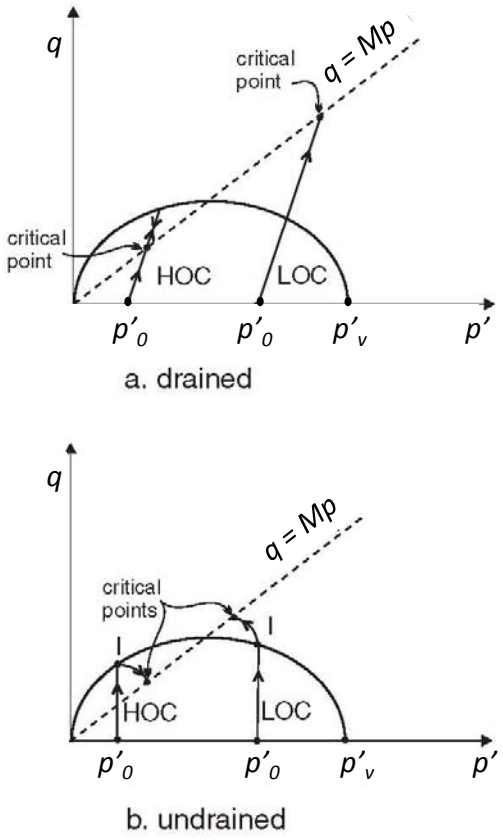

Figure 2-18: Effective stress paths for drained and undrained triaxial compression tests using the Cam-clay model (modified after Itasca, 2008).

Figure 2-19 shows a summary of all the test results obtained for residual soil and transition zone samples from O'Sullivan (2009). The Cam-clay constitutive model could represent the behaviour of this type of soil well as it can be seen that undrained samples follow the same shape as the stress paths shown in Figure 2-18. The stress paths for drained samples are controlled, and thus are not indicative of soil response. In the undrained condition, the stress path goes straight up at 90° from the horizontal, and after reaching the yield surface, curves towards critical state. In the drained condition, the stress path moves towards the yield surface (at a slope of 1 in *t* versus *s'* space) and if highly overconsolidated, it reaches the yield surface and then curves down towards the critical state line. If lightly overconsolidated, it goes up towards the critical state line after yield. Several of the drained tests in Figure 2-19

exhibit highly overconsolidated behaviour, as it can be seen that most of them reach a certain point (yield) and travel back down (towards critical state). O'Sullivan's plot is in *t-s'* space rather than *q-p'* space. These terms are defined in Section 2.6.1.

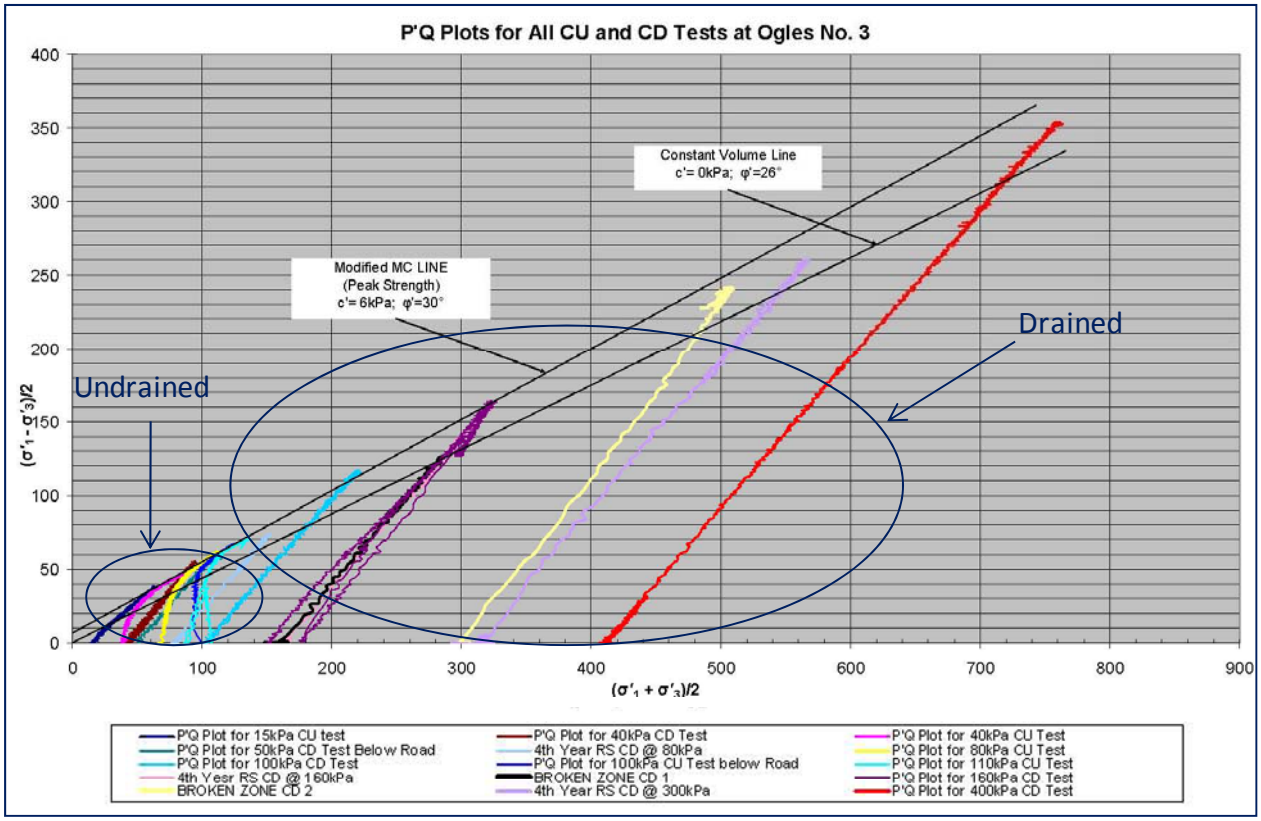

Figure 2-19: Summary of test results obtained from residual soil & transition zone soil specimens (O'Sullivan, 2009).

Muir-Wood (1990) also shows that data of peak strengths from carefully conducted tests on overconsolidated clays fall on a normalized *q* versus *p'* plot. This is the Hvorslev surface (Figure 2-20) which was discussed in Section 2.6.5 with respect to reconstituted clays. *M* is the slope of the critical state line and is equal to *q/p'*.

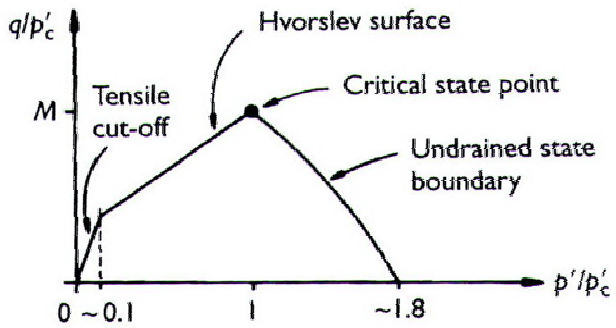

Figure 2-20: Tensile cut-off, Hvorslev line, critical state point and Cam-clay undrained state boundary in a normalized (q/p'_c, p'/p'_c) plot (Powrie, 2004).

This may be used to estimate peak strengths of overconsolidated samples that are dry of critical state. Powrie (2004) (expounded by Schofield (1980)) states that normally overconsolidated and lightly overconsolidated samples will display continuum yield as predicated by the Cam-clay type model, eventually reaching critical state. More heavily overconsolidated samples will probably rupture on planes of maximum stress ratio, according to a Hvorslev failure criterion. At very low effective stresses, failure would be expected to occur by tensile fracture (Powrie, 2004).

For heavily overconsolidated soils, the yield surface of the modified Cam-clay model, which is represented by an ellipse in the *q-p'* plane, could be replaced by a quadratic function to better represent soil behaviour on the dry side of critical state (Figure 2-21). In Figure 2-21, p_c is the mean total stress at critical state and q_{crit} is the deviatoric stress at critical state. In addition, p_v is the total stress preconsolidation pressure, F_2 and F_1 are yield surface functions, G_2 and G_1 are plastic potential functions, and p'_0 is the initial confining pressure. This modification was implemented into the Cam-clay model in the FLAC code by Benmebarek et al. (2001), but is not commercially available.

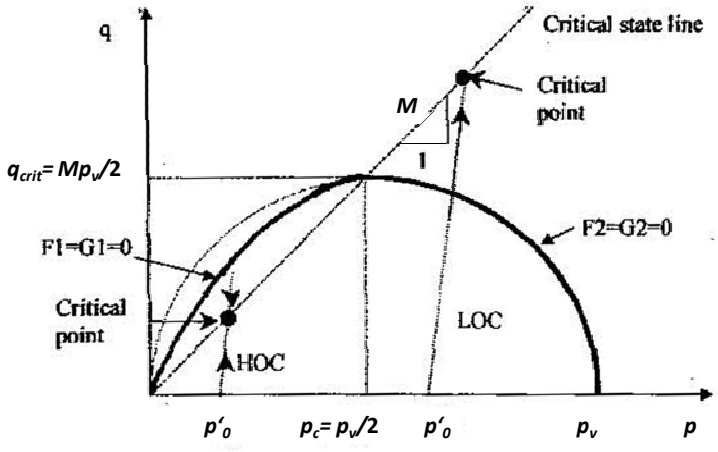

Figure 2-21: Proposed Cam-clay failure surface (modified after Benmebarek et al., 2001).

2.8.3 Modelling of DSM Columns in 2D

There are several common issues that still exist with modelling of DSM columns. In practice, 2D models have been utilized more extensively than 3D models, as they are less time consuming to develop. The limited studies that have been performed comparing 2D and 3D numerical models of DSM columns for either bearing capacity failure mitigation (Karstunen et al., 2005) or slope failure mitigation (Leung et al., 2006) show that 2D and 3D models do not always produce the same results in terms of the stress distribution, the overall ability of the columns to handle the lateral load, and in some cases, the FoS. For studying settlement, it is common for practitioners to create a 2D model by using a composite (axisymmetric) cell model (Karstunen et al., 2005). In this approach, one column, and the equivalent cylinder of soil arround it is modelled and assumed to be representative of the whole improved soil mass- a rather crude method. Figure 2-22 depicts a unit cell. Note that d is the DSM column diameter and d_e is an equivalent diameter.

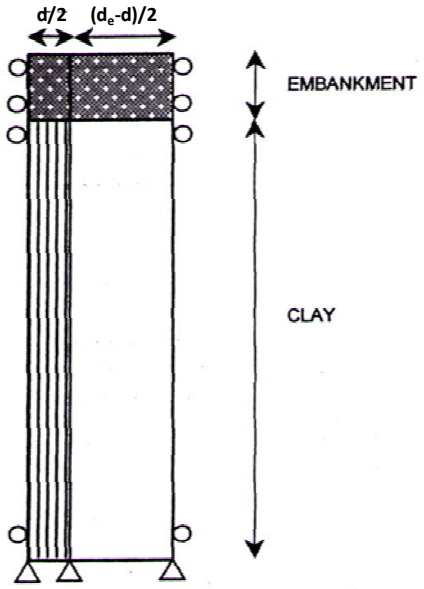

Figure 2-22: Unit cell (modified after Karstunen, 1999).

A commonly used method for modelling 2D plane strain conditions (e.g. slope stability) involves representing the rows of columns discretely, but modelling the columns together with the surrounding soil in the out-of-plane direction as a block of composite material. This is called the replacement ratio method (Leung et al., 2006). The replacement ratio method is discussed further in Chapter 6. Vogler & Karstunen (2009) use a similar method and call it the volume averaging technique. A recent study on DSM columns below an embankment found that the volume averaging technique in 2D analysis matched up well with conventional three dimensional analysis for problems involving high numbers of closely spaced columns (Vogler & Karstunen, 2009). Still, some issues remain with this technique, and discrepencies betwen 2D and 3D analysis were particularly high in problems with fewer columns. In 2D models using the replacement ratio method, the effect of stress distribution for different column spacings is not taken into account because the variation of column spacing is modelled by adjusting the composite column properties. 2D models show higher shear stresses compared to 3D ones becasuse the shear stresses in the 2D models are the equivalent shear stresses acting in the columns (calculated using the equivalent stiffness) (Leung et al., 2006).

Interaction of DSM columns with the surrounding soil mass is complex, and may significantly differ from the design assumptions, particularly as the relative stiffness of the columns to the soil increases or the column spacing increases (Karstunen et al., 2005). Several authors have pointed out that further research is required into how the relative stiffness of the columns and the soil influence the behaviour of the system (Karstunen et al., 2005; Leung et al., 2006; Porhaba, 2000).

2.8.4 Modelling of Group Effects and Soil Arching in Plan View

As discussed in Section 2.3.5, the performance of DSM columns under lateral loading is a function of their ability to work as a group to transfer load from the soil to the columns. This behaviour has been studied extensively for piles. In 2D in plan view, the primary difference between DSM columns and piles are the column spacing and diameter, and the changes to soil properties around the columns or piles (i.e. we can ignore stiffness differences in this 2D scenario). An analytical solution has been developed for piles whereby if the load is non-dimensionalized with respect to the soil strength and the diameter of the pile, it is found that the load factor on a cylinder varies between $6 + \pi$ (= 9.14) for a smooth pile and $4\sqrt{2} + 2\pi$ (= 11.94) for a rough pile (Randolph & Houlsby, 1984). The analysis of lateral loading on two piles in plan view was further developed by Chen & Martin (2002) and a similar analysis of a single pile was also carried out by Bransby (1996). The results show that the arching effect exists in both drained and undrained conditions. Closer column spacing leads to higher initial stiffness for load-displacement curves for drained conditions. The development of arching is limited by spacing. Closer column spacing results in an increase in soil arching while further column spacing results in a reduction in arching.

2.8.5 Modelling of DSM Columns in 3D

Due to the high computational requirements for modelling in 3D, few studies have been performed that examine the performance and behaviour of DSM columns in 3D under lateral loading. However, several studies have been done for piles in these conditions (Ahmadi & Ahmari, 2009; Chandrasekaran et al., 2010; Hsiung, 2003; Imancli et al., 2009; Peng et al., 2010; Shen & Teh, 2004; Yang & Liang, 2006). Many of these studies reference two particular analytical solutions of laterally loaded piles for validation (Davisson & Gill, 1963;

Reese & Hudson, 1956). However, TurboJET DSM columns are composed of about 35% grout and 65% soil, and thus behave as soil more than a structural element (compared to reinforced concrete piles or steel piles) in terms of both their strength and stiffness properties. In addition, they often fail in shear rather than in bending (which is a more common mode of failure for steel piles). Therefore, these analytical solutions applicable to piles are not directly applicable to DSM columns. However, the decoupled approach developed by Kourkoulis et al. (2012) where the geometry of a slope stabilized by piles or DSM columns is separated from the computation of the pile lateral capacity provides a method for simplifying the 3D analysis of laterally loaded piles or DSM columns. This method is discussed further in Chapter 8.

2.9 Summary of Methods Used in this Study

Areas identified for further research described at the beginning of this study have been investigated through field testing, laboratory testing, and numerical modelling. The following points summarize how each of the areas has been examined:

- The general soil properties of the soil have been investigated through soil classification tests, triaxial testing and oedometer testing which contributes to the body of knowledge about this soil type.

- To determine if variations exist between field sites within the Northland Allochthon Mangakahia Complex, soil properties (classification tests and strength properties) have been compared between different field sites.

- In situ field testing methods (sDMT and CPT) have been utilized to acquire soil parameters. These parameters add to the overall characterization of the soil.

- To determine if soil structure is contributing to soil strength, triaxial testing has been performed on reconstituted and intact specimens of Northland Allochthon soil. The method developed by Burland (1990) has been used.

- To assess their suitability for representing Northland Allochthon soil from the Mangakahia Complex, several constitutive models have been examined and compared to laboratory results.

- A case study of a road slip failure has been analysed through numerical modelling using Plaxis finite element software in order to propose a plausible failure mechanism that corresponded to observed field behaviour. In addition, the failure mode of the columns (as modelled) is examined.

- As a method for investigating if property changes around DSM columns occur, field testing (sDMT) has been performed before and after DSM column installation.

- Group interaction of DSM columns has been studied through a carefully validated numerical model (using Plaxis finite element software) of DSM columns that are laterally loaded, in plan view. By varying column spacing, the increased ability of the columns to handle lateral load (at a given displacement) can be quantified. Through this same model, the effects that soil property changes around the columns have on the ability of the columns to handle lateral load has also been investigated.

- In order to examine how appropriate the 2D replacement ratio method is for representing DSM columns in a laterally loaded scenario, a 3D model of lateral loaded DSM columns using Plaxis 3D Tunnel has been developed and compared to a similar 2D model using Plaxis 2D.

3.0 Field Testing and Soil Classification Tests

3.1 Introduction

This chapter details the results of soil classification tests done on Northland Allochthon residual soil from the Mangakahia Complex acquired from three different sites. This chapter also contains the results of field testing, which includes some tests performed in close proximity to DSM columns. The method of sample collection is described, and the results of soil classification tests (specific gravity and Atterberg limits) are also discussed. CPT and sDMT testing results are used to determine the undrained shear strength, sensitivity, *OCR*, and unit weight of the soil at one of the three field sites. The results of these two types of tests are compared to one another. The exposure of DSM columns installed to mitigate a road slip, and the results of Atterberg limits in the soil in close proximity to the columns are also discussed. sDMT testing performed before and after DSM column installation at a fourth field site (not located in Northland) are examined.

3.2 Site Descriptions

Soil samples and soil testing results for this study have been acquired from three different field sites in Northland Allochthon derived soil where road slips have occurred. These are Mountain Road, Ogles No. 3, and Kaeo. Figure 3-1 shows the approximate locations of each of the sites. Soil samples collected for evaluation of soil structure through triaxial testing have been acquired from the Mountain Road site. Classification tests were also performed on samples acquired at the Mountain Road site. Samples from the Kaeo site were acquired for classification tests only. Testing done at the Ogles No. 3 site was performed by O'Sullivan (2009) and included drained and undrained triaxial tests on natural samples as well as classification tests.

Figure 3-1: Field site locations.

Kaeo is in undifferentiated Mangakahia Complex containing structurally complex units of tectonically intercalated sandstones and mudstones. Ogles No. 3 is in the Hukerenui Mudstone of the Mangakahia Complex (well-bedded, multicoloured mudstone). Mountain Road is in undifferentiated melange which is comprised of a matrix of predominantly Mangakahia Complex mudstones, commonly with included blocks of Mangakahia Complex, Motatau Complex, and Te Kuiti Group lithologies (Edbrooke & Brook, 2009).

The bedrock at the Mountain Road site has been identified in a consulting report (MWH, June 2002) as being in the Opahi Group (a now obsolete synonym for the Mahurangi limestone of the Motatau Complex), with reference to the "Geological sheet map of New Zealand, Sheet 2A, Whangarei", Thompson (1961). This map, however, is outdated and new sources of information have changed several of the geological descriptions and boundaries. The map "Geology of the Whangarei Area" by Edbrooke & Brooke (2009) provides a more recent and revised interpretation. In addition, the boreholes at Mountain Road describe the underlying Northland Allochthon rock as a dark grey or dark brown homogenous, completely

weathered mudstone. This confirms (as shown on Edbrooke & Brooke's map, Figure 3-2) that the area is in a block of the Mangakahia Complex as Mangakahia mudstones are the dominant rock type in Northland Allochthon undifferentiated melange.

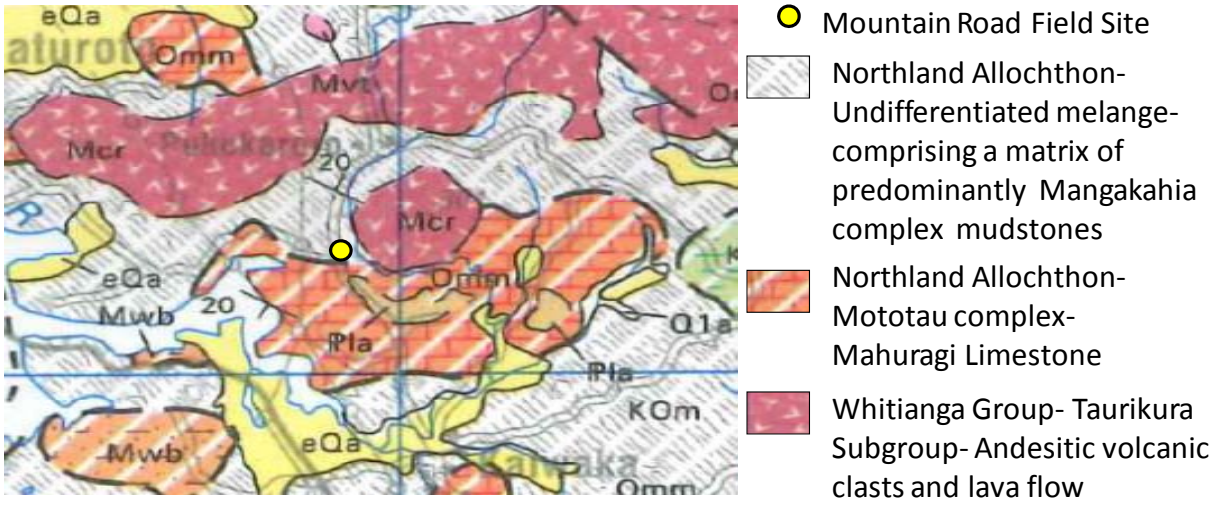

Figure 3-2: Location of Mountain Road Site on 1:250,000 map "Geology of the Whangarei Area."

At Mountain Road and Ogles No. 3, soil samples were collected from both the upper zone- (referred to as the "residual" zone) and the lower zone (referred to as the "transition" zone). The lower zone tends to retain the sheared fabric of the underlying rock, and may have gravel sized clasts of this parent rock. The upper zone tends to be lighter in colour with a lower permeability (Winkler, 2003). The residual soil tends to be 2 to 9 m thick. The transition zone is approximately 5 m thick, and the underlying rock is between 10 to 35 m thick. Figure 3-3 shows the upper (residual) and lower (transition) zone at Mountain Road.

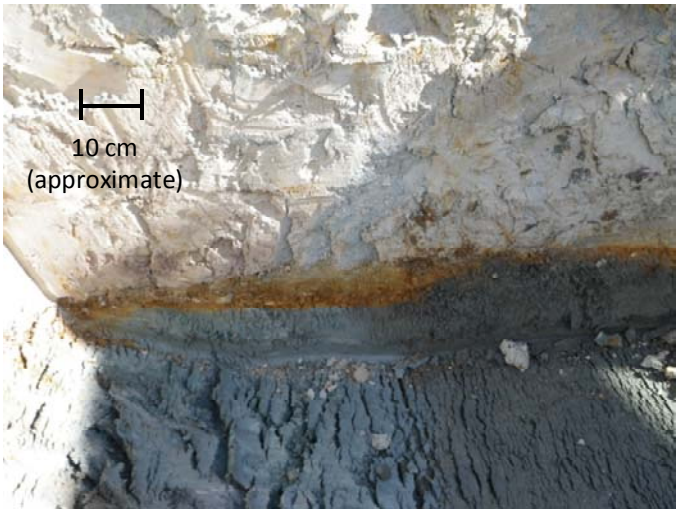

Figure 3-3: Upper (residual) and lower (transition) soil zones at Mountain Road.

Figure 3-4 shows three types of weathering profiles for residual materials. Many types of residual soils have a gradual weathering profile, but for some, such as the weathered basalt soils found on the North Island of New Zealand, the boundary between the residual soil and rock is abrupt with only a thin zone of transition material (Wesley, 1988). In stratified deposits such as interbedded sandstone and mudstone, the soil profile is more complex and is likely to reflect both the weathering sequence and the differences in the parent rock (Wesley, 1988).

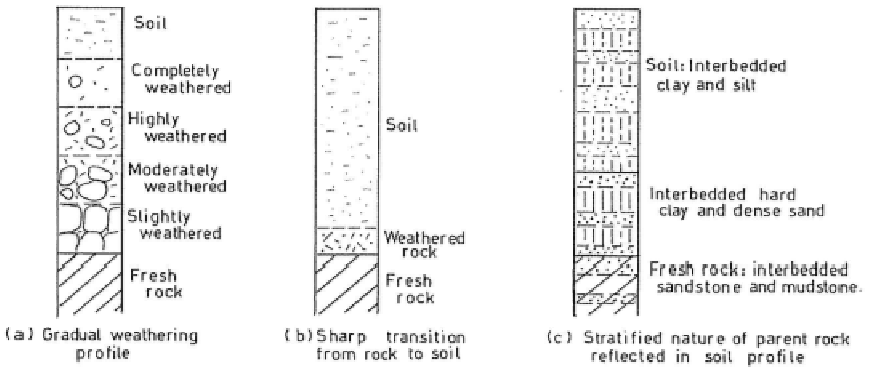

Figure 3-4: Variations in residual soil profiles (Wesley, 1988).

The soil profile at Mountain Road appears to fall into category b in Figure 3-4. Lentfer (2007) also noted a sharp transition from residual soil to the underlying transition zone, and the underlying rock.

Since the Mountain Road site is in close proximity to Mahurangi limestone according to the geological map (Figure 3-2), another method of determining if the parent rock could have been limestone was utilized. Mahurangi limestone is an argillaceous limestone (Carter, 1969). Argillaceous limestones are limestones consisting predominantly of calcium carbonate, (but include 10-40% clay minerals), and the presence of carbonates in soil derived from this rock should be easily assessed with a dilute hydrochloric acid (HCl) solution. To confirm or refute the presence of carbonates ($CaCO_3$) in soil, a drop of HCl applied to a soil sample is widely used as a quick test. No single standard HCl concentration is specified for detecting carbonates, but 1M and 3M solutions are the most commonly used (Kaisaki, 1994). Dolomitic carbonates or specimens with a low content of carbonates may be more easily recognized with acid concentrations greater than 1M. Therefore, a 3M solution of HCl was utilized as extra precaution (although dolomite and dolomitic limestone is not found on the North Island of New Zealand (Williams, 2009)). This test was performed on soil samples from both the upper and lower zones from Mountain Road, and on soil samples from Kaeo. All of the soil samples were found to be non-effervescent, confirming that the soil is not carbonaceous and is likely to be derived from Mangakahia Complex mudstone.

Another field site from which sDMT data is examined in this study is located outside of the boundaries of Northland Allochthon soils, in the city of Hamilton. It is located at Carrs Road, off Wairere Drive. The top few metres are in Hamilton Ash, with the remainder (>30 m depth) in the Puketoka Formation. The top 6 to 7 m is described as firm to stiff silty clay, underlain by approximately 4 m of soft silt (Anderson, 2010). This site is included in this study because sDMT testing was performed before and after DSM column installation and the results provide general insight into the changes that may occur to soil stiffness and strength due to column installation.

3.2.1 Mountain Road Field Investigation

In 2002, a field investigation was performed at the Mountain Road site on State Highway 1 (SH1) to investigate subsidence approximately 35 m in length. The initial report stated that the likely failure mechanism was long term creep movement due to saturation and weakening of the soils under and surrounding the road (due, in part to inadequate drainage) (Yang, 2002). The field investigation included two boreholes and 5 CPT tests. Three rows of DSM columns were installed in 2003. In 2011, due to the widening of the highway, an additional 4 rows of columns and a mechanically stabilized earth (MSE) wall were installed. Prior to design and installation, sDMT testing was performed on site, Shelby tube samples were collected and two test pits were dug to examine the existing DSM columns. A map of the locations of the sDMT tests, Shelby tube samples, and test pits is shown in Figure 3-5 based on survey coordinates. Note that sDMT 5, 6 and 7 were performed on the same day that the Shelby tube samples were collected and test pits were dug, while sDMT 1, 3 and 4 were performed two weeks earlier. Based on drawings from geotechnical reports, CPT tests 01, 02 and 04 are in the vicinity of the area shown in Figure 3-5, however their exact locations cannot be determined because survey coordinates are not available.

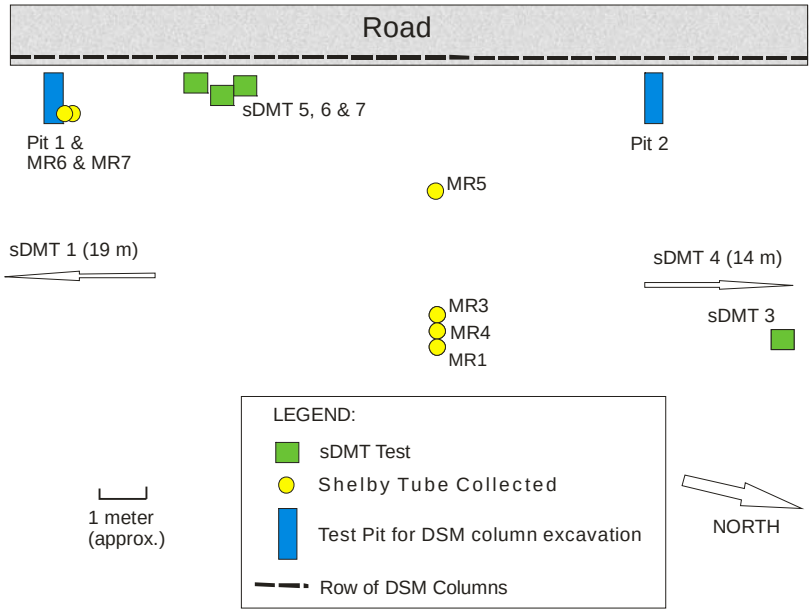

Figure 3-5: Approximate relative locations of testing and sample collection at the Mountain Road field investigation.

3.2.2 Kaeo Field Investigation

In mid 2011, a field investigation was performed at the Kaeo site located on State Highway 10 to investigate a small slip that occurred on the side of the road. Three boreholes were drilled, and soil sample were acquired in Shelby tubes. Three rows of DSM columns were installed. There was no official report for this project, and details regarding the field investigation were acquired from Hiway Stabilizers Ltd. (O'Sullivan, pers. comm., 2011a).

3.2.3 Ogles No. 3 Field Investigation

The Ogles No. 3 site is located on State Highway 1. The road in question was constructed around 30 years ago. Despite remedial efforts involving the installation of drains in the 1990's, the carriageway embankment suffered major failure. Following this, fill was imported to buttress the embankment and provide toe support. The toe buttress increased the stability such that wholesale movement no longer occurred, but the embankment was still subject to ongoing deformation with time. In 2006, a shallow geotechnical investigation was completed,

and in 2007, Hiway Stabilizers Ltd. was commissioned to complete an investigation and remedial works. As part of these investigations several boreholes were drilled, standpipe piezometers were installed, and soil samples were acquired for laboratory analysis.

3.3 Sampling Methods and Preparation

Sample disturbance can occur during any of the following six stages: boring, tube sampling, storage, extrusion, preparation, and testing (Hight, 2000). The following characteristics of Northland Allochthon residual soil provide the biggest obstacles to selecting a sampling method (O'Sullivan, 2009):

1. High sensitivity to changes in moisture (samples potentially liable to shrink/swell)
2. Large number of lithic fragments and delicate structure which are susceptible to breakage along pre-existing planes

While it is widely reported in literature that samples cut from carefully extracted blocks provide the best laboratory results, the above characteristics of Northland Allochthon residual soil make it difficult to trim them without excessive pitting. Therefore, a different approach was taken which is similar to that of O'Sullivan (2009).

Samples were collected in 72 mm diameter Shelby tubes so that the soil specimens could be extruded from the tubes and placed directly into a triaxial cell with virtually no additional trimming. The Shelby tubes were hydraulically jacked into the ground using a special rig and a jacking frame at a slow, controlled rate (typically around 20 minutes/tube). The frame and ram were fabricated for a University of Auckland study (O'Sullivan, 2009). The jacking device is shown below in Figure 3-6.

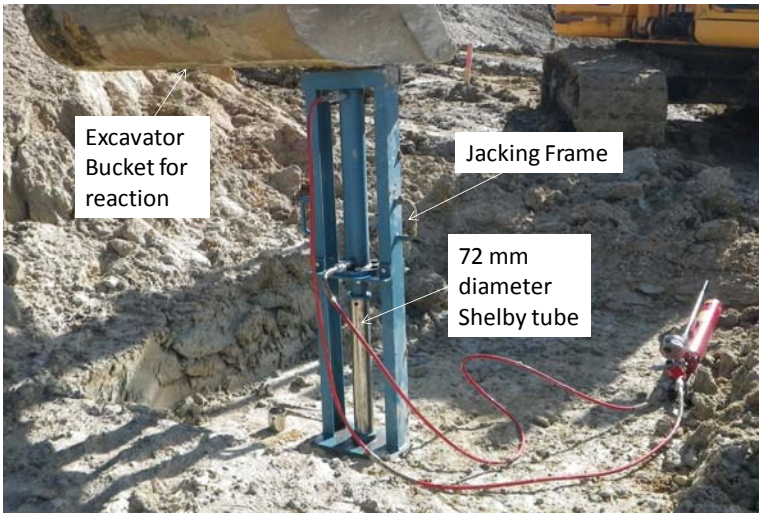

Figure 3-6: Shelby tube jacking frame and ram.

The adopted sampling procedure is summarized as follows:

1) Excavate a shallow pit to the desired depth using an excavator bucket- ensuring the base of the excavation is level and smooth

2) Jack the 450 mm long, 72 mm diameter stainless steel tubes into the ground very slowly (over a period of around 20 minutes)

3) Excavate the tubes carefully by hand with a spade

4) Wax seal both ends of the tubes with a minimum of 20 mm of wax

5) Double wrap the tubes in plastic bags and seal tightly

6) Transport back to the laboratory for storage

Mountain Road

Six Shelby tube samples were collected for testing at the University of Canterbury. Testing included drained and undrained triaxial testing of undisturbed and reconstituted samples, Atterberg limits, specific gravity, and water content. Table 3-1 summarizes the Shelby tubes collected and approximate depth from ground surface.

Table 3-1: Summary of samples acquired at Mountain Road.

Shelby Tube #	Soil Type	Depth below ground level (m) at start of sampling
MR1	Residual Allochthon/Transition	3.4
MR3	Residual Allochthon/Transition	3.2
MR4	Residual Allochthon/Transition	3.2
MR5	Residual Allochthon	1.5

Kaeo

Six Shelby tube samples were collected at this site in the residual soil. The sample depths were between 1.5 m - 6.4 m at two locations. Testing on these samples included Atterberg limits, specific gravity, and natural water content.

Ogles No. 3

Shelby tube samples were collected by O'Sullivan (2009) in both the upper zone and the underlying transition zone. Various tests were performed by him including Atterberg limits, ring shear and consolidated drained and undrained triaxial tests. The results are reported and analysed by O'Sullivan (2009) and are used in this study as comparative reference for the residual clay soil properties.

3.4 Soil Classification Tests

3.4.1 Soil Description

Below is a description of the soil at each of the three field sites based on visual inspection (Kaeo and Mountain Road) and borehole logs (Ogles No. 3).

Kaeo- Residual Soil: Light brown, mottled with iron staining and lithic fragments, moderately weathered, firm clay with some silt and traces of gravel and sand.

Mountain Road- Residual Soil: Light to medium brown, homogenous, completely weathered, firm to stiff silty clay with traces of coarse sand and minor iron staining.

Mountain Road- Transition Zone: Dark brown to grey, moderately to completely weathered, stiff clayey silt.

Ogles No. 3- Residual soil: Light coloured, completely weathered, clayey slightly sandy silt, with some sand or gravel sized clasts.

Ogles No. 3- Transition zone: Moderately to completely weathered clayey silt. Pervasively sheared and slickensided.

Photos of the soil from the site investigations at the Kaeo site and Ogles No. 3 site such as that shown in Figure 3-3 were not available. Figure 3-7 shows photos of samples extruded from Shelby tubes from Kaeo and Mountain Road prior to triaxial testing. Note that the Kaeo specimen was trimmed, and smearing from extrusion from the Shelby tube is evident in the Mountain Road specimens. However, the photos show the homogeneity of the MR soil compared to the Kaeo soil, and differences in colour between the two sites.

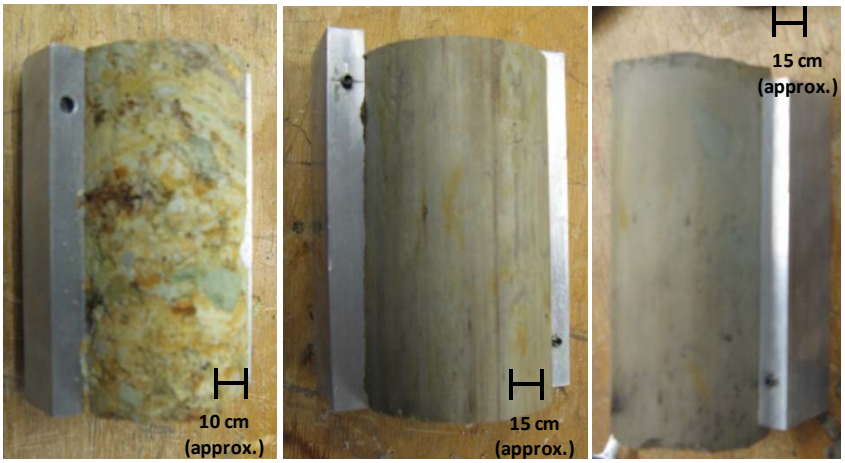

(a) **(b)** **(c)**

Figure 3-7: Photos of samples- (a) Kaeo (residual soil), (b) Mountain Road (residual soil) and (c) Mountain Road (transition zone).

The material index (I_D) is acquired from the sDMT as follows:

$$I_D = \frac{p_1 - p_0}{p_0 - u_0} \qquad (3.1)$$

where p_0 is the initial pressure reading of the dilatometer membrane, p_1 is the second pressure reading (after inflation), and u_0 is the equilibrium pore pressure.

The sDMT can be used to estimate the soil type based on the material index I_D, shown in Table 3-2.

Table 3-2: Soil classification based on I_D (Marchetti, 1980).

Soil Type	Clay		Silt			Sand	
	Clay	Silty Clay	Clayey Silt	Silt	Sandy Silt	Silty Sand	Sand
I_D Value	0.1	0.35	0.6	0.9	1.2	1.8	3.3

The sDMT results at Mountain Road predominantly indicate a soil type of silty clay or clayey silt, which is consistent with visual classification as described above. The results of the soil descriptions determined from I_D for sDMT 3, 4, 5, 6 and 7 are presented in Appendix A.

3.4.2 Specific Gravity

Specific gravity (G_s) was determined in accordance with ASTM D854-38. For most soils it lies within the range of 2.7 ± 0.1 (Zhou, 2006), but for clays and silts, specific gravity will depend on the amount and type of clay minerals present (Fratta et al., 2007). The results are shown Table 3-3.

Table 3-3: Specific gravity for selected samples.

Sample Name	Depth from Original Ground Level (m)	Specific Gravity (G_s)	Unit Weight (kN/m^3)	
			Lab Testing Results	sDMT Results
Kaeo-S1	1.5	2.61		
MR5a	1.5	2.61	18.8	16.9
MR4a	3.2	2.62	19.1	15.9
MR3b	3.4	2.60	19.3	17

3.4.3 X-ray Diffraction

X-ray diffraction is the most widely used method for identification of fine grained soil minerals and the study of their crystalline structure (Mitchell & Soga, 2005). X-ray diffraction results give an indication of the clay mineralogy present in the soil. Mineralogy is the primary factor controlling the size, shape and properties of soil particles- which determine the possible ranges of physical and chemical properties of a given soil (Mitchell & Soga, 2005). Thus, knowledge of clay mineralogy can give valuable insight into soil behaviour.

X-ray diffraction was not completed as part of this study. However, Lentfer (2007) included x-ray diffraction on the parent rock for the three Northland Allochthon lithofacies within in the Mangakahia Complex. The field sites for his study were on the southern edge of the Northland Allochthon isopaches. Results from Lentfer (2007) indicated the following mineralogy for some of the Mangakahia lithofacies:

- Hukerenui Mudstone: 89% smectite, 8% illite, <3% kaolinite and <1% chlorite
- Punakitere Sandstone: 47% smectite, 13% illite, 19% kaolinite, 21% chlorite
- Whangai Formation: 90% smectite, 5% illite, 5% kaolinite, traces of chlorite

Although variation in mineralogy exists between samples of the same complex or formation (Lentfer, 2007), knowledge of clay mineralogy can assist in confirming the parent material.

These previously performed x-ray diffraction results indicate that smectite is the most abundant clay mineral in the Hukerenui Mudstone of the Mangakahia Complex. Smectite is by far the most "active" clay mineral group (Mitchell & Soga, 2005). Activity (*A*) is defined by:

$$Activity = \frac{PI}{\%<2\ \mu m} \qquad (3.2)$$

where *PI* is the plasticity index. The greater the activity, the greater the influence the clay fraction has on the soil properties. More active clays will be at higher water contents and lower densities than inactive clays, and will exhibit greater time dependant responses (i.e. creep) (Mitchell & Soga, 2005). This follows well with the behaviour seen at the field sites (road slips) in the soils of the Mangakahia Complex.

3.4.4 Atterberg Limits

The Atterberg limits for the samples tested are shown in Table 3-4.

Table 3-4: Atterberg limits.

Site	Kaeo	Ogles No. 3*		Mountain Road (Residual)				Mountain Road (Transition)	
Sample	BH2- 1.5-2m	BH1/BH2- 1- 4m		MR3c	MR4a	MR5a	MR5a-Dried	MR3a-1	MR3a-2
Plastic Limit	27.5%	28.9%	36.4%	25.70%	25.3%	28.7%	27.9%	23.7%	23.0%
Liquid Limit	59.0%	69.0%	72.9%	48.0%	49.1%	50.1%	42.9%	33.1%	33.0%
Plasticity Index	31.5	40.1	38.6	22.3	23.8	21.4	15.0	9.4	10.0
Natural Water Content	39.1%	34.3%	48.4%	33.9%	33.8%	36.0%	36.0%	30.4%	30.4%

*From O'Sullivan (2009)

A plot of the results of plasticity index (*PI*) versus liquid limit (*LL*) from all sites examined with relation to the A-line is shown in Figure 3-8. Note that the Ogle's No. 3 results are from O'Sullivan (2009). Two additional results from field sites also within the Mangakahia Complex are also shown on the figure:

1) Silverdale site (a town about 30 km north of Auckland)- Hukerenui Mudstone- Lentfer (2007)
2) A site also located in Silverdale, along State Highway 1- Whangai Formation- Melrose & Willis (2010) as cited in Harris (2013)

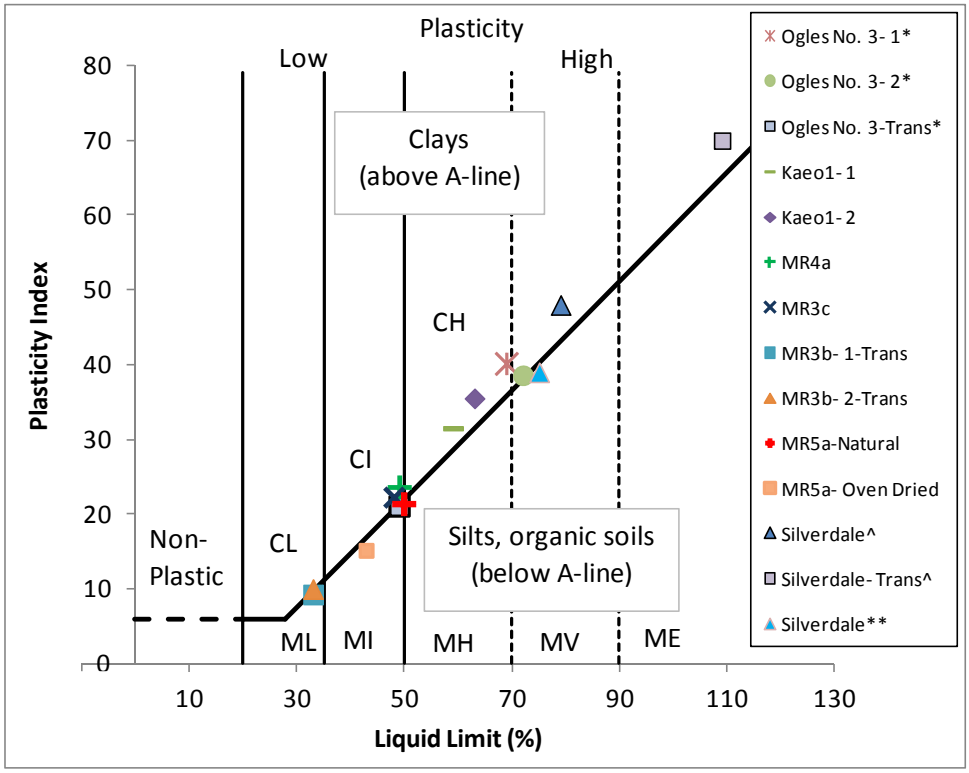

C = Clay	L = Low Plasticity	LL< 35%
M = Silt	I = Intermediate Placticity	35% < LL < 50%
O = Organic	H = High Plasticity	50% < LL < 90%
Pt = Peat	V = Very High Plasticity	70% < LL < 90%
	E = Extremely High Plasticity	LL > 90%

*O'Sullivan (2009)
^Melrose & Willis (2010) in Harris (2013)
**Lentfer (2007)

Figure 3-8: Results of Atterberg Limits as plotted on a conventional plasticity chart.

Oven drying has been found to reduce the plasticity of clays (Burland et al., 1996). Rao et al. (1989) tested a variety of clay specimens and found that oven drying can significantly reduce the liquid limit, and can also (but less significantly) reduce the plastic limit. Atterberg limits tests done on sample MR5a before and after oven drying show that oven drying reduced the liquid limit from 50% to 43% and the plastic limit from 29% to 28%. Atterberg limits testing on all other samples was performed prior to any drying.

The residual soil samples range from medium to high plasticity from all of the sites. The transition zone samples from Mountain Road have a low plasticity. The results from the Ogles No. 3 site also show that the transition zone has a lower plasticity than the residual soil at that site. However, results from Harris (2013) which are also from the Mangakahia Complex, but are from the Whangai Formation, are more plastic than the other sites, and show a higher plasticity in the transition zone than in the residual soil. All the samples plot on or slightly above or below the A-line, indicating a clayey silt or silty clay soil type. Most inorganic soils with sheet type clay minerals follow the A-line (Nagaraj et al., 1994). As mentioned, Hukerenui mudstone has been found to contain a significant amount of smectite (89%), with 8% illite, kaolinite < 3% and chlorite <1% (Lentfer, 2007). The Allochthon soil derived from this mudstone group is likely to have high smectite content as well. High smectite content tends to result in a very high liquid limit, and high plasticity (Berti, 2003). Samples sitting just above the A-line are likely to be high in illite, and samples sitting higher up along the A-line (Ogles No. 3 and the results from Harris (2013)) are likely to have a larger percentage of smectite compared to those further down (Berti, 2003).

The results of index tests on related soils tend to plot in a straight line which is often approximately parallel to the A-line. Figure 3-9 shows the plots of several soil types in relation to the A-line (Muir-Wood, 1990). This soils in this figure are as follows: 1- gumbo clays (Mississippi, Arkansas, Texas; 2- glacial clays (Boston, Detroit, Chicago, Canada); 3- clay (Venezuela); 4- organic silt and clay (Flushing Meadows, Long Island); 5- organic clay (New London, Connecticut); 6- kaolin (Mic, Washington); 7- organic silt and clay (Panama); 8- micaceous sandy silt (Cartersville, Georgia); 9- kaolin-type clays (Vera, Washington, and South Carolina) (after Casagrande, 1947). From this relationship, it is clear that the soils from

Mountain Road, Ogles No. 3, Kaeo, and the other two field sites (Harris (2013) and Lentfer (2007)) are related in this sense.

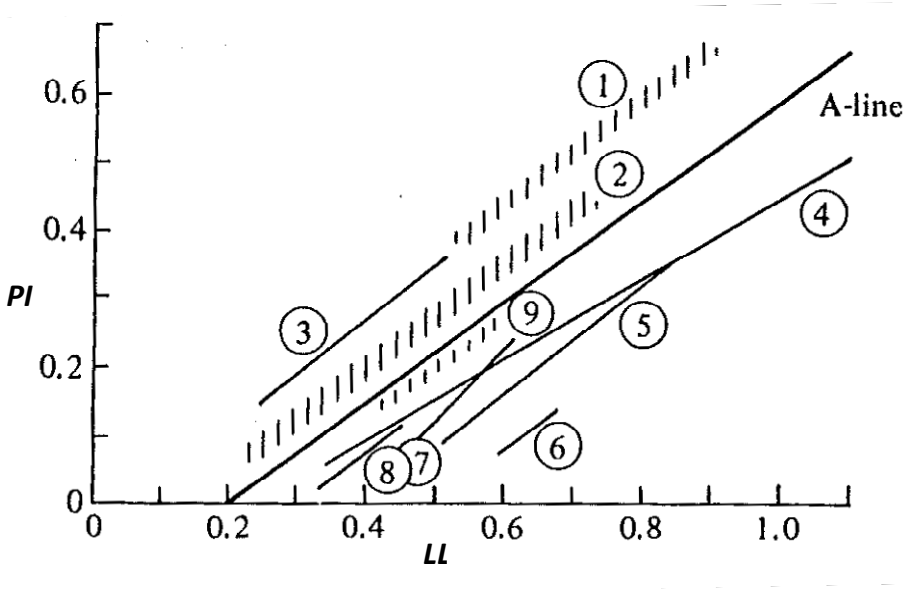

Figure 3-9: Relation between liquid limit and plasticity index for several clays (modified after Muir-Wood, 1990).

The lines drawn parallel to the A-line in Figure 3-10 show a proposed division of residual soils into clay, silty clay and silt. The results of Northland Allochthon residual clay soil fall into this classification as a silty clay- parallel and close to the A-line.

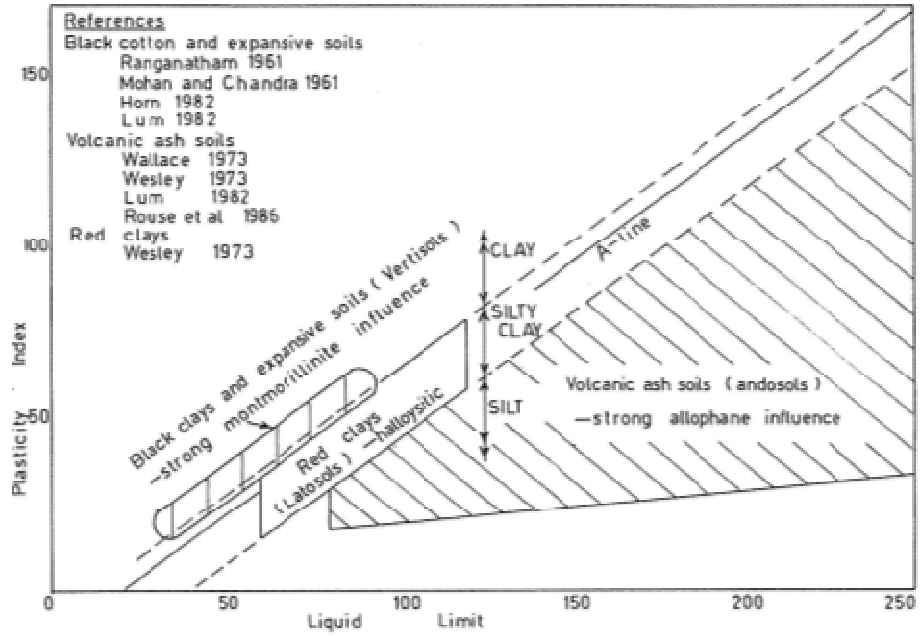

Figure 3-10: Possible division of plasticity chart for use with residual soils (Wesley, 1988).

Figure 3-11 shows the leaching process for a Norwegian clay (Muir-Wood, 1990). The effect of leaching moves the clay down the line in the plasticity chart by reducing the sodium chloride content and other minerals in the soil.

Examination of Figure 3-11 suggests that the Northland Allochthon residual and transition zone soils of the Mangakahia Complex at different sites (as plotted in Figure 3-8) are indeed related. Note that *PI* is given as I_P and *LL* is given as w_L in Figure 3-11. It is possible that varying degrees of leaching could account for some of the movement along the A-line on the plasticity chart.

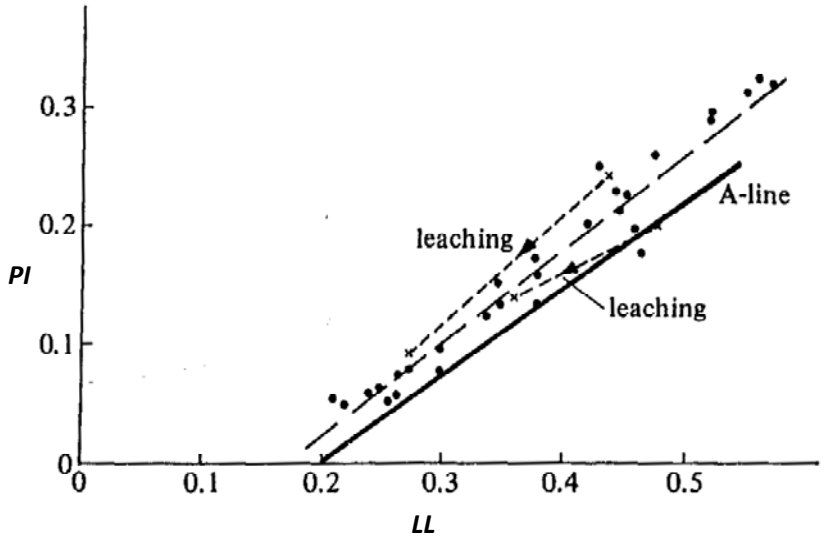

Figure 3-11: Influence of leaching on the relationship between liquid limit and plasticity index for Norwegian marine clays (data from Bjerrum, 1954, 1967) (modified after Muir-Wood, 1990).

Finally, Schofield and Wroth (1968) suggested that the critical state lines for all soils pass through a single point in the ln(p'):v plane, which they call the Ω-point. Muir-Wood (1990) revised this to propose that all related soils (perhaps of similar activity) pass through an Ω-point (Figure 3-12). In terms of critical states, this implies that moving down the A-line leads to a reduction in compressibility and so changes the critical state line from A to B to C in Figure 3-12. In Figure 3-12, p' denotes mean effective stress, p'_P is the mean effective stress at the critical state for a water content equal to the plastic limit and p'_L is the mean effective stress at the critical state for a water content equal to the liquid limit. The water content is denoted by w and the specific volume by v.

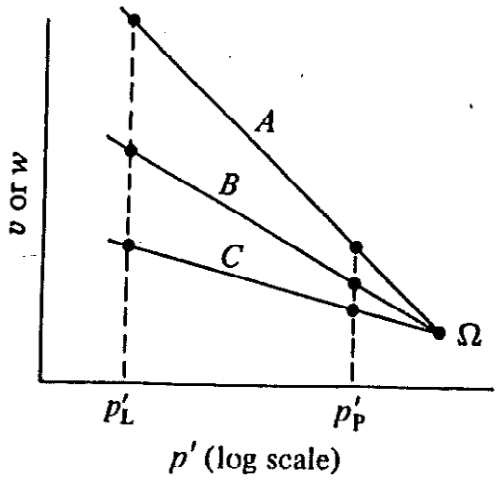

Figure 3-12: Critical state lines for related soils A, B and C passing through a single Ω-point in compression space (Muir-Wood, 1990).

3.4.5 Organic Content

The organic content test by loss of ignition was performed on sample MR5b (residual soil) in accordance with Germaine and Germaine (2009). It was found to be 5.5%. At a value higher than 2%, the soil is no longer considered completely inorganic (Germaine & Germaine, 2009). It is therefore likely that the organic content plays a role in the behaviour of the soil. Albert et al. (2003) found that removing the organic content of Bothkennar clay (measured at 3-8%) resulted in a reduction of the *PI* from approximately 40 to approximately 20.

3.5 CPT and sDMT Testing at Mountain Road

3.5.1 Undrained Shear Strength

The five CPT tests carried out at the Mountain Road site were performed along the estimated centre line of the slip, to depths of 8 to 12 m (refusal). The soil encountered in the boreholes is described in Section 3.4.1, with the underlying Allochthon rock being described as a dark grey, homogenous, highly weathered mudstone. The undrained shear strength can be estimated from CPT results though the following empirical equation:

$$c_u = \frac{q_c - \sigma_{v0}}{N_k} \quad (3.3)$$

where c_u is the undrained shear strength (kPa), q_c is the cone penetration resistance (kPa), σ_{vo} is the total in situ vertical stress, and N_k is an empirical cone factor. N_k is a function of a soil's plasticity index or stiffness. Kjekstad et al. (1978) found that for non-fissured overconsolidated clays, using c_u from triaxial compression tests as the reference strength, the average value of N_k was 17. The findings by Lunne et al. (1976) from five sites in Scandinavia show that the N_k values are in the range of 15 to 19 for marine clay and 11 to 13 for soft clay. The stiffness and overconsolidated behaviour of the soil at Mountain Road was compared to that of the clays examined by Lunne et al. (1976) and Kjekstad et al. (1978), and an N_k value of between 11 and 17 was estimated based on their results.

Seven sDMT tests were performed at Mountain Road. As discussed in Section 2.7.2, several soil parameters can be derived from sDMT results. Undrained shear strength (c_u) is estimated from sDMT results using the equation below.

$$c_u = 0.22\sigma'_{v0}(0.5K_D)^{1.25} \quad (3.4)$$

where K_D is the horizontal stress index, measured directly from the dilatometer, and σ'_{v0} is the in situ effective vertical stress (Marchetti et al., 2001). This formula is only valid for a material index (I_D) of less than 1.2, which is the case for the test results at Mountain Road.

The results of c_u from the approximate depths of sample collection at Mountain Road (1.5 m to 4 m) are shown in Table 3-5 for the CPT and sDMT results. The CPT results are averaged based on minimum and maximum q_c values from N_k values of 11 and 17. Aside from the 4 m deep location, the results show reasonable agreement. Examining the whole soil profile, the CPT results showed a marked increase in c_u with depth, which is to be expected as c_u has been found to be directly related to vertical effective stress (Muir-Wood, 1990), while sDMT results did not appear to show any overall trend.

Table 3-5: Undrained shear strength from 1.5 to 4 m below ground level from sDMT and CPT testing at Mountain Road.

Depth (m)	Undrained Sheared Strength (c_u) kPa									
	sDMT3	sDMT4	sDMT5	sDMT6	sDMT7	CPT 01	CPT 02	CPT 04	Average (CPT)	Average (sDMT)
1.50	58	54	61	84	22	72	27	35	52	56
2.00	64	74	40	31	35	79	15	34	46	49
2.50		66	32	35		85	49	40	51	44
3.00	69	52	25	26	80	125	25	69	59	50
3.50	63	99	24	24	31	124	65	76	63	48
4.00	57	69	48	55	52	142	112	120	82	56

Holtringter (2010) examined the CPT and sDMT correlations for several soil parameters at 10 field sites in northern New Zealand, some of which were located in Northland Allochthon derived soil, and found that c_u agreed well between the two tests at most of the sites examined. The results shown in Table 3-5 agree well from 1.5 to 3 m depth, but begin to deviate more substantially below this.

3.5.2 Soil Sensitivity

The ratio of undisturbed to remoulded strength is defined as soil sensitivity, S_{tr} (Muir-Wood, 1990):

$$S_{tr} = \frac{c_u}{c_{ur}} \qquad (3.5)$$

where c_{ur} is the remoulded undrained shear strength. Note that S_{tr} which is the ratio of c_u to c_{ur} (as defined here by Muir-Wood (1990)), is slightly different than the strength sensitivity (S_t) as defined by Cotecchia and Chandler (2000) (discussed in Section 2.6.5), which is the ratio of c_u to the reconstituted c_u at the gross yield point. The difference between reconstituted and remoulded clay lies in the mixing technique and water content at mixing. As mentioned in Section 2.6.5, reconstituted soil is mixed at a water content of 1.1-1.5 times the liquid limit. Remoulded samples, however, are homogenized by hand mixing at a water content of around the liquid limit. The mixing affects the mechanical properties of the soil (Messerklinger, 2006). Soil sensitivity is generally expected to be slightly higher when the reconstituted c_u is used to determine it, because reconstitution is a more thorough mixing technique that destroys more of the soil structure than remoulding.

The remoulded shear strength of a soil can be estimated from the liquidity index (*LI*) (Muir-Wood, 1990):

$$c_{ur} = 2\ x\ 100^{(1-LI)} \qquad (3.6)$$

This relationship, however, has not been established for residual soils, and is therefore an estimate.

LI can be found from:

$$LI = \frac{w-PL}{LL-PL} \qquad (3.7)$$

where *w* is the natural moisture content as measured from the acquired soil samples, *PL* is the plastic limit, and *LL* is the liquid limit.

From the above equations, and the estimated in situ undrained shear strength from CPT/sDMT testing, the sensitivity was estimated at three different depths at Mountain Road. The results are shown in Table 3-6. Table 3-7 shows the classification of the sensitivity of clays (Skempton & Northey, 1952).

Table 3-6: Estimate of soil sensitivity (S_{tr}) at 1.5 m, 3.2 m and 3.4 m below ground level.

Approximate Depth (m)	Remoulded c_u (kPa)	Liquidity Index	Estimated In situ c_u (kPa)	Estimated S_{tr}
1.5	42	0.34	54	1.28
3.2	38	0.36	55	1.43
3.4	8	0.71	56	7.33

Table 3-7: Classification of the sensitivity of clays (Skempton & Northey, 1952).

S_{tr}	Description of Sensitivity
0 to 1	insensitive clays
1 to 2	low sensitivity clays
2 to 4	medium sensitivity clays
4 to 8	sensitive clays
>8	extra-sensitive clays
>19	quick clays

The sensitivity of the soil is slightly above 1 for the samples at 1.5 m and 3.2 m. This indicates a low sensitivity, and that the c_u of the in situ soil is slightly higher than the c_{ur}. At 3.4 m, the clay is sensitive. It should be emphasized that since c_{ur} based on *LI* is only an estimate for residual soils, the S_{tr} values are also estimates. Related soils show a clear trend of increasing sensitivity with increasing liquidity index, and that leaching results in increased sensitivity (Muir-Wood, 1990). The values in Table 3-6 reflect this trend.

3.5.3 Volume Change Potential

The implication of high shrink-swell potential, in general, on slope instability and the specific shrink-swell potential of Northland Allochthon clay soils are briefly discussed in Section 2.5. The most widely used parameter for determining the shrinkage and swelling potential of a soil is the *PI*. BRE (1993) developed a modified plasticity index (*PI'*) to assess the potential for volume change due to shrinking and swelling of a soil. *PI'* was developed in order to take into account the sand and gravel content of the soil which may exist in situ. These larger sized particles, which are removed during the determination of the *PI*, will result in a reduction in the volume change potential of the soil compared to considering only the fraction less than 425 μm. It is therefore a closer approximation to field conditions to account for these larger particles in some way. In order to obtain the *PI'*, the *PI* is modified based on the percentage of particles less than 425 μm. *PI'* is equal to (BRE, 1993):

$$PI' = \frac{PI \times (\%<425\ \mu m)}{100\%} \qquad (3.8)$$

Estimated volume change potential with *PI'* is shown in Table 3-8. Hazelton and Murphy (2007) discuss a similar relationship between *PI* and volume change potential to that shown in Table 3-8.

Table 3-8: Clay volume change potential (BRE, 1993).

***PI'* (%)**	**Volume Change Potential**
>60	Very High
40-60	High
20-40	Medium
<20	Low

Grain size distribution curves are only available for the soil from Silverdale (Melrose & Willis, 2010 as cited in Harris, 2013). The grain size curves in that study show approximately 98% passing at 0.425 μm. This is a high percentage. It has been assumed that the soil from the other Northland Allochthon field sites has a similar percent passing 0.425 μm which is conservative (i.e. tending towards a higher shrink-swell potential). The results are shown in Table 3-9. The results from the transition zone at Silverdale (Harris, 2013) show two different values based on two different grain size curves for the transition zone (one with approximately 98% passing 0.425 μm and the other with approximately 90% passing 0.425 μm).

Table 3-9: Volume change potential based on *PI'* at Northland Allochthon sites.

Site	**Soil Type**	***PI'* (%)**	**Volume Change Potential**
Mountain Road	Residual	21-23	Medium
Kaeo	Residual	31	Medium
Ogles No. 3*	Residual	38-39	Medium
Silverdale^	Residual	48	High
Mountain Road	Transition	9-10	Low
Ogles No. 3*	Transition	21	Medium
Silverdale^	Transition	63-69	Very High

*O'Sullivan (2009)
^Harris (2013)

The volume change potential shown in Table 3-9 shows large variation between field sites. The results from the residual soil agree more closely and are all within, or close to, the

medium range. The transition zone soils vary between low to very high, which could be a result of varying degrees of weathering at different sites.

3.5.4 Overconsolidation Ratio and Coefficient of Lateral Earth Pressure at Rest

The overconsolidation ratio (*OCR*) can be estimated from sDMT results through the following equation (Marchetti et al., 2001):

$$OCR = (0.5\ K_D)^{1.56} \qquad (3.9)$$

where K_D is the horizontal stress index measured by the sDMT. This equation was developed based on results for uncemented clays.

K_0, the coefficient of lateral earth pressure at rest, can also be estimated from K_D:

$$K_0 = (\frac{K_D}{1.5})^{0.47} - 0.6 \qquad (3.10)$$

Data collected by Powell and Uglow (1988) from several sites in the United Kingdom using a self-boring pressuremeter (SBP), triaxial testing, and sDMT results showed some deviation from this correlation. Figure 3-13 is a plot of overconsolidation ratio versus horizontal stress index K_D.

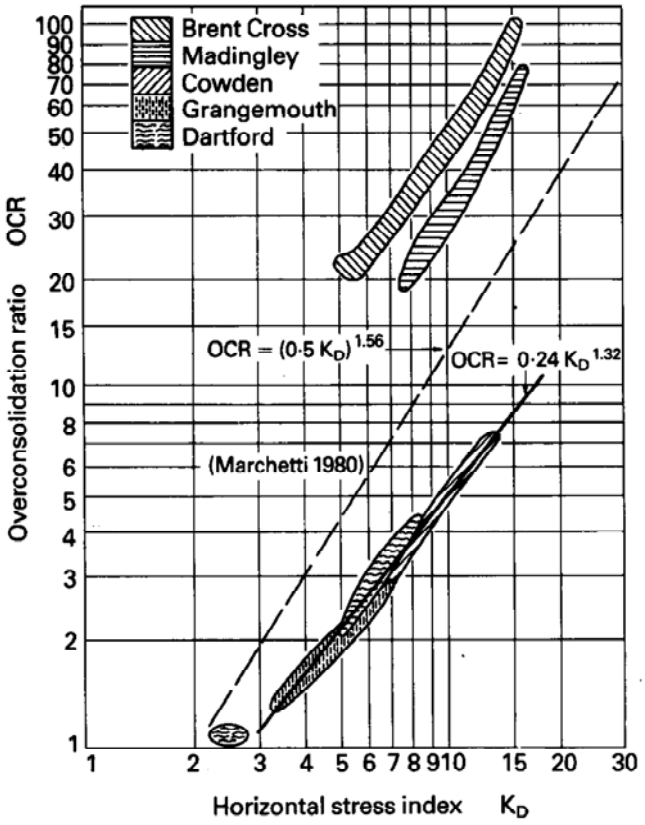

Figure 3-13: Comparison of sDMT and SBP for *OCR* versus K_D for several U.K. clays (Powell & Uglow, 1988).

While the results from Powell and Uglow (1988) follow a narrow band that is parallel to Marchetti's initial correlation line, the equation itself would either over or underestimate the *OCR* for their soils. These results show the importance of site specific correlations, and emphasize the importance of wariness when these correlations are unavailable. The data collected by Powell and Uglow (1998) on the coefficient of lateral earth pressure at rest (K_0) shows a similar trend against Marchetti's correlation for the horizontal stress index (K_D). They suggested that young clays tend to lie below Marchetti's correlations for both *OCR* and K_0 while older clays tend to lie above. While a new correlation was suggested for "young" clays, the authors suggested that for "old" clays, existing experience on that soil type should be used (or, if one or two values of K_0 are available, a new correlation can be drawn through them, parallel to the Marchetti line).

While the rocks of Northland Allochthon themselves range in age from 90 to 25 million years old, emplacement of the Northland Allochthon rocks began in the Miocene era and continued to the early Burdigalian stage (about 22 million years ago) (Isaac et al., 1994). Assuming the soil derived from Northland Allochthon rocks began forming after emplacement, the silty clay at Mountain Road is likely to be an "old" clay, i.e. significant time has passed to allow it to undergo the processes that result in soil ageing. There is nothing in the geologic history of the residual soil derived from the Northland Allochthon rock (Isaac et al., 1994) to suggest that the present overburden stress of the soil has been exceeded in the past (i.e. through mechanical one dimensional loading). Wesley (1990) studied three different residual soils, and found that they all behaved in a manner not unlike that of moderately or heavily overconsolidated soils. However, similar to the Northland Allochthon residual clay soil studied here, at least two of the soils had never been subjected to consolidation pressures higher than their present overburden pressure, and thus stress history was not a significant influence on their behaviour. Since "preconsolidation" pressures of this soil bear no relation to stress history, this is therefore likely to be the result of weathering processes. For this reason, the preconsolidation pressures of such residual soils are often termed pseudo-preconsolidation pressures (Wesley, 1990). The mechanisms that could have led to the pseudo-preconsolidation pressures (*OCR*s higher than 1) include desiccation (especially near the surface), drained creep (long term secondary compression), and physiochemical processes (natural cementation due to carbonates and silica, and other causes of bonding due to ion exchange). In addition, cemented or structured soil may behave like overconsolidated soil (Mitchell & Soga, 2005). Harris (2013) states that the presence of the montmorillonite clay greatly increases the susceptibility of Northland Allochthon soil to weathering, due to the mechanical process of expansion and contraction from repeated cycles of wetting and drying, such as rainfall events. In addition, in his field study, Harris (2013) found that the volumetric water content of the soil at shallow depths fluctuated significantly during each rainfall event (though there was very little fluctuation at deeper depths). This suggests frequent rising and falling of the groundwater table. Through the examination of the effects of weathering, Bhattarai et al. (2006) confirm that the fluctuation of the groundwater table is a weathering process.

Studies in soft clay have found good correlation to Marchetti's original correlation between K_D and *OCR* (Iwasaki et al., 1991; Wong et al., 1993). Results from several studies were compiled by Kamei and Iwasaki (1995) and found that the overall trend was similar to Marchetti's equation. However, averaging results from various locations does not do justice to site-specific variations.

OCR can also be determined from CPT results by correlating the ratio of c_u to σ'_{v0} to the plasticity index for the soil as shown in Figure 3-14. Note that in Figure 3-14 c_u is given as s_u, *PI* is given as I_p and p'_v is given as p'_c.

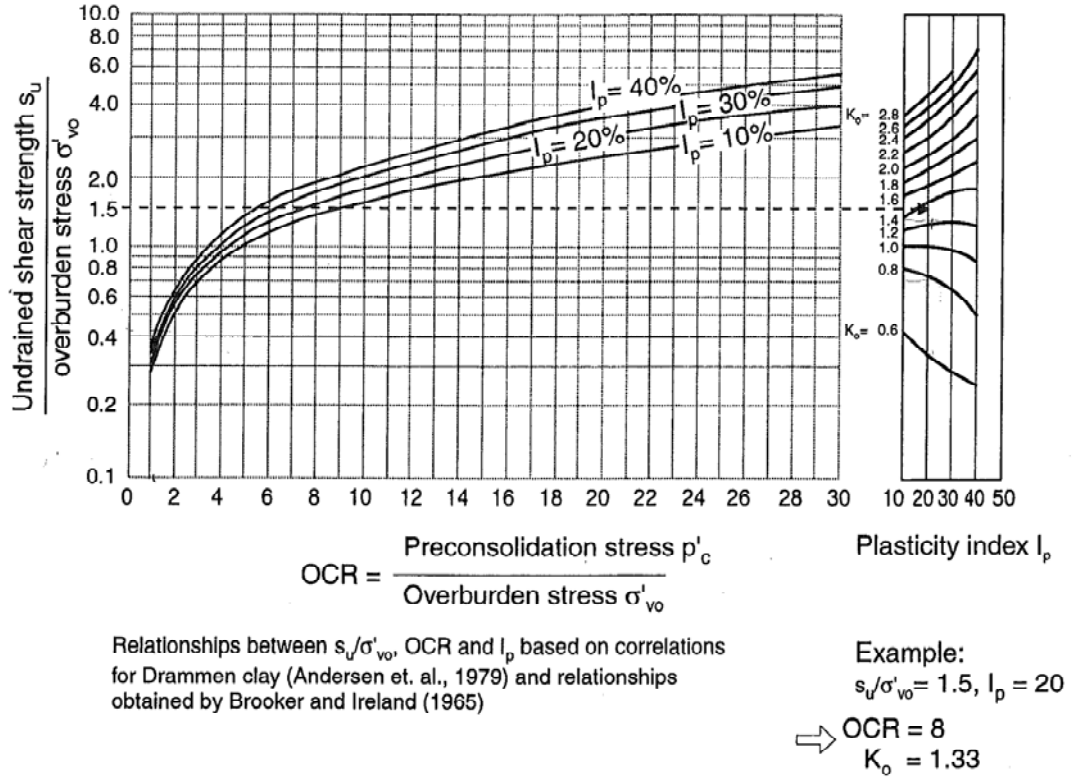

Figure 3-14: *OCR* and K_0 from c_u/σ'_{vo} and plasticity index (Lunne et al., 1997).

This relationship is appropriate for soils that have been mechanically overconsolidated, and caution should be taken when applying such relationships to cemented or aged soils.

The results from 1.5-4 m for *OCR* and K_0 at Mountain Road are shown in Table 3-10.

The comparison of the *OCR* from CPT results to sDMT results at locations where samples were available (for a plasticity index (*PI*) value) are shown in Table 3-11. Undrained shear strength was estimated from an average value of sDMT and SPT results. The CPT results show a lower approximation of both the *OCR* and K_0 compared to the sDMT.

Table 3-10: *OCR* and K_0 from sDMT in the depth range of sample collection at Mountain Road.

Depth	Overconsolidation Ratio						Coefficient of Lateral Earth Pressure at Rest					
(m)	sDMT7	sDMT6	sDMT5	sDMT4	sDMT3	Average	sDMT7	sDMT6	sDMT5	sDMT4	sDMT3	Average
1.40				23.45		23.4				2.36	2.08	2.22
1.50	5.74	31.01	20.75			19.2	1.34	2.62	2.25			2.07
1.60				15.61	16.96	16.3				2.02	2.12	2.07
1.75	7.66	5.77	8.39			7.3	1.51	1.34	1.57			1.47
1.80				11.13	17.76	14.4				1.76		1.76
2.00	7.64	6.21	8.46	17.47		9.9	1.51	1.38	1.58	2.11		1.64
2.20				12.36		12.4				1.84	1.86	1.85
2.25	5.33	4.77	3.28			4.5	1.29	1.32	1.24			1.28
2.40				8.90	12.70	10.8				1.61	1.8	1.71
2.50	3.20	5.62	4.89			4.6	1.25	1.13				1.19
2.60				10.75	11.74	11.2				1.74	1.63	1.69
2.75	4.9	3.95				4.4		0.74	0.96			0.85
2.80				7.08	9.23	8.2				1.46	1.47	1.47
3.00		1.71	2.83	6.67	7.12	4.6	1.17	0.99	0.95	1.42		1.13
3.20				8.25	7.16	7.7				1.56	1.47	1.52
3.25	4.29	3.01	2.72			3.3	1.08	0.93	0.93			0.98
3.40				8.14	7.10	7.6				1.55	1.46	1.51
3.50	3.62	2.61	2.61			2.9	1.45	1.33	1.15			1.31
3.75	6.91	5.70	4.12			5.6						
3.80				8.59	8.05	8.3				1.59	1.54	1.57
4.00	6.41	6.72	5.76	7.99	5.95	6.6	1.4	1.43	1.34	1.54	1.36	1.41

Table 3-11: *OCR* and K_0 from CPT results (compared to sDMT).

Depth (m)	c_u (kPa)	σ'_{v0} (kPa)	*PI* (%)	c_u/σ'_{v0}	*OCR* (CPT)	*OCR* (sDMT)	K_0 (CPT)	K_0 (sDMT)
1.5	48	38.3	21.3	1.3	6	18	1.3	2.1
3.2	55	81.6	24.4	0.7	3	5	0.8	1.5
3.4	55	86.7	22.3	0.6	3	5	0.8	1.5
3.6	56	91.8	9.6	0.6	3	4	0.7	1.4

The results in Table 3-10 show a higher overconsolidation ratio at around 1.4 m-1.5 m compared to the rest of the soil profile up to 4 m. The *OCR* above 1.4 m (not shown in the table) is very high for all sDMT reading locations, and is in excess of 50 for the top 50 cm near ground surface. These high apparent levels of overconsolidation ratio are consistent with a stress history consisting of frequent fluctuations in the groundwater table near ground surface, resulting in high soil suctions. Although no potentiometric data are available for the Mountain Road site, several researchers have noted that seasonal fluctuations of the groundwater table, which is typically located within the top few meters of ground level, are prominent in Northland Allochthon soil (Harris, 2013; Lentfer, 2007; O'Sullivan, 2009). Volumetric water content sensors installed by Harris (2013) at 0.5 m below ground level at the toe and the middle of a road slip in Silverdale (Whangai Formation) indicated that the volumetric water content fluctuated considerably with rainfall events at this depth. The groundwater table was not encountered during the shallow excavations preformed as part of the site investigation for Shelby tube sample collection at Mountain Road. Results from sDMT testing indicate that U_D (discussed in Section 2.7.2) begins to go above zero at 3.25 m below ground level at sDMT 3, 4, 5, 6 and 7, suggesting that the ground water level was at approximately this depth at the locations and time of the sDMT testing.

In Table 3-11, which shows a summary of the *OCR* for the samples collected, the *OCR* varies from 4 to 18. In light of the research done by Powell and Uglow (1998), and the fact that the sDMT has not been thoroughly calibrated in this soil type, the *OCR* of the soil as determined by other methods (such as laboratory testing or a self-boring pressuremeter) may be slightly offset from the values given by the sDMT.

As mentioned, the frequent rise and fall of the groundwater table and changes in the degree of saturation of the soil are sources of weathering that contribute to the high OCR near ground level. Although Northland Allochthon residual clay soil has a low permeability (Harris, 2013), frequent expansion and contraction of the soil leads to fissures which can be 1 to 2 m deep (Lentfer, 2007). These fissures reduce the overall permeability of the soil, making it more susceptible to wet and dry cycles from both surface water and groundwater. Lentfer (2007) also noted water ponding at the surface at field sites in Northland Allochthon during winter months, confirming a groundwater table at ground level during these periods. Wierzbicki (2009) noted a similar spike in OCR values near ground level, as determined from CPT and sDMT results in a sedimentary soil deposit. He also attributed this to frequent changes in the groundwater table.

3.5.5 Locating the Slip Surface Location with the Horizontal Stress Index (K_D)

A method for detecting active or old slip surfaces in overconsolidated clays was developed by Totani et al. (1997) using the sDMT parameter K_D. It is based on the premise that the sliding and remoulding occurring in a slip surface cause the clay to be remoulded and undergo a loss of structure. This reduces the K_D value to approximately 2- which is that of a normally consolidated clay. The method was validated by inclinometers and documented slip surfaces.

At Mountain Road, K_D drops to a value of 2 at approximately 8 m below ground at sDMT 7, 6 and 5. These data are contained in Appendix A. 8 m below ground at this location corresponds to the interface between the transition zone soil and the underlying mudstone. Borehole logs suggest that the possible slip surface is at the interface between the residual soil and transition zone (MWH, 2002). This method could prove useful, but requires further investigation for use in Northland Allochthon residual clay slopes.

3.5.6 Unit Weight

The saturated unit weight was determined by two methods in the laboratory. Method one involved first determining the bulk density of each sample. Prior to triaxial testing (in the undisturbed state) each sample was weighed and the dimensions of the sample were taken to find the mass per unit volume. Unit weight (γ) was then determined from:

$$\gamma = \rho * g \qquad (3.11)$$

where g is 9.81 m^2/s, and ρ is the measured bulk density of the sample. Method two is the more common method. For method two, the water content of the sample at the end of an undrained triaxial test was used to determine the void ratio (e). Then, the unit weight was determined from:

$$\gamma = \left[\frac{G_s+e}{1+e}\right]\gamma_w \qquad (3.12)$$

where e is the void ratio, G_s is the specific gravity and γ_w is the unit weight of water. Both methods have sources of error. Method one requires the direct measurement of soil specimen dimensions. Soil specimens are imperfect, and highly accurate dimensions can be difficult to obtain. Method two relies on the accurate measurement of G_s and e, and determination of these parameters have their own sources of error associated with their measurement.

A chart for determining the unit weight from the material index (I_D) and the dilatometer modulus (E_D) was developed by Marchetti and Crapps (1981). A comparison of the unit weight as determined from laboratory testing to the original sDMT correlation is shown in Table 3-12. The sDMT results tend to underestimate the unit weight as found through laboratory testing. This is because the chart developed by Marchetti and Craps (1981) is presented as a "good average for 'normal' soils". As with the *OCR* and K_0, the chart needs to be modified to better match local soil conditions.

Table 3-12: Unit weight at Mountain Road.

Depth from Original Ground Level (m)	Unit Weight (kN/m^3)		
	Lab Testing Results		sDMT Results
	Method 1	Method 2	
1.5	18.8	18.0	16.9
3.2	19.1	18.2	15.9
3.4	19.3	18.2	17

3.5.7 Shear Wave Velocity (V_s) and Small Strain Shear Modulus (G_0)

The small strain shear modulus (G_0) is directly proportional to shear wave velocity, V_s. The results for the top 5 metres for sDMT tests 5, 6 and 7 are shown in Figure 3-15. Results indicate a G_0 of approximately 20 MPa for 1 to 3 m, increasing to 30 MPa at 3.5 m and 50 MPa at 4 to 5 m.

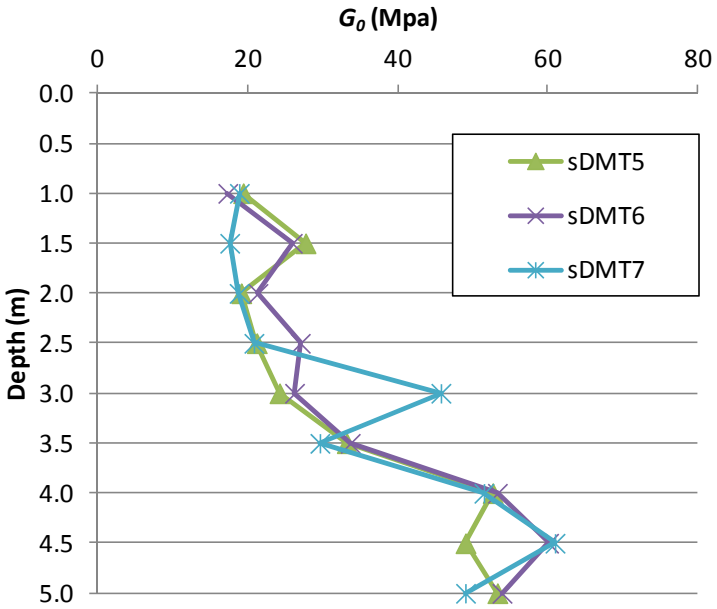

Figure 3-15: G_0 from sDMT 5, 6 and 7 for 0 to 5 m below ground level.

The shear modulus (G) is related to Young's modulus (E) and Poisson's ratio (ν) through the following equation:

$$G = \frac{E}{2(1+\nu)} \qquad (3.13)$$

Since all of the shear stress is carried by the soil skeleton (as pore water is unable to withstand shear), the effective shear stress is the same as the total shear stress, and the effective shear modulus G' is equal to the total stress shear modulus G_u (Powrie, 2004). Thus,

using the above equation, with an estimate of Poisson's ratio (v), and a value of G_0 from shear wave velocity results, an estimate of Young's modulus at small strains (E_0) can be determined. E_{u0} is the total stress Young's modulus at small strains.

Table 3-13: Estimates of Young's modulus at small strains from shear wave velocity data.

Depth	G_0 (kPa)	Poisson's Ratio	E_{u0} (kPa)	E_0 (kPa)
1- 3 m	20000	0.5	60000	
	20000	0.2		48000
	20000	0.3		52000
3 - 3.7 m	30000	0.5	90000	
	30000	0.2		72000
	30000	0.3		78000
3.7 - 5 m	50000	0.5	150000	
	50000	0.2		120000
	50000	0.3		130000

With Poisson's ratio ranging from around 0.2 to 0.3, E_0 is approximately 48000 to 52000 kPa from 1 to 3 m depth. This is consistent with the visual description of the soil as "stiff". The E values acquired from laboratory testing will be discussed in Chapter 4.

3.6 Exposure of DSM Columns at Mountain Road

The DSM columns installed at Mountain Road were constructed using twin mixing blades (Colmix) each with a diameter of 30 cm and spaced 2.1 m apart. Two of the DSM columns installed in 2003 at Mountain Road were exposed during the May 2011 field investigation with an excavator. Figure 3-16 shows the exposure of one of the columns. Layers of pavement where the road has been repaired can be seen in the soil profile. There did not appear to be significant evidence of the cement mixture permeating the soil surrounding the column (i.e. the columns were distinct). The column material was significantly harder than the surrounding soil and could not be readily excavated. The surrounding soil was stiff, but could be excavated with some effort. The columns appeared to be intact and straight.

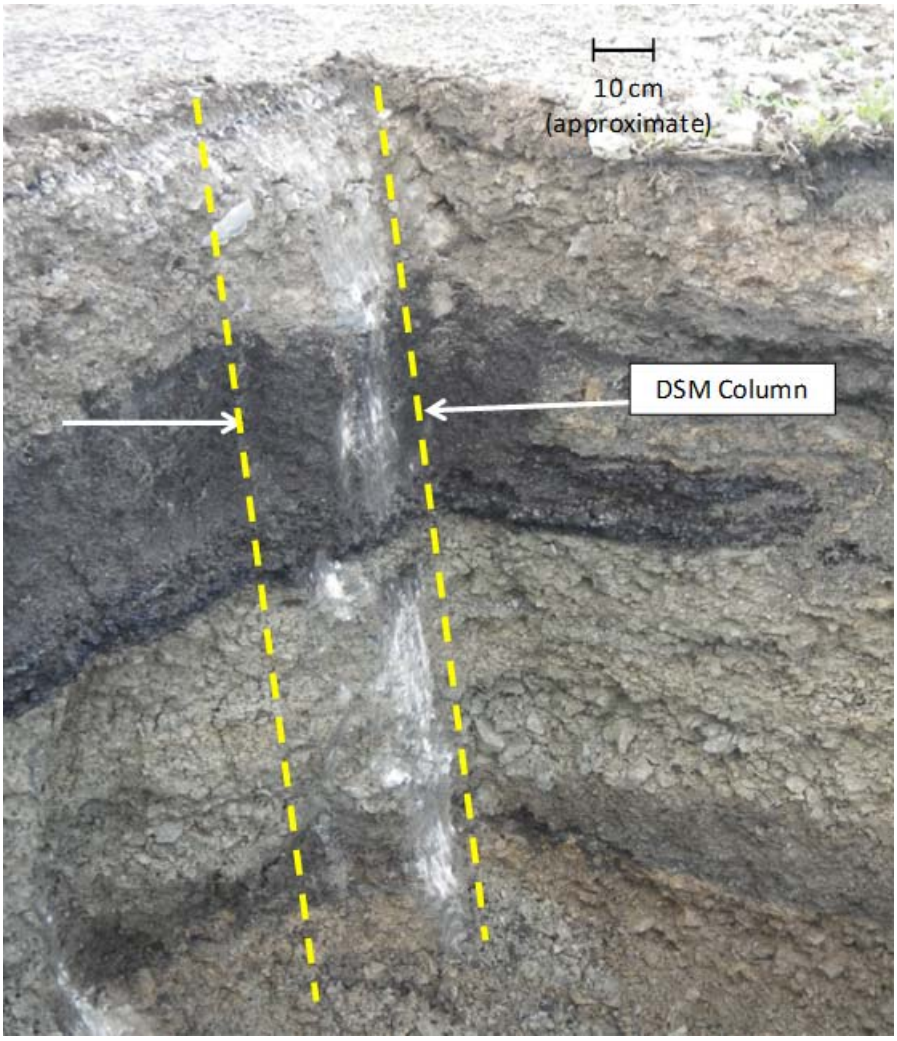

Figure 3-16: DSM column exposure at Mountain Road.

Larsson and Kosche (2005) investigated the changes to the soil surrounding DSM columns in a small scale test (50 mm diameter columns) in Kaolin clay. They found that the transition zone (the area around the column with increased strength parameters) propagated with time up to approximately 28 mm (56% of the column diameter) after 100 days. The kaolin soil being tested had liquidity index (*LI*) of 0.93, in its unaltered state. The *LI* was found to be in the range of 0.2 to 0.3 at the column periphery and increased linearly towards 1 at a distance of 60% of the column diameter from the column periphery.

Two Shelby tubes were pushed laterally into the soil approximately 15-20 cm from DSM columns as shown in Figure 3-17. For the 30 cm diameter columns, 15-20 cm is about 50-60% of the column diameter away from the column periphery. Based on the study discussed above, this should be just within the boundary of the transition zone. Atterberg limits were performed to determine if a decrease in *LI* could be observed. The *LI* was found to be an average of 0.36 based on two tests from Shelby tube MR7. The *LI* of the residual soil further from the columns was 0.38. From these results, a significant change in *LI* around the columns cannot be deduced. The change in *LI* seen by other researchers in the transition zone around DSM columns is mainly due to a change in water content (associated with cation exchange) and a slight increase in the *PL* (Shen et al., 2008). As no significant change in *LI* has been seen here, it is possible that less cation exchange is occurring than that seen in other studies. However, the sample collection at this site was performed over a year after DSM column installation, while in the other studies cited it was performed approximately 40 days (or much less) after installation. This significant difference in time may also affect the observed changes in *LI*. In addition, more samples should be collected to draw a firm conclusion.

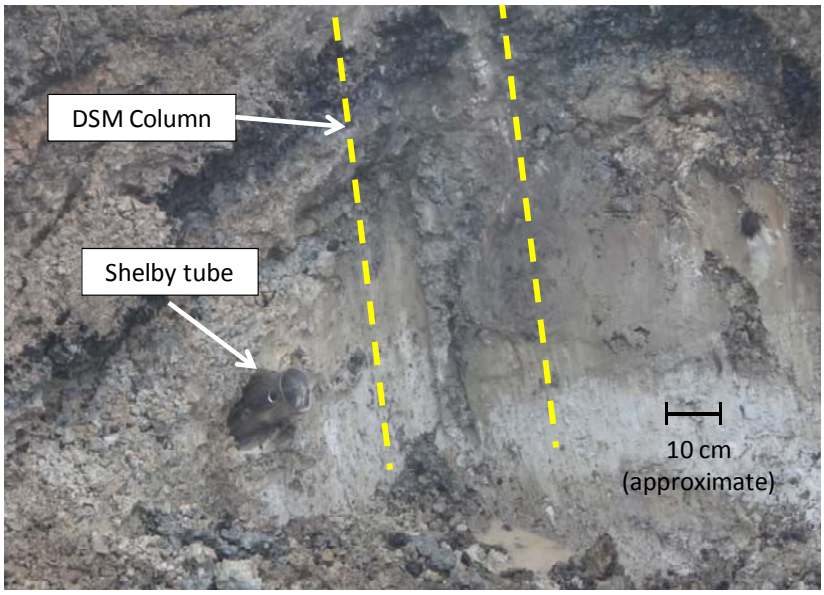

Figure 3-17: Sample acquisition next to DSM column.

3.7 sDMT Testing at Wairere Drive

A numerical modelling study on improvements to soft clay surrounding stone columns after installation indicated an increase in soil stiffness and K_0 after construction of the columns due to consolidation of the clay and increased confinement (Guetif et al., 2007). A similar effect has been found around DSM columns (Chai et al., 2005). The use of the seismic flat plate dilatometer (sDMT) between DSM columns was performed to examine whether such changes are taking place around TurboJET DSM columns.

The testing was performed at Wairere Drive near the Carrs Road Bridge in Hamilton in the Hamilton Ash and Puketoka Formation. The soil is classified as firm to stiff silty clay up to approximately 7 m, and soft and sensitive silt from approximately 7 m to 12 m. The change in soil stiffness due to DSM column installation is dependent on the amount of displacement due to column installation, which is reliant on the type of DSM, the injection pressure, the mass injected, and the radius of the column (Chai et al., 2005). Although the soil type at Wairere Drive is similar in some regards, it is not the same as the Northland Allochthon residual clay soil examined in the rest of this study. As such, the sDMT results are meant only to examine whether changes in soil properties surrounding DSM columns may take place, and no attempt is made to quantify these changes.

sDMT testing before and after DSM column installation was undertaken at distances of 300, 600 and 900 mm away from the column periphery for columns 0.6 m in diameter (and 8.5 m deep) as shown in Figure 3-18. The columns were spaced 2.4 cm apart from centre to centre. Testing was performed before column installation and five days after column installation.

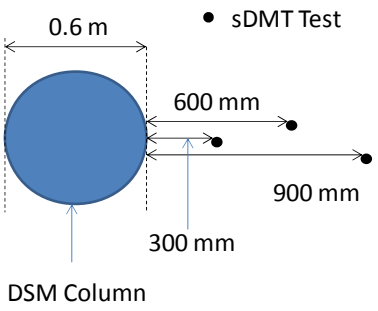

Figure 3-18: sDMT testing locations before & after column installation.

3.7.1 Horizontal Stress Index (K_D)

Figure 3-19 shows a general increase in the horizontal stress index (K_D) after column installation indicating greater confinement of the soil. The most notable increase in K_D is at the location 900 mm from the column edge, which could be due to overlapping confinement from surrounding columns at this location (Figure 3-20).

Relaxation of lateral stresses has been found to occur in soil surrounding some types of ground improvement, such as sand compaction piles (SCP) (Harada et al., 2010). Based on a thorough literature review, there are no available studies on the amount of stress relaxation that occurs over the long term after DSM column installation. The destruction of soil fabric is one of main contributors to stress relaxation (Spira et al., 2005). The installation of DSM induces less volumetric strain in the surrounding soil compared to other methods of ground improvement (such as stone columns and SCP), and thus there is less destruction of the soil fabric and realignment of the particles (Terzaghi, pers. comm.., 2014). As such, in the case of DSM, the degree of stress relaxation with time is likely to be less than that seen in other types of ground improvement methods. However, further research is required to verify the amount of stress relaxation around DSM columns.

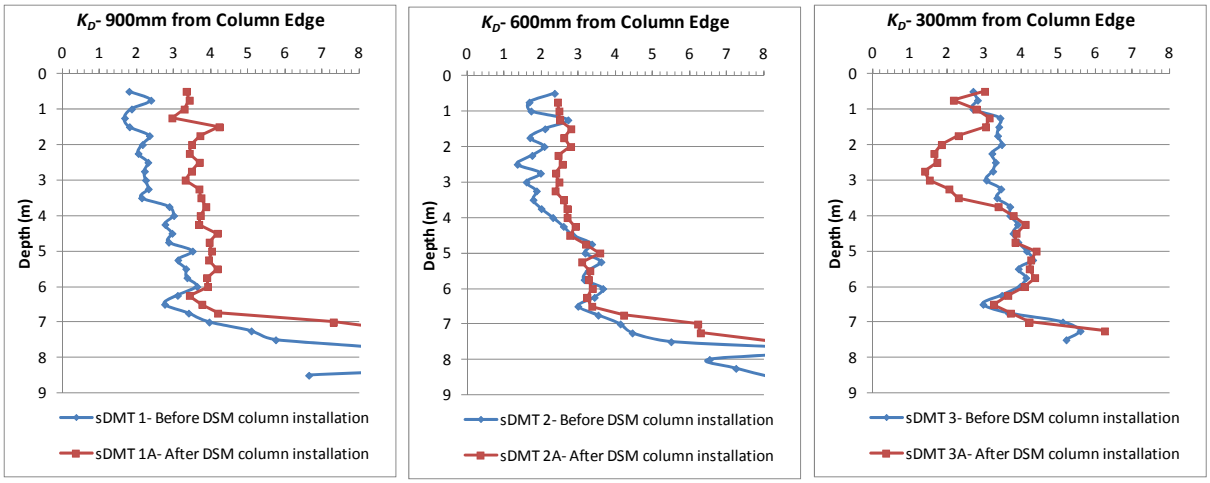

Figure 3-19: Horizontal stress index (K_D) versus depth before and after DSM column installation.

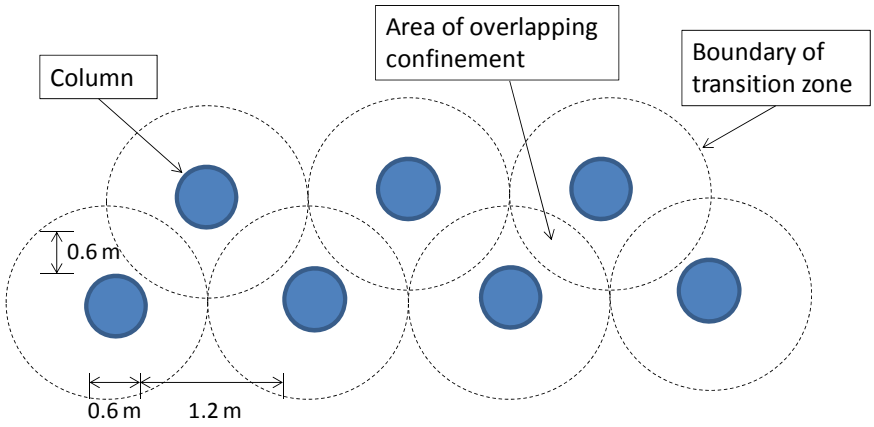

Figure 3-20: Column installation pattern and overlapping column confinement.

3.7.2 Material Index (I_D)

I_D gives an indication of soil type, but reflects the mechanical behaviour or "rigidity" of the soil, rather than being representative of sieve analysis (Marchetti et al., 2001). The results show a marked increase in I_D at 300 mm away from the column edges, a slight increase at 600 mm and no noticeable difference at 900 mm. This could be interpreted as an increase in

the rigidity of the soil due to DSM column installation, especially close to the column (at 300 mm).

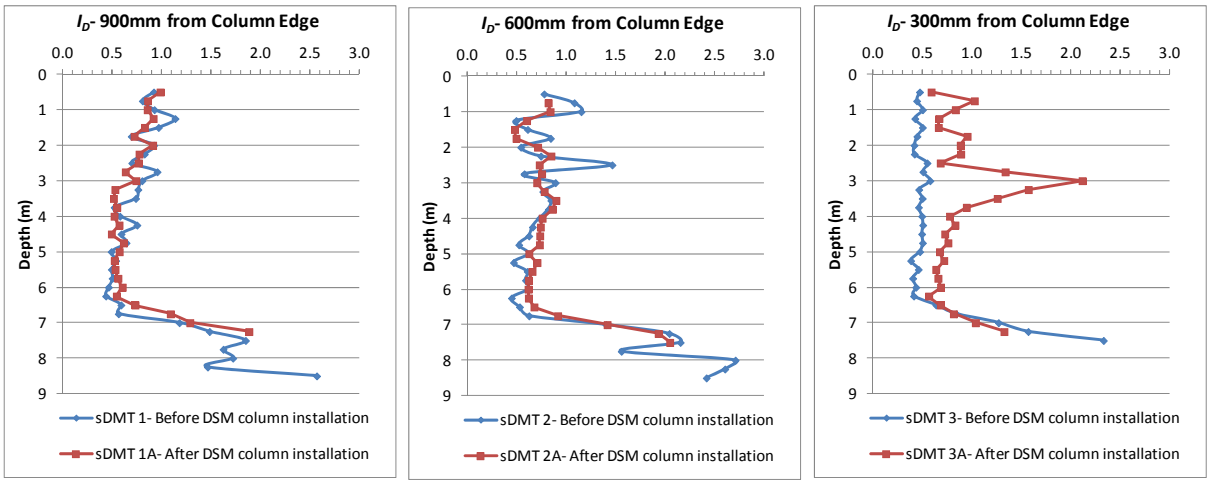

Figure 3-21: Material index (I_D) versus depth before and after DSM column installation.

3.7.3 Shear wave velocity (V_s)

Shear wave velocity readings were expected to increase after DSM column installation, but do not show any significant trend, and are thus inconclusive. The results are shown in Figure 3-22. The lack of change observed in V_s (while changes in K_D and I_D were observed) is likely due to differences in the measuring tools. Seismic phones (attached to the DMT) were used to measure V_s while the DMT itself was used to measure K_D and I_D. While empirical correlations have been developed between G_{max} (as determined from V_s) and E_D (as determined from DMT) (Hryciw, 1990), there are no such correlations between K_D or I_D and V_s.

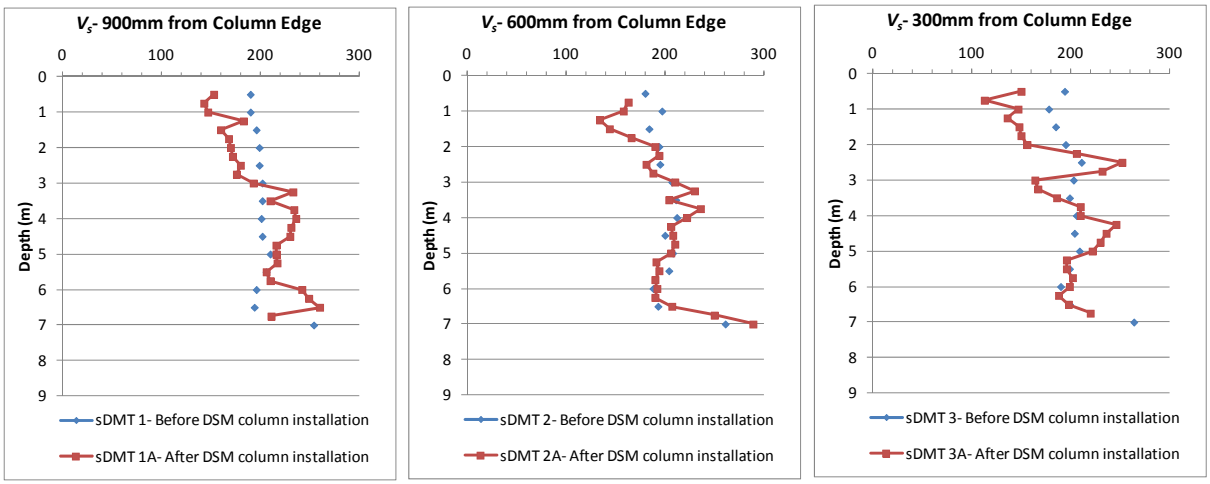

Figure 3-22: Shear wave velocity (V_s) measurements versus depth before and after DSM column installation.

3.8 Conclusions

Shelby tubes were collected from Mountain Road and Kaeo field sites. As part of another study (O'Sullivan, 2009) samples were collected in a similar fashion from the Ogles No. 3 field site. The residual soil at all three of these sites can be classified as silty clay or clayey silt, confirmed through the location of the Atterberg limits results on a plasticity chart. The residual and transition zone soil at these sites can be considered to be "related", as the results fall in a row along the A-line. The specific gravity of the soil was found to be between 2.60 and 2.62. X-ray diffraction performed on this soil type indicated the dominant clay mineral is smectite (Lentfer, 2007).

CPT and sDMT testing at Mountain Road indicated a c_u of 44 to 56 kPa (sDMT) and 46 to 82 kPa (CPT). The sensitivity was determined at 3 different depths and was found to be between low sensitivity to sensitive.

The volume change potential from several field sites was found generally to be medium within the residual soil at the three field sites for which it was estimated. It ranged between low to very high in the transition zone for the same three field sites.

The *OCR* was found to range from 3-6 (CPT) and 4-18 (sDMT) at the depths of sample collection at Mountain Road. The overall soil profile showed a substantial spike in the *OCR* near the ground surface, likely due to frequent groundwater fluctuations. The pseudo-preconsolidation pressures that exist are likely due to weathering processes (Wesley, 1990), since the geological history of this soil does not suggest any preconsolidation. The importance of using caution with direct use of results from the sDMT has been highlighted in this chapter based on literature. This is an important consideration for practitioners in areas where the correlations developed for this instrument have not been calibrated to local soil conditions.

The Atterberg limits are a valuable tool for evaluating residual soils (Wesley, 2010b). Results in this chapter have demonstrated that the *PI'* (as derived from the *PI*) can be useful for evaluating the volume change potential of Northland Allochthon soils. Northland Allochthon residual soil has several similarities to other residual soils. It is common for residual soils to have varying *PI* due to different degrees of weathering (Rahardjo et al., 2004), and significant variation is seen in the results from the Northland Allochthon field sites examined in this study. In addition, results in this chapter have demonstrated the existence of a pseudo-preconsolidation pressure. This type of behaviour has also been noticed in residual soils from other places (Wesley, 1990).

Similarities also exist with sedimentary soils. The Atterberg limits of Northland Allochthon residual clay soil from several sites fall in a line parallel to the A-line, which is a trend that has been demonstrated for several types of sedimentary clays (Muir-Wood, 1990). In addition, research on sedimentary soils has shown that c_u tends to increase with depth (Muir-Wood, 1990), a trend which was also seen at the Mountain Road field site.

The exposure of DSM columns at the Mountain Road site showed that they were intact, and no permeation of the column material into the surrounding soil was visible. There were no significant changes to the Atterberg limits of the soil for samples acquired at 15- 20 cm from the column periphery.

sDMT testing performed before and after DSM column installation at Wairere drive in Hamilton (in Hamilton Ash and Puketoka Formation) indicated an increase in horizontal

stress index (K_D) and material index (I_D) at some locations. This confirms an increase in soil confinement due to column installation, an important finding for practitioners who use DSM, as it provides evidence that the ground improvement provided by DSM columns exists outside of the columns themselves.

4.0 Mechanical Behaviour of Reconstituted Northland Allochthon Residual Clay and the Effects of Structure

4.1 Introduction

Based on triaxial testing performed in his study, O'Sullivan (2009) suggested that in situ weathering of Northland Allochthon residual clay soil may impart forms of structure on the soil which could influence its behaviour. Burland (1990) found that the structure of a clay soil can lead to an increased resistance to compression and shearing and a change in the state boundary surface. This chapter attempts to fill the knowledge gap in understanding the effects of structure on Northland Allochthon residual clay soil. Triaxial testing results of several reconstituted specimens and a small number of natural specimens of Northland Allochthon residual clay soil from the Mountain Road site are summarized. Triaxial testing of reconstituted soil gives a robust framework for comparison to intact soil (Burland, 1990). It also provides a well-defined critical state and critical state parameters, which can be difficult to attain with natural specimens. The peak strength results for both the reconstituted and natural specimens are normalized by the equivalent one dimensional pressure σ_{ve}*, acquired from oedometer testing, as discussed in the literature review (Chapter 2, Section 2.6.5) in order to determine how much, if any, of the soil strength is related to soil structure. The stress paths, stress-strain behaviour, and critical state parameters of the material are analysed and compared to other clay soils.

4.2 Reconstituted Sample Preparation

For this study, a consolidation device (consolidometer) was constructed in order to reconstitute soil into 50 mm diameter specimens. The soil was mixed with water to a water content of 1.25 to 1.5 times its liquid limit (Burland, 1990) and then slowly consolidated over time. The consolidation device utilizes the application of pressure to the top of the sample through the addition of weights. Two-way drainage (top and bottom) is allowed. Figure 4-1 is a diagram detailing the consolidometer. Figure 4-2 is a photograph of the device.

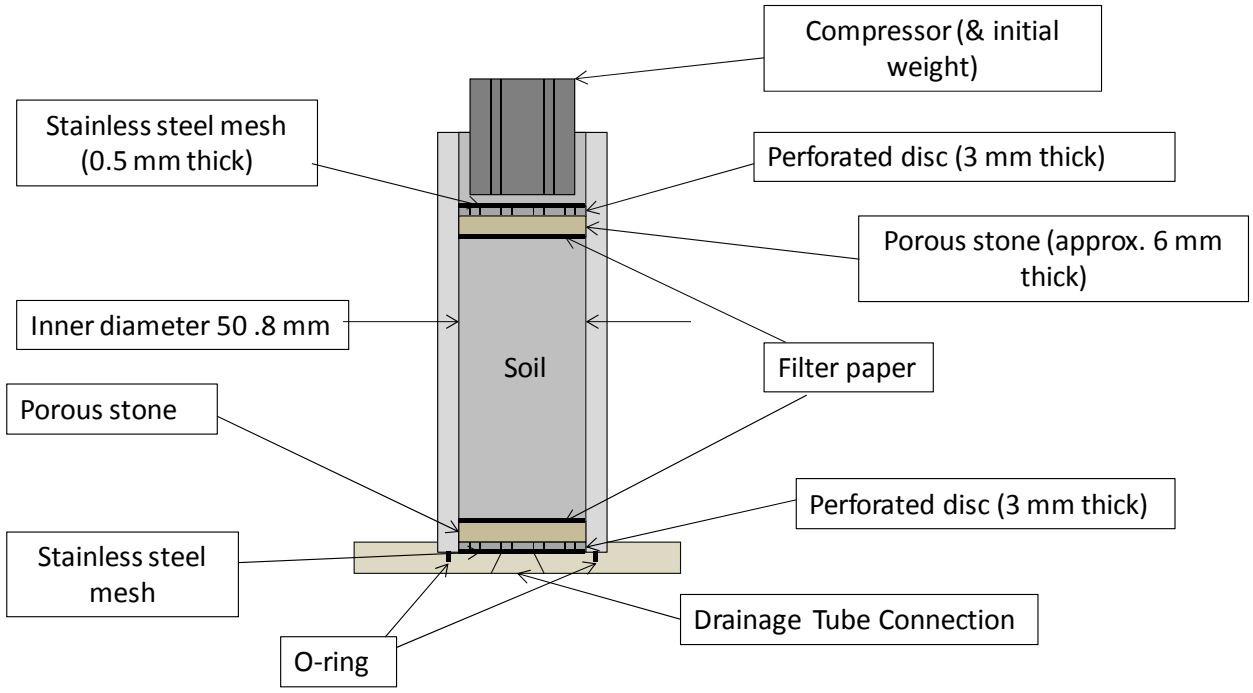

Figure 4-1: Diagram of consolidometer.

Figure 4-2: Photograph of consolidometer.

Pressure (weight) was increased in stages as per the method for consolidation described for oedometer consolidation tests (Head & Epps, 2011). The weight sequence and corresponding effective stress is shown in Table 4-1. The change in height was monitored and plotted versus the log of time to ensure full consolidation was reached. The next weight sequence was added when the plot showed a flattening out from the steeper part of the curve to a straight line which is less steeply inclined, as shown in Figure 4-3.

Table 4-1: Weight sequence for consolidation of reconstituted soil.

Weight Type	Weight (kg)	Cumulative Weight (kg)	Stress (kPa)	Cumulative Stress (kPa)
Initial Compressor	0.83	0.83	4.17	4.17
1 kg weight	1.00	1.83	5.00	9.16
Top part of hanger (without 1kg weight)	1.58	3.41	7.87	17.03
Remaining part of hanger	2.66	6.07	13.27	30.31
1 + 4 kg weights	5.00	11.07	24.98	55.29
10 kg weight	10.00	21.07	49.96	105.25
10 kg weight	10.00	31.07	49.96	155.21

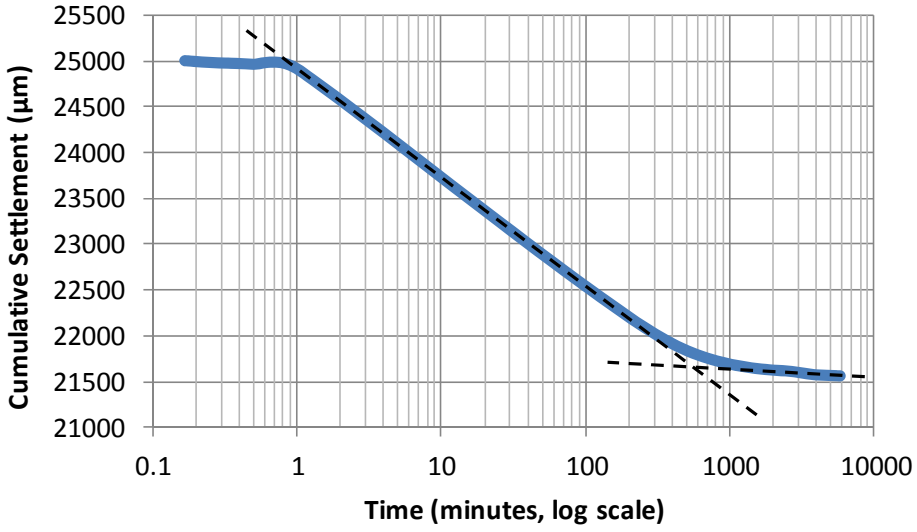

Figure 4-3: Cumulative settlement versus square root of time for one consolidation stage.

All specimens were consolidated to 155 kPa vertical effective stress before extrusion. The method used for trimming and extruding the samples was the same as that used for the intact samples, and is discussed in Section 4.4. The displacement at the end of the consolidation was used to determine the final void ratio. This value was cross-checked with the void ratio based on water content of the specimen at the end of consolidation, and the values of water

content were generally within 0.1 of one another between specimens. The void ratio based on the water content was used as the final value.

When time permitted, a second sample could be reconstituted in the apparatus (using a second metal tube) while the first sample was stored temporarily (prior to extruding it for triaxial testing) by sealing it at the ends with a paraffin wax and petroleum jelly mixture. Paraffin was mixed with petroleum jelly at a 1:1 ratio (Germaine & Germaine, 2009).

4.3 Tests Conducted

Burland et al. (1996) consolidated their reconstituted samples isotropically in the triaxial apparatus to relatively high effective stresses (between 700 kPa and 1000 kPa), and then allowed them to swell to a lower effective stress in order to obtain a variety of overconsolidation ratios. The same method was adopted here. Table 4-2 summarizes the tests performed on reconstituted samples. The second column indicates whether the triaxial tests were consolidated drained (CD) or consolidated undrained (CU). Consolidation pressures were kept to a maximum of 800 kPa for reconstituted specimens and 130 kPa for the larger intact specimens due to a load cell limitation of 2 kN. Table 4-3 summarizes the triaxial tests performed on intact specimens

Table 4-2: Summary of tests performed on reconstituted specimens.

Name	CD/CU	Effective Stress (kPa)	Consolidaton Pressure (kPa)	*OCR*
MR5a-R1	CD	80	800	10
MR5a-R2	CD	83	250	3
MR5a-R3	CD	160	800	5
MR5a-R4	CD	114	800	7
MR5a-R5	CU	125	250	2
MR5a-R6	CU	250	250	1
MR5a-R7	CU	400	400	1
MR5a-R8	CU	550	550	1
MR5a-R9	CU	800	800	1
MR5a-R10	CU	800	800	1
MR5a-R11	CU	800	800	1
MR5a-R12	CU	550	550	1
MR5a-R13	CU	400	400	1

Table 4-3: Summary of tests performed on intact specimens.

Name	CD/CU	Effective Stress (kPa)
MR5a	CU	110
MR5b	CU	190
MR5d	CU	130

4.4 Triaxial Testing Methods & Preparation of Intact Samples

Sivadass et al. (2003) found sample size (diameter) to have a significant effect on the results obtained for triaxial tests on a residual clay soil. They found that the maximum deviatoric stress decreased for increasing sample diameters of 38 mm, 50 mm and 100 mm. They also found that peak and residual frictional components of strength decreased with increasing sample size. However, Sivadass et al. (2003) make no comments as to the possible reason for this. For this study, larger diameter samples of 72 mm were used in order to better capture the soil behaviour. Samples were extruded from the undisturbed stainless steel tubes with an

inner diameter of 72 mm using a motorised hydraulic ram fitted with a 70 mm shoe as shown in Figure 4-4.

The wax seal end caps were trimmed off and the samples further extruded and then re-trimmed using a thin steel wire saw. Samples were trimmed towards the centre of the sample to reduce the risk of breakage. Once a sufficient length had been extruded for the current test, the remaining sample within the tube (if any) was sealed with the paraffin wax and petroleum jelly mixture, double wrapped at both ends using cling film and the tube placed in two tightly sealed plastic bags. The samples were then placed in a plastic sealed box with water at the bottom to ensure that they were in a moist environment, which further reduces the possibility for the loss of moisture from the specimens, a method commonly used at some research institutions in Japan (Hosono, pers. comm., 2011).

Figure 4-4: Sample extrusion.

4.4.1 Preparation

Samples were prepared and tested in accordance with ASTM D 4767-04- Standard Test Method for Consolidated Undrained Triaxial Compression Test for Cohesive Soils. Once extruded, the samples were taken to the preparation area in a mitre box. The mitre boxes were specially made for the 72 mm diameter and 50 mm diameter sample sizes, and were used to

trim the samples as shown in Figure 4-5. Trimmings were weighed and dried to verify moisture content.

An advanced stress-path GDS triaxial apparatus was used for triaxial testing.
Prior to placing the soil sample into the triaxial apparatus, the following checks were performed:
1. Filter papers for side drains as well as porous discs were de-aired by allowing saturation in de-aired water for a minimum of 30 minutes.
2. Water for cell pressure and back pressure was de-aired
3. Back pressure and pore pressure lines were filled with water and de-aired.

The de-aired porous stones were placed in the top and bottom platens and the filter paper fitted around the sample. Enlarged end platens (82 mm diameter) with lubricated ends were specially made for the 72 mm diameter samples and were used throughout testing to promote uniform deformation and reduce specimen barrelling. Two layers of greased membranes at the same diameter of the specimen (72 mm) and cut to fit around the porous stones in the centre were placed on each of the platens (Figure 4-6). Each of these membranes was 0.25 mm thick. For the reconstituted specimens, conventional platens 50 mm in diameter with 50 mm diameter porous stones were used.

72 mm or 50 mm diameter membranes were fitted over the soil samples using a split mould device of 73 mm or 51 mm diameter with a vacuum applied while the sample was sitting on the bottom platen. Once the membrane was on the sample and over the top and bottom platens, the vacuum was released. The sample was then carefully placed in the triaxial apparatus and the base raised until the top cap was in contact with the load cell, but no load was applied. Two types of top caps were used- a knob-and-dimple top cap and a top cap with a vylastic sleeve shown in Figure 4-7.

Figure 4-5: Mitre box and sample trimming.

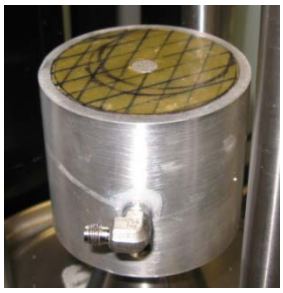

Figure 4-6: Bottom platen showing membranes used for lubricated ends and small centred porous stone.

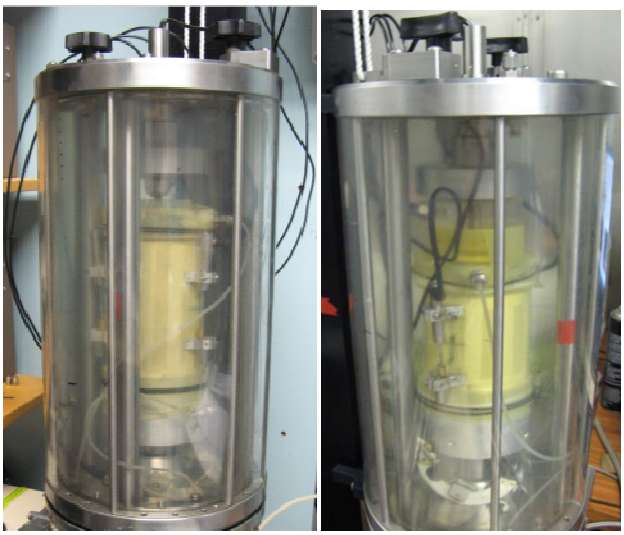

Figure 4-7: Sample in triaxial apparatus- knob-and-dimple top cap (left), top cap with vylastic sleeve (right).

Typically, a sample height-to-diameter ratio of 2:1 is used for triaxial testing (ASTM, 2007). However, due to restraints of the apparatus and platen sizes, this was reduced to 1.8:1 (130 mm high to 72 mm diameter) for test MR5a where the knob-and-dimple top cap was used and 1.4:1 (100 mm high to 72 mm diameter) for test MR5b where the top cap with the vylastic sleeve was used. The top cap with the vylastic sleeve was also used for MR5d, but due to issues with trimming the sample (friability), the height-to-diameter ratio of this sample was 1.1:1. Several studies have shown that the use of rigid, lubricated end platens (as used in this testing), inhibits the propagation of temporarily developing non-uniform deformations within short specimens with a sample height reduction to 1:1 (Amsiejus et al., 2009; Goto & Tatsuoka, 1988; Lade & Uzair, 1988). Therefore, as lubricated end platens have been used, a reduction in sample height has been deemed acceptable for this study.

Lubricated end platens are enlarged with regard to the size of the specimen (approximately 10% larger in diameter than the specimen diameter), and use two layers of lubricated membranes fitted around a small (1 cm diameter) porous stone to allow end movement. Standard platens use a platen that is the same diameter of the soil specimen, and a larger porous stone which is also the same diameter as the soil specimen. With both types of

platens, the bottom platen is fixed, while the load is applied to the top platen during shearing. In this study, the top platen (cap) comes into contact with the load cell through either a knob in the top cap with a dimple provided by the load cell, or with a vylastic sleeve where the top cap and load cell make contact on a flat surface. These are discussed further in Section 4.4.8.

4.4.2 Strain Measurement Errors in Triaxial Testing

There are several errors that can occur during triaxial testing which may give rise to an overestimation of axial strain (Jardine et al., 1984). These errors include:

a) Compliance of the loading system
b) Alignment errors due to a non-uniform specimen
c) Seating errors due to non-uniform contacts between the ram/internal load cell and the top cap, and between the top cap/base pedestal and the porous discs
d) Bedding errors at the specimen ends due to local surface irregularities and voids
e) Drift of local transducers during testing

External measurement of strains can result in errors that are too large to give a good definition of the stress-strain behaviour at smaller strains, particularly for soil that has a high stiffness at these strains. Calibrating the apparatus carefully can enable quantification of errors arising from the compliance of the loading system, but other errors are more difficult to account for. In order to ensure these errors do not mask the true soil behaviour, an accurate measurement of soil stiffness over the small strain range in triaxial tests is important. Measuring the strains locally, inside the triaxial cell, using high resolution transducers allows for highly accurate measurement of small strains. While axial strain is a critical measurement during triaxial testing, accurate measurements of radial strain are valuable for determining the secant shear modulus (G_{sec}) and shear strain (ε_q). Local measurements of radial strain can also be combined with axial strain to provide another measurement of volumetric strain in drained tests (in addition to the measurement of volumetric strain that can be determined through the measurement of water volume loss from the sample).

4.4.3 Axial and Radial LVDTs

The local displacements were measured by using axial and radial submersible on-sample (or local) LVDTs (linearly variable differential transformers), as shown in Figure 4-8, Figure 4-9

and Figure 4-10. The photo in Figure 4-9 is courtesy of GDS instruments as it was difficult to get a front view photo of the axial LVDT due to the triaxial set up. For the axial LVDTs, the armature rested on a lower mount, which was fitted with a knobbed screw that enabled small adjustments of the armature to be performed when the sample was set up. The design of the mounts allows the sample to barrel or develop a shear plane without causing the armature to jam. This kind of transducer has a linear calibration over a range of displacements of about 10 mm and has relatively small noise. To resolve the very small strains at the start of the shearing, the LVDTs were set at their electrical zero by adjusting the zero potentiometer in the transducer amplifier. This allowed the data logger to work in its most sensitive range. An LVDT for the measurement of radial displacements was mounted on the reconstituted samples (which had 50 mm diameters) using a radial belt designed for samples of this diameter. The radial LVDT was fitted over the axial LVDT as shown in Figure 4-10. The resolution of the LVDTs is approximately 0.15 μm.

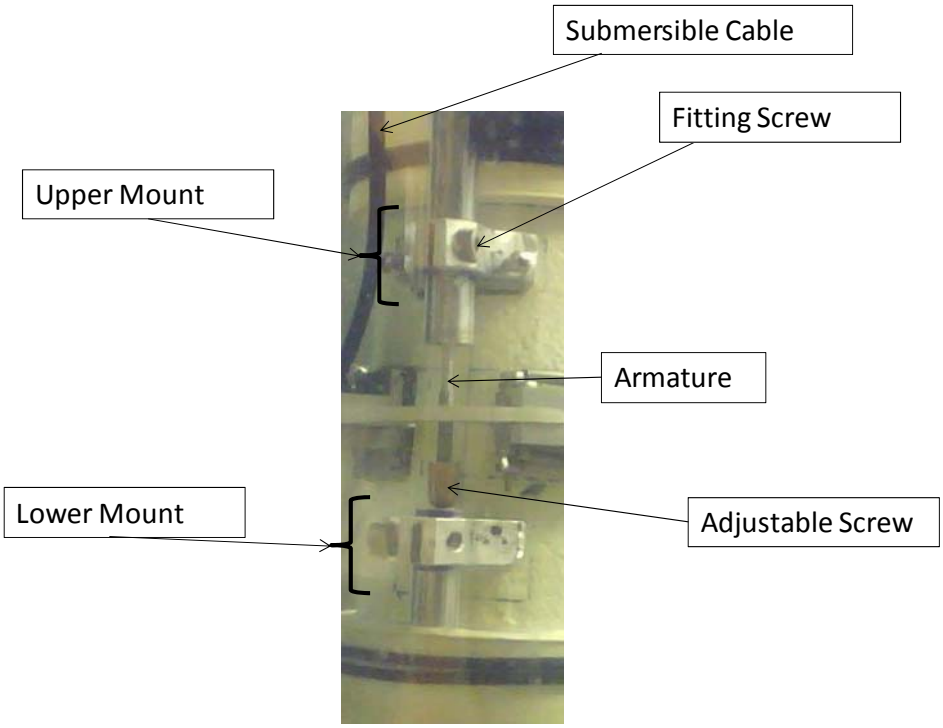

Figure 4-8: Axial LVDT with adjustable screw.

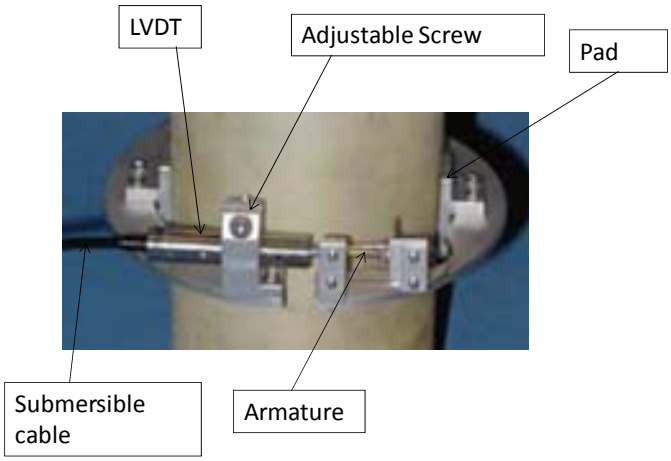

Figure 4-9: Radial strain belt.

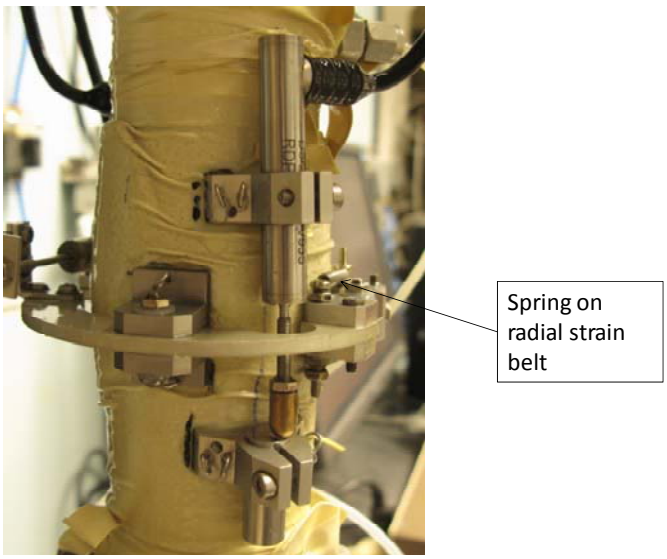

Figure 4-10: Fitting of radial strain belt over axial LVDT.

4.4.4 Saturation

The saturation of each specimen was carried out for a minimum of 24 hours. However, with the use of lubricated end platens which had much smaller porous stones (Figure 4-6), the saturation process often took as long as 5-7 days. Saturation was completed in stages of 100 kPa up to a back pressure of between 400 kPa and 1000 kPa. The requirement of such

high values for back pressure is typical for low permeability clays (Day, 2001). The cell pressure was kept at 10 kPa higher than the back pressure throughout saturation. The Skempton B value was checked after each 100 kPa increment as well as at the end of the saturation period. (Head, 1998). The relationship between the B value and the saturation ratio is dependent on the soil type, and this relationship was not investigated in this study. A minimum B value ($\Delta u/\Delta\sigma$) of 0.95 was attained for all specimens, which is typically utilized to ensure full saturation (Head, 1998; Rees, 2012).

4.4.5 Consolidation

Following saturation, pressure ramps were used to bring the difference between the cell pressure and back pressure to the desired effective stress for the test. When the knob-and-dimple top cap was used, the sample was left undocked during this period. When the top cap with the vylastic sleeve was used, a deviatoric stress of 1 kPa was targeted during this stage to ensure that the top cap remained in contact with the load cell, in order to eliminate seating errors (which are further discussed in Section 4.4.8). Consolidation continued until the volume change had stabilized. This typically took between 2-5 days.

4.4.6 Loading

Sample loading was performed at an axial strain rate equal to or less than the rate computed from the consolidation stage from Head (1998), pg 227. For this method, the plot of volume change versus the square root of time from the consolidation stage is utilized to determine the time intercept ($\sqrt{t_{100}}$). The value of t_{100} is then multiplied by the appropriate factor to estimate the 'significant testing time' or time to failure (Table 4-4).

Table 4-4: Factors for calculating time to failure (Head, 1998).

Time of Test (any diameter) **(2:1 ratio)**	***NO side drains***	***WITH side drains***
Undrained (CU)*	0.53 x t_{100}	1.8 x t_{100}
Drained (CD)	8.5 x t_{100}	14 x t_{100}

*For plastic deformation of non-sensitive soils only

The factor for no side drains was utilized for the intact specimens because while side drains are used in conjunction with lubricated end platens, they are not connected in any way to the porous stone, and therefore provide little or no assistance with drainage in or out of the sample (although they were thought to assist with equalisation within the sample). The time to failure can then be used to compute a maximum strain rate for the loading stage. The ASTM method for determining the maximum strain rate was compared to the method summarized by Head (1998) for each test. The two methods generally compared well, and the lower of the two strain rates was utilized, not exceeding 4.5% per day for undrained tests and 1.5% per day for drained tests. It is noted that these two methods have been developed for specimens with a 2:1 height to diameter ratio. Literature on samples where a reduction in the height to diameter ratio has been utilized do not propose a reduction to loading rates (Amsiejus et al., 2009; Goto & Tatsuoka, 1988; Lade & Uzair, 1988), and thus no reduction in loading rate has been used for specimens with a height to diameter ratio of less than 2:1 in this study. Figure 4-11 is a graphical representation of how the volume change dissipation is used to derive the time to failure.

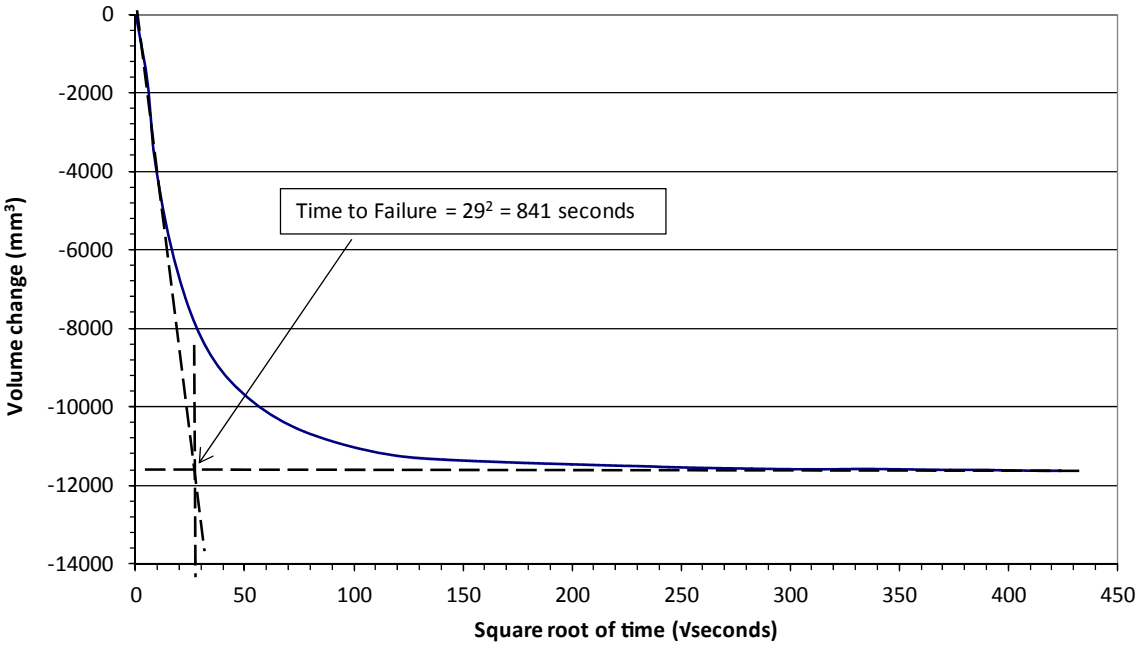

Figure 4-11: Representation of volume change dissipation for deriving time to failure.

Loading was generally carried out to 25%-30% axial strain, and deviatoric stress was monitored during loading in an attempt to reach critical state conditions.

4.4.7 Effects of End Restraint on Triaxial Testing Results

Germaine and Ladd (1988) discuss the pros and cons using of lubricated versus frictional ends specifically for saturated cohesive soils, with data compiled from several studies (Table 4-5).

Table 4-5: Comparison of lubricated and frictional triaxial ends (Germaine & Ladd, 1988).

Frictional Ends		Lubricated Ends	
Reasons For	Reasons Against	Reasons For	Reasons Against
> Easy set-up procedures	> Nonuniform stress and strain	> Improves uniformity at *all* strain levels	> More difficult to assemble
> Simple, efficient drainage	> Nonuniform excess pore pressure	> Reduces strain rate effects	> Reduces small strain precision
> Stiff apparatus for axial	> Water migration	> Reduces uncertainty in area correction	> Increases consolidation time
> Simple cell geometry	> Larger strain rate effect	> Essential for large strain behaviour	
	> Formation of rupture surfaces		

Germaine & Ladd (1988) do not provide firm recommendations on when to use either, as there are problems caused by frictional ends but practical difficulties with lubricated ones. They recommended that frictional end tests should be done slowly enough to allow equilibration of pore pressures to reduce water migration and non-uniform pore pressure distribution. They recommend lubricated ends when reliable data is required at large strains for highly overconsolidated soil (OCR >6).

Results have shown that end restraint does not significantly affect the failure envelope but may cause significant changes in measured volume change behaviour, especially with highly dilatant materials (Duncan & Dunlop, 1968; Lee, 1978). Few laboratories use lubricated ends for routine testing due to the increased consolidation time and reduction in small strain precision (Germaine & Ladd, 1988). The issues in small strain precision can be overcome with internal contact measuring devices (such as submersible LVDTs).

For this study, reconstituted soil was tested using frictional ends. Small strain precision was accurately measured through the use of LVDTs. A consolidation stage followed by a swelling stage was required to bring the samples to a variety of overconsolidation ratios, which made

the use of lubricated ends much less practical for these tests, as it would result in both of these stages being significantly more time consuming.

An increase in the degree of soil structure (with respect to the same soil in the reconstituted state) causes an increase in inhomogeneities due to end restraint, which can result in partial drainage and bulging of the sample during loading (Liyanapathirana et al., 2005). Due to the high stiffness of the soil at Mountain Road (and tendency to be slightly dilatant), as well as the possibility of inhomogeneities and significant structuration, the use of lubricated ends were deemed more likely to capture the true constitutive behaviour of the intact soil. Therefore, lubricated ends were utilized for the intact soil testing, in conjunction with LVDTs. There was no attempt made to compare the results for the same test condition with the two different types of end restraint for intact specimens. Test MR5a-10 on a reconstituted specimen had lubricated ends and was compared to MR5a-12 and MR5a-9 (also reconstituted specimens) which had frictional ends. However, seating errors in tests MR5a-9 and MR5a-10 make it difficult to compare the effects of end restraints in these tests. These seating errors are discussed further in the following section.

4.4.8 Seating Errors due to Knob-and-Dimple Top Cap Type

As mentioned, the GDS triaxial system used in this study comes equipped with two types of top cap set-ups: a knob-and-dimple top cap and a top cap with a vylastic sleeve. Figure 4-12 and Figure 4-13 are close-up photographs of each of these top-cap types.

Figure 4-12: Knob-and-dimple top cap.

Figure 4-13: Top cap with vylastic sleeve.

The knob-and-dimple top cap was used for several tests in this study, but was replaced after some tests due to problems seen in the stress-strain response of specimens. As the load cell makes contact and the knob moves into place, there is potential for realigning the top of the soil specimen. Stress and strain non-uniformity in the early stages of loading can be developed as the ball seating, if not initially well aligned, pulls the specimen to the side. This can sometimes be seen from differential strains measured on each side of the specimen, and may result in pore pressure changes in the case of undrained testing, leading to changes in the mean effective stress during the early part of loading. Figure 4-14 shows the initial LVDT readings during loading for a specimen set-up with a knob-and-dimple top cap (MR5a-R7) where the sample is particularly poorly aligned. There is a slight extension on the local strain device on one side of the specimen, giving a very clear indication of tilting of the specimen. LVDT readings may not always detect the realignment to this extent, as it will depend on the direction of tilt with respect to the locations of the strain devices.

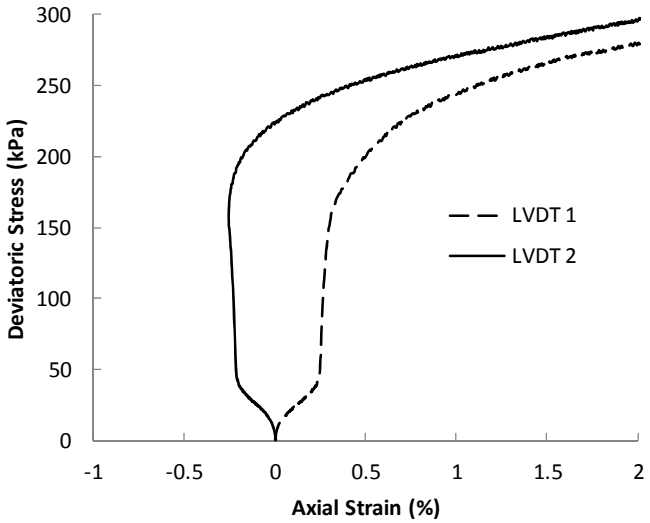

Figure 4-14: Initial LVDT readings from MR5a-R7 showing extension on one side of the specimen.

Kok (2006) completed several triaxial tests on natural clay specimens and also noticed bedding errors due to misalignment in his stress versus strain curves where the knob-and-dimple top cap was used. He attributed it to the fact that slightly eccentric docking leads to the load cell being docked on the slope side of the recess. Then, when compression begins, the load cell (i.e. knob) glides on the sloping side of the recess, and the load acting on the sample is not initially fully mobilised. When the load cell eventually becomes fully docked in the recess, the strength of the sample is mobilised, resulting in a hump feature in the stiffness-strain profile, which usually occurs at small to intermediate strains. As a result, the measured strains are overestimated and the initial stiffness is underestimated. Figure 4-15 explains the phenomenon.

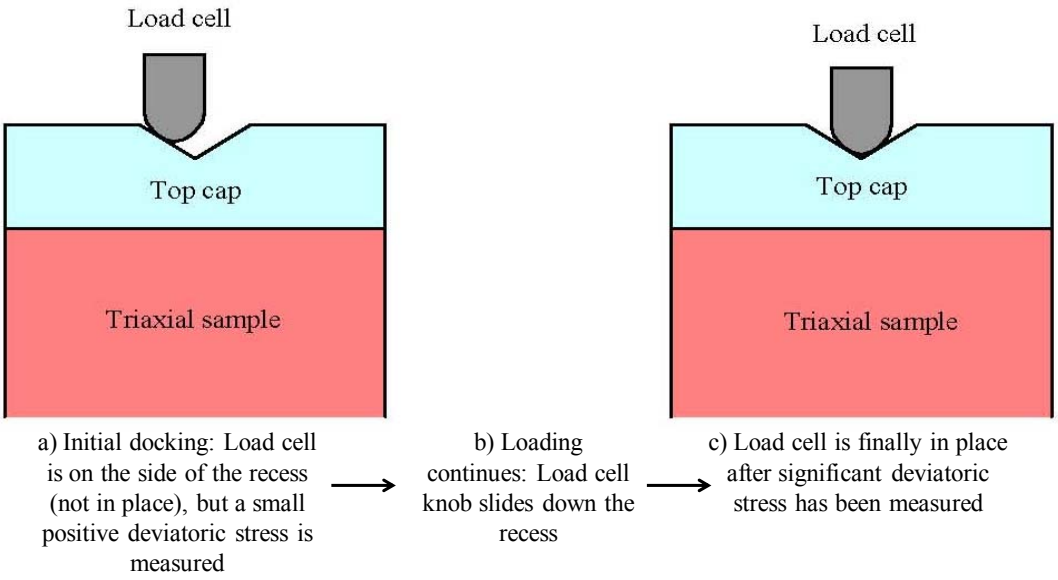

Figure 4-15: Improper docking of the load cell in the recess of the top cap (modified after Kok, 2006).

Atkinson and Evans (1985) suggested joining the load cell and the top platen at the start of the test (before any compression or consolidation phases) so that errors due to misalignment would be eliminated at the start of shearing, rather than just before the deviator stress is applied, as is often the practice. They suggested that the load cell and top platen could be joined inside the cell body by using a suction cap. This is similar to the top cap with the vyalstic sleeve set-up. Therefore, three of the undrained, normally consolidated triaxial tests on reconstituted specimens were repeated with the use of the vylastic sleeve provided by GDS. Figure 4-16 shows the undrained stress paths for these tests. Tests MR5a-R7, MR5a-R8, MR5a-R9, and MR5a-R10 were all completed using knob-and-dimple top cap configurations. MR5a-R11, MR5a-R12 and MR5a-R13 are repeats of MR5a-R7, MR5a-R8 and MR5a-R9 respectively, using the top cap with the vylastic sleeve set-up. In attempt to eliminate the phenomenon shown in Figure 4-15, test MR5a-R10 (completed with enlarged platens) had a deviatoric stress of 1 kPa applied during the consolidation stage in order to align the knob. Despite pre-alignment of the knob prior to shearing, seating errors are still significant. It is possible that although the knob appeared to be fully in place, slight misalignment of the specimen was still present.

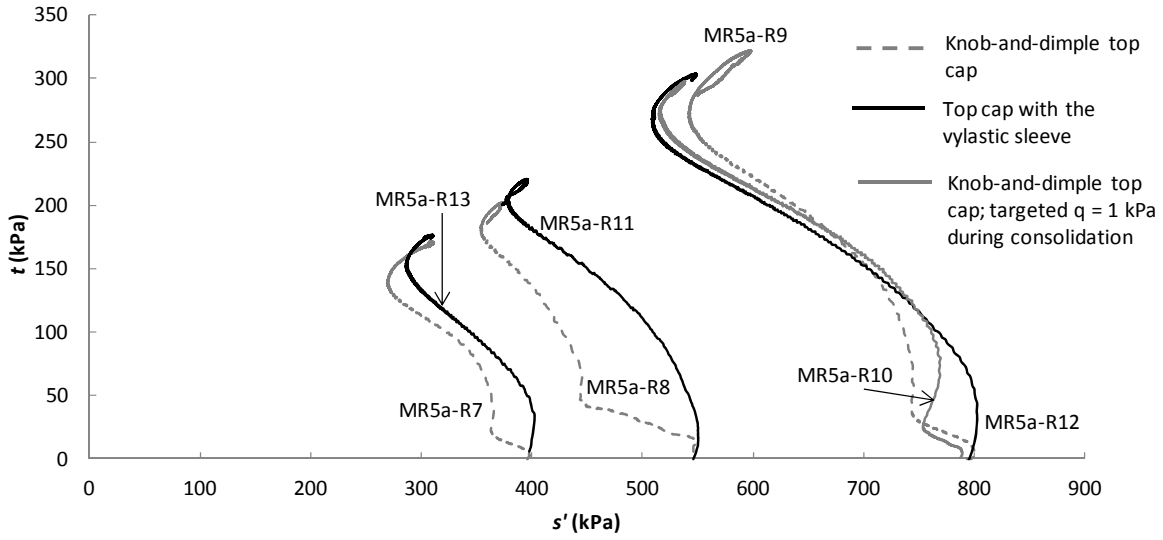

Figure 4-16: Undrained stress paths showing the difference between the knob-and-dimple top cap and the top cap with the vylastic sleeve.

The bedding errors due to misalignment in the tests with the knob-and-dimple top cap set-up can be seen in the initial part of the curves. As straining continues, the stresses readjust, giving a realistic stress path after this point which matches up well with the tests where the top cap with the vylastic sleeve was used.

The seating error is reflected in both the load cell readings as well as the pore pressure. This is demonstrated in Figure 4-17 and Figure 4-18 which show the load cell readings versus axial strain and pore pressure versus axial strain (respectively). These figures also show the corrected axial strain (using only the local LVDT readings for the first part of the stress versus strain curve) for specimens that were tested with the knob-and-dimple top cap.

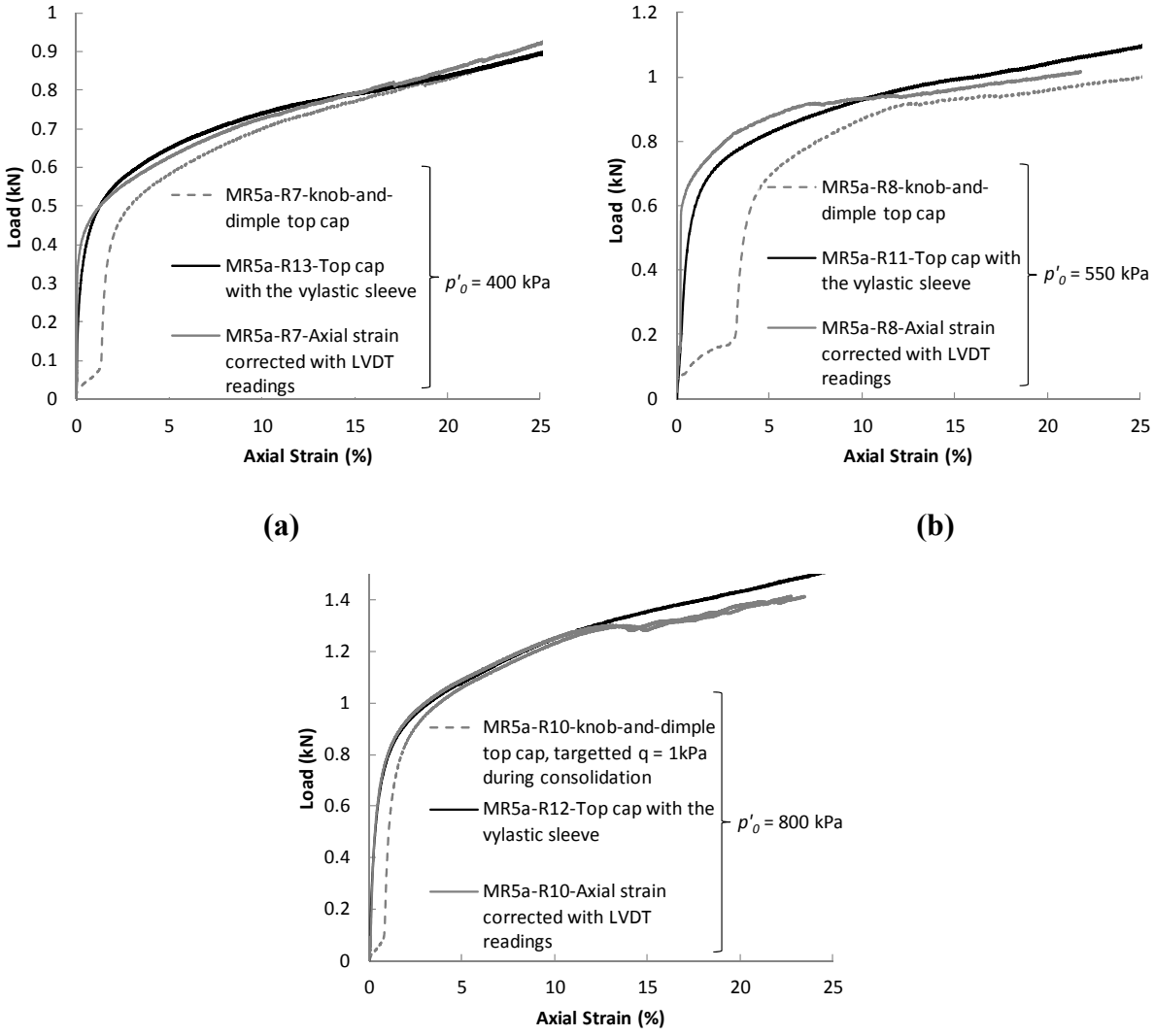

Figure 4-17: Comparison of load cell readings versus axial strain between the knob-and-dimple top cap and the top cap with the vylastic sleeve at (a) p'_0 = 400 kPa, (b) p'_0 = 550 kPa and (c) p'_0 = 800 kPa.

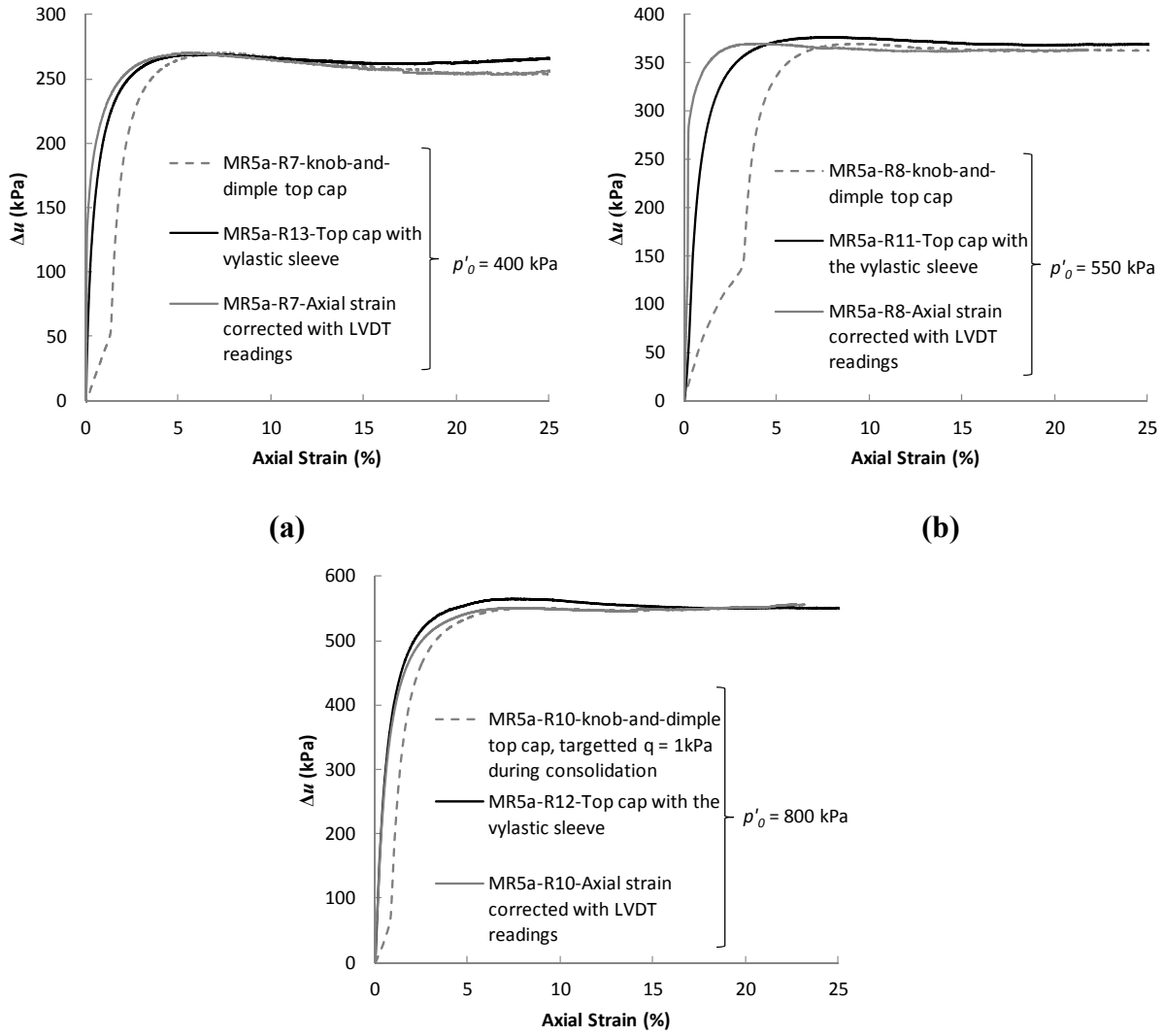

Figure 4-18: Comparison of change in pore pressure versus axial strain between the knob-and-dimple top cap and the top cap with the vylastic sleeve at (a) p'_0 = 400 kPa, (b) p'_0 = 550 kPa and (c) p'_0 = 800 kPa.

Figure 4-17 and Figure 4-18 show that the seating errors can be eliminated with the use of LVDTs wherever the results are a function of strain. A closer examination at strains from 0-4% can be found in Appendix B.

These results demonstrate that the knob-and-dimple top cap type is very susceptible to seating errors, which are exacerbated by specimen tilting and misalignment. These errors can

be reduced significantly with the use of the vylastic sleeve to attach the top cap to the load cell prior to shearing.

4.5 Oedometer Testing

Oedometer testing on reconstituted soil was performed to acquire an intrinsic compression line (ICL) (Burland, 1990), discussed in Chapter 2, Section 2.6.5. After completing trial tests on sand and clay to ensure the equipment was calibrated, three tests were performed on reconstituted Northland Allochthon clay soil from Mountain Road (soil from sample MR5c). The soil was mixed to a water content approximately equal to its liquid limit. The oedometer apparatus was controlled by air pressure, and load increments were applied through computer control. The apparatus is shown in Figure 4-19.

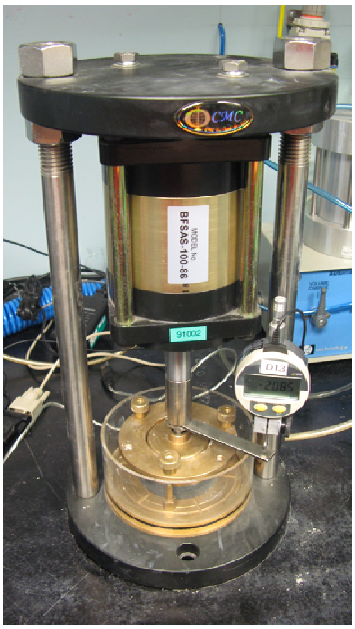

Figure 4-19: Oedometer apparatus.

The load increments were applied in the sequence suggested by Head and Epps (2011) starting with a load of 3-6 kPa as suggested for soft soils. Deformation was monitored to ensure primary consolidation was nearing completion prior to increasing the applied stress,

similar to the method used for consolidating the reconstituted soil specimens for triaxial testing in Figure 4-3. The results of the three tests are shown in Figure 4-20 and Table 4-6 where λ is the gradient of the normal compression and critical state line and κ is the slope of the swelling line.

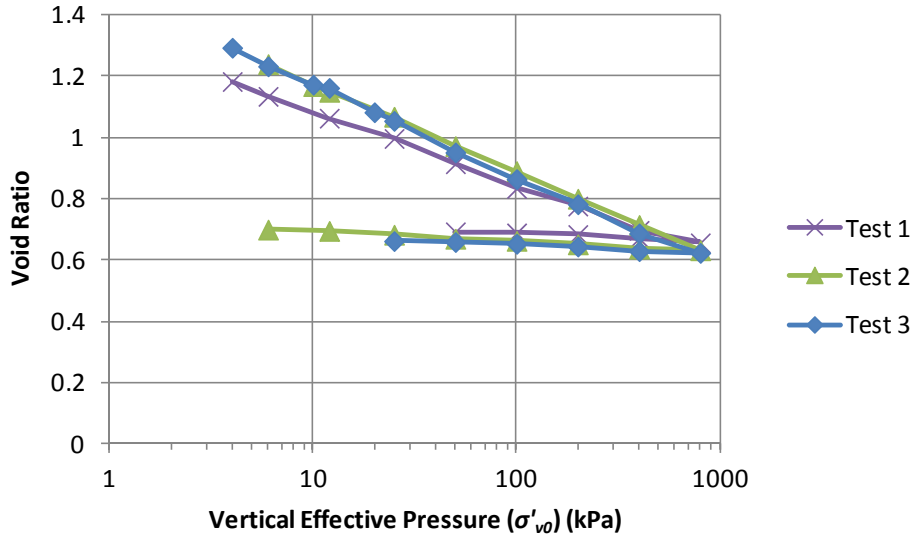

Figure 4-20: Intrinsic one dimensional compression and swelling curves from three oedometer tests on reconstituted specimen MR5c.

Table 4-6: Parameters acquired from oedometer results.

Test #	C_c	C_s	λ	κ
Test 1	0.240	0.036	0.104	0.016
Test 2	0.285	0.034	0.124	0.015
Test 3	0.308	0.033	0.134	0.014
Average	0.278	0.034	0.121	0.015

The average λ value of 0.121 is typical of clay soils and is quite similar to the typical value for London clay (λ = 0.1), and less than that for kaolin clay (λ = 0.2) (Atkinson & Evans, 1985). The relationship between λ and the plasticity index is λ/PI = 1/176, which compares

well to the value of 1/170 given by Schofield and Wroth (1968) through their examination of the relationship between these two parameters for five different clay soils. The λ/κ value is approximately 8.1, which is larger than the values for clay soils (2-5) given by Schofield and Wroth (1968) based on five clay soils.

The compression index (C_c) of reconstituted clays (i.e. the intrinsic compression index) that lie on or slightly above the A-line can be estimated using the following equation (Burland, 1990):

$$C_c = 0.253e_L - 0.04 \qquad (4.1)$$

where e_L is the void ratio at the liquid limit. While this equation has been developed from sedimentary clay soils, its use has been applied here to examine its relevance for Northland Allochthon residual clay soil, as no such relationship has been developed for residual soil. In addition, intrinsic (reconstituted) soil behaviour is independent of its natural state (Burland, 1990), which would suggest that a soil's intrinsic properties are not associated with the method of deposition (i.e. residual or sedimentary). Using this equation gives a C_c of 0.290 for two samples of residual clay soil from Mountain Road, which matches reasonably with the average C_c of 0.278 attained from the oedometer tests. The results from using this equation for these tests and several others from Mountain Road, Kaeo, and Ogles No. 3 are shown in Table 4-7.

Table 4-7: Computed and laboratory determined C_c values for samples from Mountain Road, Kaeo and Ogles No. 3 based on the liquid limit void ratio.

Sample Name	Soil Type	Water Content At Liquid Limit	Specific Gravity	e at Liquid Limit	Intrinsic C_c from oedometer results	Computed Intrinsic C_c
MR3b	Transition	0.33	2.60	0.86		0.178
MR3c	Allochthon	0.48	2.60	1.25	0.278	0.277
MR4a	Allochthon	0.49	2.63	1.29	0.278	0.287
MR5a	Allochthon	0.50	2.61	1.31	0.278	0.291
Kaeo-1	Allochthon	0.59	2.61	1.54		0.351
Sample Name	**Soil Type**	**Water Content At Liquid Limit^**	**Assumed Specific Gravity***	**e at Liquid Limit^**	**Intact C_c from oedometer results^**	**Computed Intrinsic C_c**
Ogles No. 3- 1	Allochthon	0.71	2.61	1.85	0.070	0.430
Ogles No. 3- 2	Allochthon	0.71	2.61	1.85	0.110	0.430
Ogles No. 3- 3	Allochthon	0.71	2.61	1.85	0.080	0.430
Ogles No. 3- 4	Allochthon	0.71	2.61	1.85	0.130	0.430
Ogles No. 3- 5	Allochthon	0.71	2.61	1.85	0.110	0.430

Note: Ogles No. 3 oedometer testing was performed on intact samples, not reconstituted (i.e. intrinsic)
*Specific gravity was not found for Ogles No. 3 residual or transition zone soil and was therefore estimated to be the same as the residual clay soil at Mountain Road
^Results from O'Sullivan (2009)

Intrinsic C_c values tend to be lower than that of the intact clay (Burland et al., 1996). The intact values of C_c acquired for Ogles No. 3 (O'Sullivan, 2009) appear to be suspect as they are significantly lower than computed intrinsic C_c values and are out of the range for most clays (Burland, 1990). This may have been due to the problems that occurred during the oedometer testing portion of that study (i.e. sudden increase in displacements and instrument drift) (O'Sullivan, 2009), and the difficulties associated with the oedometer testing of intact residual clay soil in general as discussed in Chapter 2, Section 2.6.3.

4.6 Triaxial Testing Results

4.6.1 Reconstituted Specimens

Figure 4-21 shows the deviatoric stress versus axial strain and the pore pressure change versus axial strain for the CU triaxial tests on both the normally consolidated and overconsolidated reconstituted specimens. Deviatoric stress is denoted as σ_a-σ_r where σ_a is

axial stress and σ_r is radial stress. Also, $\sigma_a = \sigma_1$ and $\sigma_r = \sigma_3$ in a conventional triaxial test. Figure 4-22 shows the corresponding deviatoric stress versus axial strain and volumetric strain versus axial strain for the CD tests.

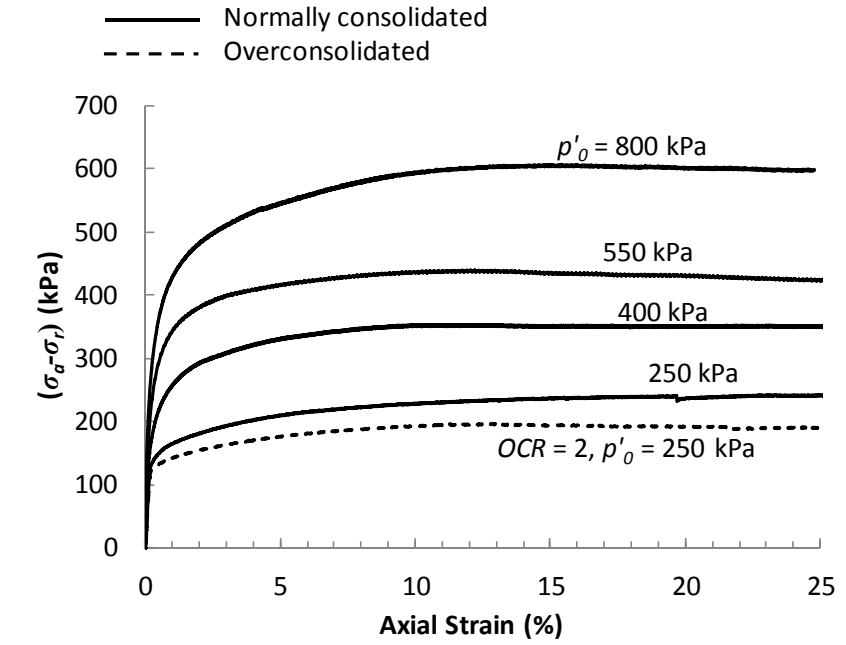

(a)

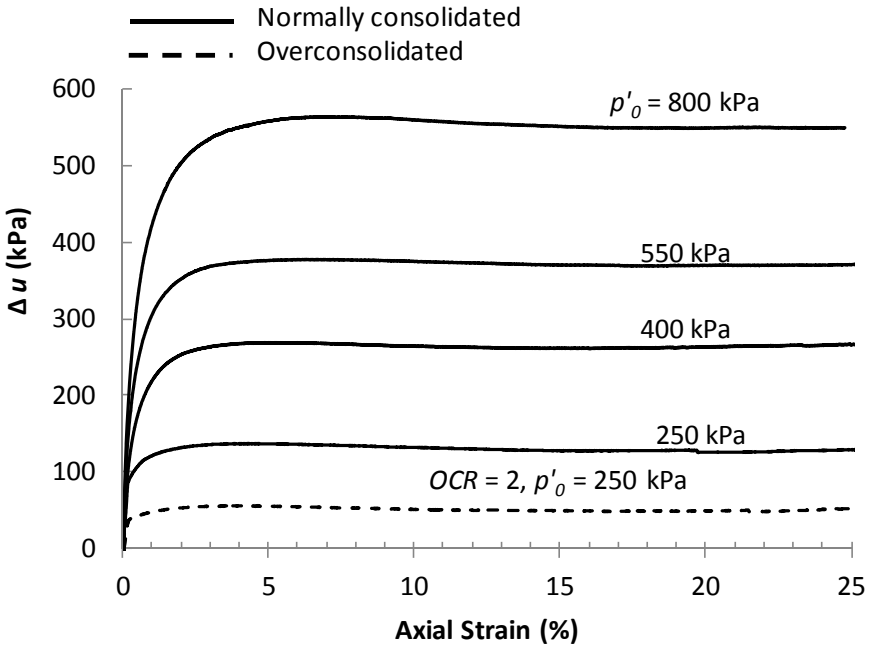

(b)

Figure 4-21: (a) Deviatoric stress versus axial strain; (b) pore pressure change versus axial strain for the consolidated undrained triaxial tests on reconstituted specimens.

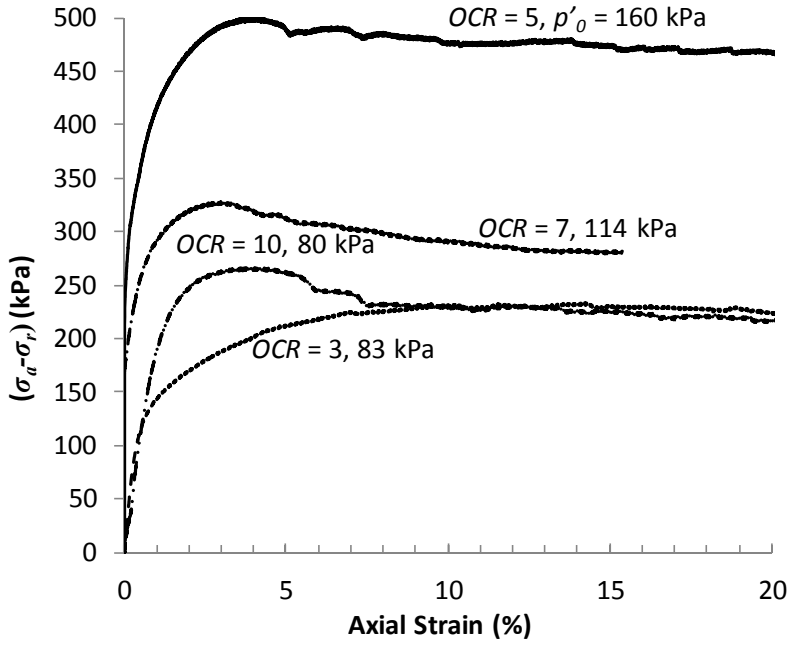

(a)

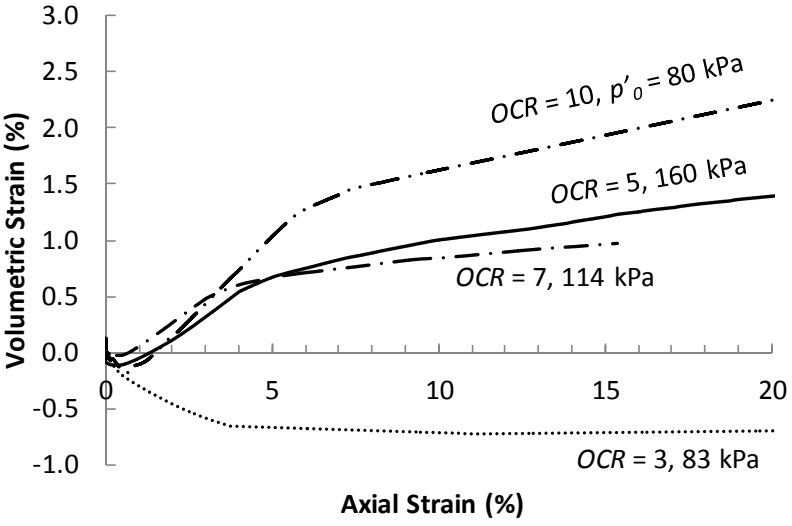

(b)

Figure 4-22: (a) Deviatoric stress versus axial strain; (b) volumetric strain versus axial strain for consolidated drained tests on reconstituted specimens.

The consolidated undrained (CU) tests performed on normally consolidated (NC) samples exhibited well-defined critical states. Failure took place after slight bulging, and most of the

samples did not develop shear bands. The CU test performed on a slightly overconsolidated sample (*OCR* of 2) exhibited similar deformation to the samples that were normally consolidated. The consolidated drained (CD) tests were performed on overconsolidated specimens, and all displayed failure along shear bands after slight bulging. The stress versus strain curves for the CD tests show post-peak reductions in shear strength, except at the lowest *OCR* of 3. Photographs of the soil specimens at failure are contained in Appendix C.

Figure 4-22 (b) shows contraction followed by dilation for the specimens at *OCR* values of 5, 7 and 10. At an *OCR* of 3, the behaviour is purely contractive. The *OCR* 7 sample shows less dilation than the *OCR* 5 sample, which was not expected. The normally consolidated intrinsic failure line in *t-s'* space is shown in Figure 4-23.

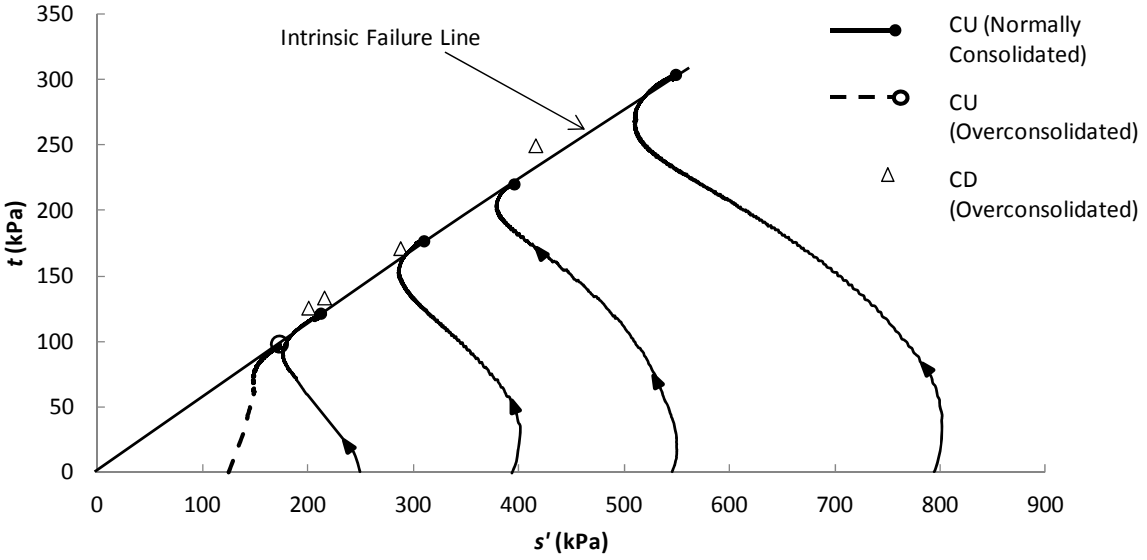

Figure 4-23: Peak strengths and undrained stress paths for the reconstituted specimens.

The intrinsic failure line is defined by the peak strengths of the normally consolidated specimens. It is very slightly curved. The intrinsic critical state angle of internal shearing resistance (φ^*_{cs}) at s' = 550 kPa is 33.6°, while at s' = 210 kPa, it is 34.9°. The peak strengths for the overconsolidated drained samples lie slightly above the intrinsic failure line. This

behaviour can also be seen in the results for all four of the stiff clays tested by Burland et al. (1996).

The effective stress paths of material give an indication of whether that material is dilatant or contractive through the change in pore pressure. Figure 4-24 demonstrates this.

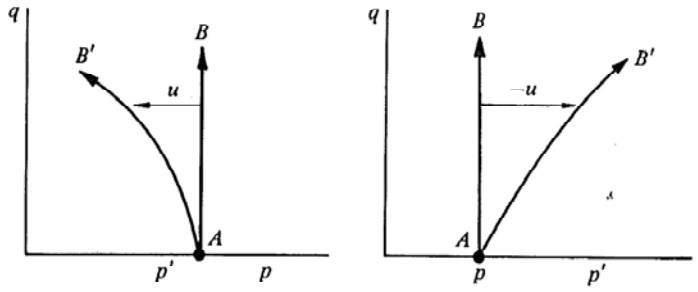

Figure 4-24: Total and effective stress paths for undrained triaxial tests on a soil that wishes to contract as it is sheared (left) and a soil that wishes to expand as it is sheared (right) (Muir-Wood, 1990).

The sharp bend to the right in the undrained stress paths in Figure 4-23 indicate the material is slightly dilatant. The shape of the stress paths for this material are very similar to the residual "red clay" of Indonesia studied by Wesley (1990), and the residual tropical clay soil of Bangladesh studied by Hossain (2001). They are unlike the stress paths for the four stiff clays examined by Burland et al. (1996), as they show a tendency to dilate (a bend to the right near the end of the test) even in normally consolidated tests on reconstituted specimens. The undrained stress paths for these soils are compared in Appendix D.

The results in Figure 4-23 have been normalized using the void ratio of each sample at failure and the one dimensional compression curves from Test 2 in Figure 4-20 to acquire the intrinsic Hvorslev strength envelope, shown in Figure 4-25.

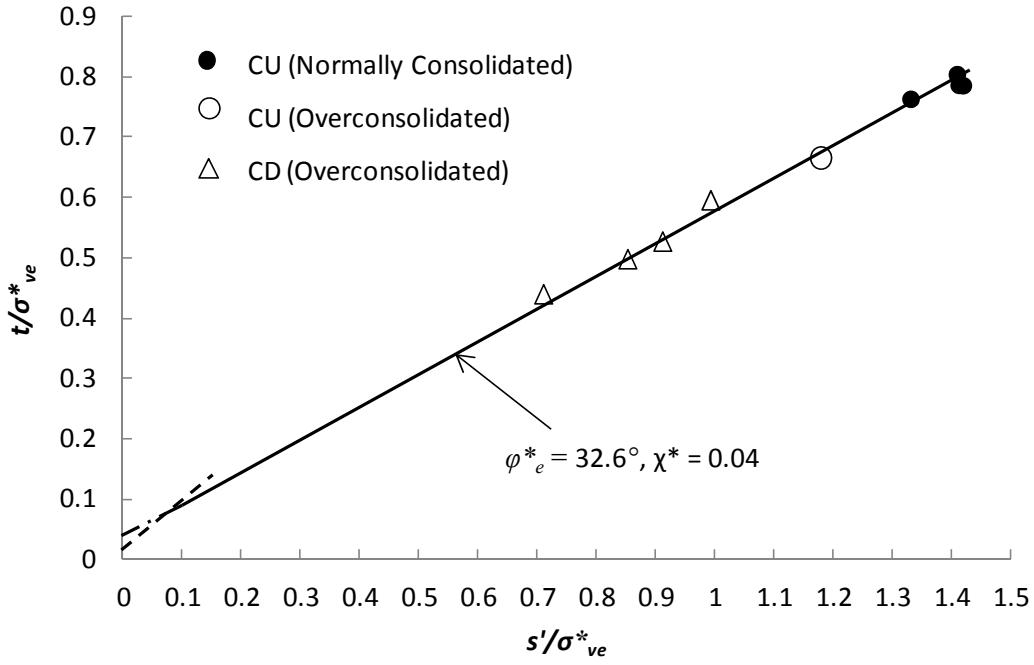

Figure 4-25: Intrinsic Hvorslev strength envelope for Northland Allochthon residual clay soil from Mountain Road.

The Hvorslev true angle of internal shearing resistance (φ^*_e) is 32.6°, shown on Figure 4-25. The intrinsic Hvorslev cohesive intercept, χ^*, is 0.04. The value of s'/σ^*_{ve} at critical state is 1.5. This is slightly higher than the four stiff clays tested by Burland et al. (1996). The three Italian clays had s'/σ^*_{ve} of 0.75 and the Corinth marl had s'/σ^*_{ve} of 1.2. The slight dilatancy of the Northland Allochthon residual clay as it approaches critical state would contribute to this higher s'/σ^*_{ve}.

A plot of the stress ratio (deviatoric stress divided by mean effective stress, q/p') versus axial strain for the normally consolidated undrained tests on reconstituted specimens is shown in Figure 4-26.

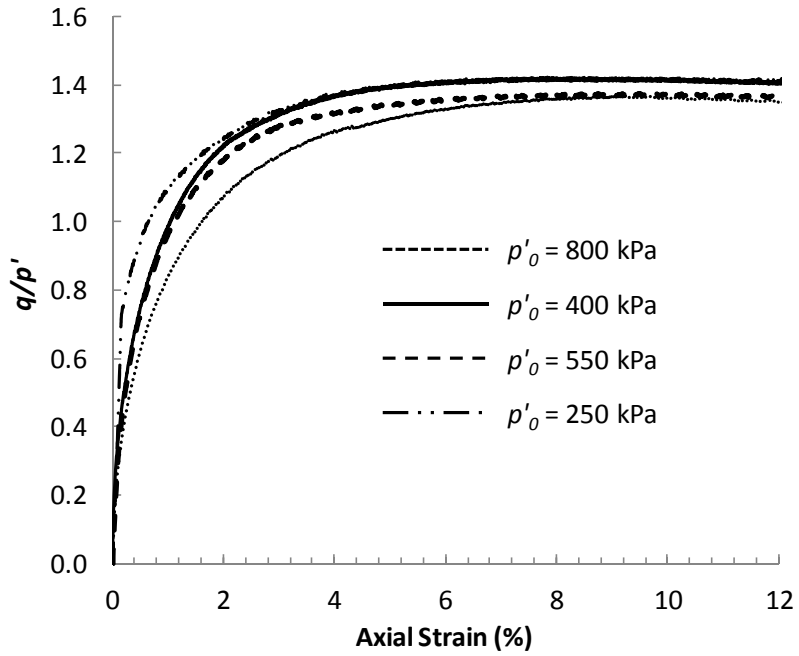

Figure 4-26: *q/p'* versus axial strain for undrained tests on normally consolidated reconstituted specimens.

The stress ratio at critical state for this soil is approximately 1.36 – 1.4. This is the value of M in the equation:

$$q = Mp' \qquad (4.2)$$

The value of φ'_{crit} can be determined from:

$$sin\varphi'_{crit} = 3M/(6 + M) \qquad (4.3)$$

Giving a value of 33.7° to 34.6° for φ'_{crit}, similar to the values of 33.6° to 34.9° from the intrinsic critical state line in *t-s'* space.

In order to examine the small strain stiffness, the secant shear modulus (G_{sec}) versus shear strain (ε_q) was examined. G_{sec} was computed as follows:

$$G_{sec} = \frac{\frac{q}{\varepsilon_a - \varepsilon_r}}{3} \qquad (4.4)$$

where q is the deviatoric stress, ε_a is the axial strain, and ε_r is the radial strain. The following equation was used to compute the shear strain:

$$\varepsilon_q = \varepsilon_a - \varepsilon_r \qquad (4.5)$$

G_{sec} versus ε_q for three of the normally consolidated reconstituted specimens is shown in Figure 4-27. G_{max} is the maximum secant shear modulus. Note that G_0 (small strain shear modulus) was not determined due to limitations on the minimum shear strain obtainable from the LVDT results. Therefore, G_{max} was used in Figure 4-27 (b) to normalize the results in lieu of G_0.

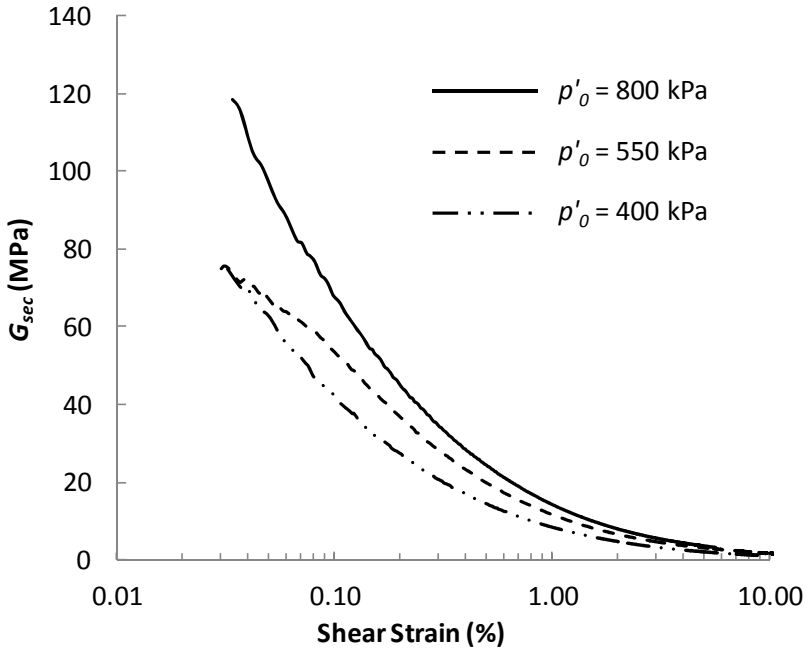

(a)

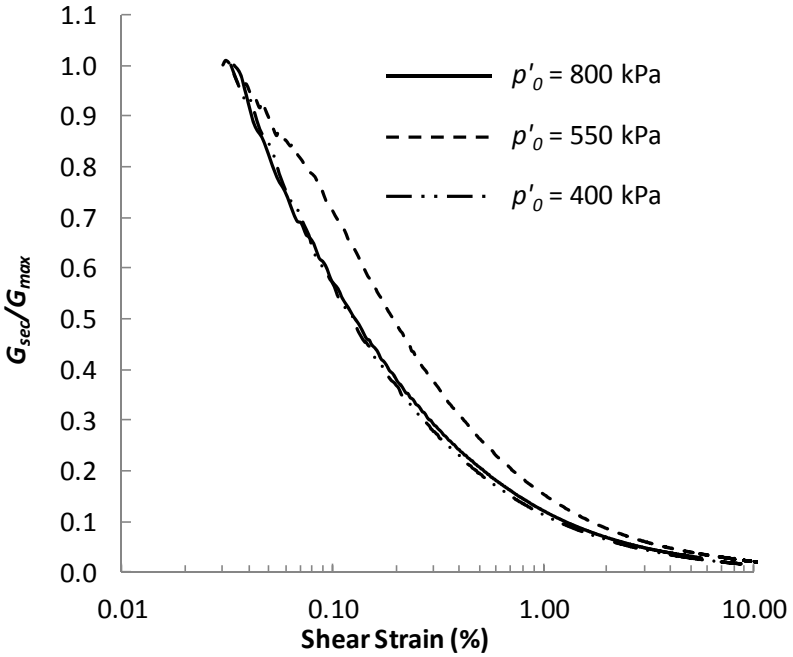

(b)

Figure 4-27: (a) Secant shear modulus (G_{sec}) versus shear strain (ε_q) and (b) G_{sec}/G_{max} versus shear strain (ε_q) for normally consolidated reconstituted specimens at p'_0 = 800 kPa, 550 kPa and 400 kPa.

Figure 4-27 (a) shows a higher G_{sec} and stiffer response for tests at a higher mean effective stress. The stiffness-strain curves are highly non-linear, which is typical of those commonly found for soils in which small strains are carefully measured (Jardine et al., 1984). Normalization of the results by p'_0 as used by some researchers (i.e. Allman & Atkinson (1992), Grammitikapoulou et al. (2008), and Hight et al. (2007)) was found to reduce the scatter between the results of the three tests only slightly, while normalization by G_{max} reduced the scatter significantly. Vardanega and Bolton (2013) also found that the maximum shear modulus, G_{max}, is successful as a normaliser for shear modulus data. In addition, Vardanega and Bolton (2013) concluded that the commonly used surrogates (such as p'_0 and c_u) are not acceptable.

4.6.2 Intact Specimens

Three triaxial tests were performed on intact specimens of Northland Allochthon residual clay all from the same vicinity at the Mountain Road site at 110 kPa (MR5c), 130 kPa (MR5d) and 190 kPa (MR5b). A range of confining pressures that would encompass the in situ effective stresses of the samples was desired. Confining pressures greater than 190 kPa were not possible due to load cell limitations. Figure 4-28 shows the deviatoric stress versus axial strain and the pore pressure change versus axial strain for these tests. Note that σ_a is the axial stress and σ_r is the radial stress, which are equivalent to σ_1 and σ_3, respectively, in a conventional triaxial test.

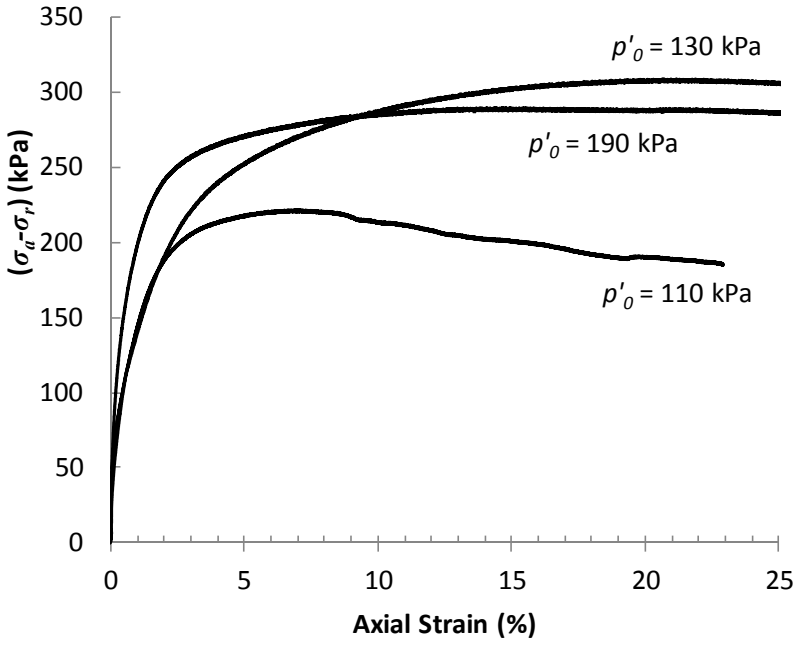

(a)

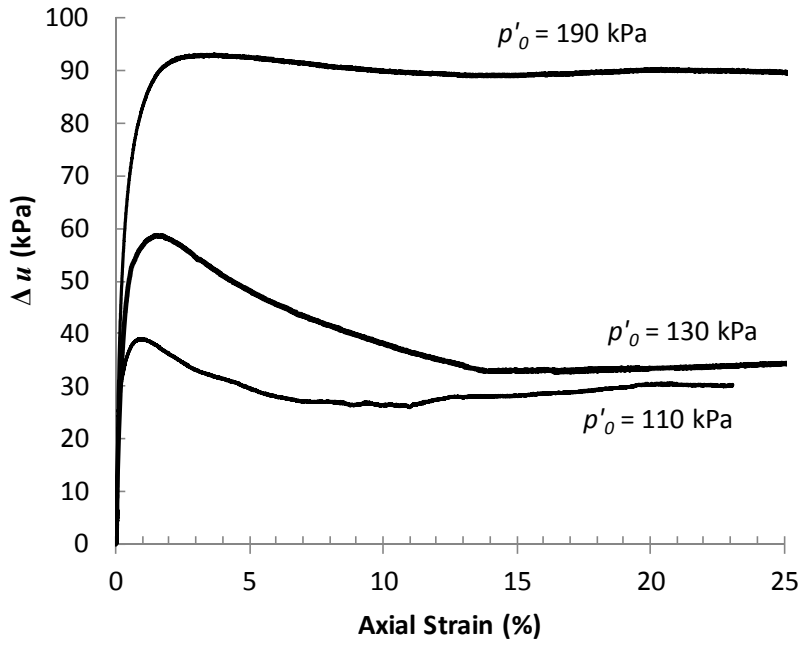

(b)

Figure 4-28: Deviatoric stress versus axial strain (a) and pore pressure change versus axial strain (b) for the consolidated undrained triaxial tests on intact specimens.

The samples tested at 190 kPa (MR5b) and 130 kPa (MR5d) exhibit well-defined critical states, and failure of these samples took place after slight bulging and development of small shear bands. The specimen tested at 110 kPa (MR5c) showed a gradual post peak reduction in strength, and developed a single slip surface. Photographs of the soil specimens at failure are contained in Appendix C.

The specimen tested at 130 kPa exhibits a higher peak deviatoric stress (q) than the 190 kPa test. Although this is not expected, this sort of behaviour does occasionally occur in intact specimens due to their variability, and can be seen in the results on drained specimens of Todi clay in Burland et al. (1996). The pore pressure change in Figure 4-28 (b) however, still exhibits a higher peak with higher confining stress.

The undrained Young's modulus of the material at 0.1%-0.2% strain is estimated to be approximately 34000 kPa from the 190 kPa test, 21000 kPa from the 130 kPa test, and 12000 kPa from the 110 kPa test. These values are of the same order of magnitude but lower than the undrained Young's modulus of 60000 kPa estimated from shear wave velocity testing at the approximate depth of these soil samples, presented in Chapter 3, Section 3.5.7. Rampello & Vigianni (2001) compared the small strain stiffness between in situ and laboratory measurement for five well-researched clays. They found that the ratio of stiffness between the laboratory and field was between 0.75 and 1 for these clays, averaging at 0.8. They deduced that different strain rates are the primary reason for the differences between laboratory and field results, and mention that sample disturbance could also play a role. It is likely that these factors are also contributing to the difference between field and laboratory measurements of Young's modulus at low strain levels (though precautions were taken to minimize sample disturbance during sample collection in the field and specimen preparation in the laboratory as discussed in Section 3.3 and Section 4.4.1).

The normally consolidated intrinsic failure line in *t-s'* space (approximated using a trend line) is shown in Figure 4-29.

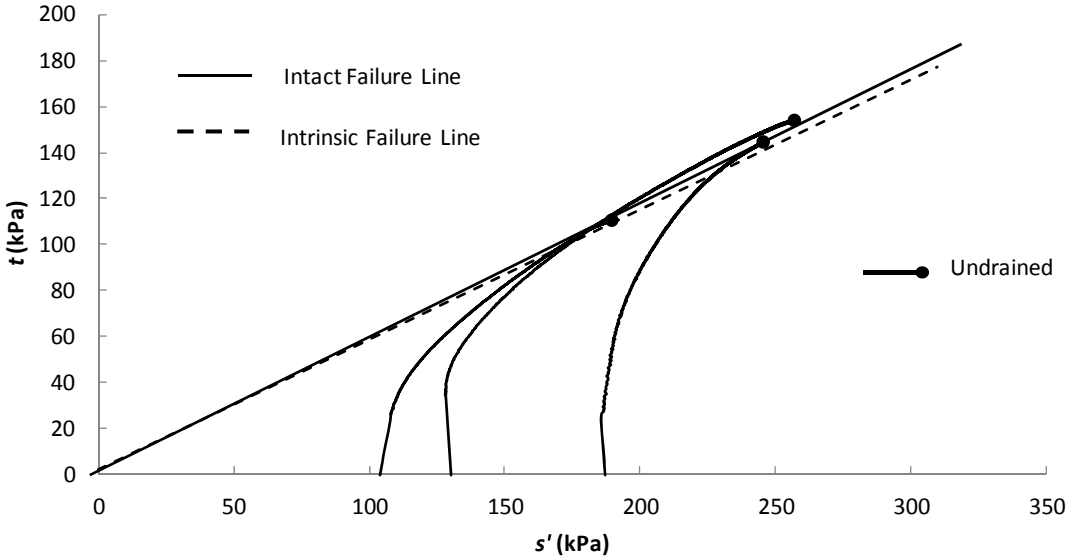

Figure 4-29: Peak strengths and undrained stress paths for the intact specimens.

These stress paths show dilatant behaviour (i.e. they are bending to right). The behaviour is more dilatant at p'_0 = 110 kPa and 130 kPa than at p'_0 = 190 kPa. Clay soils do not tend to demonstrate dilatancy except when highly overconsolidated (Plaxis, 2008; Terzaghi et al., 1996). The intact peak effective angle of internal shearing resistance from these results (φ'_{peak}) is approximately 35.6°, and the effective cohesion (c') is approximately 2.5 kPa.

The peak intact strengths lie close to the intrinsic failure line for the reconstituted material, however, this does not necessarily indicate that the microstructure of the soil is not contributing to the soil strength. Figure 4-30 evaluates where the intact soil failure envelope sits in comparison to the intrinsic failure envelope in normalized $t/\sigma^*_{ve} - s'/\sigma^*_{ve}$ space.

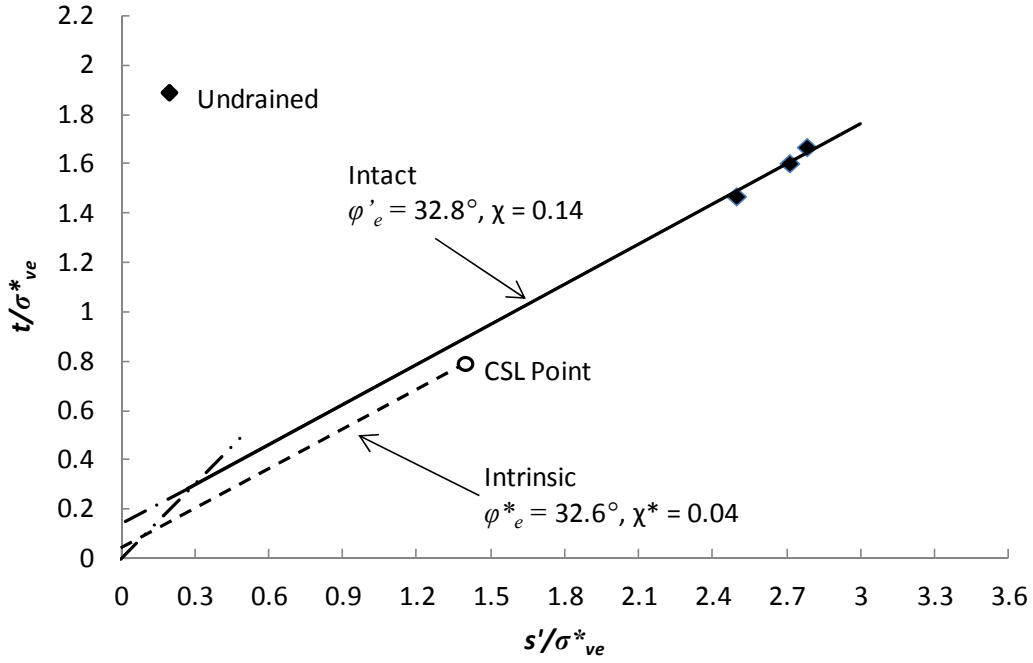

Figure 4-30: Comparison of intact and intrinsic Hvorslev failure envelopes.

The Hvorslev failure line for the intact material has been demonstrated by Burland et al. (1996) to run parallel to that of reconstituted material to the end point of the CSL, and in some clays can show some curvature after this point. The Hvorslev failure line for the intact soil from Mountain Road lies above the intrinsic line, and extends right, past the intrinsic CSL. The Hvorslev cohesive intercept for the intact material, χ, is 0.14, giving a ratio of χ/χ^* of 3.5. The ratio of the normalized strengths at intrinsic critical strength (T) is 1.2, indicating there is an influence of structure on the strength of the intact soil. This falls close to the lower end of the range of T values obtained by Burland et al. (1996) for the four stiff clays which they tested, which ranged from 1.23 to 1.5.

Research by Calabresi (1980) led to the identification of two stages of post-peak strength reduction: the first and most important occurring immediately after peak for a relative displacement of less than 1 mm; the second taking place gradually as the relative displacement increases, tending towards residual strength conditions. Calabresi found that the immediate post-peak strength envelope lies above the residual strength envelope and has an angle of internal shearing resistance corresponding approximately to the intrinsic angle of

internal shearing resistance. He suggested that the immediate post-peak strength is representative of the initial strength along a recently formed pre-existing discontinuity. Burland (1990) and Georgiannou & Burland (2001) used the term 'post-rupture strength' to define the point at which the strength drops to a reasonably constant value along the rupture surface after a relative displacement across the surface of only a few millimetres. Burland (1990) found that for Todi clay and London clay the post-rupture Coulomb strength lines are close to the intrinsic critical state Mohr-Coulomb failure lines. The post-rupture strength for the intact specimens from Mountain Road was estimated by locating the point after peak strength (and the instigation of shear bands) where approximately 3 mm of displacement had occurred. The following equations were used to obtain the intrinsic failure line and post-rupture points in Mohr-coulomb space. The shear stress (τ) was computed as follows (Craig, 2004):

$$\tau = t sin\theta \qquad (4.6)$$

where θ is defined as:

$$\theta = 45° + \frac{\varphi'}{2} \qquad (4.7)$$

where φ' is the effective angle of internal shearing resistance and can be computed from:

$$sin\varphi' = \frac{t}{s'} \qquad (4.8)$$

The effective normal stress (σ') was determined from:

$$\sigma' = s' + tcos2\theta \qquad (4.9)$$

The post-rupture Coulomb strengths compared to the intrinsic Mohr-Coulomb failure line are shown in Figure 4-31. A posture-rupture Coulomb failure envelope was estimated from a linear trend line.

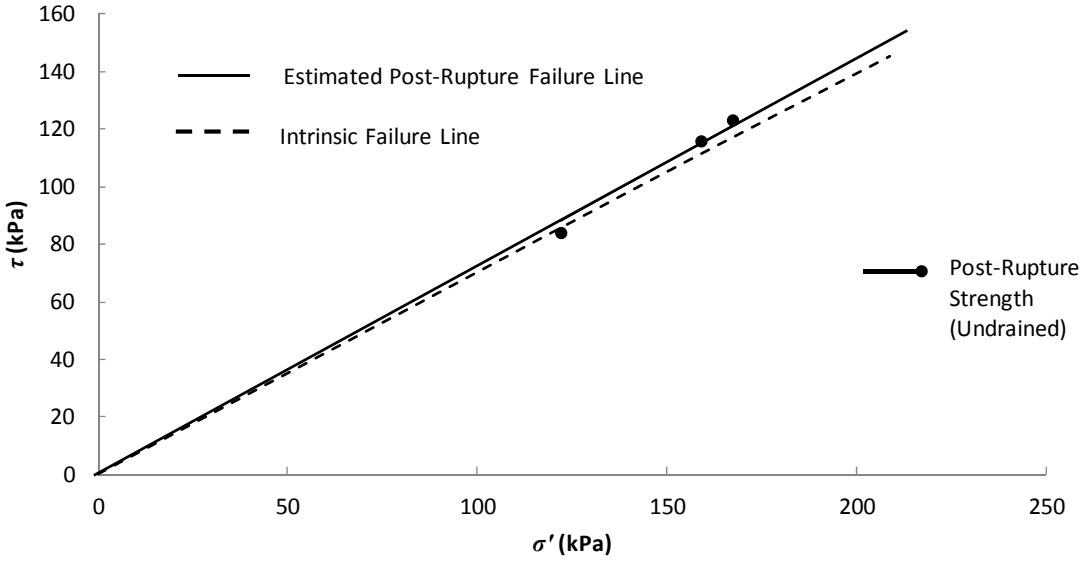

Figure 4-31: Post-rupture Coulomb strengths compared to the intrinsic Mohr-Coulomb failure line.

Figure 4-31 shows that the post-rupture strengths fall close to the intrinsic failure line. The implications of this are discussed in Section 4.7.1.

4.7 Discussion of Results

4.7.1 Critical State Angle of Internal Shearing Resistance and Operational Strength

The use of φ'_{crit} for assessing first time failure in clay slopes suggested by Skempton (1977) and Chandler (1984), and further established by several other researchers, was discussed in Section 2.5.1. Burland et al. (1996) found that the post-rupture strength for the four stiff clays examined in their study nearly coincided with φ'_{crit}, and suggested that this gives further support to the use of φ'_{crit} for evaluating first time failure in clay slopes, and provides an explanation in terms of the microstructural behaviour (e.g. the breakdown of structure has led to a reduction in strength down to critical state). The near coincidence of the Coulomb post-rupture points with the intrinsic Mohr-Coulomb failure line in Figure 4-31 suggests that φ'_{crit} is likewise a relevant parameter for evaluating first time failure in the clay soil from Mountain Road. The evaluation of reconstituted specimens from Mountain Road has given rise to a well-defined φ'_{crit}. This points to the value of testing high quality reconstituted specimens- which are more easily obtainable than intact specimens (due to the friability and

other issues associated with sample collection in Northland Allochthon soil (discussed in Section 3.3).

4.7.2 Comparison of Results to Other Soils

Burland et al. (1996) found that φ'_e was similar for intact and reconstituted specimens for all four of the stiff clays that they tested. The results for the Northland Allochthon residual clay soil also showed similar φ'_e for intact and reconstituted specimens (see Figure 4-30). The CU tests on normally consolidated reconstituted specimens of Northland Allochthon residual clay from Mountain Road reached a well-defined critical state. The value of M (1.36-1.4) corresponding to a critical state angle of 33.7° to 34.6° is quite high for a clay. It is similar to the value of M =1.38 (corresponding to an angle of internal shearing resistance of 34°) attained for reconstituted Bothkennar clay by Allman and Atkinson (1992). They attributed this high critical state angle of internal shearing resistance to the high silt content and organic content of this soil. Table 4-8 compares the critical state parameters acquired from the Mountain Road residual clay soil to several other soil types.

Table 4-8: Comparison of critical state parameters from the Mountain Road site to other soils.

Soil	λ	M	φ'_{crit} (°)
Glacial till[1]	0.09	1.18	29.5
London clay[1]	0.16	0.89	22.8
Kaolin clay[1]	0.19	1	25.4
Bothkennar clay[2]	0.18	1.38	34.1
Tropical residual clay (Dhaka- Borehole 1)[3]	0.07	1.05	25.8-26.5
Tropical residual clay (Dhaka- Borehole 2)[3]	0.06	0.96	24.2-24.4
Tropical residual clay (Dhaka- Borehole 3)[3]	0.05	0.84	21.6
Northland Allochthon residual clay (Ogles No. 3)[4]	n/a	1.03	26.0
Northland Allochthon residual clay (Mountain Road)	0.12	1.36-1.4	33.7-34.6

[1]Atkinson (1993)

[2]Allman & Atkinson (1992)

[3]Hossain (2001)

The values acquired by Hossain (2001) for tropical residual soil of Dhaka, Bangladesh were based on a limited number of tests that reached critical state. In his results, there is a clear inconsistency between boreholes 1 and 2 and borehole 3, which are all considered to be in the same formation. O'Sullivan (2009) estimated a peak strength angle of internal shearing resistance for Northland Allochthon residual clay soil at the Ogles No. 3 site to be 29.5°, and a φ'_{crit} of 26°, based primarily on CD triaxial tests. The Atterberg limits indicate that the soil acquired at the Mountain Road site has a higher silt content (lower plasticity) than the soil acquired at the Ogles No. 3 site, which could, in part, explain the higher M (and φ'_{crit}) for this soil. The variation in the values of φ'_{crit} acquired by Hossain (2001) for tropical residual clay, and the differences in this parameter in Northland Allochthon residual clay between the Ogles No. 3 site (O'Sullivan, 2009) and the Mountain Road site suggest that the critical state parameters of residual soils that are considered to be of the same formation can vary between locations. Atkinson (1993) suggested that the intrinsic critical state parameters (λ and M) may vary due to differences in grading and mineralogy from sample to sample, and depend primarily on the nature of the soil. Rahardjo et al. (2004) state that residual soil properties vary from region to region due to their heterogeneous nature and highly variable degree of

weathering, controlled by regional climatic and topographic conditions and the nature of the bedrock. In residual soils, different degrees of weathering due to location could certainly alter the mineralogy as well as the grading of the soil, and this is discussed further in Section 4.7.3. Note that Harris (2013) acquired a φ'_{peak} of 36° for the Northland Allochthon residual clay soil from the Whangai Formation, though no φ'_{crit} is mentioned.

Muir-Wood (1990) summarizes the relation between *PI* and *M* in the following equation based on data from Mitchell (1976) for several normally compressed soils:

$$sin\varphi' = 0.35 - 0.1\ln(PI) \qquad (4.10)$$

This equation has been developed from sedimentary soils. No such relationship has yet been developed from residual soils. It has been applied here in order to compare how well the relationship holds for Northland Allochthon residual clay soil. Using this relationship, φ'_{crit} is approximately 29.5° to 30.4° for the Mountain Road site and 26.2° to 27.8° for the Ogles No. 3 site (compared to 34° and 26° from triaxial tests, respectively). The correlation, though loose, holds reasonably well and demonstrates that a lower *PI* will result in a higher φ'_{crit}.

For Bothkennar clay, the Muir-Wood relationship of *M* to *PI* results in a φ'_{crit} of 26.5° based on a *PI* of 38. Allman and Atkinson (1992) obtained a φ'_{crit} of 34° from reconstituted triaxial results, therefore for this soil type, this relationship does not hold well. However, when the organic content was removed from the Bothkennar clay, the *PI* reduced to 18-20 (Albert et al., 2003), resulting in an estimated φ'_{crit} of 30°-31° from the Muir-Wood *M-PI* relationship, which is a notably better match to the φ'_{crit} of 34° acquired from triaxial testing results. The relationship between *PI* and *M* (after Muir-Wood 1990) with the addition of data from the Northland Allochthon residual clay as well as Bothkennar clay and Dhaka clay (from three boreholes) is shown in Figure 4-32.

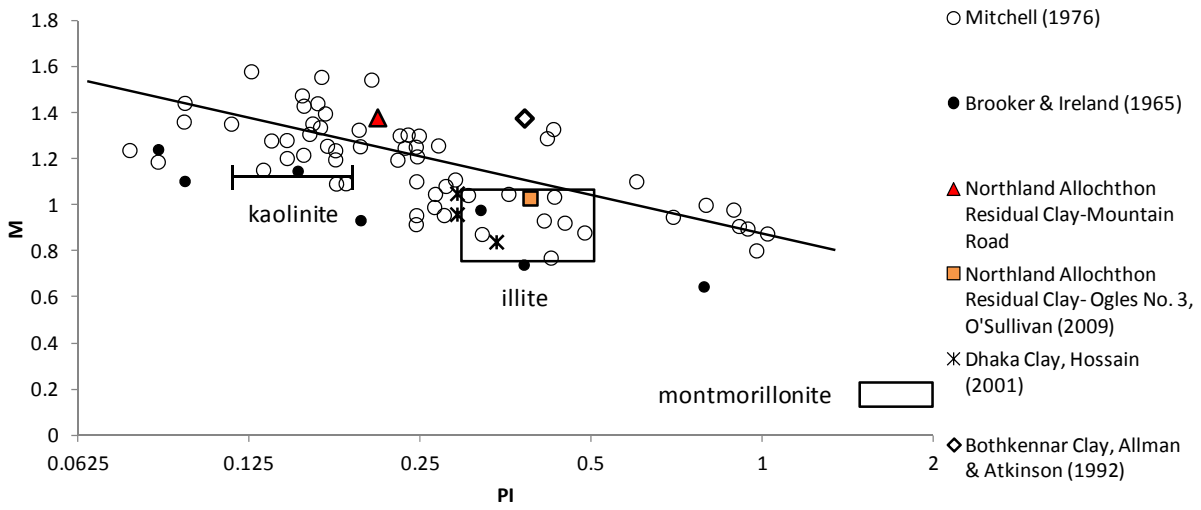

Figure 4-32: Relationship between *M* and plasticity index (*PI*) after Muir-Wood (1990).

Figure 4-32 shows that the residual clay soil from Mountain Road falls close to the trend line. It is offset above it and outside the realm of the pure soils of koalinite and illite, suggesting that the presence of multiple clay minerals are playing a role in its plasticity index and strength at critical state.

Further substantiation to the argument that the high φ'_{crit} of the Mountain Road soil is related to its higher *LI* can be found by examining correlations between *LI* and the residual angle of internal shearing resistance from numerous clays by Mesri & Cepeda-Diaz (1986). Based on their correlations, the residual angle of internal shearing resistance should be 12°-14° for the Ogles No. 3 soil. Values of 11°-14° were obtained from shear box tests (O'Sullivan, 2009). For the Mountain Road site, the *LI* correlates to a residual angle of internal shearing resistance of 21°-22°. It follows that φ'_{crit} is likely to be much higher at Mountain Road as well.

Clays undergo either turbulent or sliding shearing mechanisms as they fail. The type of mechanism that will govern depends on the plasticity of the clay and the content of platy clay minerals. Clays undergoing turbulent shearing are those with a low content of platy clay minerals while clays that undergo sliding shearing are those with a high content of these minerals (Lupini et al., 1981). Vaughan et al. (1978) suggested that the *PI* could provide a

dividing line. Clays having a *PI* less than 25 undergo turbulent shear at large strain so that peak and residual angles of internal shearing resistance are similar. Clays having a *PI* greater than 30 undergo sliding shear so that residual angles of shearing resistance are much lower than peak. The use of *PI* as an indicator of the type of shearing has restricted applicability. Large inter-void spaces (such as in Allophane rich clays or clays with high organic content) can produce turbulent shearing and dilatant stress path behaviour.

The undrained strength of low plasticity clay is strongly influenced by water content as the soil undergoes turbulent shearing, and its behaviour in an overconsolidated state is basically ductile (Gasparre, 2005). Plastic clays, instead, undergo sliding shearing, so their peak undrained stress is controlled by the initial stress before shearing, and their shearing behaviour in an overconsolidated state is generally brittle (Figure 4-33). The brittleness is thought to be due to the presence of bonding, as this increases the peak strength of the material, but has no influence on the large strain strength (Jardine et al., 2004).

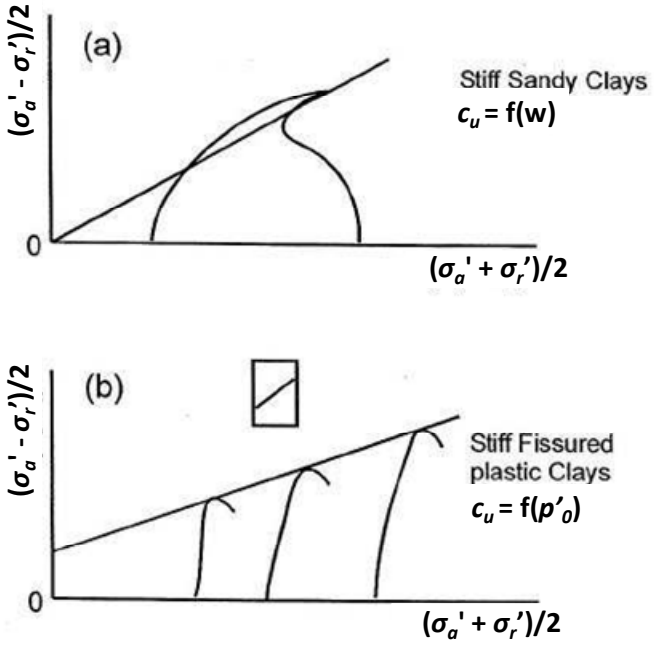

Figure 4-33: Idealized undrained shearing behaviour of overconsolidated clays with (a) low plasticity and (b) high plasticity (modified after Jardine et al., 2004).

Comparing Figure 4-33 to the stress paths the of Northland Allochthon clay, the Northland Allochthon clay is more akin to the stiff sandy clays in Figure 4-33 (a) than the stiff fissured plastic clays in Figure 4-33 (b). The behaviour at lower confining pressures (the first curve in Figure 4-33 (a)) is similar to the intact specimens (Figure 4-29). The reconstituted specimens (which were tested at higher confining pressures) behave very similarly to the second curve in Figure 4-33 (a). Although the Northland Allochthon residual clay soil examined in this study has been classified as a medium to high plasticity clay, its stress path behaviour is more similar to a low plasticity clay (that is overconsolidated, even in the normally consolidated state). This can be explained by the amount of platy clay minerals, as discussed above. The MR soil has a *PI* of under 25 (it is 21), and it is therefore likely to be undergoing turbulent shearing, causing some dilatancy in its stress path behaviour. In addition, the high organic content contributes to larger inter-void spaces which could also be playing a role in causing turbulent shearing and dilatant behaviour. This dilatant stress path behaviour in the absence of overconsolidation is also seen for the Indonesian residual red clay examined by Wesley (1990), which has a high plasticity, and the Bangladeshi residual clay examined by Hossain (2001), which has a medium to high plasticity (Appendix D).

4.7.3 Summary of Properties and Behaviour of Northland Allochthon Clay Soil

This section summarizes the main findings regarding the properties and behaviour of Northland Allochthon soil from this study and other studies.

The soil properties for the residual Northland Allochthon clay soil are summarized in Table 4-9. Table 4-10 summarizes results for transition zone soil. Note that these tables include the more commonly used soil parameters, and some parameters obtained by other authors (such as those from the volumetric water content analysis performed by Harris (2013)) have not been included. In the tables, φ_{res} is the residual angle of internal shearing resistance, φ^b is the unsaturated angle of internal shearing resistance, and CSD indicates constant sheared stress drained triaxial test.

Table 4-9: Summary of Northland Allochthon residual clay soil properties from this study and other studies.

Parameter	Unit	Field Site	Results from this thesis		*Results from other studies*		
			Mountain Road	Kaeo	*Ogles No. 3* [1]	*Silverdale* [2]	*Silverdale* [3]
		Complex/ Formation	Undifferentiated Mélange, predominantly Mangakahia Complex mudstones	Undifferentiated Mangakahia Complex	*Mangakahia Complex-Hukerenui Mudstone*	*Mangakahia Complex-Whangai Formation*	*Mangakahia Complex-Hukerenui Mudstone*
General Properties							
γ	**kN/m^3**		18-19.3		*20*	*17-18, 17.2* [3]	*17.4*
γ_{dry}	**kN/m^3**					*13-14, 12.9* [3]	*12.2*
k_x	**m/second**					*8.85 x 10^{-10}*	
k_y	**m/second**				*1x10^{-11} (field); 4.8 x 10^{-7} and 1.5 x 10^{-8} (lab)*	*10.19 x 10^{-10}*	
G_s			2.61	2.61		*2.59-2.65* [#]	
Strength Parameters							
c'	**kN/m^2**		2.5		*6*	*0, 1*, 0* [CSD], *20.6-33.6* [unsat]	
φ'_{peak}	°		35.6		*30*	*27*, 36, 41* [CSD]	
φ'_{crit}	°		33.7-34.6		*25^, 26*		
M			1.36-1.4		*1.03*		
φ^b	°					*20, 33*	
φ_{res}	°				*11-14*	*19*	
Stiffness Parameters							
λ	**(intrinsic)**		0.12				
κ	**(intrinsic)**		0.05				
λ	**(intact)**				*0.04*		
Plasticity Indices							
PI			21.4-23.8	31.5	*38.6-40.1*	*49* [#], *45* [3]	*76*
LL	%		48-50.1	59	*69-72.9*	*80* [#], *70* [3]	*110*

[1] O'Sullivan (2009)

[2] Harris (2013) unless otherwise specified by * or [#] or [3]

[3] Lentfer (2007)

*Tilsley (1998) as cited in Harris (2013)

^Value obtained from correcting O'Sullivan (2013) results with area correction- discussed in Section 5.4

[#] Melrose & Willis (2010) as cited in Harris (2013)

[CSD] Strength properties acquired from CSD triaxial tests (Harris, 2013) rather than standard CD or CU

[unsat] Value acquired from unsaturated triaxial tests (Harris, 2013)

Table 4-10: Summary of Northland Allochthon transition zone soil properties from this study and other studies.

Parameter	Unit		Results from this thesis	*Results from other studies*		
		Field Site	Mountain Road	*Ogles No. 3* [1]	*Silverdale* [2]	*Silverdale* [3]
		Complex/ Formation	Undifferentiated Mélange, predominantly Mangakahia Complex mudstones	*Mangakahia Complex-Hukerenui Mudstone*	*Mangakahia Complex-Whangai Formation*	*Mangakahia Complex-Hukerenui Mudstone*
General Properties						
γ	**kN/m^3**				*17.6* [3]	*20.4*
γ_{dry}	**kN/m^3**				*11.5-15, 12.9* [3]	*16.9*
k_y	**m/second**				*1 x 10^{-10} - 2x 10^{-9}*	
G_s			2.6			
Strength Parameters						
c'	**kN/m^2**			*0*	*19; 22-23*, 4* [CSD], *20.7* [unsat]	
φ'_{peak}	°			*26*	*16; 24-31*, 21* [CSD]	
φ [b]	°				*20*	
φ_{res}	°				*9*	
Plasticity Index & Liquid Limit						
PI			9.4-10	*21.2*	*70* [#]	*35*
LL	%		33	*49.1*	*109* [#]	*54*

[1] O'Sullivan (2009)

[2] Harris (2013) unless otherwise specified by * or [#]

[3] Lentfer (2007)

*Tilsley (1998) as cited in Harris (2013)

[#] Melrose & Willis (2010) as cited in Harris (2013)

[CSD] Strength properties acquired from CSD triaxial tests (Harris, 2013) rather than standard CD or CU

[unsat] Value acquired from unsaturated triaxial tests (Harris, 2013)

The soil properties in Table 4-9 and Table 4-10 show substantial variation between the four field sites, particularly for the strength parameters and the Atterberg limits. However, there does appear to be a loose correlation between *PI* and the strength parameters, such a φ'_{peak}, as shown by the trend line in Figure 4-34. Note that there are two values for φ'_{peak} from the Silverdale site (Whangai Formation). One result is from Harris (2013) and the other result is from Tilsley (1998) (as cited in Harris (2013)). Only one *PI* result is available from this site, performed by Melrose and Willis (2010) (as cited in Harris (2013)).

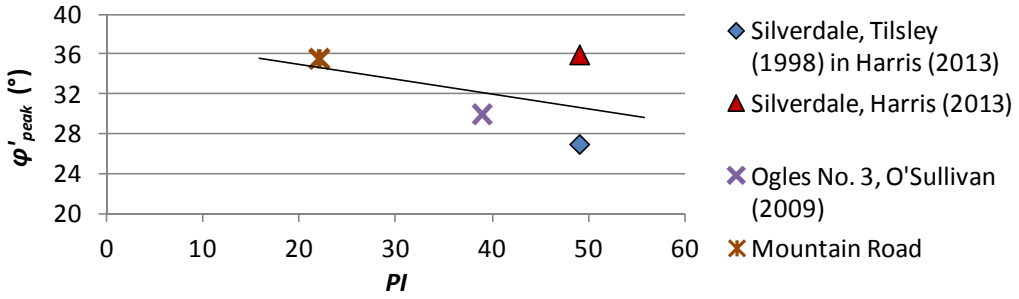

Figure 4-34: φ'_{peak} versus *PI* for Northland Allochthon residual clay soil from three field sites.

The effects of the varying degrees of weathering were mentioned in Section 4.7.2. Research by Rahardjo (2004) on Singapore residual soils provides further evidence of the tendency for the properties of residual soils to vary geographically and with depth due to different degrees of weathering. Rahardjo et al. (2004) found that the residual soil from Bukit Timah (a geological formation) had a liquid limit ranging from 20%-40% and a plastic limit ranging from 40%-60% due to different degrees of weathering. The angle of internal shearing resistance was found to range between 27° and 38°, and the specific gravity ranged between 2.55 and 2.78 (due to varying mineralogy imparted by differences in the amount of weathering).

The cohesion in the Northland Allochthon residual soil was found to be quite low (0 – 6 kPa) from all three of the sites where triaxial testing was performed, but Harris (2013) and Tilsley (1998) as cited in Harris (2013) found the transition zone had significantly higher cohesion. Harris (2013) also alluded to the likelihood that different (lower) cohesion in the residual soil was from significantly more weathering of the clasts which are present in the transition zone soil. Harris (2013) also found that there was a significant difference between the cohesion in CSD (constant stress drained) triaxial testing results compared to the CD triaxial testing results (as shown in Table 4-10). This suggested that the failure mechanism (i.e. a stress path induced from either a CD or CSD, as described in Section 2.4) drastically affected the exhibited shear strength parameters of the soil.

In addition to the aspects of Northland Allochthon residual soil behaviour from other studies discussed in Section 2.4, the following points summarize the main aspects of the soil behaviour that have been noted during this study:

- The appearance of a pseudo-preconsolidation pressure in the soil at Mountain Road from in situ testing results was discussed in Chapter 3. The slightly dilatant behaviour of the intact specimens demonstrated by their undrained stress paths means that they are behaving as overconsolidated at these confining pressures. This provides further substantiation to the overconsolidated behaviour of the soil under the conditions generally encountered (i.e. shallow slips), and the likelihood of a pseudo-preconsolidation pressure. O'Sullivan (2009) also found that triaxial testing results of soil from the Ogle's No. 3 site displayed a behaviour similar to that of an overconsolidated clay, which is discussed in Section 2.8.2 (under the Cam-clay model), though no evidence of a preconsolidation pressure was found in the oedometer testing results of that study.
- O'Sullivan (2009) stated that Northland Allochthon residual soil, by some definitions, could be considered a structured soil, and recommended that this be included as a topic for future research. Following the technique established by Burland (1990) to compare intact specimens to reconstituted specimens where the structure has been reduced to its intrinsic state, it has been demonstrated in this chapter that soil structure contributes to an increased strength in the residual soil from the Mountain Road site. In addition, the post-rupture Coulomb strength of the soil is close to that of the critical state strength, suggesting that the reduction in strength due to the breakdown of structure brings the soil strength towards critical state. This suggests that φ'_{crit} can be an important parameter for modelling first time failure in Northland Allochthon clay slopes, an advantage of which is that critical state strength can be acquired from reconstituted specimens, which are much easier to obtain.
- Slope failure mechanisms as examined in this thesis and other studies in Northland Allochthon clay slopes are briefly discussed in Section 6.4.1.

4.8 Conclusions

Triaxial testing was completed on reconstituted and intact specimens of Northland Allochthon residual clay soil from the Mountain Road site. Samples were prepared according to the ASTM standard and LVDTs were used for local strain measurement. Seating errors occurred with the use of the knob-and-dimple top cap, but were resolved with the use of the top cap with the vylastic sleeve. Triaxial testing of reconstituted Northland Allochthon clay soil had not been performed prior to this study, and it provides a method for determining the intrinsic soil properties for comparison to intact specimens.

Oedometer testing was completed on reconstituted soil in order to acquire an intrinsic compression curve to be used for normalizing the Hvorslev strength envelopes. A λ value of 0.121 was acquired which is typical of clay soils. The C_c value acquired was 0.278. This value matches well with the C_c obtained from the relationship derived by Burland (1990) between C_c and the liquid limit.

The CU tests performed on NC reconstituted samples exhibited well-defined critical states, and formed the intrinsic failure line. The Hvorslev true angle of internal shearing resistance (φ^*_e) was found to be 32.6°. The intrinsic Hvorslev cohesive intercept, χ^*, was 0.04. The value of M (1.36-1.4) corresponding to a critical state angle of 33.7° to 34.6° is quite high for a clay, and higher than the value acquired for the Ogles No. 3 site of 26° (O'Sullivan, 2009). A correlation made by Muir-Wood (1990) relating M (and therefore also φ'_{crit}) to the PI indicates that the higher φ'_{crit} is likely related to the low PI. These results suggest that selecting a φ'_{crit} for Northland Allochthon residual clay soil can be based approximately on the PI of that soil.

The shape of the stress paths for the undrained reconstituted specimens appear to be slightly dilatant prior to reaching peak strength. This dilatant behaviour could be attributed to turbulent shearing, which is typical in clay soil with a PI less than 25 (Vaughan et al., 1978).

The Hvorslev cohesive intercept for the intact material, χ, is 0.14, giving a ratio of χ/χ^* of 3.5. The ratio of the normalized strengths at intrinsic critical strength (T) is 1.2. These results indicate that the microstructure of the intact soil is stronger than that of the reconstituted soil and that bonding plays a role in the strength of the intact soil. The value of φ'_e was not

affected, which suggests that the difference is cohesive in nature (i.e. related to the Hvorslev cohesive intercept only). The influence of microstructure on the strength of the Northland Allochthon residual clay soil falls within the range of that determined for the four sedimentary clays examined by Burland et al. (1996).

The post-rupture Coulomb strengths for the intact specimens were plotted with the Mohr-Coulomb intrinsic failure line. Near coincidence of the Coulomb post-rupture points with this line suggests that φ'_{crit} is a relevant parameter for evaluating first time failure in this soil, as it demonstrates that the degradation of structure reduces the soil strength to critical state. Reconstituted specimens from Mountain Road have produced a well-defined φ'_{crit}, suggesting that there is value in testing reconstituted specimens. This is an important finding because reconstituted specimens are significantly easier to obtain than intact specimens, given the difficulties associated with acquiring high quality undisturbed samples in this soil type.

The results in this chapter provide groundwork for interpreting future laboratory tests on intact samples of Northland Allochthon residual clay soil, as well as in situ tests, and have demonstrated that soil structure contributes to the shear strength of this soil type.

The soil properties of Northland Allochthon residual soil from this study and other studies have been summarized in a tabular format in this chapter. This can be used as a reference for practitioners. A comparison of the soil properties between field sites reveals that they vary substantially, which is an important consideration for practitioners working with this problematic soil. The use of simple Atterberg limits tests can give an indication of the expected soil behaviour at a given site, given that *PI* loosely correlates to the angle of internal shearing resistance at peak strength, and also, as mentioned, at critical state.

5.0 Numerical Simulation of Triaxial Tests

5.1 Introduction

The Mohr-Coulomb (MC) model, Hardening Soil (HS) model, Hardening Soil small (HS small) model, and Cam-clay model are introduced in Section 2.8.2 (Chapter 2). In this chapter, these constitutive models are used to examine the behaviour of the soil at the Ogles No. 3 site and the Mountain Road site by comparing numerical simulations of triaxial tests to triaxial laboratory results. The results in this chapter from the Ogles No. 3 site provide a basis for the soil parameters used in following chapters. As the Cam-clay model has been developed based on other reconstituted clay soils, an examination of whether reconstituted Northland Allochthon residual clay soil from the Mountain Road site can be represented with this model is performed.

5.2 Influence of Soil Parameters on Soil Behaviour

The following sections describe the influence of basic soil parameters on the observed soil behaviour in each of the constitutive models considered.

5.2.1 Mohr-Coulomb and Hardening Soil Models

Elastic Properties: Young's Modulus and Poisson's Ratio

The elastic properties in the Mohr-Coulomb model can be defined either through the shear modulus (G) and bulk modulus (K), or Young's modulus (E) and Poisson's ratio (v). For this analysis, the latter two have been utilized. Changes in E alter the initial slope of the stress versus strain curve, as shown in Figure 5-1 (a), where q is the deviatoric stress and ε_a is the axial strain. Changes to v affect the initial slope of the volumetric strain, ε_{vol} versus axial strain curve in a drained triaxial test. Note that ε_{vol} is given as ε_p in Figure 5-1 (b). A lower v will result in a lower initial slope of this curve, as shown in Figure 5-1. (In undrained tests, v is 0.5 as there is no change in volume).

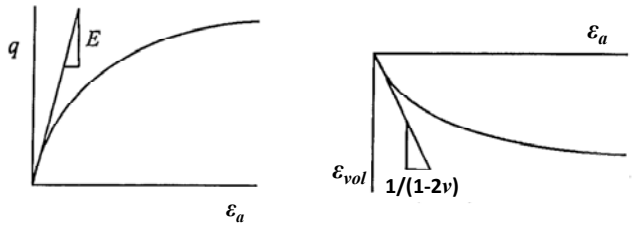

(a) **(b)**

Figure 5-1: Young's modulus and Poisson's ratio from initial stages of a conventional drained triaxial test (modified after Muir-Wood, 2004).

Elastic Properties in the Hardening Soil Model

Unlike plasticity based models, the elastoplastic HS model (described in Section 2.8.2) does not involve a fixed relationship between the drained triaxial stiffness and the oedometer stiffness for one dimensional compression. Instead, these stiffnesses are inputted independently. E_{oed} is the tangent stiffness modulus. Figure 5-2 shows how E_{oed}^{ref} is determined from oedometer test results. The value of p^{ref} is at a vertical effective stress of $\sigma'_1 = \sigma'_3/K_0^{NC}$ (where K_0^{NC} is the coefficient of lateral earth pressure at rest under normally consolidated conditions, σ'_3 and σ'_1 are the minor and major principal effective stresses, respectively). Note that Figure 5-2 is based on an oedometer test which is a drained test and there is no distinction between total and effective stress. Therefore σ_1 in the figure could also be labelled σ'_1.

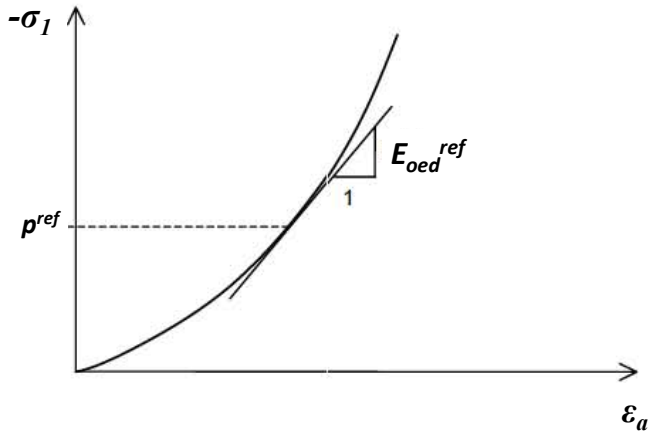

Figure 5-2: Definition of E_{oed}^{ref} in oedometer test results (modified after Plaxis, 2008).

The power *m* is applied in the derivation of all three stiffness parameters. In essence, it allows the stiffness of the soil to change hyperbolically depending on the current stress. This can be described by the following relationship (as an example, E_{50} and E_{50}^{ref} are used. E_{ur} and E_{ur}^{ref} have the same relationship. E_{oed}^{ref} also has the same relationship, except that σ'_3 is divided by K_0^{NC}):

$$E_{50} = E_{50}^{ref} \left(\frac{c\cos\varphi' - \sigma'_3 \sin\varphi'}{c\cos\varphi' + p^{ref}\sin\varphi'}\right)^m \qquad (5.1)$$

The default value in Plaxis for *m* is 0.5. To simulate logarithmic compression as seen in soft clays, *m* should be taken equal to 1 (Plaxis, 2008). Figure 5-3 below depicts how E_{50} varies with E_{50}^{ref} at different values of *m* (while φ', σ'_3 and p^{ref} remain constant at 25°, 5 kPa, and 100 kPa respectively). It shows that at an *m* value of 0.5, E_{50} will be higher (stiffer) than at an *m* of 1 for any given E_{50}^{ref} value.

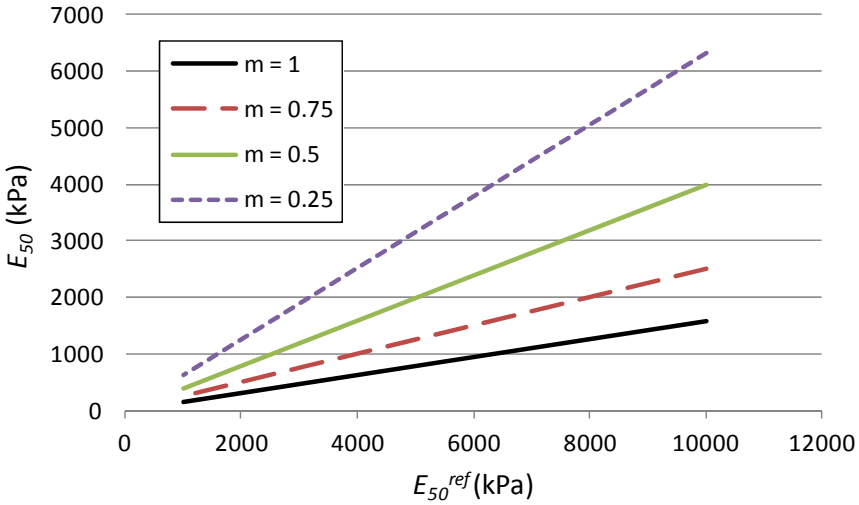

Figure 5-3: E_{50} versus E_{50}^{ref} at different values of m (φ'= 25°, σ'_3= 5 kPa and p^{ref}= 100 kPa).

The HS small model is similar to the HS model, but it incorporates an initial (or very small strain) shear modulus G_0 and a shear strain level ($\gamma_{0.7}$) at which the secant shear modulus (G_{sec}) is reduced to about 70% of G_0. The G_0 value is used instead of Young's modulus at very small strains (less than 1 x 10^{-6}). G_0 and $\gamma_{0.7}$ therefore influence the very initial elastic behaviour of the soil. They enable the simulation of the non-linear decrease in soil stiffness with increasing strain in the initial part of the stress-strain curve.

Strength Properties: Angle of Internal Shearing Resistance, Cohesion and Dilatancy

Increases to the angle of internal shearing resistance or the cohesion in a numerical model will alter the failure envelope of the soil and result in higher peak or critical state strength.

The peak angle of internal shearing resistance depends on the angle of dilation (ψ), which in turn depends on density and pressure. Shear stress versus shear strain curves for tests with the same angle of internal shearing resistance, but different dilatancy values are shown in Figure 5-4. Both the volume changes and the apparent strengths vary with the angles of dilation. Shear strain is denoted as ε_q.

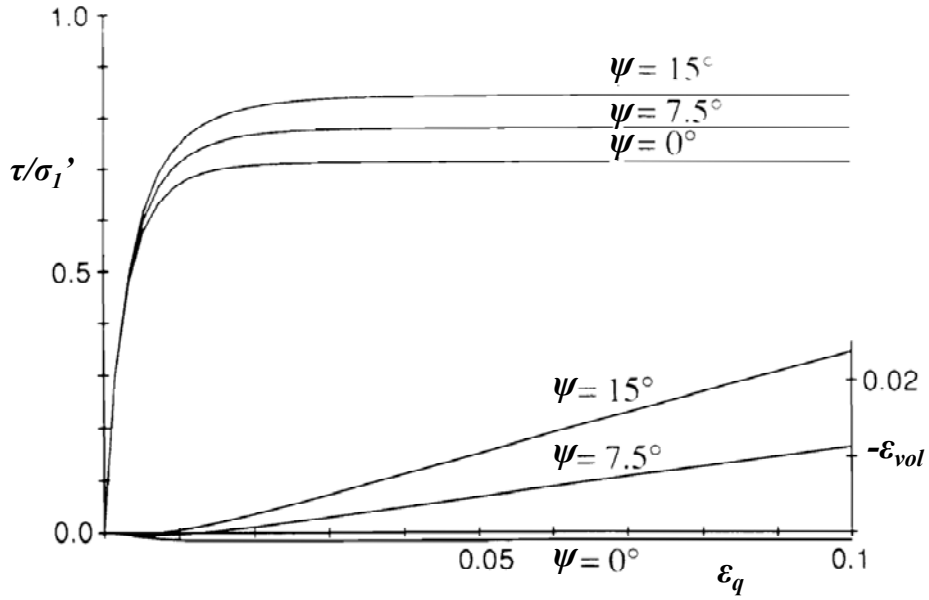

Figure 5-4: Shear stress versus shear strain curves for different dilatancy values (modified after Houlsby, 1994).

A slope stability problem was examined by Zienkiewicz et al. (1975). Two slopes with the same angle of internal shearing resistance (20°) were examined. One slope had an angle of dilation of 0°, and the other had a theoretical dilation angle value of 20°. The deformations of the slope are shown in Figure 5-5, and are found to be rather different. Factor of safety analysis was also performed by reducing tan(φ') and cohesion in the same proportions until failure (similar to phi-*c* reduction performed in Plaxis, which is discussed further in Chapter 6). The factor of safety was found to be unaffected by the angle of dilation. This is because although the amount and direction of movement has changed, the location of the slip surface and the original strength parameters along it (φ' and c') remain unaltered.

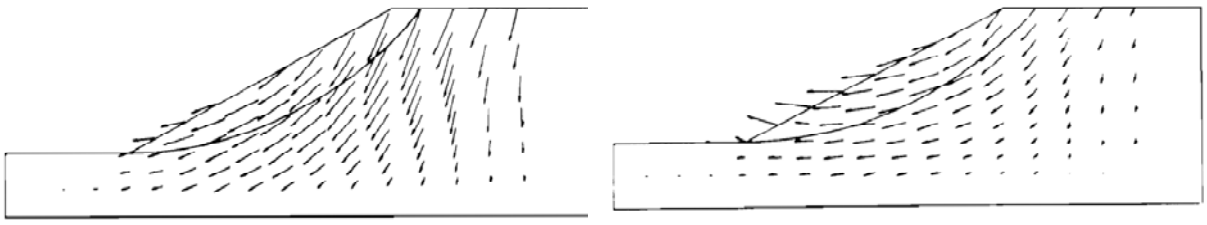

Figure 5-5: Deformation of a slope with $\psi = 0°$ (left) and $\psi = 20°$ (right) (Zienkiewicz et al., 1975).

5.2.2 Cam-Clay Model

Elastic Properties: Poisson's Ratio, Lambda, Kappa and Initial Void Ratio

Kappa (κ) and the initial void ratio (e_0) characterize the elastic response of the soil. The hardening rule incorporates lambda (λ), which characterizes the plastic response of the soil (along with the slope of the critical state line (M)). The magnitude of the plastic strain that occurs is controlled largely by λ-κ (i.e. the difference between the two values) rather than the values of λ and κ themselves (Muir-Wood, 2004).

Strength Properties: Slope of the critical state line

As discussed in Chapter 4, M is linked to the critical state angle of internal shearing resistance (φ) in triaxial compression. Numerically, an increase in M will result in an increase in the ultimate strength of the soil under examination.

5.3 Procedure for Numerical Simulations of Triaxial Tests

The procedure for element testing was performed in stages to coincide with the stages performed on the triaxial test in the laboratory. This included applying gravity loading, consolidation to the desired effective stress, and then applying axial strain to 25%. Each of these steps (aside from gravity loading) was performed using consolidation analysis in order to ensure the same time frame as the actual triaxial test. The geometry of the model is the same as the actual laboratory test, and is shown in Figure 5-6.

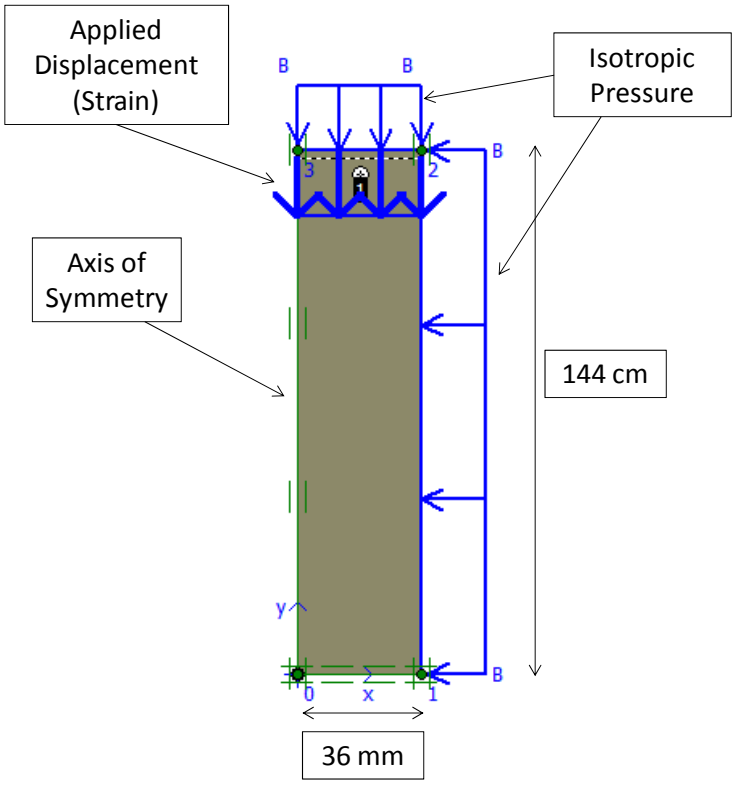

Figure 5-6: Model set-up for element tests in Plaxis.

The following sections show comparisons between the laboratory results and the results of the numerical simulations. It should be noted that there were significantly more numerical simulations performed (with varying soil parameters) than those shown in order to assist with validating the constitutive models utilized. In addition, for each of the soils and constitutive models, the selected parameters were examined against at least one other laboratory test under a different confining pressure. A small number of the numerical simulation results were selected for presentation in this chapter. The parameters that were varied in the simulations presented were found to be the most difficult to select, and to have the largest influence on matching the numerical and laboratory behaviour.

5.4 Ogles No. 3 Site

Numerical simulations of triaxial tests were performed for the residual soil from the Ogles No. 3 site in O'Sullivan (2009). The soil is reanalysed here with slight changes to the soil properties. In addition, the deviatoric stress results have been area-corrected as discussed

below. The base soil properties were estimated from the laboratory testing results from O'Sullivan (2009), and are shown in Table 5-1. Certain parameters in Table 5-1 (E^{ref} and E_{50}) were varied to determine their influence on how well the constitutive models matched the actual lab testing results. The parameters k_x and k_y are the hydraulic conductivities in the horizontal and vertical directions, respectively. The hydraulic conductivity at this site was determined from on-site dataloggers which is discussed further in Section 6.4. Although Northland Allochthon soils are presumed to have some degree of anisotropy, variation between k_x and k_y are often due to the layering of the soil and the effects of a vertical overburden stress (Al-Tabbaa & Wood, 1987). Harris (2013) found that for Northland Allochthon residual clay soil acquired from the Silverdale site examined in his study (Whangai Formation), there appeared to be little difference between the horizontal and vertical permeability of the soil. He also states that as a residual soil, this is expected because there is no deposition which causes a layering effect, and hence leads to anisotropic permeability and in situ stress as discussed by Wesley (2010a). O'Sullivan (2009) also presumed k_x was equivalent to k_y for the Ogles No. 3 site. Based on the above information, it seems reasonable to assume that k_x is equal to k_y for the purpose of this study.

Note that during triaxial testing, the cross sectional area of the soil specimen is usually corrected during the consolidation and shearing phases, as the area of the specimen will increase. For this correction, it is assumed that the specimen deforms as a right circular cylinder, and it is used in the standard test method (ASTM D4767) for CU tests. The area correction is given by the following equation.

$$A_c = \frac{A_o(1-\varepsilon_{vol})}{1-\varepsilon_a} \qquad (5.2)$$

where A_c is the corrected area of the specimen, A_o is the initial area of the specimen, ε_{vol} is the volumetric strain and ε_a is axial strain. The deviatoric stress (q), which is computed by dividing the load cell reading by the cross-sectional area of the specimen, is slightly reduced when the area correction is used. The area correction was not used in O'Sullivan (2009), but was applied during this investigation to results available from that study, which resulted in a reduction in the φ'_{crit} value from the original estimation by O'Sullivan (2009) of 26° to 25° (shown in Table 5-1). The value of φ'_{crit} has been used instead of φ'_{peak} because the soil

parameters are being assessed for use in the examination of a slope (Chapter 6) undergoing first time failure (as discussed in Section 2.5.1).

Table 5-1: Soil parameters used in numerical simulation of triaxial tests on intact Ogles No. 3 soil.

Soil Properties			
Model	**Parameter**	**Units**	**Value**
MC	E^{ref}	kN/m^2	5000
	ν		0.25
HS	E_{50}^{ref}	kN/m^2	5000
	E_{oed}^{ref}	kN/m^2	4000
	E_{ur}^{ref}	kN/m^2	22500
	power (m)		0.1
HS Small	$\gamma_{0.7}$		0.0001
	G_0^{ref}	kN/m^2	40000
HS, HS Small & Mohr-Coulomb	γ (unsat)	kN/m^3	20
	γ (sat)	kN/m^3	20
	k_x	m/day	0.064
	k_y	m/day	0.064
	c	kN/m^2	6
	φ	°	25
	ψ	°	2

5.4.1 Intact Soil: Hardening Soil, Hardening Soil Small and Mohr-Coulomb

This section examines the suitability of the HS, HS small and MC models for representing the behaviour of intact soil at Ogles No. 3. The Cam-clay model was also considered as a constitutive model for intact soil at Ogles No. 3. However, a thorough examination was not performed due to the heavily overconsolidated behaviour of this soil (sitting "dry" of critical state) and the unavailability of modifications to the Cam-clay model for this situation in Plaxis, as discussed in Chapter 2, Section 2.8.2.

The results for the HS, HS small, and MC models are shown in Figure 5-7 and Figure 5-8. In the legend, p'_0 refers to the initial effective stress of the test. The parameters used are as shown in Table 5-1 unless otherwise stated in the legend.

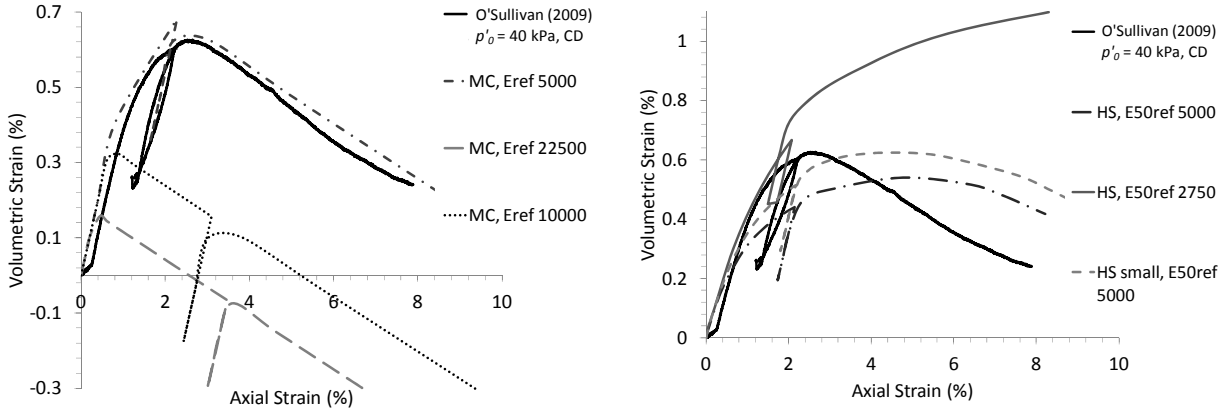

Figure 5-7: Volumetric strain versus axial strain- Mohr-Coulomb (left) and Hardening Soil and Hardening Soil small models (right) in Plaxis.

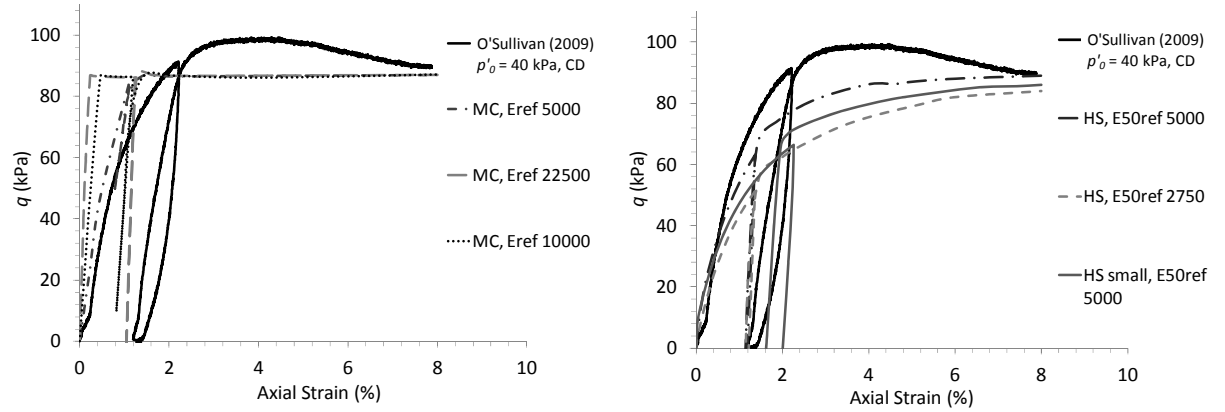

Figure 5-8: Deviatoric stress versus axial strain- Mohr-Coulomb (left) and Hardening Soil and Hardening Soil small models (right) in Plaxis.

5.4.2 Conclusions on Constitutive Models for Ogles No. 3 Site

The results show a good match of the MC model to triaxial results for volumetric strain versus axial strain with the soil parameters as shown in Table 5-1. An E^{ref} of 5000 kPa is more suitable than the higher values of 10000 kPa or 22500 kPa. The deviatoric stress versus axial strain behaviour is best captured by the HS model due to its strain hardening capabilities. An E_{50}^{ref} of 5000 kPa is more suitable than the lower value 2750 kPa which allows for excessive volumetric strain. The MC model as well as the HS model with an E_{50}^{ref} of 5000 kPa both underestimate the peak strength by approximately 13 kPa. The MC model underestimates the critical state strength by 3 kPa, while the HS model with E_{50}^{ref} of 5000 kPa underestimates it by less than 1 kPa. The HS model with an E_{50}^{ref} of 2750 kPa underestimates it by 5 kPa. The HS small model with an E_{50}^{ref} of 5000 kPa underestimates the critical state strength by 6 kPa. The HS small model appears to best represent the unload reload loop in deviatoric stress versus axial strain space.

Muir-Wood (2004) stated "The more complex the model, the more the modelling itself will obscure the underpinning mechanics of soil behaviour and the geotechnical system behaviour which we are trying to probe and understand". The modelling of DSM columns in Northland Allochthon slopes involves varying stratigraphy, soil-structure interaction, and varying groundwater levels. The HS and HS small models are significantly more complex than the MC model. As the MC model is well understood and has provided a reasonable match to the soil behaviour, it has been selected as the primary constitutive model for the numerical analysis performed in the following chapters of this thesis.

5.5 Mountain Road Site

The geometry of the numerical simulations of triaxial tests performed on the Mountain Road specimens was identical to Figure 5-6 for the tests on intact specimens. This was reduced to 50 mm in diameter and 100 mm in height for the tests examining reconstituted specimen behaviour, so as to be identical to the actual laboratory dimensions. (However, specimen dimensions do not affect the results. This is because the cell pressure is applied to the sample homogenously, and the sample weight is negligible in comparison to the external stress level (Xing-Cheng, pers. comm., 2014a)).

The soil parameters used for the numerical simulation of triaxial tests on Mountain Road soil were derived from laboratory testing results presented in Chapter 4. Table 5-2 shows the reconstituted soil parameters and Table 5-3 shows the intact soil parameters. The intact tests were undrained. Undrained effective stress analysis with undrained strength parameters was used in Plaxis. For the reconstituted soil from Mountain Road, the Cam-clay and MC models have been examined. For the intact soil, the MC model has been examined.

Table 5-2: Soil parameters used in numerical simulation of triaxial tests on reconstituted Mountain Road soil.

Soil Properties			
Model	**Parameter**	**Units**	**Value**
Mohr-Coulomb	E^{ref}	**kN/m^2**	17500
	c	**kN/m^2**	2
	φ	°	36
	ψ	°	0
Cam-Clay & Mohr-Coulomb	ν		0.25
	γ **(unsat)**	**kN/m^3**	20
	γ **(sat)**	**kN/m^3**	20
	k_x	**m/day**	0.064
	k_y	**m/day**	0.064
Cam-Clay	λ		0.121
	κ		0.015
	e_0		0.9
	M		1.37

Table 5-3: Soil parameters used in numerical simulation of triaxial tests on intact Mountain Road soil.

Soil Properties			
Model	**Parameter**	**Units**	**Value**
Mohr-Coulomb	E^{ref} **(undrained)**	**kN/m^2**	20000
	c **(undrained=** c_u**)**	**kN/m^2**	110
	φ **(undrained)**	°	0
	ψ	°	0
	ν **(undrained)**		0.495
	γ **(unsat)**	**kN/m^3**	20
	γ **(sat)**	**kN/m^3**	20
	k_x	**m/day**	0.064
	k_y	**m/day**	0.064

5.5.1 Reconstituted Soil: Cam-Clay

The Cam-clay model was evaluated for the reconstituted CD test with an *OCR* of 3. A preconsolidation pressure of 250 kPa was applied to the soil, initiated prior to allowing the soil to swell back to 83 kPa. The *OCR* and κ were varied from the "Base Model". For the Base Model, the soil parameters shown in Table 5-2 were used. Figure 5-9 and Figure 5-10 show the volumetric strain versus axial strain and deviatoric stress versus axial strain results. In the legend, "p'_0" indicates the effective stress of the test (in kPa).

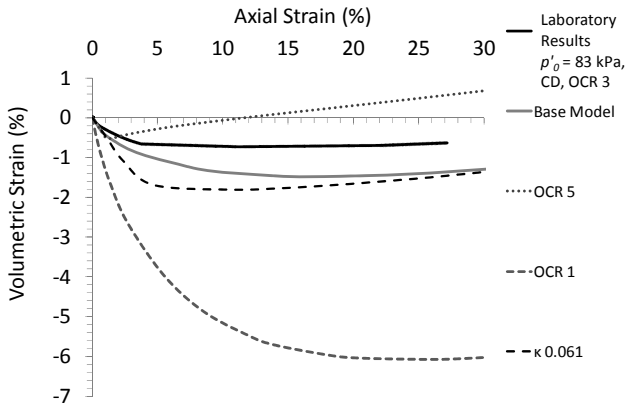

Figure 5-9: Volumetric strain versus axial strain- Cam-clay model.

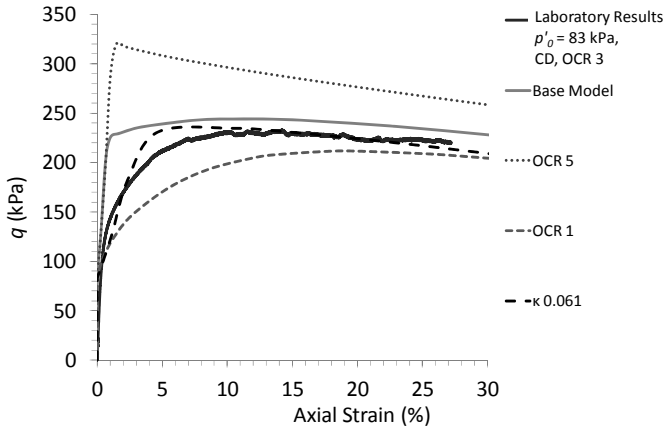

Figure 5-10: Deviatoric stress versus axial strain- Cam-clay model.

Figure 5-9 shows that the volumetric strain is slightly overestimated with the Cam-clay model. Figure 5-10 shows that reducing λ/κ from a value of 8 to a value of 2 results in a good match between numerical and laboratory results for the deviatoric stress versus axial strain relationship, but does not improve the volumetric strain versus axial strain relationship.

Figure 5-9 shows a similar volumetric strain versus axial strain response with increasing *OCR* to that seen in the CD test results on reconstituted specimens in Figure 4-22 (Chapter 4).

An increase in *OCR* in the Cam-clay model will result in an increasing peak stress, but a minimal increase in the critical state stress. This is shown in Figure 5-11, where η is the stress ratio (*q/p'*) and ε_q is the triaxial shear strain. This behaviour is clearly seen in Figure 5-10.

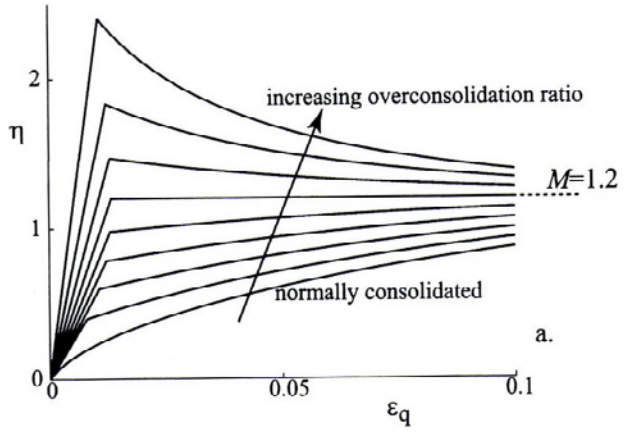

Figure 5-11: Cam-clay stress versus strain response with increasing *OCR* (Muir-Wood, 2004).

5.5.2 Reconstituted Soil: Mohr-Coulomb

The MC model was also evaluated for the reconstituted CD test with an *OCR* of 3. The soil parameters shown in Table 5-2 were used. Figure 5-12 and Figure 5-13 show the volumetric strain versus axial strain and deviatoric stress versus axial strain results, respectively.

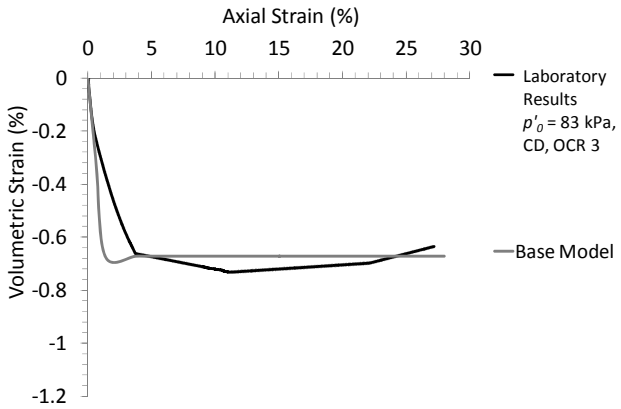

Figure 5-12: Volumetric strain versus axial strain- Mohr-Coulomb model, reconstituted soil.

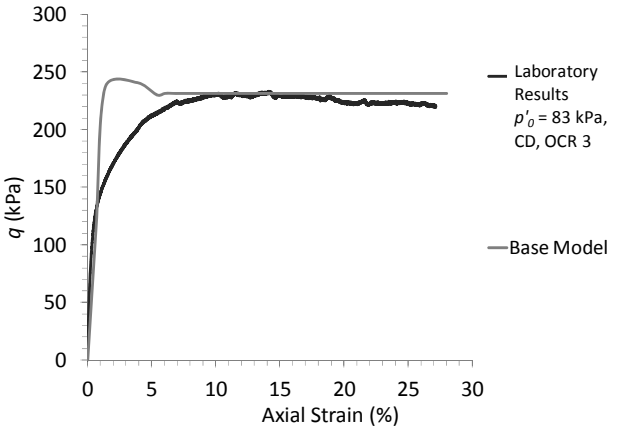

Figure 5-13: Deviatoric stress versus axial strain- Mohr-Coulomb model, reconstituted soil.

As anticipated, the model does not capture the strain hardening that occurs in the deviatoric stress versus axial strain curve prior to reaching peak strength. Aside from this, however, both Figure 5-12 and Figure 5-13 show a reasonable match between the MC constitutive model results and the laboratory results.

5.5.3 Intact Soil: Mohr-Coulomb

The MC model was evaluated for the intact consolidated undrained (CU) test at an effective stress of 110 kPa. The soil parameters shown in Table 5-3 were used. Figure 5-14 and Figure 5-15 show the pore pressure versus axial strain and deviatoric stress versus axial strain results, respectively.

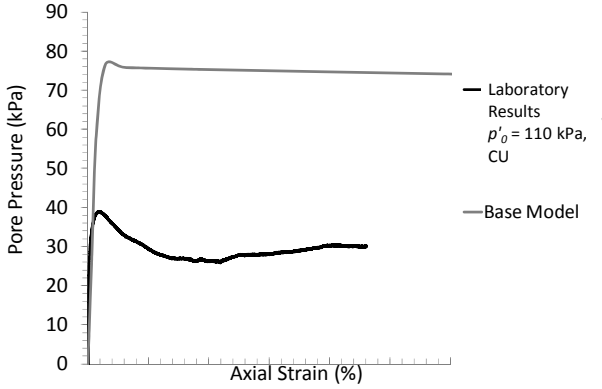

Figure 5-14: Pore pressure versus axial strain- Mohr-Coulomb model, intact soil.

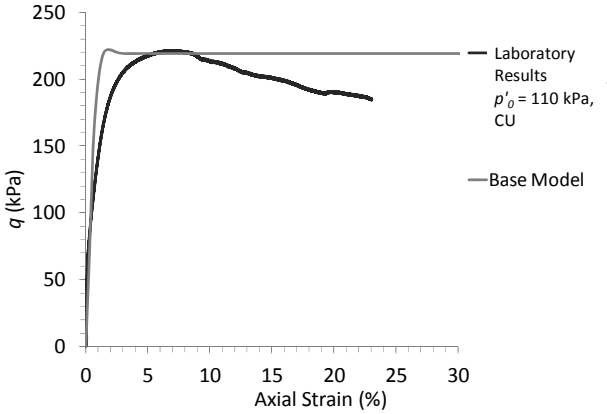

Figure 5-15: Deviatoric stress versus axial strain- Mohr-Coulomb model, intact soil.

Note that although the MC model is a simplification of reality (as it does not account for anisotropy and assumes elastic behaviour), it is perhaps the most popular constitutive model in geomechanics (Masin & Herle, 2005). As such, its use has been evaluated to determine how well it can match the behaviour of the Northland Allochthon residual clay soil examined in this study. Its limitations are evident in the undrained test (pore pressure response) of the intact soil. In an undrained test, the pore pressure change reflects the change in total stress. Theoretically, in a conventional triaxial test on an isotropic elastic material where the total stress path change in deviatoric stress divided by the change in mean stress is equal to three ($\Delta q/\Delta p$ = 3), there will be a pore pressure change $\Delta u = \Delta q/3$ at all stages of the test. This is exhibited in the numerical simulation of the intact triaxial test using the MC model in Figure 5-14 and Figure 5-15. The actual pore pressure change on the intact specimen is different to that predicted however, due to the fact that in reality it is neither isotropic nor elastic. The departure from theory depends on the past history of the soil and the tendency of the soil to dilate or contract (Muir-Wood, 1990). The intact specimen displays a significantly lower peak pore pressure than that of the MC model, suggesting it is more dilative than an idealized soil with similar strength properties. This is also reflected in the stress path behaviour of the soil, as seen in Figure 4-29, Chapter 4.

As with the reconstituted specimen, the MC model does not capture the strain hardening of the soil prior to reaching peak strength. Similar peak strengths are reached between the MC model and the laboratory test.

The Cam-clay model was not considered for the intact material due to the unavailability of intact compression and swelling characteristics (λ and κ).

5.6 Conclusions

The behaviour of the soil at the Ogle's No. 3 site under triaxial compression based on the 40 kPa CD test can be represented suitably with either the MC model or the HS model. The HS model captures the strain hardening of the soil well, while the MC model seems to capture the volumetric strain behaviour better. Due to clarity and simplicity of the MC model, it has been selected for use as the primary constitutive model for this soil in the numerical modelling investigations that follow.

The behaviour of the reconstituted soil from Mountain Road with respect to the CD test performed at an effective stress of 83 kPa (at an *OCR* of 3) is well represented by the Cam-clay model when λ/κ is reduced from 8 to 2. The MC model also provides a reasonable match to the laboratory results.

The deviatoric stress versus axial strain of the CU triaxial test performed at an effective stress of 110 kPa on an intact specimen from Mountain Road is well represented by the MC model. The pore pressure, however, is overestimated by the MC model due to the dilatant nature of the intact soil which cannot be captured by the constitutive model.

6.0 Case Study of the Ogles No. 3 Road Slip

6.1 Introduction

This chapter examines the failure and remediation (with DSM columns) of a road slip at the Ogles No. 3 site in Northland Allochthon residual clay soil using Plaxis 2D (Version 9).

Laboratory testing results and field results from other studies have provided a basis for this analysis. Initial remediation work for the road slip at the Ogles No. 3 site involved the construction of a buttress at the embankment toe. However, when slope failure continued, the slope was remediated again using a combination of DSM columns and drainage works. The following analysis provides an interpretation of the slope failure, involving initial failure and subsequent seasonal movement as the shear strength is reduced toward residual along the shear surface. This type of slope failure mechanism has not previously been examined for this soil type. The slope failure and performance of the DSM columns, as installed, are examined and the replacement ratio method (RRM), commonly used in industry, is utilized to represent the DSM columns in two dimensions. This method does not allow for the effects of soil movement past the columns and soil arching to be implemented. These aspects are examined in the following two chapters.

6.2 Site Description

Location and Previous Works

As discussed in Chapter 3, the Ogles No. 3 site is located on State Highway 1 in the Northland region of New Zealand and lies within the Hukerenui Mudstone of the Mangakahia Complex in Northland Allochthon. The area is comprised of shallow slopes of 10° or less and around 250 m long. The road in question was constructed around 30 years ago. Despite remedial efforts involving the installation of drains in the 1990's, the carriageway embankment suffered major failure. Following this, fill was imported to buttress the embankment and provide toe support. The toe buttress increased the stability such that wholesale movement no longer occurred, but the embankment was still subject to ongoing deformation with time. In 2006, a shallow geotechnical investigation was completed, and in 2007, Hiway Stabilizers Ltd. was commissioned to complete an investigation and remedial

works. As part of these investigations several boreholes were drilled, standpipe piezometers were installed, and soil samples were acquired for lab analysis including triaxial tests and Atterberg Limits (O'Sullivan, 2009).

The site consists of residual clay soil (2 to 9 m thick), characterised as an overconsolidated clay underlain by a broken ("transition") soil (5 m thick) which is underlain by weathered and pervasively sheared mudstone. The interpreted geology is depicted in Figure 6-1.

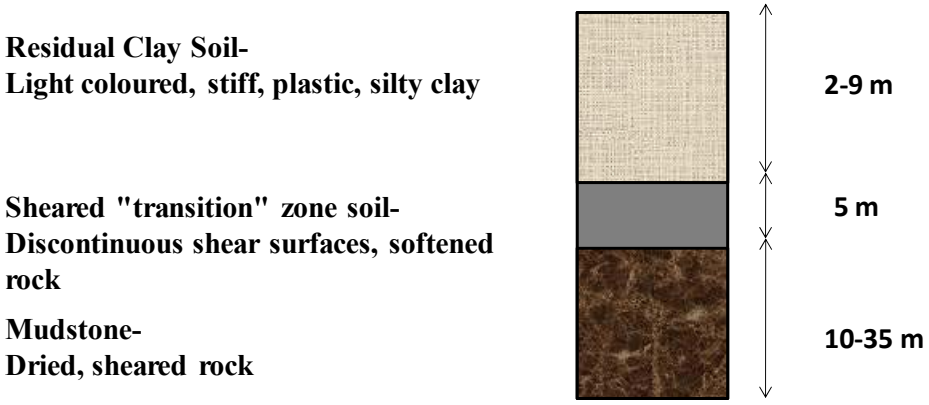

Figure 6-1: Interpreted geological profile.

6.3 Model Calibration

The soil properties for the residual soil were derived from triaxial laboratory test data from O'Sullivan (2009) (as discussed in Chapter 5). The properties for the transition zone were directly interpolated from triaxial testing results from O'Sullivan (2009).

6.4 Slope Model Description

The Mohr-Coulomb (MC) constitutive model was used to examine the original slope failure, subsequent on-going movement and eventual remediation. Given that the on-going movement of the slope appears to be related to long-term soil behaviour, only the drained condition has been considered here.

The hydraulic conductivity of the residual soil was estimated to be 7.4 x 10^{-7} m/s, calculated using Hvorslev's method (Hvorslev, 1951) with constant water head readings obtained from dataloggers in piezometers installed in two boreholes in the field. (The piezometers were screened at 3.5 to 5.5 m and 7.0 to 7.5 m below ground level and constant head readings from these were 4.8 m (0.5 m below ground level) and 5.8 m (1.5 m below ground level) (O'Sullivan, 2009).

Preliminary analysis was performed to include traffic loading on the road surface in order to determine its impact on reducing slope stability. The same model was used (as described in Sections 6.4.1, 6.4.2 and 6.4.3), with an estimated average load of 10 kPa (Shave et al., 2010) applied across the road during the road construction stage and subsequent high groundwater stage. The impact on the factor of safety (FoS) of the slope due to the estimated traffic load was determined. The results indicated that the traffic loading reduced the FoS from 1.01 to 1.00. Given that the change was nominal, traffic loading was not utilized in the remainder of this study.

6.4.1 Slope Failure Mechanism

Slope failures in Northland Allochthon soil are considered to be associated with large rainfall events and the frequent rise and fall of the groundwater table (Lentfer, 2007). Harris (2013) used Mohr-Coulomb failure criterion and factor of safety analysis while assessing a slope failure at the Silverdale site (Whangai Formation), but also incorporated changes induced by volumetric water content (or matric suction) through seepage analysis. However, O'Sullivan (2009) offered the proposition that failure in Northland Allochthon slopes could not be explained by strength considerations alone (i.e. factor of safety analysis). From his research on infinite slope analyses utilizing soil properties derived from the Ogles No. 3 site, he concluded that pre-failure deformations within the Mohr-Coulomb envelope could provide a plausible explanation for observed movements in slopes which he found had a factor of safety of greater than 1.4 using strength-based analysis (i.e. factor of safety analysis). The case study presented in this chapter proposes a more conventional and simpler explanation for slope movements in Northland Allochthon clay soil after initial slope failure, whereby the soil strength is reduced to its residual value along a pre-existing failure plane. O'Sullivan

(2009) observed non-recoverable deformations in the soil from the Ogles No. 3 site at axial strain levels of less than 0.1% during unload-reload loops from triaxial testing results. This suggests that small levels of movement at the site would promptly lead to plastic (irrecoverable) deformation, and a reduction of soil strength, providing further support to the possibility of the development of a pre-existing failure plane. The use of residual strength on pre-existing shear surfaces in clay slopes was proposed by Skempton (1964) and has since been found to be effective in many other studies (e.g. Fletcher et al. (2002), Insley et al. (1977)). For a smooth and continuous failure surface to form, the presence of an adequate proportion of clay sized particles are required (Muir-Wood, 1990) (i.e. a high plasticity soil). Thus, the proposition of this type of mechanism in Northland Allochthon clay soil accounts for the high plasticity of this soil type.

6.4.2 Model Phases

Slope instability processes can be divided into four stages: pre-failure, first time failure, post-failure, and reactivation (Leroueil, 2001). The numerical model examined in this case study examines all four stages, with DSM columns installed in the post-failure stage. For the initial slope failure, the location of the shear surface was determined via back-analysis using parameters derived for the intact soil and most-probable ground water level. During the reactivation stage, the slope is considered to become active along its pre-existing rupture plane, where soil strength is reduced to residual. At this point, a predefined slip surface where soil parameters were reduced to estimated residual values was inputted along the failure plane found during the back-analysis for the stages after road construction.

Plastic analysis was used for the calculation phases with the following stages in order to perform back analysis of the slope failure:

1) Gravity Loading: To develop initial stresses (use of “total multipliers” rather than “staged construction”).
2) High Groundwater: Water level raised to near ground surface.
3) Road Construction: Road is placed, at low groundwater.
4) High Groundwater.
5) Factor of Safety Calculation: Slip surface is noted.

Once the failure plane was determined, the slope model was re-run with residual strength properties along the failure surface, and the following stages were added:

6) Buttress Installation: Buttress installed. A weakened residual shear zone along the shear plane noted in Step 5 is activated.
7) Factor of Safety Calculation.
8) DSM Column Installation (using replacement ratio method).
9) Factor of Safety Calculation.

6.4.3 Model Geometry and Soil Properties

The sheared zone resulting from first time failure of the road embankment is shown in Figure 6-2. Figure 6-3 is a photograph of the deformation in the road carriageway and subsidence of the embankment. A close-up of the slope detailing the geometry of the model after installation of the buttress is shown in Figure 6-4. Plaxis utilizes phi-*c* reduction for computation of FoS. In this method, the slip surface is not defined by the user and the method can only localize the most critical slip surface. In some cases, such a slip surface may suppress other relevant failure modes, especially if the factor of safety for different slip surfaces differs only slightly (Kupka et al., 2009). In order to ensure that the FoS computation would relate to a deep-seated failure located at the road embankment under examination (and thereby avoiding domination of the FoS calculation by a shallow slip along the upper slope location), a zone approximately 1.5 m thick with an increased angle of internal shearing resistance was placed along the upper slope as shown in Figure 6-4 ("Higher Phi Zone").

Soil properties were acquired from the most recent geotechnical investigation at the Ogles No. 3 site, and interpreted from lab testing results (Chapter 5). The residual clay soil is a high plasticity clay, as described in Chapter 3.

Ring shear testing indicated a residual angle of internal shearing resistance of 11° to 14° (O'Sullivan, 2009) which matched well to correlations with the liquid limit of 12°-14° (Mesri & Cepeda-Diaz, 1986). A value of 14° was chosen for this analysis. The soil properties utilized are shown in Table 6-1. Note that this table summarizes soil and column properties prior to failure. Stark et al. (2005) recommend that in first time slide situations (i.e. fully softened conditions) the effective stress cohesion be set to zero. As Plaxis does not allow for

a value of exactly 0, 0.1 kPa was selected for cohesion of the residual soil and transition zone material.

Amongst practitioners, there has not been widespread agreement on the most appropriate strength envelope for deep mixed materials for use in stability analyses of column-supported embankments. Brandl (1981), Takenaka and Takenaka (1995) and Terashi et al. (1980), state that the tensile strength of soil improved by the wet DSM method is 10% to 20% of the unconfined compressive strength. Terashi (2005) points out that in Japan, the practice is to use a total stress, $\varphi = 0$ and $c = ½\ c_u$ envelope for deep-mixed material. Kitazume et al (1996) reports that a value of 15% is used in Japan with wet mix methods. EuroSoilStab (2002) uses a drained, effective stress angle of internal shearing resistance of 30°, with a range of values for the cohesion intercept depending on the location of the failure surface. They also state that, for the dry methods of deep mixing, columns should not be used to resist tensile stresses. Broms (2003) uses total stress angles of internal shearing resistance in the range of 25° to 30° for deep-mixed materials. For a suitable strength envelope for deep-mixed materials for stability analysis Navin (2005) recommends (1) the total stress angle of internal shearing resistance should be set equal to zero, (2) the total stress cohesion should be set equal to 40% of the unconfined compression strength to account for the reduction from peak strength to residual strength, and (3) no tensile strength should be included. Ye et al. (1994) reported that the cohesion of soil-cement mixtures is about 20%-30% of the unconfined compressive strengths (UCS).

The design UCS of the columns in Northland Allochthon residual clay soil is 2 MPa (O'Sullivan, pers. comm., 2011b). Documented UCS testing results were not available for any of the sites mentioned in this thesis, but they were available for a road slip at Kahoe Hill, which is located on State Highway 10, close to the Kaeo field site, in the Mangakahia Complex. These results are presented in Appendix F, and show a maximum UCS of 2.7 and 3.6 MPa, indicating that 2 MPa is a conservative estimate. A UCS of 2 MPa would result in an estimated cohesion of 400 kPa to 600 kPa based on the method suggested by Ye et al. (1994). Testing done at Hiway Stabilizers Ltd. established that the cohesion of the DSM columns was approximately 667 kPa. This was established by converting the undrained shear strength (UCS/2) (i.e. the radius of Mohr's circle) to effective stress parameters by

calculating the equivalent cohesion intercept based on tangents at the angle of internal shearing resistance estimated for the column material in this soil. The estimated column angle of internal shearing resistance (under drained conditions) is 32°-36°, depending on the strength of the surrounding soil. This is similar to the values used by EuroSoilStab (2002). A cohesion of 667 kPa for full strength columns results in a cohesion value of 167 kPa using the replacement ratio method. Further discussion of this technique follows. A tension cut-off of 0 kPa was also applied to allow the possibility of the DSM columns failing in tension (as well as in shear). Poisson's ratio for the DSM columns was estimated at 0.2, as the columns are composed essentially of a blend of concrete (Poisson's ratio of 0.2) and residual soil (Poisson's ratio of 0.25, based on lab testing results from O'Sullivan, 2009). The unit weight of concrete is approximately 23.5 kN/m^3 (Craig, 2004) and the unit weight of the soil is approximately 20 kN/m^3. The DSM columns which are a blend of these two materials, have been estimated to have a unit weight of 20 kN/m^3, as the unit weight of these two materials are reasonably similar, and measurements of unit weight performed by Hiway Stabilizers Ltd. indicate the unit weight of the columns in this soil type is approximately 20 kN/m^3 (O'Sullivan, pers. comm., 2011c).

Table 6-1: Soil parameters used for Ogles No. 3 site model.

Soil Parameter	Parameter Description	Units	Residual Soil (Allochthon)	Transition (Broken) Zone	Road Fill	Mudstone	DSM Columns Full Strength
$E^{ref\ 1}$	Young's Modulus	kN/m^2	5000	20000	45000	400000	1080000
$E^{ref\ 2}$	Young's Modulus	kN/m^2	22500	20000	45000	400000	1080000
ν	Poisson's Ratio		0.25	0.25	0.20	0.20	0.20
γ (unsat)	Unsaturated Unit Weight	kN/m^3	20	20	18	20	same as soil
γ (sat)	Saturated Unit Weight	kN/m^3	20	20	20	20	same as soil
φ	Angle of Internal Friction	°	25	26.6	35	34	32-36*
ψ	Angle of Dilatancy	°	2	1	1	2	2

[1] E^{ref} based on initial loading from triaxial data

[2] E^{ref} based on unload-reload stiffness from triaxial data; used in groundwater cycling analysis

*Varies with soil type; values used: 32 for Allochthon, 35 for transition and fill, 36 for mudstone

6.5 Slope Model Results

The shear strain contours after road construction for the FoS calculation are shown in Figure 6-2. The contours range from 0 to 10% shear strain. The FoS was calculated to be 1.01.

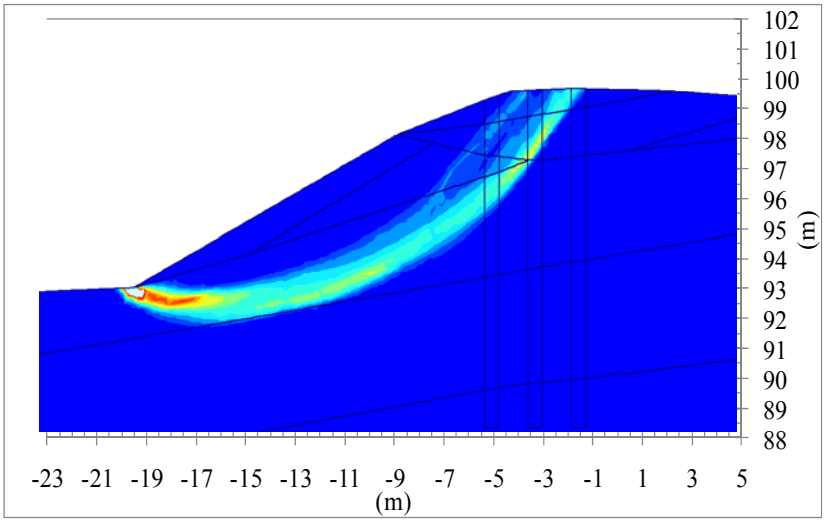

Figure 6-2: Shear zone.

A log from a borehole drilled at the road shoulder describes a highly sheared zone at approximately 4 m depth (BH 1, Appendix E). This corresponds well to the base of the shear zone as seen in Figure 6-2 at 96.5 m elevation at the location of the hard shoulder.

Note that the rightmost column as seen in Figure 6-4 does not transect the slip surface. In the original analysis performed by Hiway Stabilizers Ltd., the slip surface edge was determined to be slightly further to the right. However, Figure 6-3 shows the subsidence zone on the road surface due to failure of the underlying soil. This correlates well in terms of lateral position to the point at which the shear zone intersects the ground surface, as seen in Figure 6-2. There is no subsidence visible to the right of the road centre where the rightmost column is located.

Figure 6-3: Deformation in road carriageway and subsidence of embankment (O'Sullivan, 2009).

Based on these results, a shear residual zone was then placed in the mesh as shown in Figure 6-4 and the buttress was activated in the slope model. The groundwater within the buttress was increased incrementally until a factor of safety of 1.07 was attained. At this point, high groundwater level was found to be an average of 1 m below ground, as shown in Figure 6-4. This ground water level is consistent with piezometer/borehole data found at the site. (As mentioned in Section 6.4, standpipe piezometers read 1.5 mbgl level (screened 7 to 7.5 mbgl) and 0.5 mbgl (screened 3.5 to mbgl) (O'Sullivan, 2009)). Note that the groundwater levels in

Northland Allochthon soil vary significantly throughout the year, but are often quite high, typically 0-3 m below ground level (Lentfer, 2007; O'Sullivan, 2009).

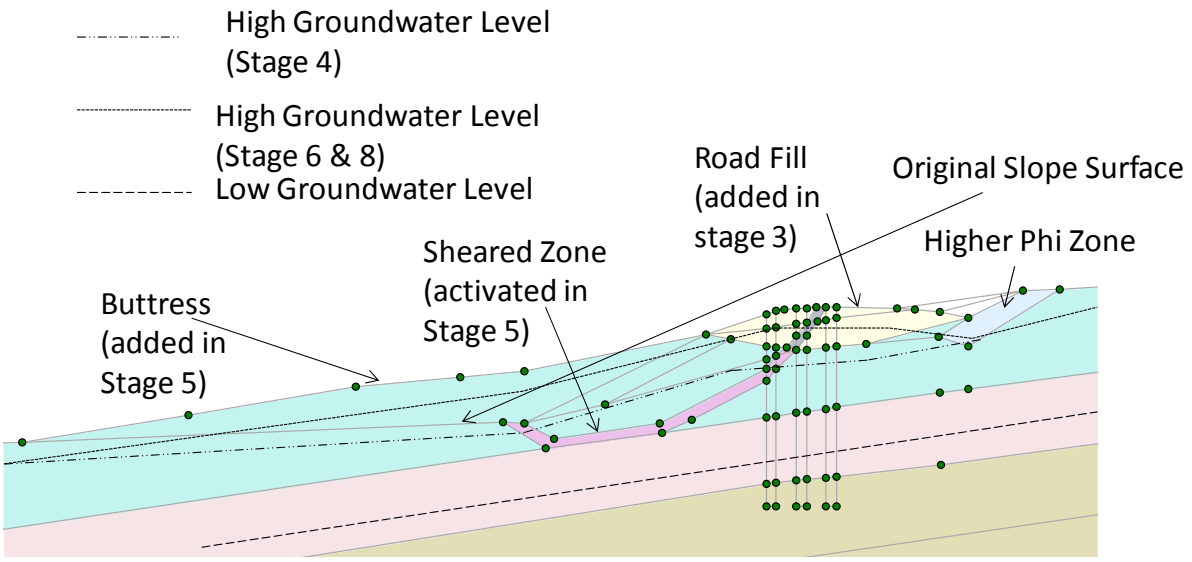

Figure 6-4: Slope model geometry.

6.5.1 Stabilized Slope Model

The final mitigation measures at Ogles No. 3 involved three rows of columns, as well as associated drainage works. The drainage works are located at the base of the ditch on the right side of the roadway, but were not included in this analysis as it was conservatively assumed that they may not function as intended throughout the lifetime of the structure.

The DSM columns were installed to depths of approximately 12 m, with rows spaced 1.2 m apart. The diameter of each of the columns was 0.6 m. Three rows of columns were installed. The DSM column installation was a wet mixing process. Approximately 300-400 kg of grout (at a ratio of 1:1 cement to water by weight) per 1 m^3 of soil was used and a small amount of lime was added to break up (flocculate) the clay. The strength of the columns was determined from samples acquired using a sampling tube similar to a long (5 m) syringe. The samples were extruded into moulds, which underwent unconfined compressive strength (UCS) testing

at 7, 14 and 28 days after column installation. This resulted in a design UCS of approximately 2 MPa.

6.5.2 Replacement Ratio Method

There are several methods that can be used to represent DSM columns in a two dimensional model. These include the composite (axisymmetric) cell model (Karstunen et al., 2005), the volume averaging technique (Vogler & Karstunen, 2009) and the replacement ratio method (Finlan et al., 2004; Gani, 2004; Leung et al., 2006; Oliveira et al., 2011; Terzhagi et al., 2004). The replacement ratio method is similar to the area strength parameters method (Goughnour et al., 1991). Navin (2005) also describes three methods that are strictly for analyses where the slip surface is circular and well-defined. The investigation described in this chapter utilizes the replacement ratio method.

With the replacement ratio method, the columns are modelled in the out-of-plane direction together with the surrounding soil as a block of composite material. This is completed by using a weighted average of the volume of soil with the volume of DSM column material in the out of plane direction. This is approximately 25% soil and 75% column material by volume based on the spacing and dimensions of the columns used at the Ogles No. 3 site. Table 6-1 shows the soil and column properties used to carry out the weighted average. Figure 6-5 is a graphical representation of the replacement ratio method.

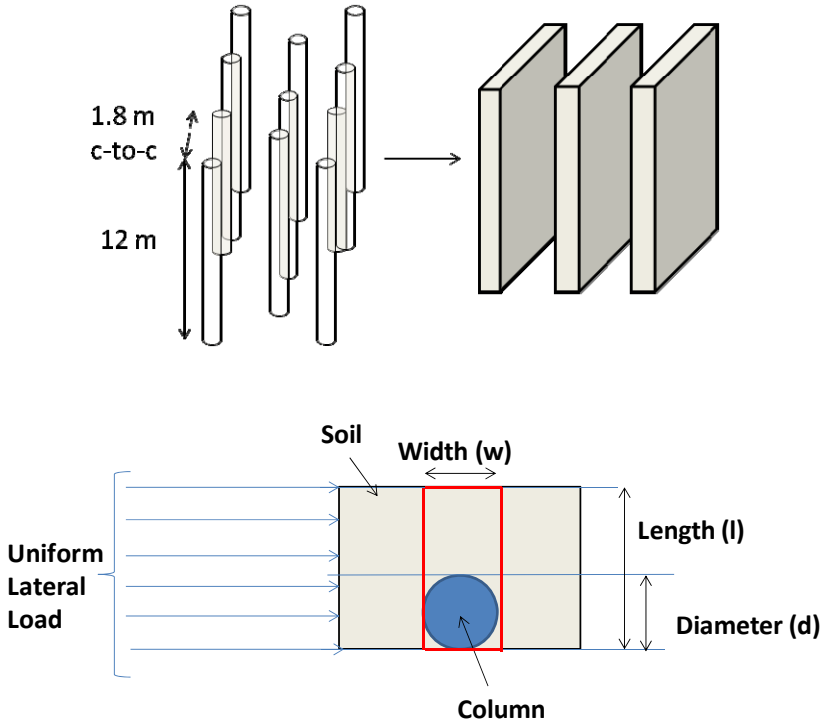

Figure 6-5: Graphical depiction of replacement ratio method.

Note that in the RRM, the replacement ratio for the DSM column material (r_{col}) corresponds to the definition of the replacement ratio that is commonly used in the design of ground improvement methods. Another term, r_{soil}, which is equivalent to 1-r_{col}, and is referred to as the replacement ratio of the soil, is used in this thesis because this value plays an integral role in defining the composition of the composite DSM column/soil material in 2D models that use the RRM. The following equation shows the computation of the replacement ratio for the column material (r_{col}).

$$r_{col} = \frac{A_{col}}{A_T} = \frac{A_{col}}{A_{col}+A_{soil}} \qquad (6.1)$$

A_{col} is the area of a column, A_{soil} is the area of the soil between two columns (together, they are the area in the red rectangle in Figure 6-5, denoted as A_T in equation 6.1). The same equation is used to compute the replacement ratio of the soil (r_{soil}) by replacing A_{col} with A_{soil}

(and A_{soil} with A_{col}). (As noted above, the value of r_{soil} could alternatively be computed as simply 1- r_{col}). The Young's modulus of the composite block would then be:

$$E = (r_{col} \times E_{col}) + (r_{soil} \times E_{soil}) \qquad (6.2)$$

where E_{col} is the Young's modulus of the column and E_{soil} is the Young's modulus of the soil. Though the composite soil/column material is undergoing shear, Young's modulus (E) is used in Equation 6.2 instead of the shear modulus (G) in order to be consistent with the soil parameters that have been used to define the soil behaviour in Plaxis. This weighted average technique is also applied to the cohesion and the angle of internal shearing resistance.

6.5.3 Previously Performed Numerical Modelling of DSM & Failure Modes

Several numerical studies have been performed that examine the failure mechanisms of DSM columns, particularly under embankments (Han et al., 2007; Huang et al., 2009; Karstunen et al., 2005; Leung et al., 2006; Oliveira et al., 2011). Most of these studies focus on settlement and displacements due to axial loading, and few studies have been performed that examine behaviour of DSM columns designed to mitigate slope failure due to lateral loading. However, important parallels still exist, particularly in regard to the findings that singular columns may exhibit bending failure (Kitazume & Maruyama, 2006, 2007). It is well known that DSM columns have low tensile strength. In the current case study, the driving moments caused by the active earth pressure of the road embankment and the underlying ground could cause the DSM columns to undergo bending failure. However, due to the implementation of a slip surface where soil strength parameters have been reduced to residual values, shear failure (along this plane) is the most likely failure mode for this case study. This is examined further in the following section.

6.5.4 Shear Failure versus Bending Failure

The soil model used in the global analysis of slope failure (Global model) was 170 m long and 50 m deep, with a fine mesh used throughout much of the model and refined further within the DSM columns. However, due to the large scale of this slope model, the maximum

refinement was one element across each column. In order to examine the possibility of bending failure within the columns, a new model was developed that "zoomed in" to the columns and embankment, reducing the model to 50 m long and 20 m deep (Local model). In this model, 4-5 elements across each column were possible. The boundary conditions for the Local model were the same as for the Global model, and the displacements in the Global model were inputted at the boundaries of the Local model at the column installation phase. The Local model exhibited a similar shearing mechanism within the columns. The deformed mesh, scaled up 10 times, is shown in Figure 6-6 for the Global and Local models. The approximate locations of points A and B, selected for stress-strain analysis are also shown in Figure 6-6. Figure 6-7 shows the failure envelopes for the soil and the columns in plane strain at the inner (point A) and outer (point B) areas of the left DSM column. Figure 6-8 is a plot of stress versus deviatoric strain and it shows a similar stress-strain response for Global and Local models. Note that deviatoric strain (ε_s) is defined as:

$$\varepsilon_s = \frac{2}{3}(\varepsilon_a - \varepsilon_r) \qquad (6.3)$$

where ε_a is axial strain and ε_r is radial strain.

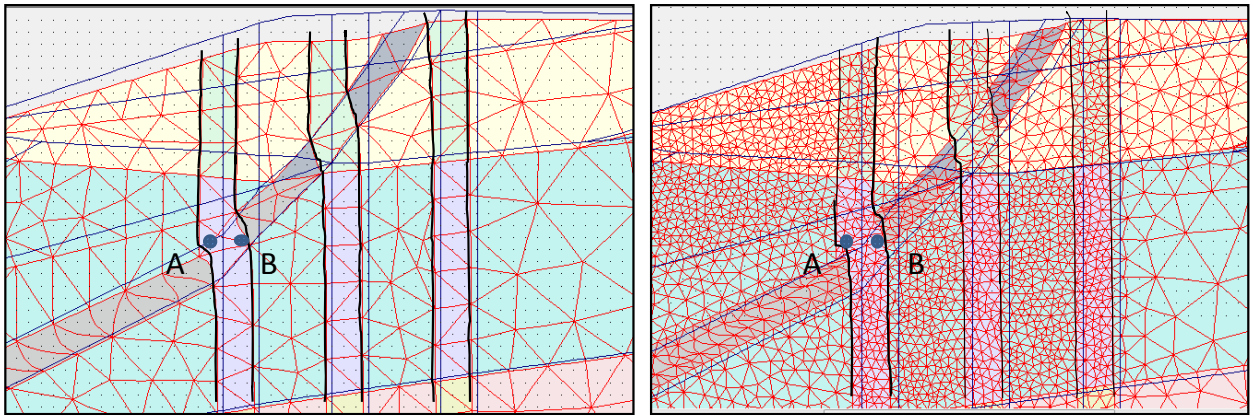

Figure 6-6: Failure mode- Global model (left), Local model (right) (scaled up 10 times).

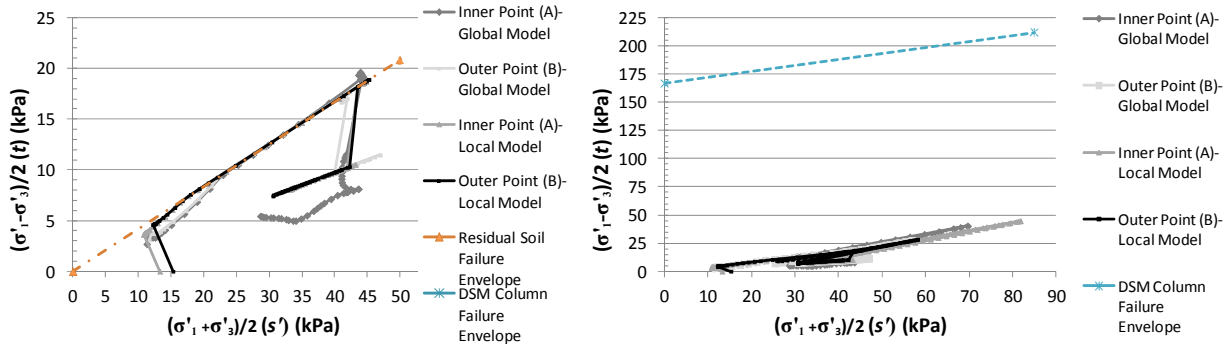

Figure 6-7: Plot of *t* versus *s'* before (left) and after (right) DSM column installation at points A and B.

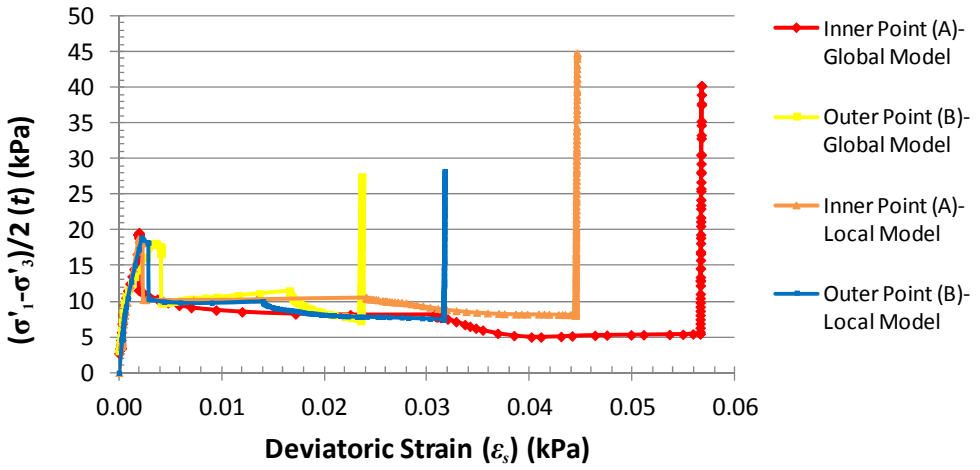

Figure 6-8: Stress versus strain at inner and outer edges of column in Global and Local models.

As seen in Figure 6-8, the installation of the DSM columns has a significant stiffening effect, and strain development is reduced to nearly zero. Minor principal stresses were examined at both points A and B to ensure that the columns were not going into tension via a bending mechanism, and were not found to drop below zero at any time.

From a consideration of the slope failure mechanism considered here (i.e. with a discrete zone of soil at residual strength and stiffness within a soil of otherwise intact properties),

bending failure of the columns may be considered as unlikely over shearing. This is because the soil above the residual zone will remain in planar mode, prohibiting bending.

6.5.5 Factor of Safety Results

The global factor of safety after each stage at high groundwater level is shown in Table 6-2. The FoS after road construction and buttress construction are 1.01 and 1.07 respectively, which are in agreement with first time and second time failure of the slope. BRANZ (1987) suggest that a FoS of greater than unity is typically used to indicate a stable slope, (though it is recommended that the results of a stability analysis be analysed on a case by case basis in order to allow the assessor to use judgement in assessing the results). Installation of the DSM columns resulted in an increase of the factor of safety from 1.01 to 1.33 at high groundwater level, indicating the columns are mitigating slope movement of the deduced failure mechanism. While 1.33 is less than the design FoS of 1.5, it does indicate that slope movement is not likely to persist. In addition, given that the slope failure zone has a residual angle of internal shearing resistance applied to it, and it could not be expected to reduce further even with additional shearing, the FoS of 1.33 seems a reasonable one (i.e. a failure scenario would have to be quite severe).

Table 6-2: Computed factors of safety for Ogles No.3 road slip.

Factory of Safety		
Road Construction	Buttress Construction	DSM Column Installation
1.01	1.07	1.33

Verifying the performance of the model

Hand calculations were performed to double check the Plaxis outputs of major and minor, total and effective, and principal stresses at point A (Figure 6-6). This was done for the high groundwater stage after road construction, and for the buttress stage. The results show a reasonable match for the end point of each calculation phase. Due to the Boussinesq effect,

there is some transfer of vertical stress outside of the loaded area, which accounts for minor differences in the Plaxis outputs. The results are shown in Table G1, Appendix G.

6.5.6 Seasonal Groundwater Fluctuations

The high groundwater table that is present in much of the Northland region during wet periods plays a significant role in instigating slope failure. During dry periods, the groundwater table drops significantly. Seasonal moisture cycles such as this have been shown to produce significant irrecoverable softening within a slope in clay (Take & Bolton, 2011). This is discussed further at the end of Section 6.5.6. In order to determine if the effects of groundwater cycles on the stability of the slope could be captured with the Mohr-Coulomb (MC) model, the model was run with 6 cycles of high and low groundwater after buttress construction, both with and without DSM columns (installed after the first groundwater cycle).

Displacement was examined both at the road shoulder and at the centre of the road. At the road shoulder, a second scenario where the stiffness, E, of the residual soil was increased from 5000 kPa to the unload-reload stiffness of 22500 kPa after the initial cycle was examined. This was done in order to examine the effects of stiffness on displacement at this location and to examine the deformation as a result of unload-reload cycling. Figure 6-9 shows the displacement at the centre of the road both with and without DSM columns at each groundwater cycle. The displacement at the road shoulder versus groundwater cycle is presented in Figure 6-10.

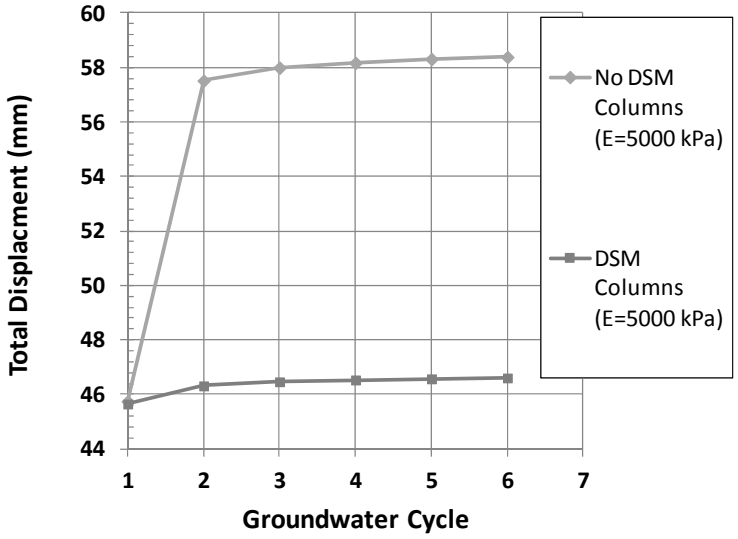

Figure 6-9: Displacement at the centre of the road versus groundwater cycle and the effect of DSM columns.

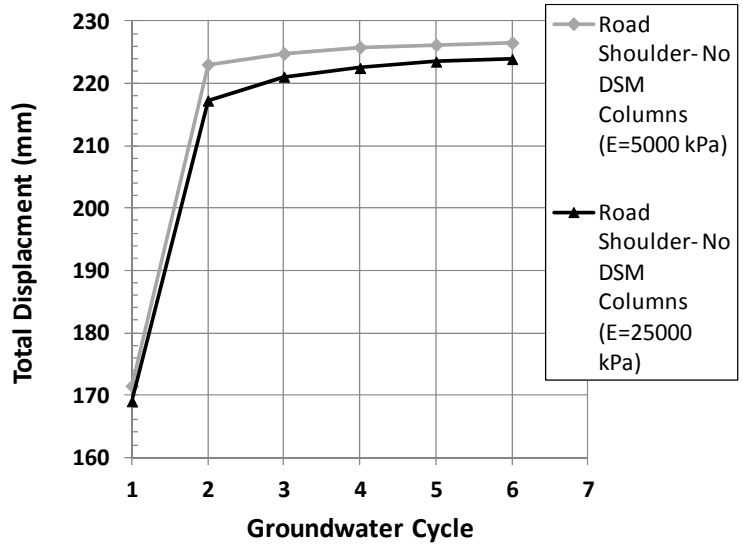

Figure 6-10: Displacement at road shoulder versus groundwater cycle and the effect of soil stiffness.

Figure 6-9 shows that the DSM columns reduce slope movement at the road centre by approximately 12 mm at the end of groundwater cycling. Much of the displacement occurs in the first groundwater cycle; however, the movement in this cycle could be largely due to re-distribution of stresses as the model is brought to equilibrium and may be superficial. The effects of groundwater cycling simulating seasonal groundwater variations appear to have a small influence on increasing movement at both the centre of the road (Figure 6-9) and the road shoulder (Figure 6-10).

Based on slope inclinometer readings from the Ogles No. 3 site, slope movement is in the order 2-5 mm over a three month period during the rainy season (May-July). This is shown by the brown line in the slope inclinometer readings (May 8th, 2006 to July 24th, 2006) in Figure 6-11.

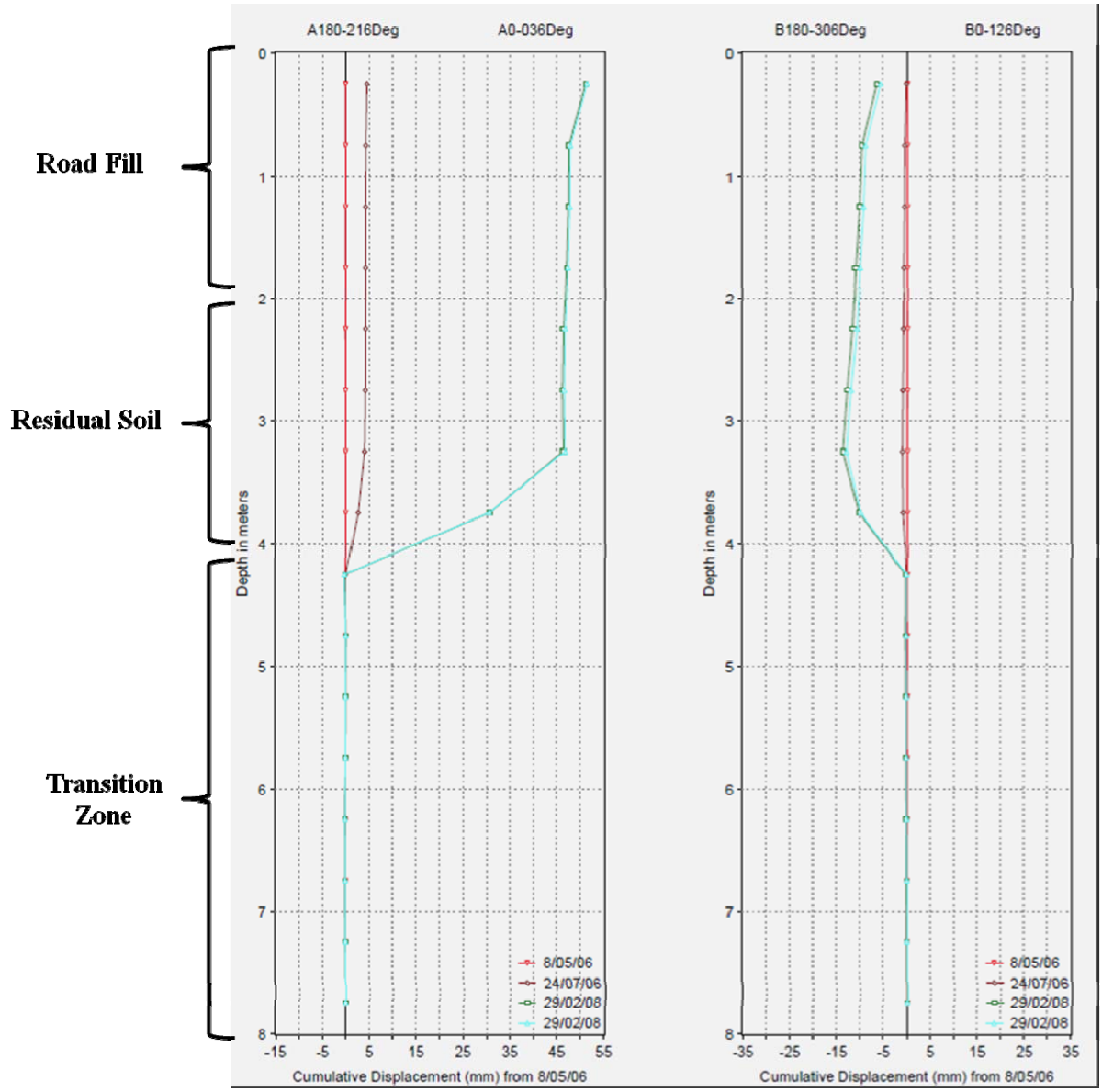

Figure 6-11: Slope inclinometer readings at the road shoulder at Ogles No. 3 (modified after O'Sullivan 2009).

During this three month winter period, approximately 40 "wet days" are experienced, on average (NIWA, 2011). Since many wet days happen sequentially (for 3-4 days at a time), it is estimated approximately 10 high-to-low groundwater cycles are experienced in this three month period. Thus, for four groundwater cycles, 1 to 3 mm of movement are anticipated. The results of the numerical model indicate that movements at the road shoulder due to

seasonal groundwater fluctuations are about 2 to 6 mm for the latter four cycles at the road shoulder in Figure 6-10, indicating that this type of "creep" movement can be captured by the cyclic Mohr-Coulomb model. The Mohr-Coulomb model features dilatancy prior to failure, which leads to ratcheting failure as the dilatancy is repeatedly induced during wet seasons. Dilatancy allows for a change in the direction of movement between wet and dry seasons. (The effect of dilatancy on slope movement was shown in Figure 5-5). The mechanisms of seasonal ratcheting and softening in clay slopes leading to failure are thoroughly examined by Take and Bolton (2011). Examination of an element in the middle of the slope shows that there is an overall displacement that is in a W pattern that is down slope. They confirm that the initial pre-rupture phase of regional softening and slope ratcheting is due to the repeated mobilization of dilatancy in successive wet seasons. If super critical stress ratios are mobilized, some dilation- irrecoverable softening- must occur. With better in situ slope movement data, further analysis could be performed with additional groundwater cycles in order to develop a stronger understanding of the slope movement mechanisms and how they may be best modelled.

6.6 Conclusions

The road embankment at Ogles No. 3 suffered from slope failure which was mitigated by the construction of a buttress, but the slope was later subject to on-going movement and settlement of the road surface. This investigation has considered that the primary mechanism for the on-going displacement after buttress construction may have been the result of a weakened shear failure plane after first-time failure, something which has not previously been proposed for slope failures in Northland Allochthon residual clay soil. The results show that the factor of safety is reduced to approximately unity after buttress installation, demonstrating that this is a useful technique and a plausible explanation for second-time failures in Northland Allochthon residual clay slopes. As such, practitioners may find that in situations where second time failure is being examined in this soil type, a pre-existing slip surface where soil strength is reduced to its residual value may provide a useful explanation for field behaviour.

To examine the influence of the effects of seasonal groundwater fluctuations of the subsequent deformation of the slope, the stiffness of the soil was varied between an initial plastic value and a subsequent elastic value during cycling. Under this altered condition, seasonal fluctuations in groundwater were found to have minimal impact on total strains. The model shows small amounts of movement with groundwater cycling similar to that seen in the field, however further analysis with more detailed field measurements are required. The model shows that the installation of the DSM columns act to reduce total displacement at the road shoulder. The analysis indicates that the DSM columns increase the global factor of safety as required and perform as intended despite being designed for a somewhat different slip surface location. The DSM columns fail in shear rather than bending, a failure mode that appears to be instigated by the pre-existing shear surface within the slope.

This case study utilizes the replacement ratio method to examine a three dimensional problem in two dimensions. Soil movement around the columns cannot be properly accounted for in this type of analysis. The following chapters examine how soil arching plays a role in the ability of DSM columns to sustain lateral load, and how the replacement ratio method in two dimensions compares to a three dimensional analysis.

7.0 Behaviour of DSM Columns under Lateral Loading in Plan View

7.1 Introduction

Due to limitations in analysis or computational time, slope stability analysis is often undertaken in two dimensions (2D), through a side-view slice of the slope. Analysis of DSM columns for road slip stabilization in Northland Allochthon is no exception. However, conventional 2D slope stability analysis does not allow for lateral movement of soil relative to the columns, and the important effects of soil arching. This chapter examines the performance of DSM columns in a Northland Allochthon derived clay soil in plan view. This study is the first of its kind to examine DSM columns from this type of two dimensional perspective. Analysis of the DSM columns in plan view allows for the examination of the effects of column spacing, changes in the transition zone around the columns, and the shape of the columns. The effects of these are investigated through examination of soil arching, and changes in pressure versus relative displacement curves for the columns, in both the drained and undrained condition. The effect of displacement of the soil around the DSM columns that is induced during column installation is also examined. In the numerical investigations in this chapter, the DSM columns are fixed in place. Therefore, it is the failure of the soil around the columns that is considered, rather than failure of the columns themselves.

7.2 Group Effects: Changes to Soil Surrounding Columns, Column Spacing & Soil Arching

7.2.1 Soil Arching

Soil arching is the term used to refer to stress transfer through the mobilization of shear strength (Wang & Yen, 1974). The amount of pressure exerted on a structure (DSM column or pile) prior to soil failure gives an indication of the effectiveness of the structure to withstand lateral loading. The transfer path of load from the soil to the piles or columns is physically manifested in the rotation of principal stress (Chen & Martin, 2002). These mechanisms can be examined in detail by modelling DSM columns in plan view. This allows examination of the passive resistance of DSM columns through pressure versus relative displacement curves.

A two dimensional (2D) numerical model was developed in Plaxis 2D (Version 9) in this thesis in order to examine how changes to the soil surrounding DSM columns and column spacing influence soil arching and pressure versus relative displacement curves.

7.2.2 Model Validation - Randolph and Houlsby, 1984

The model concept was validated by comparing the results to an analytical solution of a pile pushed laterally into cohesive soil (Randolph & Houlsby, 1984). The analysis was done using the Mohr-Coulomb constitutive model in plane strain, with similar soil and pile properties as used in Chen & Martin (2002). In their analysis, the pile was modelled using a beam element, with a surrounding "interface". Both smooth and rough interfaces were examined. A smooth interface would be similar to that of a steel pile, while a rough interface would be similar to that of a concrete pile.

Plaxis 2D is not designed to be utilized in plan view, and based on a thorough literature review, this is the first study of its kind to use Plaxis 2D in this regard. The stresses generated by gravity in the set-up of this model would be in the z-direction, and not in the conventional y-direction. Therefore, gravity had to be set to zero by setting $\sum M_{weight}=0$. By setting this value to zero, soil weight is not taken into account and all water pressures are also zero (with the exception of excess pore water pressure generated during undrained loading). In addition to this, initial (or K_0) stresses were not generated, because doing so would imply a variation in stress in the x and y directions. By taking these steps, the problem could be examined purely in the context of soil properties and boundary conditions. The validation model geometry is shown in Figure 7-1. Material properties for the model are shown in Table 7-1. *EA* is the axial stiffness of the pile, *EI* is the flexural rigidity (bending stiffness) of the pile, and W is the specific weight of the pile.

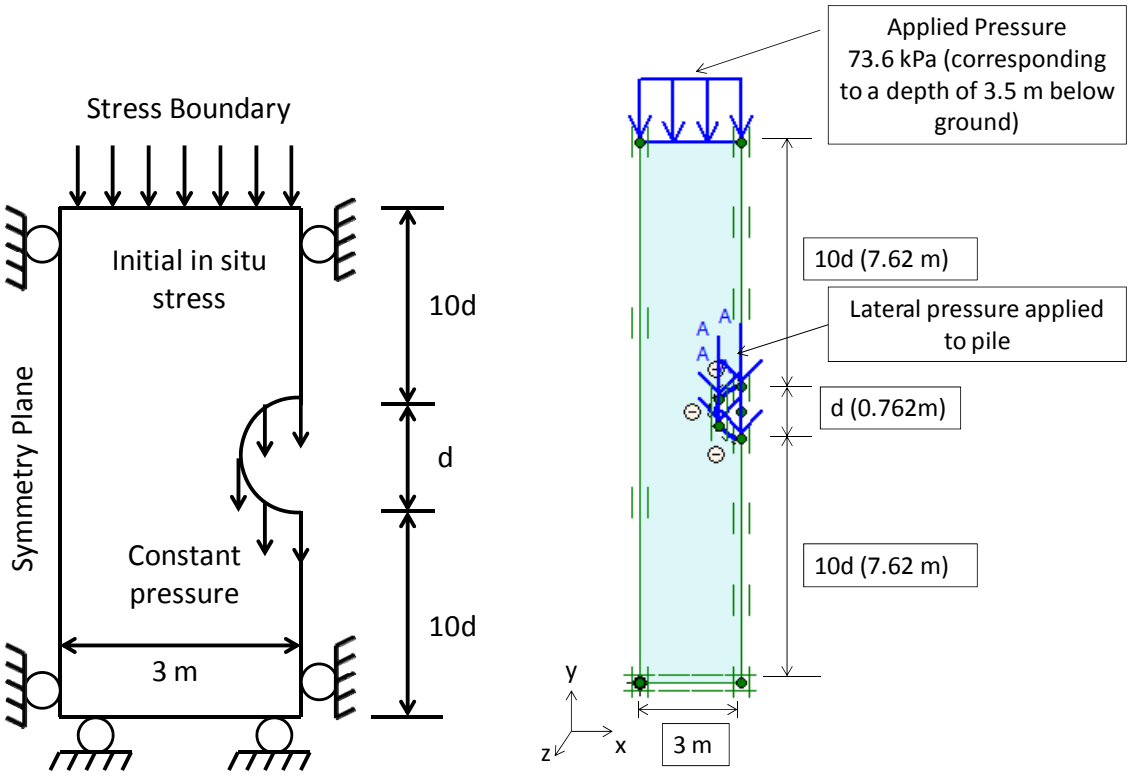

Figure 7-1: Validation model problem geometry for the limiting pressure on a pile. Left- conceptual model (modified after Chen and Martin, 2002), and right- Plaxis model.

Table 7-1: Material properties used in validation model.

Soil Parameter	Units	Material			
		Soil (Fine Grained)	Rough Interface	Smooth Interface	Steel Pipe
E^{ref}	kN/m^2	32760	32760	32760	
ν		0.3	0.3	0.3	0.27
γ (unsat)	kN/m^3	21	21	21	
γ (sat)	kN/m^3	21	21	21	
φ	°	0	0	0	
c	kN/m^2	25	125	2.5	
EA	kN/m				6.00E+09
EI	kN/m^2/m				200000
W	kN/m/m				1.54

The normalized lateral pressure is given by $p_l/(c_u d)$, where p_l is the lateral pressure on the pile, c_u is the undrained shear strength, and d is the diameter of the pile. The analytical solution for a rough interface yields a normalized lateral pressure of 11.94, and 9.14 for a smooth interface (Randolph & Houlsby, 1984). Results of the model were within 1% of the analytical solution and are shown in Figure 7-2. Updated mesh analysis was used in all numerical simulations in order to account for large strains. Lateral pressure was applied in stages at increments of 5 kPa until failure.

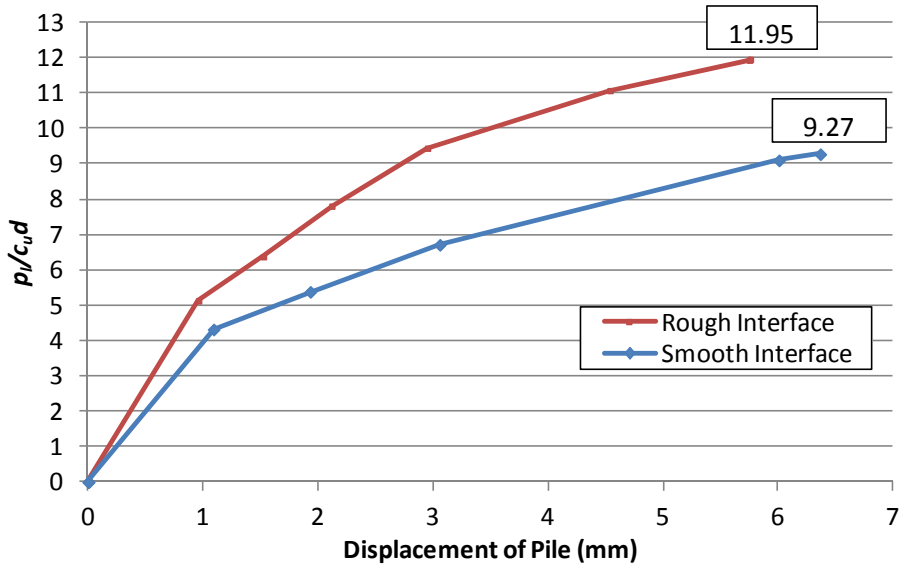

Figure 7-2: Normalized lateral pressure versus displacement of pile for validation model.

Note that the interfaces in this validation model are use to distinguish between the frictional resistance provided by a cement pile (rough) and a steel pile (smooth). The analytical solution by Randolph and Houlsby utilizes these interfaces. However, the overall aim of the validation process is to ensure that the numerical model being used can replicate an analytical solution for laterally loaded piles. Thus, the interfaces are relevant only for the validation models. Interfaces are not used in the following analyses, as the DSM columns are assumed to have frictional properties that are not significantly different from the soil around them.

7.2.3 Model Configuration

In order to examine lateral loading on two piles in plan view, a model was configured as shown in Figure 7-3.

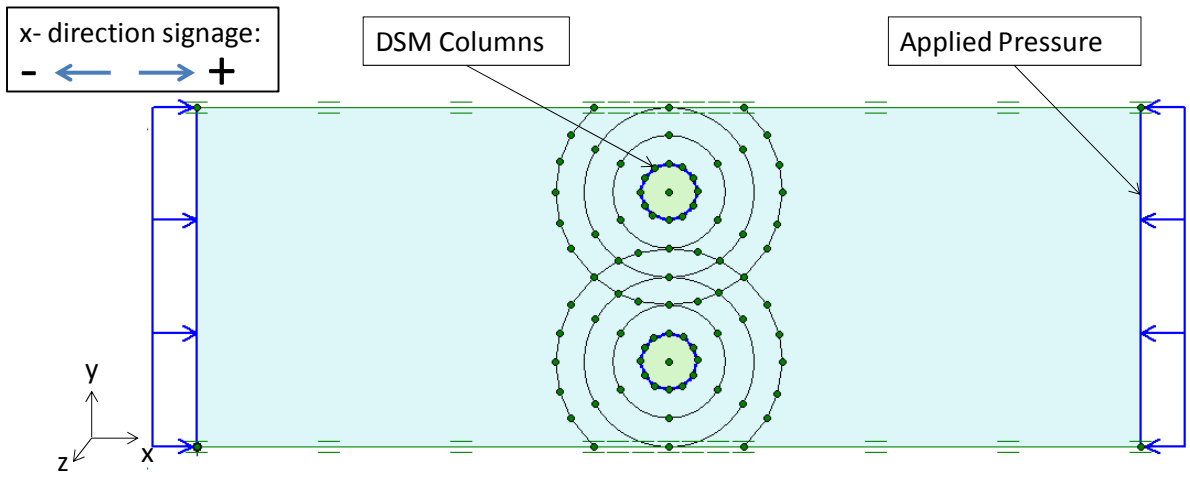

Figure 7-3: Model geometry for lateral loading of DSM columns in plan view.

The DSM columns were 0.6 m in diameter (as per typical TurboJET size). A pressure of 60 kPa was applied to the sides of the model to simulate an in situ confining pressure equivalent to total stresses 5.5 m below ground level (based on a K_0 equal to 1- sinφ with normally consolidated conditions assumed). Zero displacement vectors were applied to the edges of the DSM columns to facilitate the examination of soil movement around them. No interface was utilized for DSM column simulation, as the columns are integrated into the soil and essentially have a soil-to-soil interface rather than soil-to-structure (as with piles). The Mohr-Coulomb constitutive model was utilized, and the material properties, shown in Table 7-2, are the same as those used in the Ogles No. 3 model (Chapter 6). The unload-reload Young's modulus was used in this analysis to simulate the conditions in which lateral movement had commenced and subsequently ceased from previous high groundwater cycles. Note that for undrained analysis with undrained shear strength parameters in Plaxis, effective values must be entered for the stiffness parameters (Plaxis, 2008).

Table 7-2: Material properties used in plan view model of laterally loaded DSM columns.

Soil Parameter	Units	Material		
		Soil (Undrained)	Soil (Drained)	DSM Columns (Drained)
E^{ref}	kN/m^2	22500	22500	1080000
ν		0.25	0.25	0.2
γ (unsat)	kN/m^3	20	20	20
γ (sat)	kN/m^3	20	20	20
φ	°	0	25	32
ψ	°	0	2	2
c	kN/m^2	60	0.1	667

In stage one, the model was brought to equilibrium with an in situ confining stress at the model boundaries of 60 kPa. In stage 2, the columns were installed, with zero displacement applied at the column boundaries. Finally, a positive horizontal load was applied in increments of 5 kPa to the boundaries of the model until failure. On the left side of the model, since the initial stress is in the negative direction, the lateral load was first decreased in increments of 5 kPa until zero, and then increased in increments of 5 kPa in the other direction (positive horizontal).

7.2.4 Further Validation - Chen and Martin, 2002

In order to further validate the model configuration used in this analysis (discussed below and shown in Figure 7-3), the soil was represented as a granular material under drained conditions with the same material properties and geometry as used by Chen and Martin (2002), and with piles rather than DSM columns. The piles were modelled as fixed steel plates, as in the validation model. The results of this analysis were then compared to Chen and Martin (2002) and gave a reasonable match as seen in Figure 7-4.

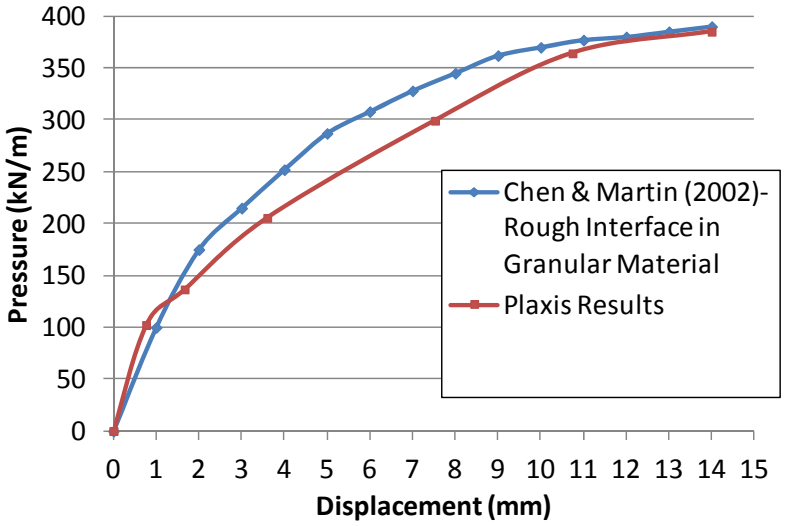

Figure 7-4: Comparison of results to Chen and Martin (2002) for piles in granular soil with a rough interface.

7.3 Influence of Changes in the Transition Zone Surrounding DSM Columns

7.3.1 Behaviour of Soil Surrounding DSM Columns

As mentioned in the Chapter 2, laboratory test results from previous studies show that two to three zones exist outside the nominal diameter of the DSM blade (Larsson & Kosche, 2005; Shen et al., 2003c). These are the expanded zone, transition zone (or influential zone) and boundary layer.

The transition zone extends 1.5 to 2 times the column diameter from the column centre, and is taken as 1.5 for this study. In the transition zone, the undrained shear strength has been found to decrease during DSM column installation, but recover after a short period of curing and further increase over the long term (Larsson & Kosche, 2005; Shen et al., 2008; Shen et al., 2003c). Beyond a distance of four times the diameter of the columns the soil strength has been found to be the same as it was prior to DSM column installation (Muntohar & Hung, 2007).

Within and beyond the transition zone, changes in stiffness parameters such as shear modulus (G), and others parameters such as the coefficient of lateral earth pressure at rest (K_0) have not been extensively studied. The sDMT testing performed at Wairere Drive before and after DSM column installation was discussed in Chapter 3. The results showed an increase in K_D, which is directly proportional to K_0. These results confirm that changes to the soil state surrounding DSM columns have taken place after DSM column installation. Due to their orientation, K_0 is not used directly in the models examined in this chapter. Applying changes to K_0 would require changing the horizontal stresses around the columns. This would require the creation of many small trapezoidal sections around the DSM columns so that the changes in stress could be applied in the appropriate directions, and would be difficult to implement in Plaxis. However, the use of a volumetric strain which is induced during DSM column installation takes changes in horizontal stress (and thus K_0) into account. This is examined in Section 7.4.

7.3.2 Analysis of Fine Grained Soil in Undrained Condition

Four parametric cases, A to D, have been considered for a fine grained soil type in the undrained (short term) condition. The property changes applied in Cases A-C within the transition zone are based on results by Shen et al. (2008). The property changes outside of this zone at up to two times the column diameter from the column centre are interpreted from results by Muntohar and Hung (2007). These cases are shown in Table 7-3.

Table 7-3: Simulated property changes to the soil around the DSM columns in the undrained condition.

Case	Time Frame	Simulated Effects
Base Case	None	Soil is modelled uniformly with properties as shown in Table 7-2 for the undrained condition.
A	Immediately after installation	A softening effect is modelled by applying 40% reduction in undrained shear strength in the column transition zone due to soil disturbance and fracturing.
B	Short term (e.g. 40-70 days after installation)	An increase in undrained shear strength of 23% in the column transition zone is applied, as well as a 12% increase beyond the transition zone out to two times the column diameter.
C	Long term	An increase in undrained shear strength of 50% in the transition zone is applied, along with a 25% increase out to two times the column diameter.
D1	Long term	Young's modulus (E) is doubled within transition zone.
D2	Long term	Young's modulus (E) is doubled out to two times the column diameter.

Pressure and displacement have been measured at the points shown in Figure 7-5. The results of the pressure versus displacement curves for Cases A, B, C, D1 and D2 are shown in Figure 7-6.

In Case A, approximately half as much pressure is acting on the column prior to failure of the soil in plastic flow around the column. Cases B and C show the opposite effect, with Case C showing an increase in pressure on the column at failure of approximately 1.5 times the base case. Doubling Young's modulus in the transition zone results in less displacement prior to failure. When this increase is extended beyond the transition zone in Case D2, there is slightly less displacement than Case D1.

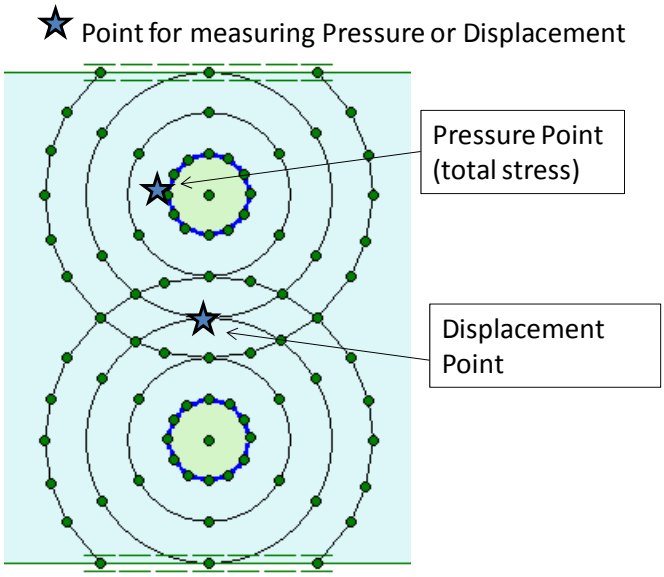

Figure 7-5: Pressure and displacement points used for curves.

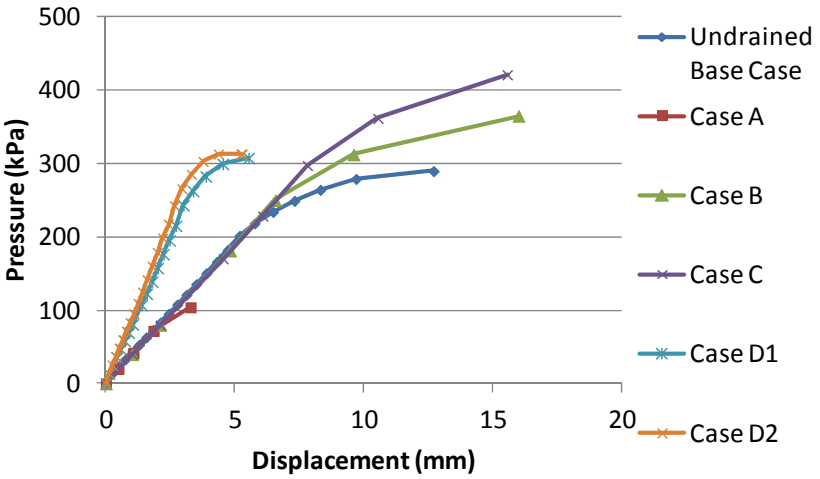

Figure 7-6: Results for undrained conditions.

In Figure 7-7, the length of each line represents the magnitude of the principal stress and the direction indicates the principal direction. The arching effect may clearly be seen to the left side of the columns as the soil flows from left to right.

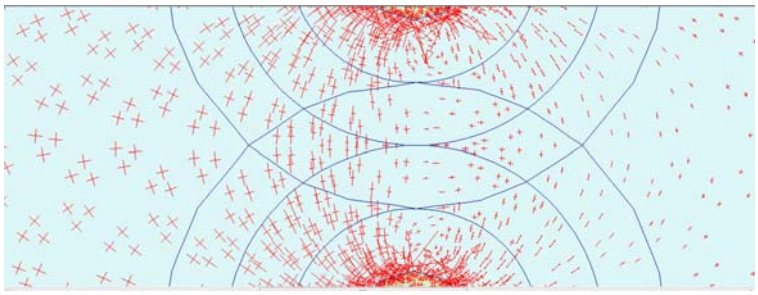

Figure 7-7: Rotation of principal stresses in undrained condition (base case).

The displacement contours in Figure 7-8 show very little soil displacement, due to arching, on the left hand side of the columns. The greater movement on right hand side is likely to be due to the boundary conditions for the model which force the soil to displace laterally rightwards, and this occurs without the "benefit" of the columns to arrest this motion.

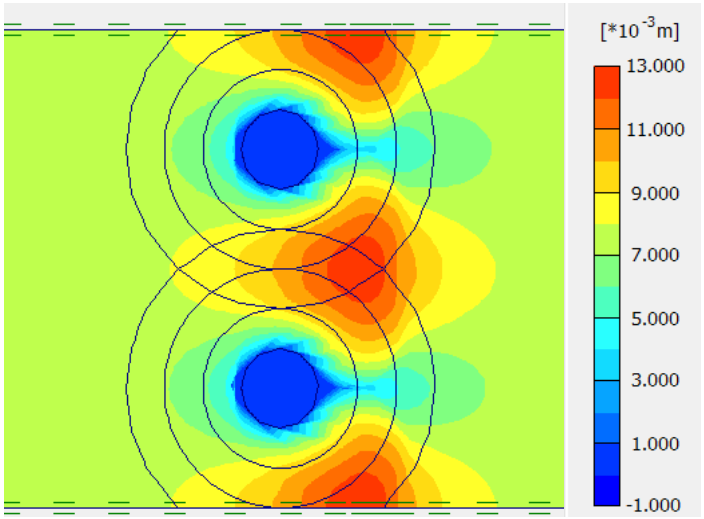

Figure 7-8: Total displacement contours in the undrained condition (base case) at failure.

7.3.3 Analysis of Fine Grained Soil in Drained Condition

Drained conditions have been considered for the scenarios shown in Table 7-4. The results of pressure versus displacement for the drained analyses are shown in Figure 7-9.

Table 7-4: Simulated property changes to the soil around the DSM columns in the drained condition.

Case	Time Frame	Simulated Effects
Base Case	None	Soil is modelled uniformly with properties as shown in Table 7-2 for drained conditions.
A	Short term (e.g. 40-70 days after installation)	An increase in cohesion to 10 kPa in the column transition zone is applied, and to 15 kPa beyond the transition zone out to two times the column diameter.
B1	Long term	Young's modulus (E) is doubled within transition zone.
B2	Long term	Young's modulus (E) is doubled out to two times the column diameter.

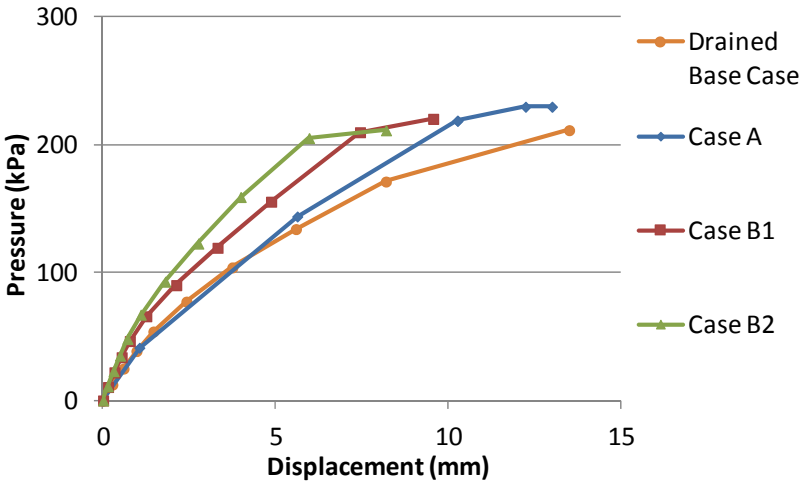

Figure 7-9: Results for the drained condition.

The results show that as with the undrained condition, the increase in shear strength assumed to occur in the soil surrounding the DSM columns results in an increase in maximum lateral pressure on the DSM columns prior to failure via soil flow of approximately 10%. The increase in Young's modulus in the transition zone (Case B1) results in less displacement and higher pressure on the column at failure. An increase beyond the transition zone (Case B2) reduces the displacement at failure even further.

7.3.4 Influence of Column Spacing

The column spacing generally has been set to three times the column diameter from centre-to-centre of the DSM columns (1.8 m). In order examine the influence of column spacing on the ability of the soil to transfer load, using the base case conditions, the column spacing has been reduced to two times the column diameter (1.2 m centre-to-centre), and increased to four times the column diameter (2.4 m centre-to-centre) for the drained condition.

Pressure (total stress) at the pile face versus displacement between the two columns has been plotted for all of the cases examined. The points taken for these curves are shown in Figure 7-5.

Pressure versus displacement is shown in Figure 7-10 for the drained condition with columns spaced at two times the column diameter (2s) as well as 3s, 4s, 6s, 8s, 12s, and 15s.

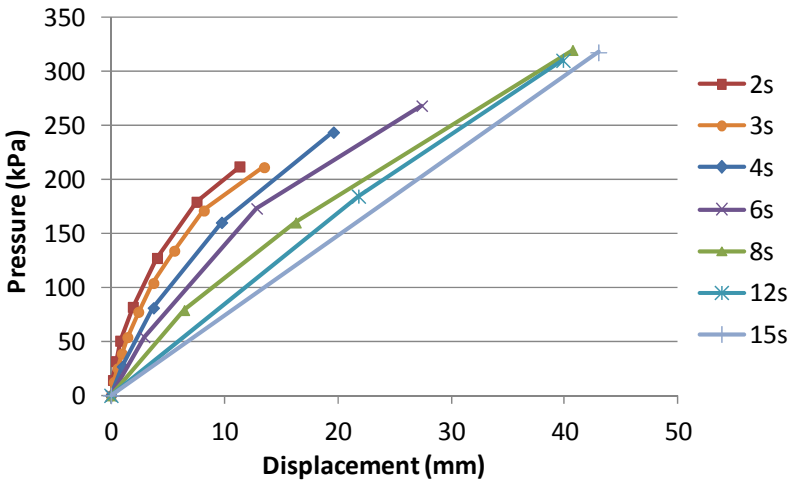

Figure 7-10: Effect of column spacing on pressure versus displacement in the drained condition.

Increasing DSM column spacing results in greater pressure on the column and more soil displacement at failure. The increase in column spacing also acts to decrease the slope of the pressure-displacement line, similar to a decrease in Young's modulus. At 12s and 15s spacing, this is no longer occurring.

Figure 7-11 shows significantly less displacement between the DSM columns at failure for 2s spacing compared to 4s (4-6 mm versus 18-20 mm).

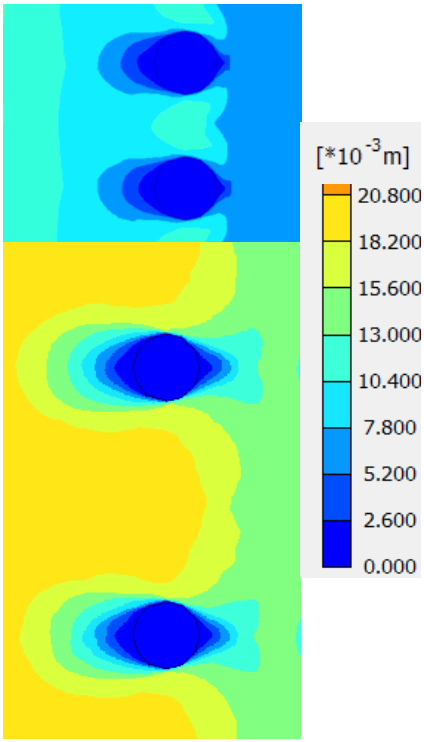

Figure 7-11: Total displacement contours at failure for column spacing of 2s (top) and 4s (bottom) in the drained condition.

Figure 7-12 shows the rotation of principal stresses for 3s, 6s and 12s at soil failure. Comparing Figure 7-12 (3s, undrained conditions) to 3s in drained conditions reveals more uniform principal stress vectors in front and behind the columns in undrained conditions than in drained conditions. This confirms that soil arching is less developed in the undrained condition. At 12s, there is no longer any rotation of principal stresses occurring between the columns.

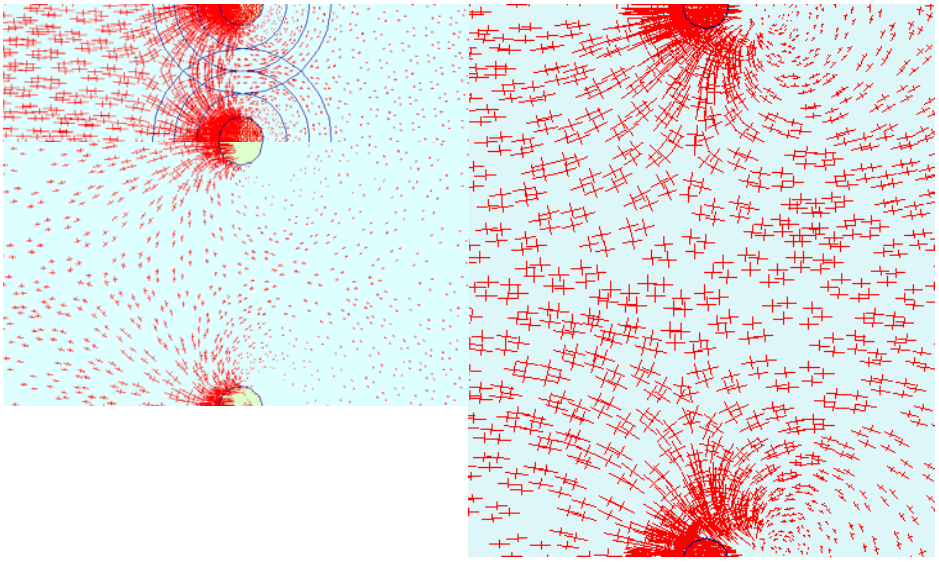

Figure 7-12: Rotation of principal stresses between columns for columns spacing of 3s (top left) and 6s (bottom left) and 12s (right) in the drained condition.

The effects of column spacing in the undrained condition on the pressure versus displacement curve are shown in Figure 7-13.

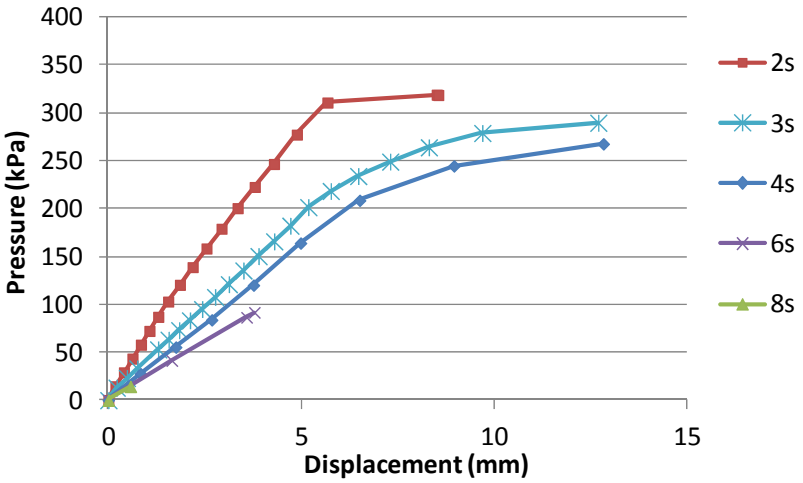

Figure 7-13: Effect of column spacing on pressure versus displacement in the undrained condition.

Figure 7-13 shows that an increase in column spacing results in a decrease in the slope of the pressure versus displacement curve, similar to a decrease in Young's modulus. The decrease in spacing also results in a lower ultimate pressure in the undrained condition.

7.4 Lateral Displacement due to DSM Column Installation

7.4.1 Methodology and Validation

The primary mechanisms that cause lateral displacement in the soil around DSM columns are the expansion and possible hydraulic fracturing in the ground due to the injection pressure and the addition of material into the ground, and it can be investigated by analysing the shearing-expanding process of a cylindrical cavity (Shen et al., 2003c). The theory of cylindrical cavity expansion is thoroughly described by Vesic (1972).

The amount of displacement occurring in the soil surrounding DSM columns can be computed through the theory behind the expansion of a cylindrical cavity (Figure 7-14).

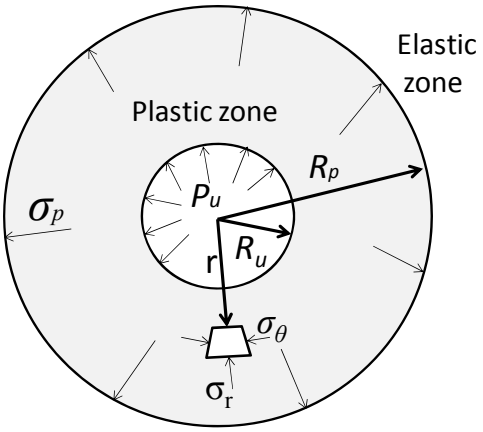

Figure 7-14: Expansion of a cylindrical cavity (modified after Chai et al., 2005).

In Figure 7-14, R_u is the radius of the cavity, R_p is the radius of the plastic zone, σ_p is the pressure at the interface of the plastic zone and elastic zone, σ_r is the radial stress on a soil element and σ_Θ is the horizontal stress on a soil element. P_u is the cavity pressure, and r is the distance from the column centre to the point where displacement is being measured.

In the case of DSM, the radius of the cavity (R_u) is not necessarily the same as the radius of the DSM column. Chai et al. (2005) back estimated the cavity radius based on measured ground displacement for several case studies for a 1 m diameter column. The results are summarized in Table 7-5. R_{u0} is the radius of the cavity corresponding to a Young's modulus of E_1.

Table 7-5: Back estimated R_{u0} based on mass injected and injection pressure (Chai et al., 2005).

Mixing Method	Mass Injected (m^3/m)	Injection Pressure (kPa)	R_{u0} (m) (E_1 = 2250 kPa)	% of True Column Diameter
Slurry Double Mixing	0.146	100-200	0.21	42%
Dry Jet Mixing	0.036	500-700	0.46	92%
Wet Jet Mixing	0.146	20000	0.58	116%

Given the slightly lower injection pressure (15000 kPa) and mass injected (0.1 m^3/m) for TurboJET compared to the generalized values for wet mixing in Table 7-5, the R_{u0} for TurboJET was estimated to be equal to the radius of the cavity (100%) as shown in Table 7-6 (for a 0.6 m diameter column). This is for soil with a Young's modulus (E_1) of 2500 kPa. Chai et al. (2005) suggest the following equation to derive a new R_u for a different soil stiffness:

$$R_u = R_{u0}\left(\frac{E_1}{E}\right)^{1/3} \qquad (7.1)$$

Based the estimated R_{u0} of 0.3 m for E_1 of 2500 kPa, TurboJET columns in Allochthon soil with an E of 22,500 kPa and a radius of 0.3 m have an estimated R_u of 0.14 m (Table 7-6).

Table 7-6: Estimated R_{u0} for TurboJET in Northland Allochthon clay soil.

Mixing Method	Mass Injected (m^3/m)	Injection Pressure (kPa)	R_{u0} (m) (E_1 = 2500 kPa)	% of True Column Diameter	R_u (m) (E = 22500 kPa)
Wet Jet Mixing	0.1	15000	0.3	100%	0.14

A sensitivity analysis was performed on the influence of the R_u value on the displacement in the soil surrounding the columns for the soil properties as shown in Table 7-2. Points at distances 0.6 m and 1 m away from the column centre (or 0.3 m and 0.7 m away from the

column edge) were examined. The results are shown in Figure 7-15. It is evident that the R_u value has more influence on the amount of displacement occurring closer to the column. At smaller R_u values, the influence on displacement is minimal. As the R_u value increases, it has a linear influence on displacement. The total difference in displacement for R_u values from 0 m to 0.4 m at 0.6 m away from the column edge is only 0.12 m.

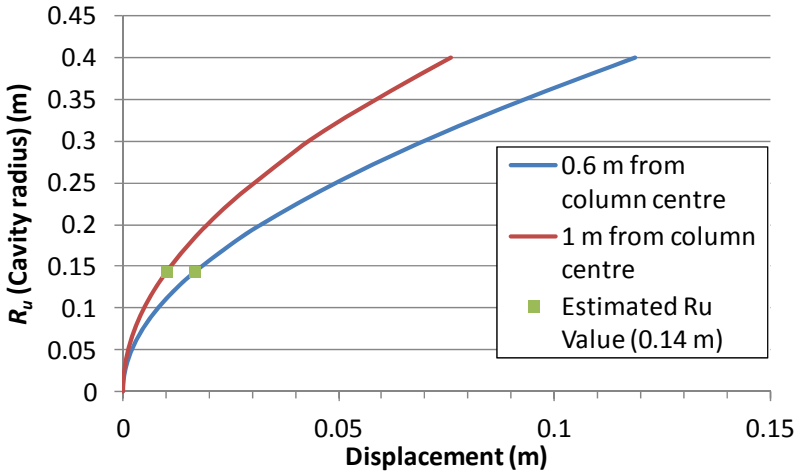

Figure 7-15: Relationship between R_u value and displacement at 0.6 m and 1 m away from column centre.

The following equations can be used to compute the displacement (δ) at a distance r from the centre of the cavity (Vesic, 1972). The cavity pressure P_u can be calculated as follows:

$$P_u = cF_c + pF_q \qquad (7.2)$$

where c is the soil cohesion, F_c and F_q are dimensionless spherical cavity factors and p is the initial mean normal stress equal to:

$$p = \frac{(1+2K_0)\sigma_{v0}}{3} \qquad (7.3)$$

For zero volumetric strain and φ=0 (undrained conditions), F_q reduces to 1 and F_c reduces to the following:

$$F_c = ln(I_r) + 1 \qquad (7.4)$$

where I_r is a rigidity index equal to G/c (where G is elastic shear modulus and c is the cohesion). From these values, σ_p (the stress at the interface of the elastic and plastic zones) can be defined:

$$\sigma_p = P_u - 2c \ln\left(\frac{R_p}{R_u}\right) \qquad (7.5)$$

where R_p is computed as:

$$R_p = R_u\sqrt{\frac{E}{3c}} \qquad (7.6)$$

The amount of displacement (δ) measured at a distance r from the column centre in the plastic zone can be computed by:

$$\delta = \delta_p \frac{2R_p+\delta_p}{2r+{}^{\delta_p R_p}/_{r}} \quad (R_u \leq r \leq R_p) \qquad (7.7)$$

where δ_p is the displacement at R_p, and R_p is the radius of the plastic zone. δ_p can be computed through:

$$\delta_p = \frac{1+v}{E} R_p(\sigma_p - p) \qquad (7.8)$$

In the elastic zone, the displacement is:

$$\delta = \frac{R_p}{r}\delta_p \quad (r > R_p) \qquad (7.9)$$

In order to validate cavity expansion behaviour, a case study for one metre diameter DSM columns in Taipei clay with an E of 14500 kPa was examined (Chai et al., 2007; Lin & Lin, 2006). The R_u value for the columns was 0.35 m, and cohesion (c) was 47 kPa with a Poisson's ratio (v) of 0.5. The above equations were input into a spreadsheet and the properties from the case study were utilized to validate that the spreadsheet was functioning

properly. A simpler model with only one DSM column and larger boundaries was developed in Plaxis 2D to validate that the program was obeying the theory of cavity expansion. The geometry of the model is depicted in Figure 7-16. The displacement computed by the spreadsheet at the column edge was used to determine the volumetric strain in the column, which was applied to the column edge in the numerical model. Final displacements within the model were tabulated at five points at varying distances from the column centre and compared to the results computed in the case study and the analytical results computed in the spreadsheet. These results are shown in Figure 7-17.

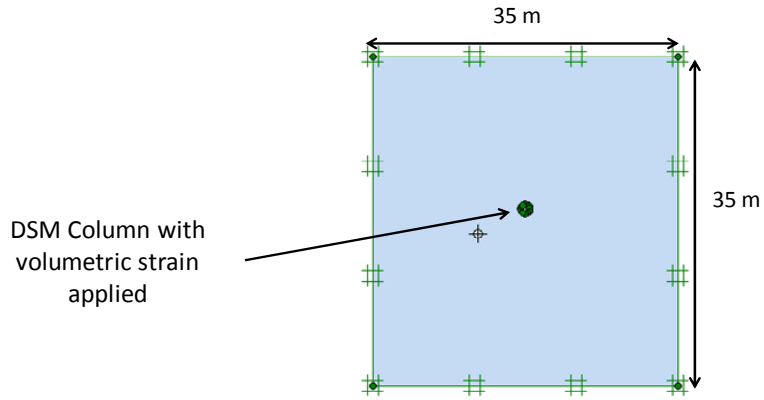

Figure 7-16: Model geometry for validation of cavity expansion.

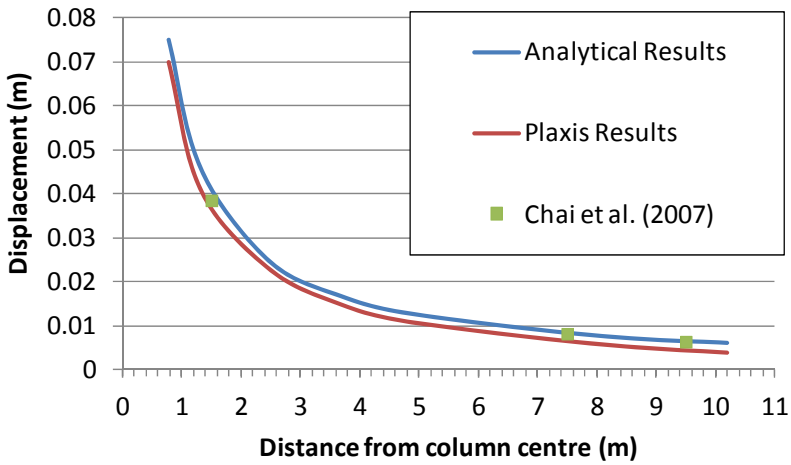

Figure 7-17: Comparison of lateral displacements results from spreadsheet (analytical), numerical model and case study for DSM columns in Taipei clay.

The results in Figure 7-17 show that numerical model as well as the analytical solution are in close comparison to the results computed by Chai et al. (2007). The equations were then used to compare the results of the numerical model to the analytical solution with Northland Allochthon clay soil properties. With the geometry of the model remaining the same, the soil properties were varied to correspond to those shown for the undrained conditions in Table 7-2. An R_u of 0.14 as estimated in Table 7-6 results in a displacement of 0.032 m at 0.3 m away from the column centre (at the column boundaries). This displacement was applied at the column boundaries. The new soil properties were inputted into the spreadsheet to compute the estimated displacement using the analytical solution at the column edge for a 0.6 m diameter column. Once again, within the numerical model, soil displacement was measured at five locations at varying distances from the column centre and compared to the analytical results for these locations. The results are shown in Figure 7-18.

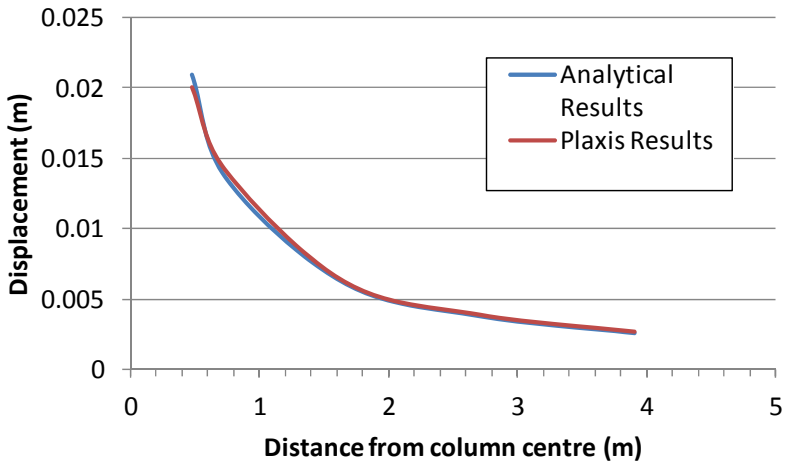

Figure 7-18: Comparison of lateral displacement results from spreadsheet (analytical) to numerical model for Northland Allochthon soil.

Due to the imperfect geometry of the numerical model (i.e. the DSM column is not a perfect circle) an exact match of the numerical model to the analytical solution is not expected. However, Figure 7-17 and Figure 7-18 show a close match, and demonstrate that the numerical model is sufficiently following the theory of cavity expansion for the material properties of both the Taipei clay and Northland Allochthon clay.

7.4.2 Effects of Lateral Displacement due to Column Installation under Lateral Loading

The effects of lateral displacement were examined using the same model configuration as Figure 7-3. The boundary conditions were also the same as those described for Figure 7-3, as were the applied stresses and staged loading. The points selected for examining stress strain curves were as shown in Figure 7-5. However, a volumetric strain was applied to the columns during the column installation stage and prior to commencing lateral loading. During this stage, the fixed boundary condition around the column edges was removed in order to allow displacement. A displacement of 0.032 m at the column edges was estimated from the analytical solution (spreadsheet) based on the estimated R_u (Table 7-6). To acquire this displacement at the column edges, a volumetric strain of 22.5% was applied to the columns.

The analysis was performed in both drained and undrained conditions. Figure 7-19 and Figure 7-20 show the results of pressure versus displacement in the undrained and drained conditions, respectively, for the base case and the case with the induced volumetric strain in the columns.

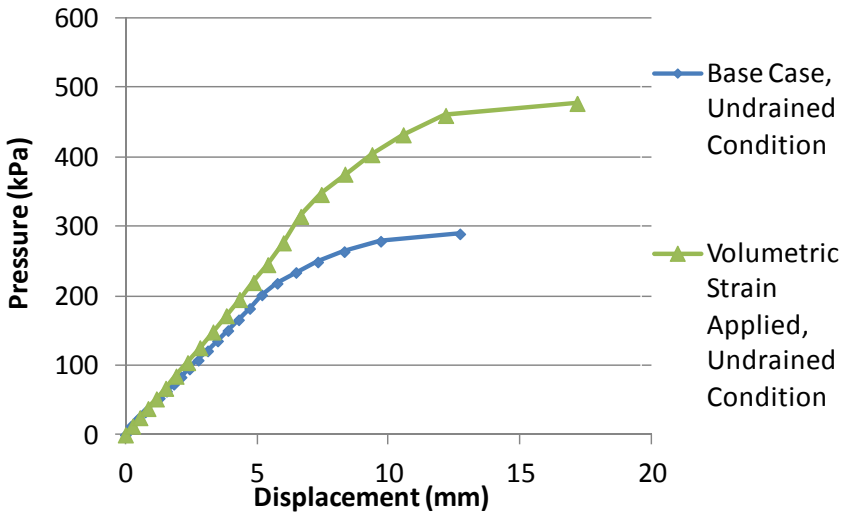

Figure 7-19: Pressure versus displacement curve with and without volumetric strain applied to the DSM columns- undrained condition.

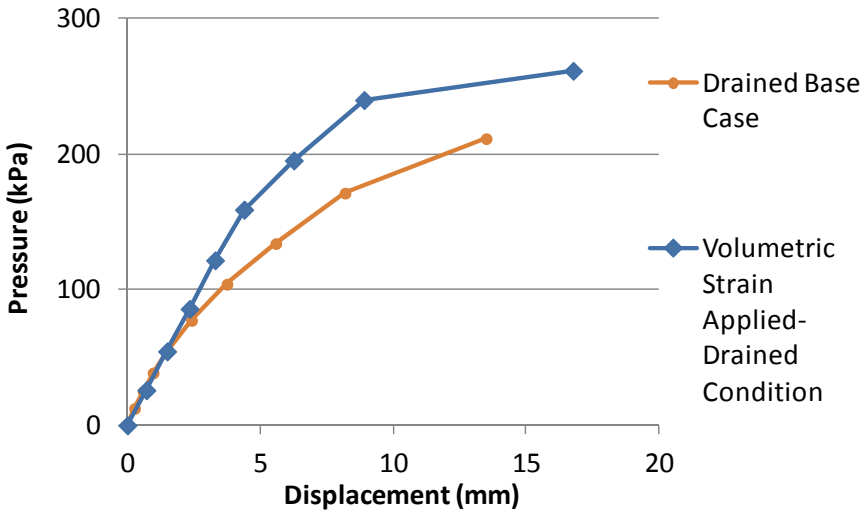

Figure 7-20: Pressure versus displacement curve with and without volumetric strain applied to the DSM columns- drained condition.

Figure 7-19 and Figure 7-20 show that there is a significant increase in the ultimate pressure acting on the front of the DSM columns prior to failure of soil in plastic flow around the columns in both the drained and undrained conditions due to the induced volumetric strain in the columns. There is approximately a 65% increase in the ultimate pressure on the columns in the undrained condition and a 23% increase in the drained condition. An increase in confining pressure (due to an increase in the depth being examined) would likely reduce the difference between the maximum pressure acting on the columns prior to failure of the soil around them in the base case compared to the case where volumetric strain due to column installation is implemented.

7.4.3 Behaviour of Square Columns versus Circular Columns under Lateral Load

The formation and shape of the arching zone in front of laterally loaded piles is a function of pile arrangement, pile shape, interface roughness and soil dilation angle (Martin & Chen, 2005). The existence of an arching foothold in front of the circular pile will cause less pressure to act on these piles than on equivalent rectangular piles (i.e. d x d, d=diameter) (Adachi et al., 1989). Square columns are introduced here because in Chapter 8, rectangular columns are utilized in a 3D analysis. Rao et al. (1999) did a series of laboratory experiments

to investigate the influence of the shape of a pile foundation on its lateral response. They found that the ultimate lateral capacity of square piles made of steel was approximately 5% to 20% more than that of circular piles with the same area, depending on the consistency index (I_c) and undrained sheared strength of the soil. I_c is defined as follows:

$$I_c = \frac{w-LL}{LL-PL} \qquad (7.10)$$

where LL is the liquid limit of the soil, PL is the plastic limit, and w is the water content. Square piles or columns have a higher lateral capacity because arching mechanisms are affected by the shape of the piles or columns to some degree.

A numerical model of equivalent square DSM columns was developed in order to examine the difference in arching mechanisms, ultimate pressure, and displacement between square and circular columns. The geometry of the model is shown in Figure 7-21. The length of the square columns was selected to be 0.6 m (equivalent to the diameter of the circular columns) to ensure that the length of the column across the model is equivalent in both cases. This is the method used by other researchers examining the difference between square and circular piles under lateral loading (Abbas et al., 2008; Adachi et al., 1989; Rao et al., 1999).

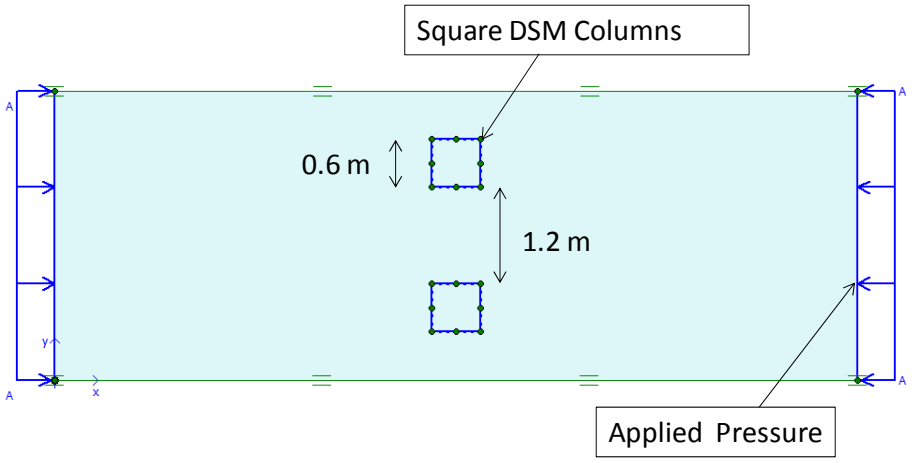

Figure 7-21: Geometry of model (square columns in plan view).

The results of the pressure versus displacement curves for square versus circular columns in undrained and drained conditions are shown in Figure 7-22 and Figure 7-23, respectively. Both the drained condition and undrained condition show a slightly higher ultimate pressure on square columns compared to circular. The ultimate pressure is approximately 10% higher in the undrained case and 5% higher in the drained case.

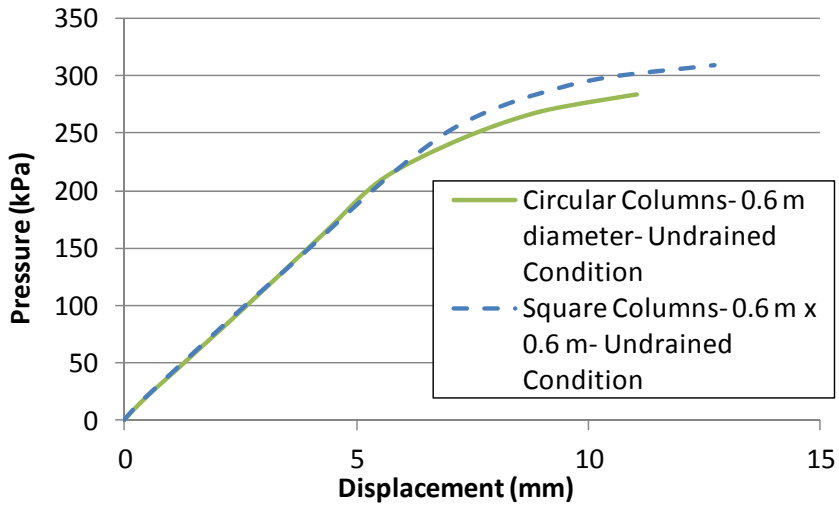

Figure 7-22: Pressure versus displacement curve for square and circular columns in undrained condition.

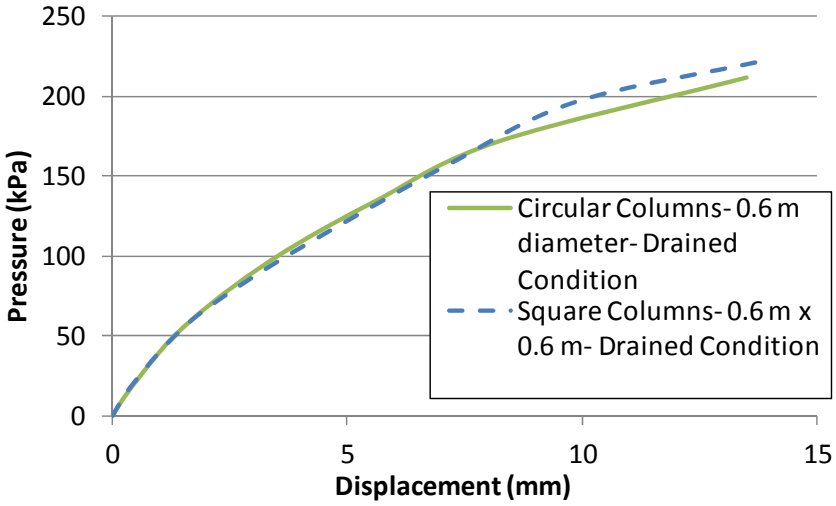

Figure 7-23: Pressure versus displacement curve for square and circular columns in drained condition.

Figure 7-24 shows the rotation of principal stresses in the drained condition for the two column shapes. Both scenarios show strong arching mechanisms between the columns, with the location of arching in similar locations. Rotation of principal stresses appears to begin slightly further to the left of the columns in the scenario with the square columns, as indicated by the longer arrow. The lateral loading acting on a pile is resisted by the earth pressure in front of the pile or column and the shear stresses acting on the sides (Rao et al., 1999). In the case of square columns, the corners of the square are in closer proximity to the arching zone, and there is better direct contact between the soil and the column in front of the column, and in shear on the sides of the column.

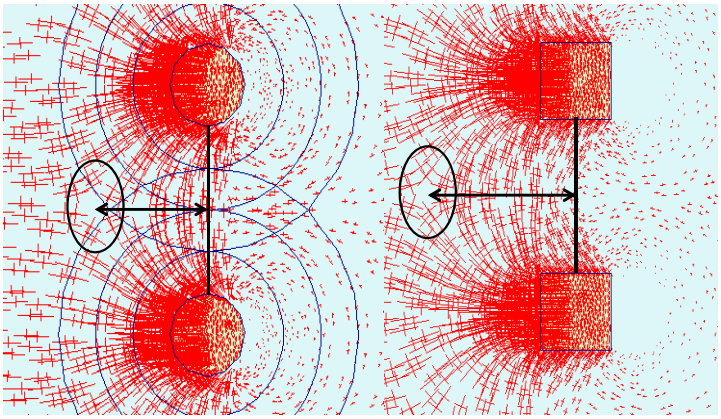

Figure 7-24: Rotation of principal stresses in the drained condition for circular and square columns.

7.5 The Use of Plaxis 2D in Plan View

Although Plaxis 2D is a common program for the modelling of DSM columns and other ground improvement techniques (Gani, 2004; Guetif et al., 2007; Krenn & Karstunen, 2009; Leung et al., 2006; O'Sullivan et al., 2009; Terzaghi et al., 2005), based on a thorough literature review there are no other published studies where Plaxis 2D has been utilized to examine a problem in plan view. Other 2D studies of this sort have used programs that allow for more user control and variation of conditions, such as FLAC (Chen & Martin, 2002) or other specially developed programs such as AVPULL (Chen & Poulos, 1993). Although the use of Plaxis 2D for the analysis in this chapter has presented some challenges, the study performed here demonstrates that it is an effective tool for this purpose. This study also provides a useful reference for those who wish to use Plaxis 2D for analysing soil-structure interaction problems in plan view.

7.6 Conclusions

Numerical modelling of piles in plan view using Plaxis 2D finite element software was successfully validated against an analytical solution and a previous study. This model was then used as a basis for examining soil arching and how it is influenced by installation effects in laterally loaded DSM columns. The increased shear strength in the soil surrounding DSM columns seen by several researchers leads to an increase in the ultimate lateral pressure acting

on the columns prior to failure of the soil in plastic flow around the columns. For the Northland Allochthon clay soil properties used in this study, the load capacity increase was approximately 50% in the undrained condition and 10% in the drained condition. An increase in soil stiffness (Young's modulus) results in less displacement prior to failure of the soil and a steeper pressure versus displacement curve. An increase/decrease in column spacing has a similar effect on the slope of the pressure-displacement curve as an increase/decrease in Young's modulus. An increase in DSM column spacing results in a lower ultimate pressure acting on the columns prior to failure of the soil around them. In addition, it results in an increase in the ultimate relative displacement on the columns in the undrained condition, and a higher ultimate pressure and ultimate relative displacement in the drained condition.

The incorporation of lateral expansion induced by DSM columns into a slope stabilization scenario (i.e. laterally loaded) has resulted in an increased ultimate pressure on the columns in both the drained and undrained conditions prior to failure of the soil in plastic flow around them. The increase is more significant in the undrained condition.

Square columns with the same dimensions as the circular columns have a slightly higher ultimate pressure acting on them prior to soil failure around the columns due to shape effects on arching mechanisms. The pressure was found to be approximately 10% higher in the undrained condition and 5% higher in the drained condition.

The results in this chapter show that for DSM columns in Northland Allochthon clay soil, the installation effects that cause changes to the soil around the columns result in an increased lateral ultimate pressure on the columns prior to plastic failure of soil around them by about 23% (drained condition) and 65% (undrained condition). The lateral expansion due to column installation in this soil type using TurboJET is significant (approximately 0.032 m at the column edge) due to the high injection pressure and the low Young's modulus of the soil.

It has been demonstrated that the plan view model developed in this chapter using Plaxis 2D is a useful method for examining load transfer mechanisms of DSM columns. Overall, the results provide practitioners with evidence of the beneficial nature of DSM column installation effects. It has been clearly demonstrated that these effects provide a substantial increase in the load that can be acting on the columns prior to failure of the soil around them.

The 2D analysis examined here does not allow for failure through the columns themselves as it is an ultimate state analysis involving failure of the soil only. In the following chapter, a laterally loaded 3D model is examined which allows for soil arching, as seen in this chapter, as well as column failure as examined in conventional 2D models.

8.0 Comparison of the Behaviour of DSM Columns under Lateral Loading in 2D versus 3D

8.1 Introduction

Often two dimensional models are used in place of more realistic three dimensional ones in practice, due to budget and time constraints. The replacement ratio method (RRM), discussed in Chapter 6, is often used to model DSM columns in 2D. This method involves modelling the DSM columns together with the surrounding soil as a block of composite material. The column spacing is accounted for by allocating averaged properties to the 2D columns, based on the ratio by volume of the soil and column material. Note that in the RRM, the replacement ratio for the DSM column material (r_{col}) corresponds to the definition of the replacement ratio that is commonly used in the design of ground improvement methods. Another term, r_{soil}, which is equivalent to 1-r_{col}, and is referred to as the replacement ratio of the soil, is used in this thesis because this value plays an integral role in defining the composition of the composite DSM column/soil material in 2D models that use the RRM. The RRM is commonly used by practitioners in New Zealand (Gani, 2004; O'Sullivan et al., 2009; Terzaghi et al., 2005), and a need for further research into how well the RRM works has been identified (Leung et al., 2006). Specifically what is needed is to determine how well this 2D method for representing the soil-column system resists lateral loading as compared to a more realistic representation of reality, where soil flow around the columns and soil arching is possible, such as a 3D model. This type of comparison will provide practitioners with an indication of whether or not the RRM is in fact a reasonable simplification, or if modifications to the RRM are required for a better representation of a 3D scenario.

Therefore, the primary goal of this chapter is to compare the performance of slope stabilizing DSM columns in a 2D model (using the replacement ratio method) to a more realistic 3D model. This chapter uses an existing and proven 3D method (developed for simplifying the design of laterally loaded piles), and applies it to laterally loaded DSM columns for a different and new purpose which has not been previously performed- to compare 3D and 2D scenarios. The simplified model of laterally loaded DSM columns with a representative region of soil surrounding them has been developed based on a hybrid method for analysing slope stabilizing piles by Kourkoulis et al. (2012). The model is examined in both 2D and 3D

with one row of columns, and with three rows of columns. Column spacing is also varied. Through the examination of the resisting force provided by the DSM columns, displacements, and total stresses, the effectiveness of the replacement ratio method and how it differs from the 3D scenario is investigated.

8.2 Hybrid Method for Slope Stabilizing Piles

8.2.1 Reason for Use

The hybrid method for slope stabilizing piles was developed by Kourkoulis et al. (2012) for the purpose of simplifying the design of laterally loaded piles (i.e. so that a piece of the slope could be modelled rather than modelling the whole slope, in order to determine the most efficient pile spacing and dimensions). The study in this chapter has a very different purpose: to compare a 3D model to a 2D model that uses the RRM. It was determined that a full scale slope model would not suffice for this analysis. This is because different slope geometry conditions will impact the difference between 2D and 3D results, especially if factor of safety (FoS) analysis is the primary method for comparing them, because the location of the slip surface is affected by the slope geometry. This means that results of a full-scale slope model would not be widely applicable. Figure 8-1 shows the slip surface location (displacement vectors) at the Ogles No. 3 site (examined in Chapter 6) after the DSM columns have been installed.

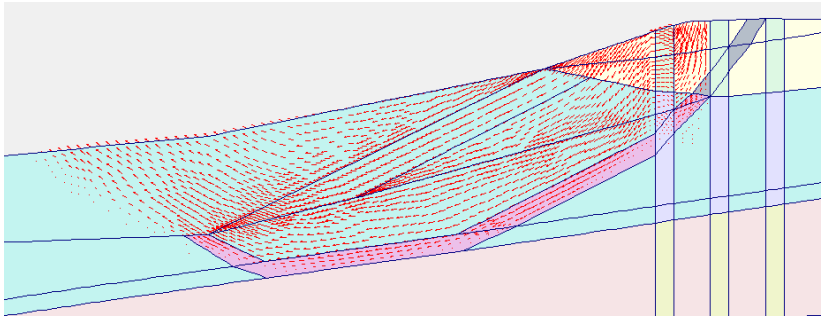

Figure 8-1: Displacement vectors for most likely slip surface after DSM column installation at Ogles No. 3.

Figure 8-1 demonstrates that the most likely slip surface has moved down slope after DSM column installation, and is no longer transecting the middle column. Therefore, in this

scenario, the strength of the columns will not have a large influence on the FoS. In addition, when a full scale slope model is used, the use of the resisting force as a measure for gauging the resistance provided by the DSM columns in 2D versus 3D would also not provide a widely applicable method for comparison in a full-scale slope model, as it too would be affected by slope geometry. In a full scale slope model, it would be difficult to ensure that failure is occurring directly through the columns, since in installing the columns, the most likely (lowest FoS) slip surface may move under or in front of the columns - which is actually part of the reason that they are installed in a particular location. In this study, it is crucial that failure occurs through the columns, as it is the effectiveness of the columns themselves that is being compared.

It was important that the method for simplifying the slope used in this chapter be based on a verified method specifically developed for a laterally loaded 3D slope that incorporates ground improvement. The simplified slope used by Kourkoulis et al. (2012), although developed for a different purpose than the goals of this study, meets these requirements, and has been validated against experimental, field and theoretical results. Therefore, this type of simplified model was deemed appropriate for the analysis in this chapter.

8.2.2 Method Description

In developing a hybrid method for designing slope stabilizing piles, Kourkoulis et al. (2012) desired to combine the accuracy of rigorous 3D finite element (FE) analysis with the simplicity of widely accepted analytical techniques. The method consists of two steps (Kourkoulis et al., 2012): (1) evaluation of the lateral resisting force (RF) needed to increase the safety factor of the precarious slope to the desired value, and (2) estimation of the optimum pile configuration that offers the required RF for a prescribed deformation level. The first step utilizes the results of conventional slope stability analysis. The second step consists of decoupling the slope geometry from the computation of pile lateral capacity, which allows numerical simulation of only a limited region of soil around the piles. A schematic illustration of the simplified decoupled method as used in this chapter for DSM columns is shown in Figure 8-2.

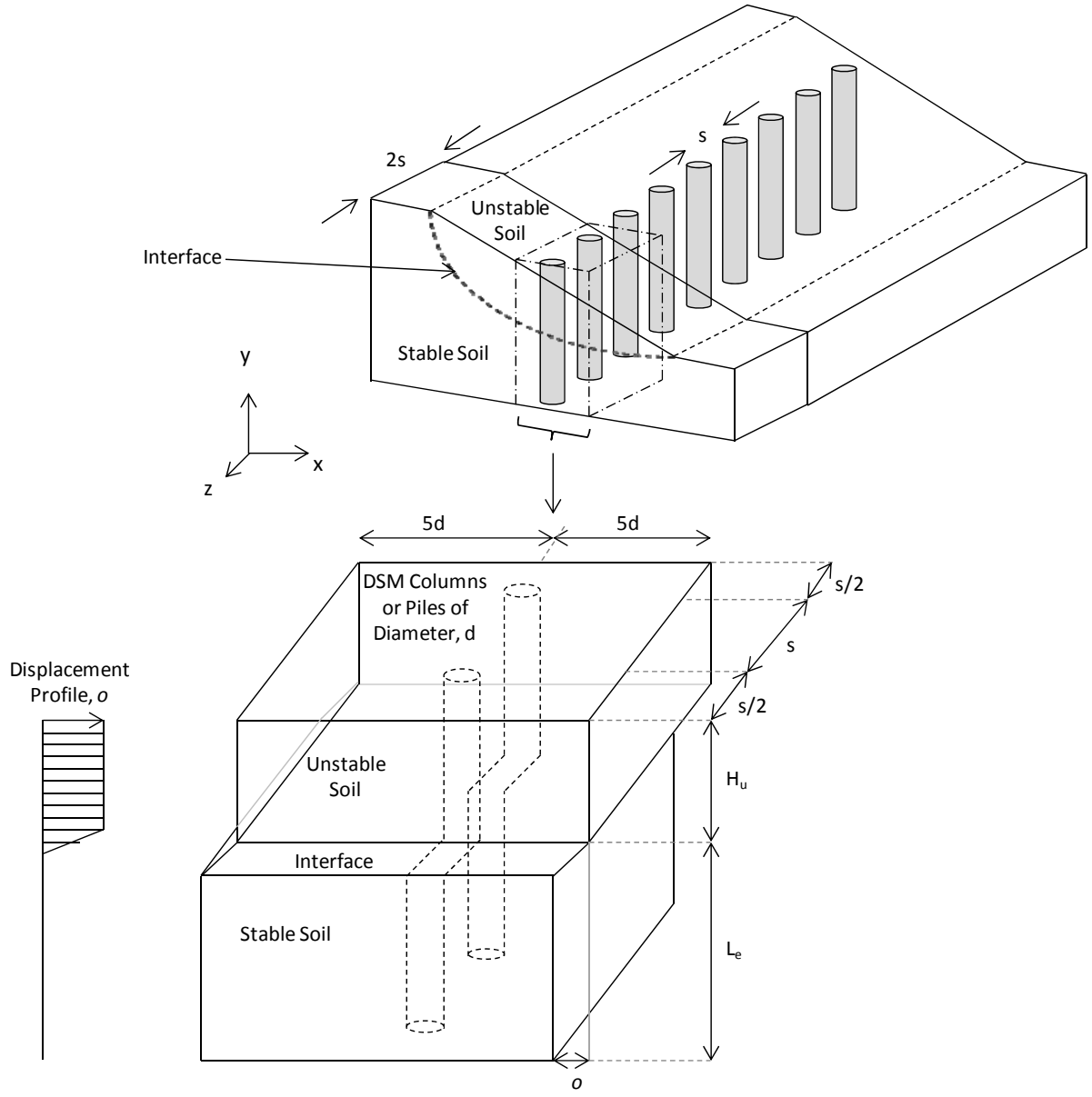

Figure 8-2: Schematic illustration of the simplified decoupled methodology for estimation of DSM column ultimate resistance (modified after Kourkoulis et al., 2012).

In Figure 8-2, instead of modelling the whole slope-soil-column system (top sketch), the focus is on the DSM columns and a representative region of soil at its immediate vicinity (boxed area). The geometry and the key parameters are show in the bottom sketch. H_u is the thickness of the unstable soil, and L_e is the distance from the top of the interface to the base of the stable soil. The interface is the pre-existing sliding plane, or the "sheared zone". In the

simplified decoupled model, column loading is in the form of the application of a uniform displacement profile along the column length in the unstable soil. The displacement tapers to zero at the base of the "interface".

As mentioned in Section 8.2.1, the above technique was used as a basis for the following investigation because it eliminates extraneous behaviour and focuses the analysis on the DSM columns themselves. The RF (discussed further in Section 8.3.3) provides a way to compare how well the soil is resisting the lateral load in the 2D model versus the 3D model.

The simplified decoupled approach that is described above is realistic when a slope failure surface pre-exists. This pre-existing plane will not change due to the installation of columns. Since in most cases, DSM columns are installed to mitigate existing road slips, this assumption is valid. Furthermore, the analysis performed in Chapter 3 provides additional evidence that it can indeed be practical to assume that the failure of Northland Allochthon clay slopes occur along pre-existing failure planes.

The study performed in this chapter is an original use of the hybrid method for designing slope stabilizing piles developed by Kourkoulis et al. (2012) because of the following:

- This study examines DSM columns rather than piles, which have different properties. In addition, Northland Allochthon soil properties are used.
- The DSM columns are loaded with incremental displacements until failure, rather than applying displacements that were acquired from a specific slope geometry.
- A 2D simplified slope model is examined. The method by Kourkoulis et al. (2012) was used by the authors only for simplifying a 3D model.
- The simplified slope models in 2D and 3D developed in this study are being utilized for a very different purpose than what the hybrid method for slope stabilizing piles was created for. That is, to compare laterally loaded DSM columns in 2D (using the RRM) to the same 3D model (rather than to simplify the design of slope stabilizing piles).

8.3 2D Model Development

8.3.1 Model Geometry

Plaxis 2D (Version 9) was used for the 2D modelling. The geometry of the model was set up as close as possible to an actual (simplified) Northland Allochthon clay slope, mitigated using DSM columns. The 2D model geometry is shown in Figure 8-3.

Kourkoulis (2009) varied the stable ground properties parametrically in order to model a dense sand (representing a low strength material), a weak rock (intermediate strength) and a stiff rock (high strength). For the case of the shallow landslide (4 m deep), all three cases led to the same value of the ultimate resisting force. The landslide being examined here is also a shallow landslide (4.3 m deep). Therefore, the properties of the lower layer are not likely to have much influence on the ultimate resisting force. The embedment depth of the columns can have a minor influence on the ultimate resisting force (Kourkoulis, 2009; Poulos, 1999). As the embedment depth increases beyond 1.2 times H_u (thickness of the unstable soil), the discrepancies amongst different depths becomes less pronounced. RF ranges from approximately 750 kN/m to 790 kN/m at 1.2 H_u (depending on the material strength) compared to approximately 440 kN/m to 780 kN/m at 0.7 H_u. The embedment depth in the geology shown in the Figure 8-3 is 1.04 H_u, as this is closest to the actual slope geology. At this embedment depth, the soil properties of the stable layer may still have some influence on the RF. However, this influence will not affect the comparison between the 2D and 3D models, as both models have the same embedment depths.

The thickness of the pre-existing sliding plane (sheared zone) in Figure 8-3 is 10 cm. The role of this zone was investigated by varying its thicknesses between 5 cm and 15 cm. It was found that the thickness of this zone did not affect the ultimate resisting force.

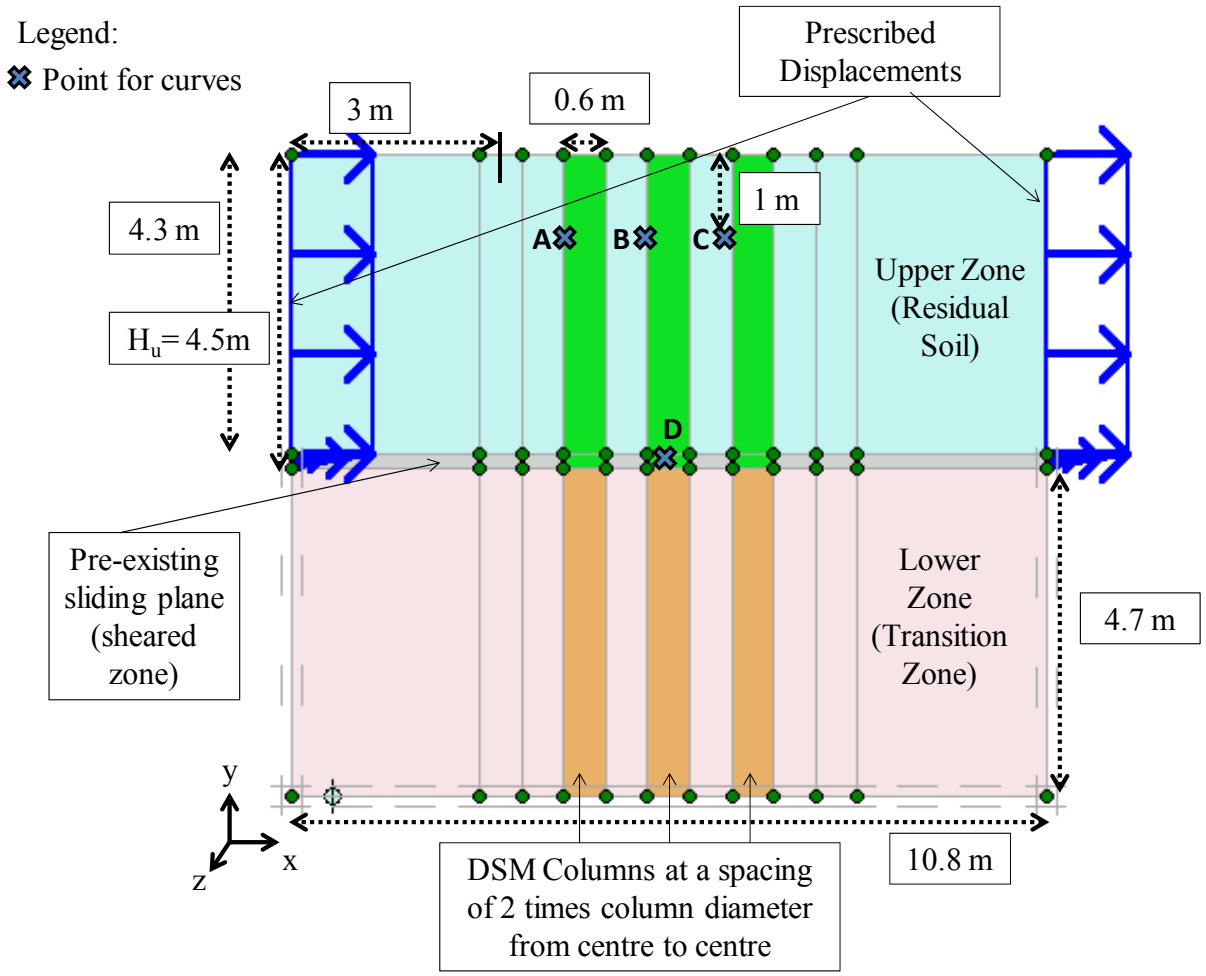

Figure 8-3: Model geometry in 2D with 2s column spacing.

Three different column spacing scenarios are examined for 0.6 m diameter columns: 2s (columns are two times the column diameter apart, from centre-to-centre), 3s, and 4s. Another scenario, where only the middle column is modelled (i.e. the column beside point B in Figure 8-3) is also examined. In this scenario, the columns in the same row as this column in the out of plane (z) direction are modelled at 3s. In Plaxis, stress points and displacement points can be selected in order to examine load and displacement curves at these points. Stress points are located around a node, while displacement points are located at a node. It is very important that when comparing stresses or displacements at certain points in the model the mesh be identical in all situations. Changes in the mesh result in changes in node locations (thus changing the stress and displacement points for curves). Therefore, all

possible column locations for the three column spacings examined are included in the mesh, and activated as desired, to ensure the mesh is the same in all scenarios. The 2D model was run with 6-node elements, which is equivalent to 15-node wedges in the 3D model as shown in Figure 8-4. The use of the 15-node elements in the 2D model is more accurate, but results in different (and more numerous) stress and displacement point locations, as well as slightly different results. The stress points and displacement points selected in the 2D model are shown in Figure 8-5 for 3s.

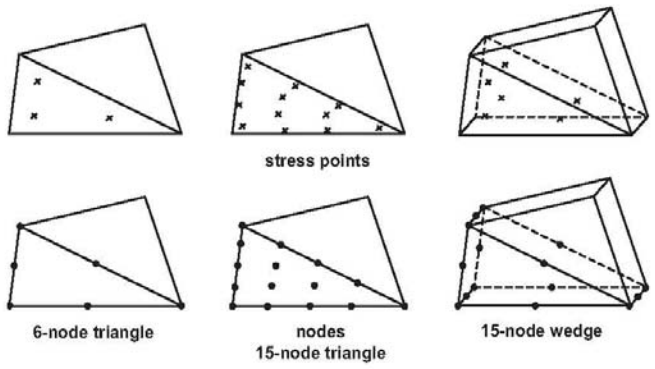

Figure 8-4: Position of nodes and stress points in soil elements in Plaxis 3D Tunnel (Plaxis, 2004).

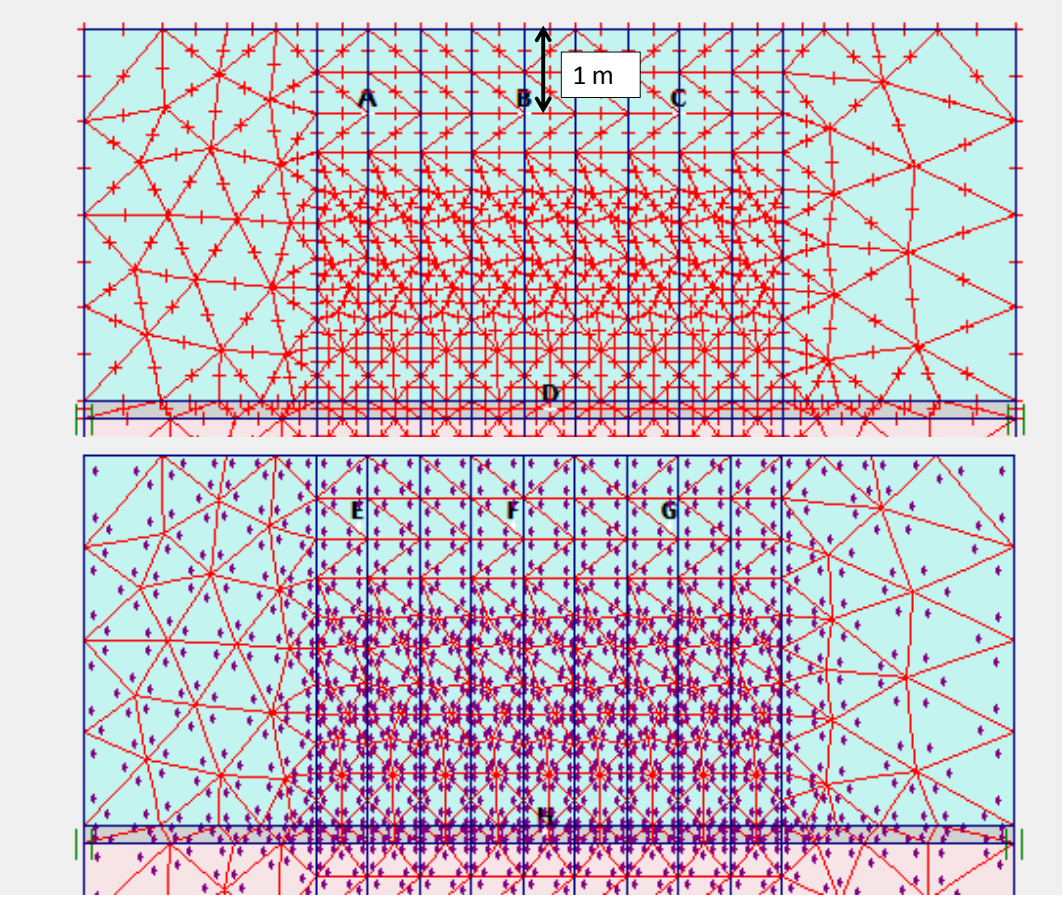

Figure 8-5: Points for curves (top: displacement points; bottom: stress points).

8.3.2 Boundary Conditions

This model simulates a representative slice of an infinitely long slope (in other words, it does not matter where the columns are actually placed within the slope). Therefore, the boundary conditions applied on the sides (left and right sides) constrain out-of-plane displacement (z-direction) but allow vertical and horizontal displacements. The vertical displacement of the bottom nodes is restrained, as is the horizontal displacement of its far left and far right side-nodes. The top boundary of the model is free to move both horizontally and vertically. Displacement was applied uniformly in the residual soil, and tapered to zero in the pre-existing sliding plane, as indicated by the blue arrows in Figure 8-3.

8.3.3 Resisting Force

The resisting force against displacements that are prescribed in the x and y direction (and in 3D, the z direction) is calculated and stored as an output parameter in Plaxis. The resisting force (RF) represents the resistance from the columns as well as the shear resistance from the soil itself within the sliding interface where failure is occurring. The reaction force is depicted in Figure 8-6, where RF_{FF} is the free field resisting force (with no columns installed), and RF_{column} is the resisting force of the columns. The RF is dependent on the vertical total stress (σ_{v0}), the angle of internal shearing resistance in the interface (sheared zone) (φ_{int}), the cohesion of the soil in the interface (c_{int}), and the area of the interface. It reaches a maximum value at failure.

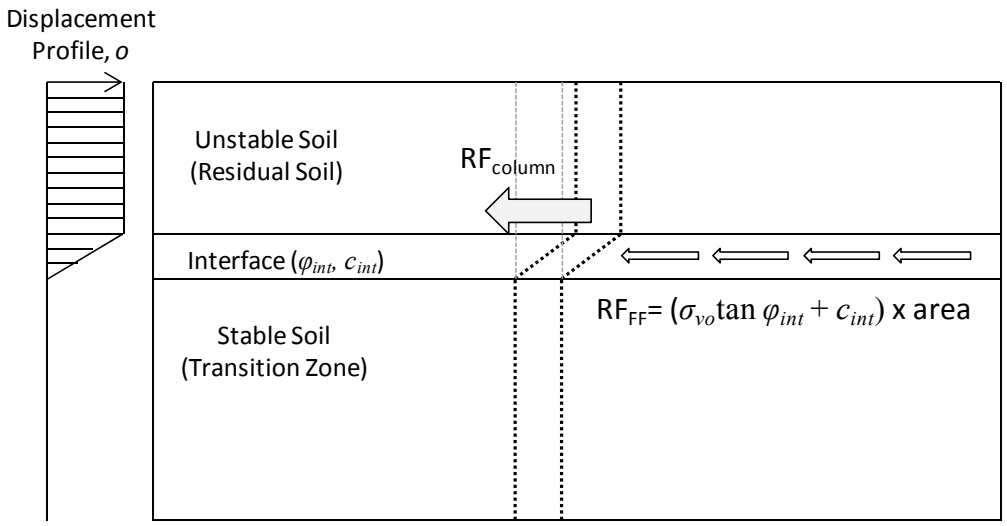

Figure 8-6: Calculation of the net resisting force of the columns (RF_{column}) against the applied displacement (o) (modified after Kourkoulis et al., 2012).

8.3.4 Soil Properties

The soil properties used in the model are shown in Table 8-1, and are similar to those used in Chapter 6. The selected parameters for the shear zone are further discussed in the next section. The Mohr-Coulomb constitutive model is used, with drained conditions. The K_0

procedure has been used to generate initial stresses. K_0 (the ratio of horizontal and vertical effective stresses) is determined in Plaxis from Jaky's formula:

$$K_0 = 1 - sin\varphi \qquad (8.1)$$

where φ is the angle of internal shearing resistance. When the K_0 procedure is applied, vertical stresses are generated that are in equilibrium with the self-weight of the soil and horizontal stresses are calculated from the specified value of K_0. Full equilibrium is only attained for a horizontal surface with any soil layers parallel to this surface, and a horizontal phreatic level, as is the case in this analysis.

Table 8-1: Soil parameters used in 2D and 3D simplified slope models.

Parameter	Unit	Residual Soil	Sheared Zone	Transition Zone
E^{ref}	kN/m^2	5.00E+03	5.00E+03	4.00E+04
v		0.25	0.25	0.25
γ (unsat)	kN/m^3	20	20	20
γ (sat)	kN/m^3	20	20	20
k_x	m/day	6.40E-02	6.40E-02	8.13E-03
k_y	m/day	6.40E-02	6.40E-02	8.13E-03
c	kN/m^2	10	0.1	10
φ	°	25	8	26.6
ψ	°	2	0	1

8.3.5 Column Properties

The purpose of this analysis is to compare the results of a 2D model (using the replacement ratio method) to a 3D model. While the properties of the soil and columns were maintained as close as possible to actual soil and column properties in a Northland Allochthon residual clay slope, it was critical to ensure that the RF was influenced by the DSM columns (i.e. the failure was occurring in the sheared zone, through columns, rather than above it in the surrounding soil). The angle of internal shearing resistance for the soil in the sheared zone was set to 8°, which is slightly lower than the residual soil strength estimated from ring shear

tests by O'Sullivan, 2009 (11°-14°). The lower angle of internal shearing resistance in this zone was selected to help ensure failure would occur in the sheared zone. DSM columns in Northland Allochthon residual clay soil are estimated to have a cohesion of 667 kPa based on laboratory testing results. However, it was found that when the DSM column cohesion was this high (i.e. 167 kPa in the 2s case using the replacement ratio method), the RF was no longer influenced by changes in the column properties, and failure was no longer occurring in the shear zone (through the columns), but rather in the soil above the slip surface. This type of failure is not appropriate for this analysis because it aims to investigate a failure mechanism that occurs along a pre-defined slip surface where the performance of the actual columns (in 2D versus 3D) are examined. This requires the failure of the columns themselves. Therefore, in order to determine the maximum DSM column cohesion that could be used while still ensuring failure through the columns, the cohesion of the columns was varied between 10 kPa to 200 kPa. This was done for the 2s and 4s cases. Figure 8-7 shows the plastic points for the base case (no DSM columns), and at a cohesion of 15 kPa, 60 kPa and 120 kPa in the DSM columns. Plastic points are stress points in a plastic state, and thus give an indication of where failure is occurring in the model.

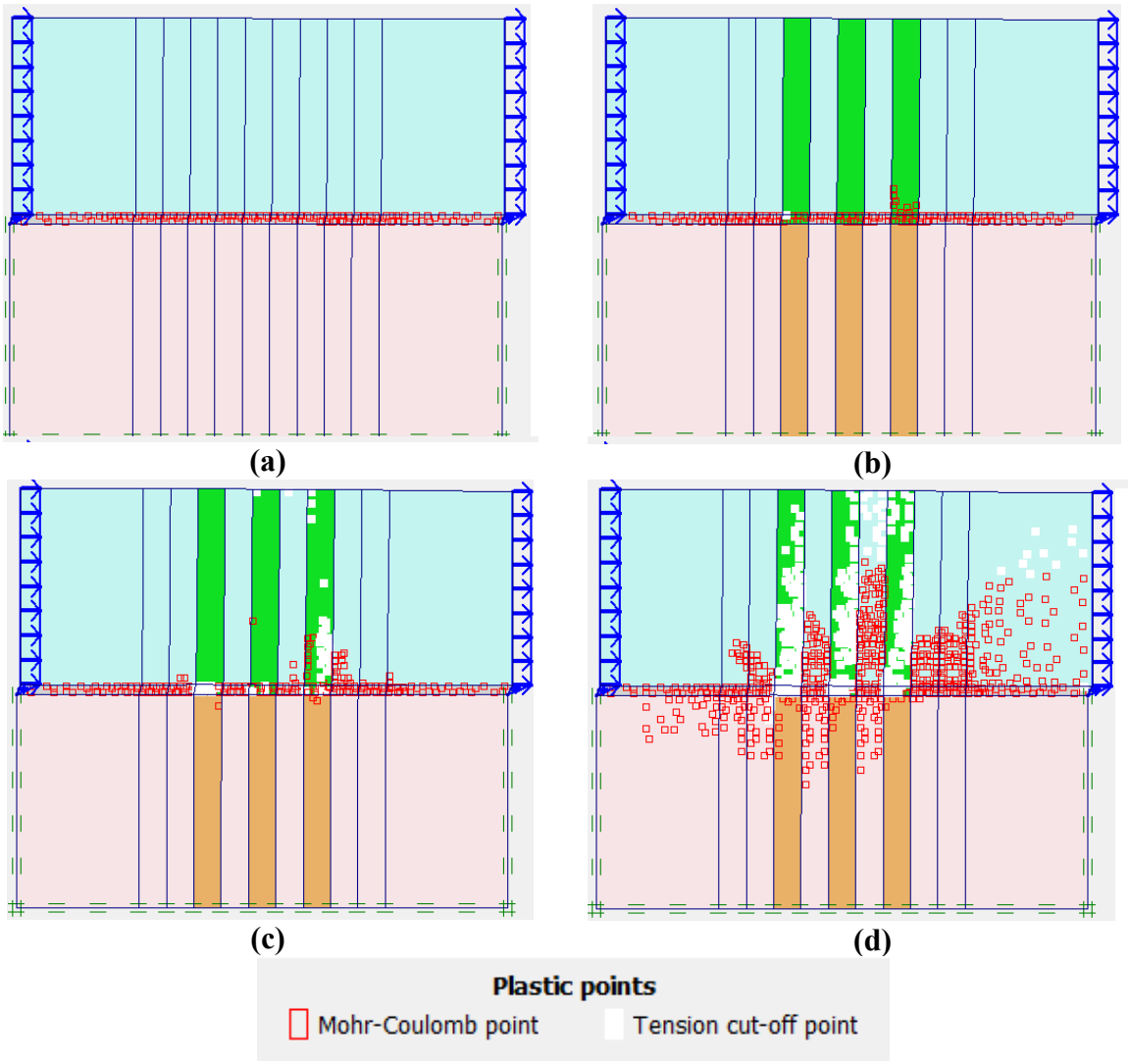

Figure 8-7: Plastic points for: (a) the base case (no columns); (b) column cohesion of 15 kPa; (c) column cohesion of 45 kPa; and (d) column cohesion of 120 kPa.

Figure 8-7 demonstrates that the plastic points are initially concentrated primarily in the shear zone when the DSM columns have nearly the same cohesion as the soil (15 kPa versus 10 kPa), but move outside of the shear zone and into the surrounding soil as the column cohesion increases. The physical significance of the high cohesion columns is that failure is occurring around the columns, rather than through them and within the sheared zone. If the columns were too "rigid", the columns would be prone to bending failure. Tension points

would develop on the left side of the columns, and, similar to high cohesion columns, failure would occur outside of the sheared zone.

The cohesion of the composite columns was varied between 10 kPa to 200 kPa for the 2s and 4s cases. Figure 8-8 shows how the resisting force at failure varies with composite column cohesion in the 2D model for the 2s and 4s cases. In both cases, the slope remains linear until approximately 70 kPa and for cohesion values greater than ~80 kPa, the resisting force changes little. A visual inspection of the failure mechanism shows that the plastic points have moved extensively outside of the pre-defined slip surface after 70 kPa. 70 kPa was hence selected as the cohesion for the 2s composite 2D columns. Back calculating via the RRM with this value gave a value of 162 kPa for the cohesion of the full strength DSM columns. The estimated unit weight and permeability of the columns is the same as that of the soil shown in Table 8-1.

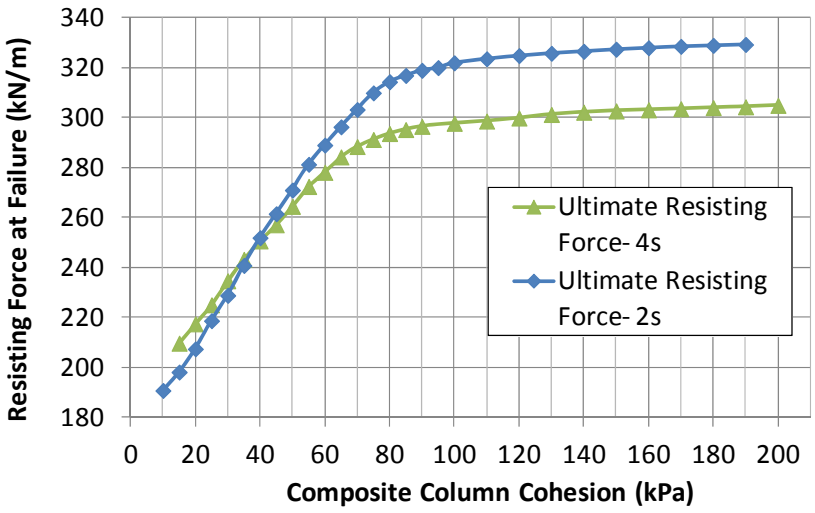

Figure 8-8: Change in resisting force with DSM column cohesion.

The column properties in the 3D model are shown in Table 8-2.

Table 8-2: DSM column properties in 3D.

Parameter	Unit	DSM Column Properties	
		Residual Soil	Transition Zone
E^{ref}	kN/m^2	1.08E+06	1.08E+06
ν		0.2	0.2
c	kN/m^2	162	162
φ	°	30	32
ψ	°	2	1

8.4 3D Model Development

The 3D model allows for soil flow around the columns in the out of plane direction, and brings into play effects of soil arching which are not possible in the 2D model. Plaxis 3D Tunnel (Version 2) was utilized for the 3D model. Due to software limitations, the column cross-sections were modelled as rectangles with dimensions of 0.6 m by 0.47 m. These dimensions ensured the volume of the columns was identical to that of circular columns with a diameter of 0.6 m. The difference in the ultimate pressure on rectangular and circular columns of the dimensions stated above at 3s spacing was examined in a plan view model in the drained condition, based on the analysis performed in Chapter 7. Note that failure of the soil around the columns rather than of the columns themselves (as is occurring in the plan view model) is more likely to occur in soft soil or soil that does not have pre-existing failure plane. Shear failure of the columns examined in this chapter is more likely to occur when the soil is stiffer and failure is occurring in a pre-existing failure plane. The soil properties for the plan view model comparing rectangular and circular columns were the same as those shown for the residual soil in Table 8-1. Figure 8-10 shows that the ultimate pressure on rectangular columns that are 0.6 m by 0.47 m in size is approximately 15% more than that of circular columns of the same area. The column dimensions with respect to the lateral load are shown in Figure 8-9.

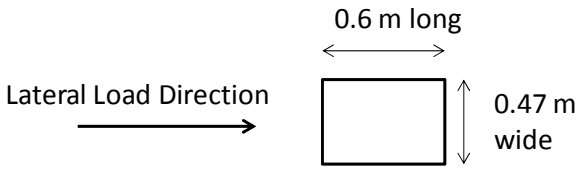

Figure 8-9: Column configuration with respect to lateral load.

The column orientation was selected to be 0.6 m long and 0.47 m wide, rather than 0.47 m long and 0.6 m wide because the other orientation would result in a slightly higher ultimate pressure due to a larger area in the direction of the load. It is evident that the ultimate capacity is influenced by column shape in an ultimate state analysis where the columns are fixed, and failure is occurring in the soil around them. However, the resisting force provided by the DSM columns in this study will be affected very little by the shape of columns. The resisting force is based on a failure mechanism occurring through the sheared zone (through the soil *and* columns) rather than in soil plastic flow around the columns. It is dependent on the frictional resistance available in the area where failure is occurring. There is much less soil arching occurring in the sheared zone because failure is occurring through both the soil and columns. Since there is very little arching in this zone, there is much less influence from column shape on the resisting force provided by the columns, and much more influence from the overall properties of the soil and columns, and the area of these, rather than the shape of the columns. Section 8.5.4 presents results that demonstrate how soil arching decreases with depth and how it is no longer effective in the sheared zone.

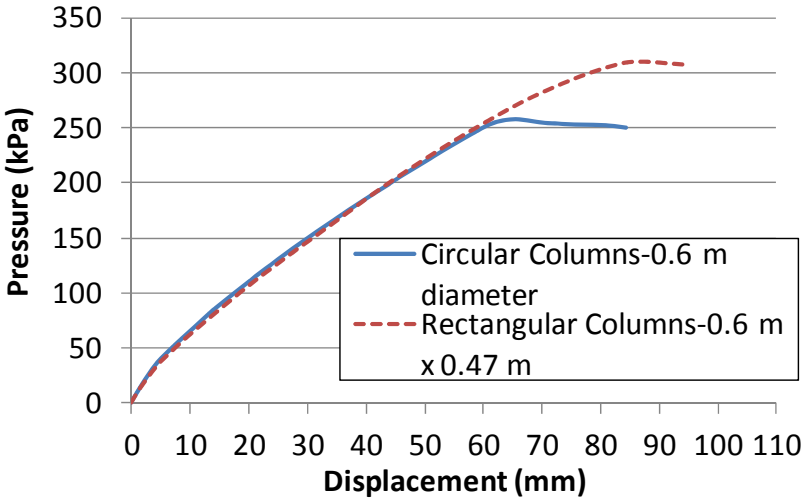

Figure 8-10: Horizontal pressure at the front of the column versus displacement between the columns for rectangular versus circular laterally loaded DSM columns in a 2D plan view analysis.

The plan view geometry of the 3D model at 2s spacing is shown in Figure 8-11. Note that column spacing in the 3D model corresponds to that of circular columns of the same area. For example, at 2s, the spacing is 1.2 m from centre-to-centre of the columns. Planes 1, 2 and 3 are the planes where the points for load-displacement curves (A, B and C in Figure 8-3) have been selected. The full 3D model at 2s spacing is shown in Figure 8-12.

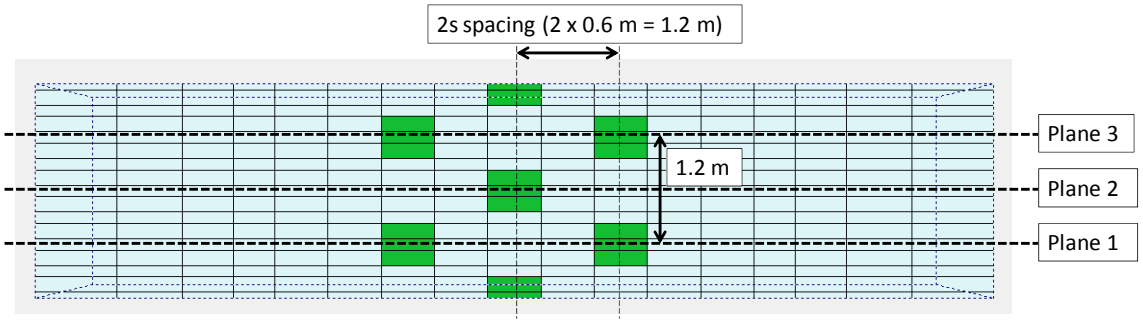

Figure 8-11: Plan view of 3D model at 2s spacing.

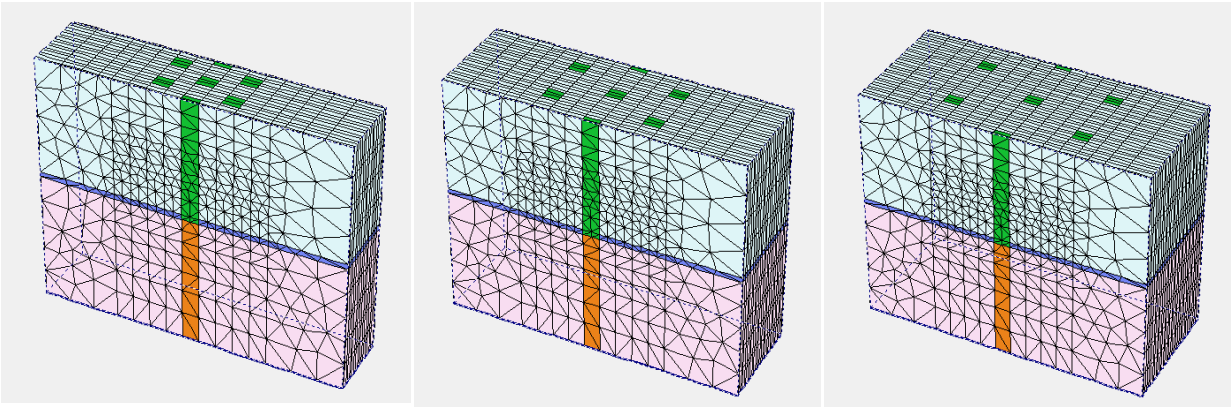

Figure 8-12: 3D model at column spacings of (a) 2s, (b) 3s, and (c) 4s.

8.5 Results of 2D Model and 3D Model Comparisons

8.5.1 Base Model

In order to ensure that the 2D and 3D models were behaving the same, horizontal stress versus displacement was compared for points A, B and C between the 2D and 3D models without any DSM columns ("base models") in Figure 8-13. For the 3D model, the plane in which these points are taken is specified in the legend. The resisting force provided by the DSM columns for each of the models was also compared in Figure 8-14. The curves were identical for both models.

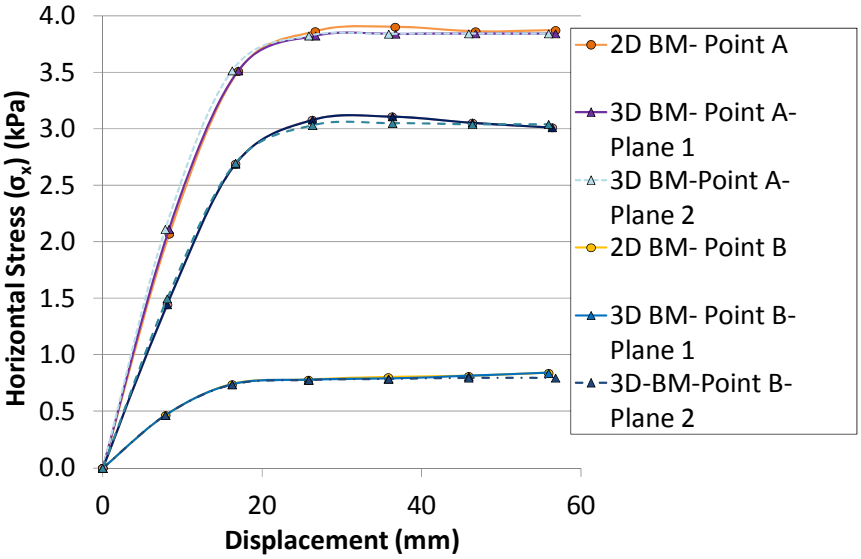

Figure 8-13: Horizontal stress versus displacement at points A, B, and C for the 2D and 3D base models.

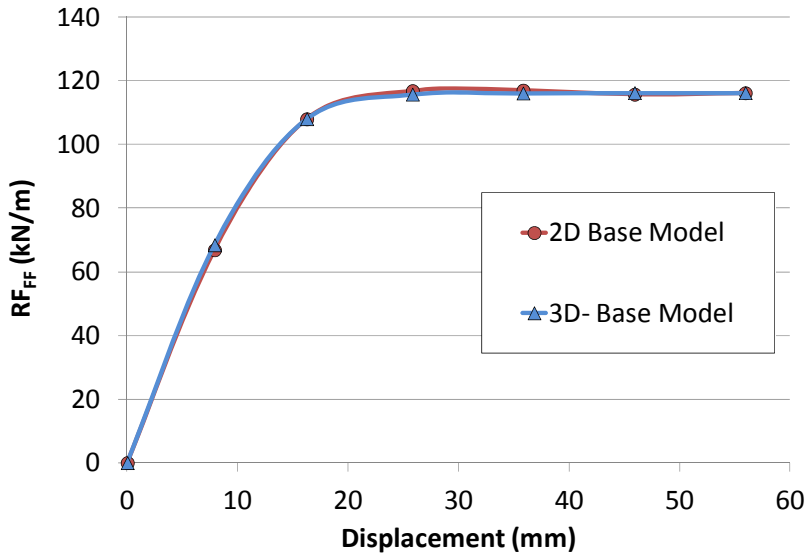

Figure 8-14: Resisting force (free field) versus displacement for the 2D and 3D base models.

8.5.2 Horizontal Stress versus Displacement

Horizontal stress versus displacement was examined at points A, B and C for all three column spacings in the 2D model. For the 3D model, plane 1 was used for points A and C and plane 2 was used for point B (i.e. points chosen to be in front of the respective staggered columns). The results are shown in Figure 8-15.

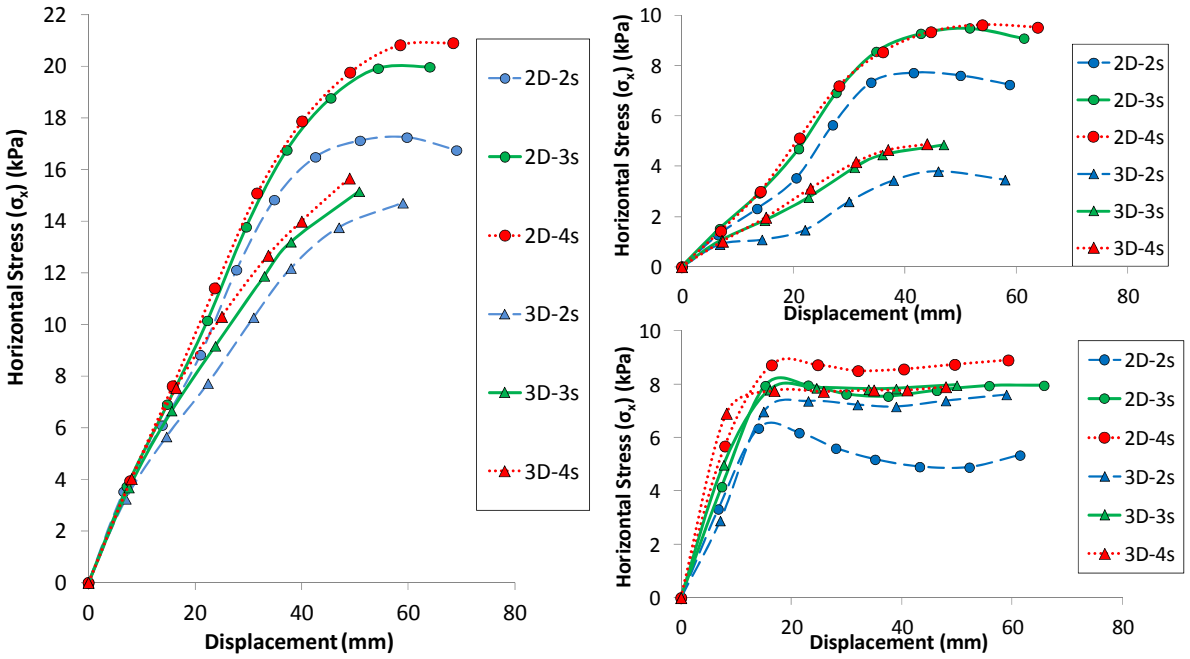

Figure 8-15: Horizontal stress versus displacement at point A (left), point B (top right) and point C (bottom right).

The horizontal stress is highest at the face of the columns on the leftmost side of the model (point A, top left figure) as these columns are carrying most of the load due to the "shadow effect".

Considering work on laterally loaded piles, the shadow effect is created from the front pile (or in this case, column) to the rear one (Reese et al., 1992) and it causes the action of soil against the rear pile to be minimal compared to that against the front one. Analytical results

(Poulos & Davis, 1980) reveal that the rear pile in a laterally loaded system may develop only about 20% of the front pile's resistance, depending on the pile distance.

The horizontal stress is higher in the 2D model than the 3D model at all column spacings at points A and B. At point C, it is the 2D-2s case that has the lowest stress. This may be due to a more significant shadow effect in this scenario. Increasing the column spacing results in a greater ultimate pressure on the column, which is in agreement with the results for drained conditions presented in Chapter 7. At point C, the 3D analyses show only a minor increase in the horizontal stress due to an increase in column spacing. This could also be due to an increased shadow effect at this location.

The ratio of the ultimate horizontal stress in 2D to 3D versus column spacing at points A, B and C is shown in Figure 8-16. As the column spacing increases, the soil moves more easily around the columns in the 3D model, but this remains impossible in the 2D model. This is reflected in the ratio of the horizontal stress in the 2D model to the 3D model, which increases as the column spacing increases. The ratio of the horizontal stress in the 2D model to the 3D model is highest at point B and lowest at point C. This is due to the configuration of the columns in the 3D model. Point B (the middle column) in the 3D model is examined in plane 2, where it has no columns in front of it. The first columns (in plane 1 and plane 3) would attract much more of the load, as they are closer to the model boundary where the displacement is being applied. The horizontal stress at point C (the rightmost column) is the least overestimated by the 2D model because in both the 2D and the 3D models there is at least one column in front of it, "shadowing" it and taking on more of the horizontal stress.

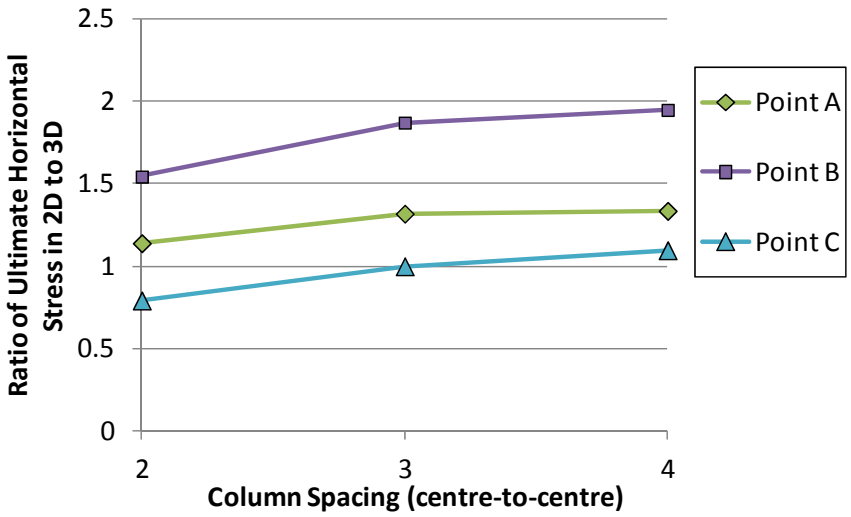

Figure 8-16: Ratio of ultimate horizontal stress in 2D to 3D versus column spacing at points A, B and C.

8.5.3 Resisting Force

The resisting force was computed for each of the three spacings as well as for one row of columns (the centre column) spaced at 3s in 2D and 3D. The free field resisting force, RF_{FF} (the resisting force computed in the base models) was subtracted from the results to give the resisting force for the columns alone (RF_{column}). The results are shown in Figure 8-17.

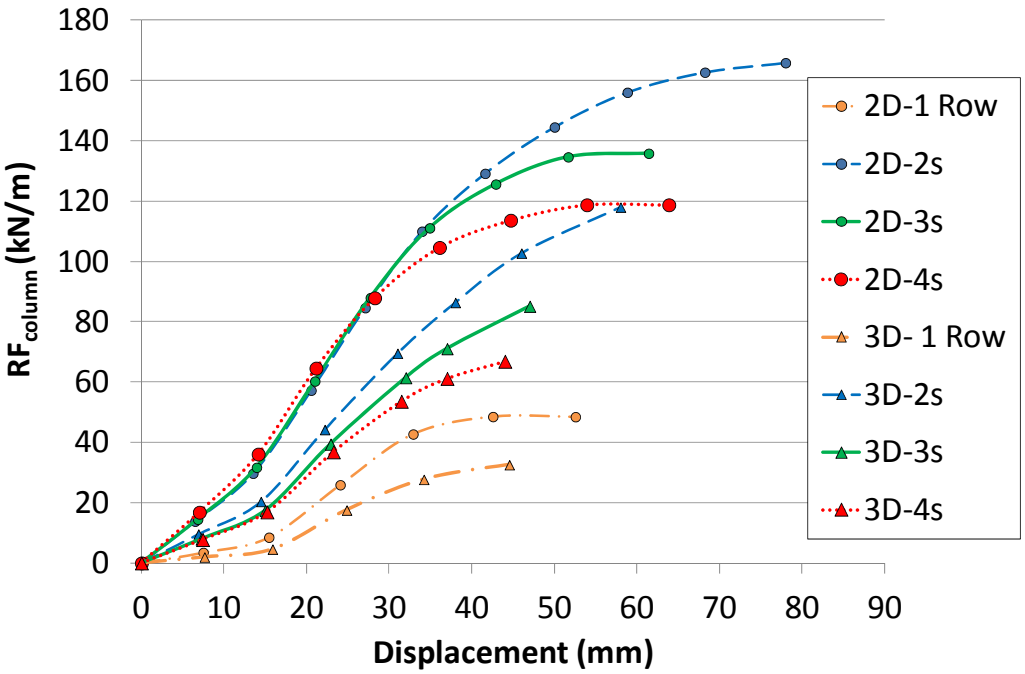

Figure 8-17: Resisting force provided by the DSM columns versus displacement for all 2D and 3D scenarios.

The results indicate that the resisting force provided by the columns is overestimated in the 2D model. Closer spacing results in less deviation between the two models with the 2D model overestimating the RF_{column} of the 3D model. The values of the RF_{column} and the ratio of 2D RF_{column} to 3D RF_{column} (in percent) are presented in Table 8-3.

Table 8-3: Ultimate resisting force provided by the DSM columns at each column spacing for the 2D and 3D models.

Model Type	Ultimate RF_{column} (kN/m)			
	2s	3s	4s	1 row at 3s
2D	166	136	119	49
3D	118	85	67	33
Difference (kN/m)	48	51	52	16
2D RF_{column} as a % of 3D RF_{column}	141%	160%	178%	149%

The 2D model with one row of columns at 3s compared to the 3D model varies less (149%) compared to the models with three rows of columns (160%). The columns have the same strength in both of these 2D models (because they are at the same spacing). This indicates that the RF_{column} is more significantly overestimated by the 2D model when more rows of columns are present. This is likely due to the fact that more columns provide a stronger "wall" to resist the applied displacement in the 2D model, while in the 3D model, the soil is still able to flow around the columns. The 2D model also has a much stiffer response in the RF_{column} versus displacement curve (i.e. it develops a greater RF_{column} for a given soil displacement) than the 3D model. This behaviour is discussed further in Section 8.6 where modifications to the RRM are made.

Figure 8-18 shows the direction of the principal stresses is rotated on the left side of the DSM columns, but not on the right side for both the 2D and 3D models. This further demonstrates the shadow effect being produced by the columns.

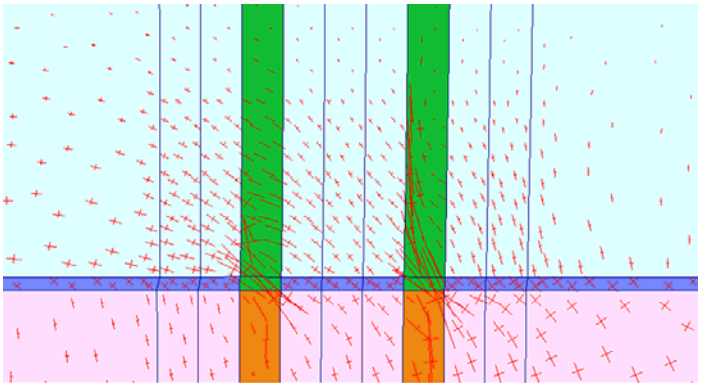

(a)

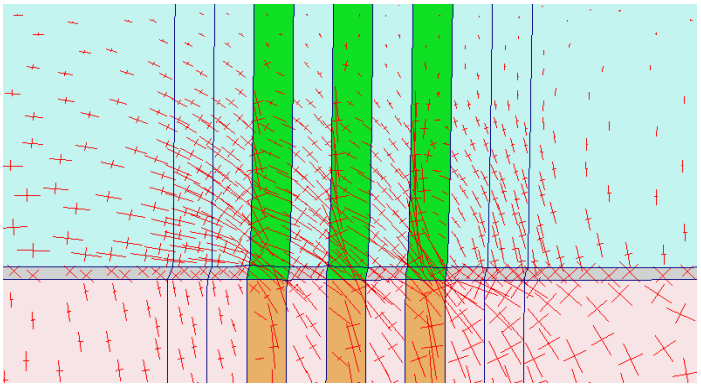

(b)

Figure 8-18: Rotation of principal stresses (a) in 2D and (b) in 3D, plane 1.

The relative shear stress gives an indication of the proximity of the stress point to the failure envelope. The relative shear stress is defined by (Plaxis, 2008):

$$\tau_{rel} = \frac{\tau^*}{\tau_{max}} \qquad (8.2)$$

where τ^* is the maximum value of shear stress (i.e. the radius of the Mohr's circle). The parameter τ_{max} is the maximum value of shear stress for the case where the Mohr's circle is expanded to touch the Coulomb failure envelope. In the 2D model, there are no intermediate principal stresses. In the 3D model, the intermediate principal stresses change during the calculation, but the centre of the Mohr's circle is kept constant at each step as the Mohr's circle is expanded (Xing-Cheng, pers. comm., (2014b)). Figure 8-19 shows the relative shear stress contours of the columns at failure in 3D, plane 1 (left) and in 2D (right) at 2s, 3s and 4s.

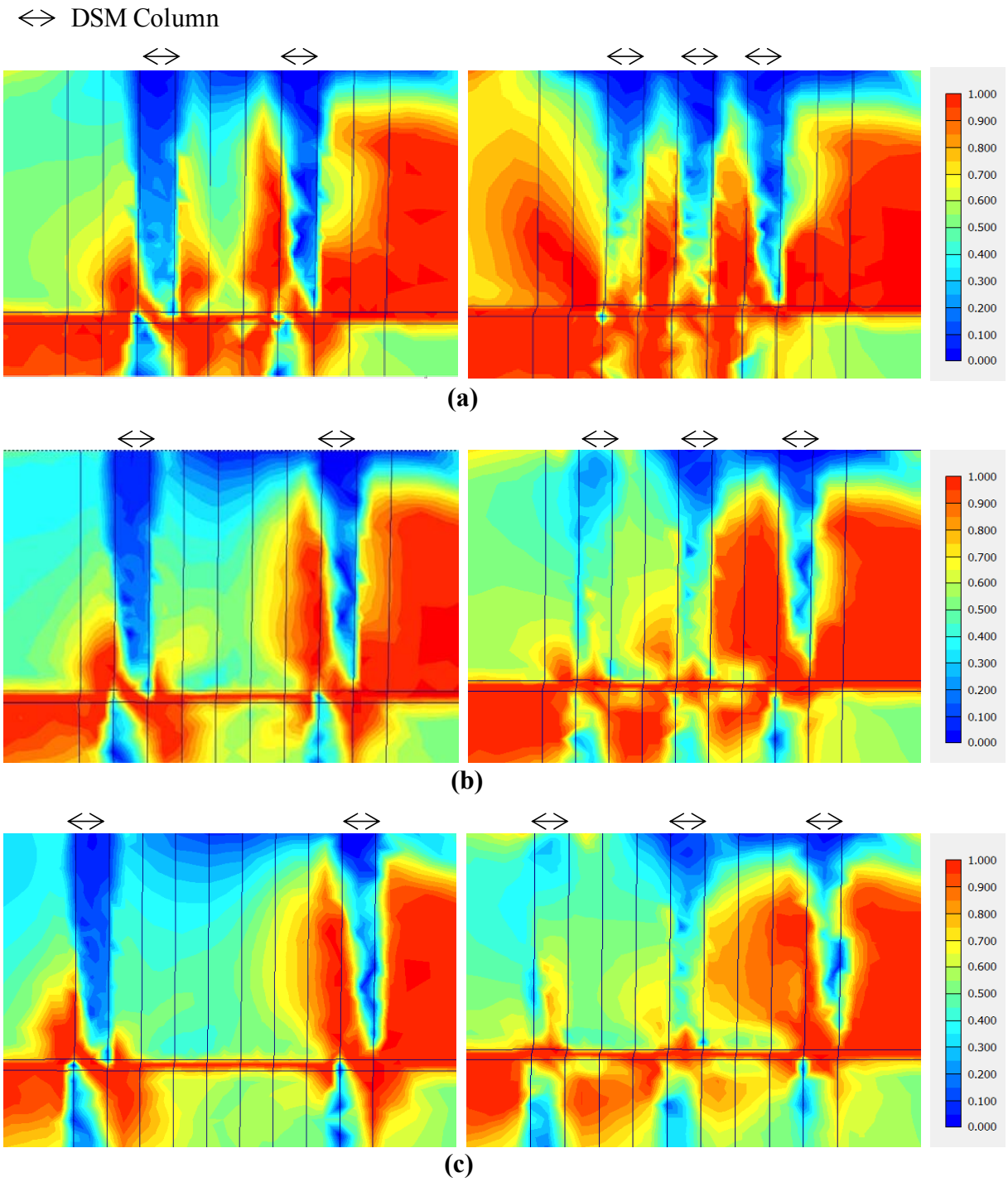

Figure 8-19: Relative shear stress contours for 3D model, plane 1 (left) and 2D model (right) at (a) 2s (b) 3s and (c) 4s.

The relative shear stresses are higher in the leftmost column than the rightmost column in the 2D cases, indicating that the front columns are closer to failure as they are "shadowing" the

columns to right of them. This effect is not as prominent in the 3D model as the soil is able to flow around the columns. All cases show high relative shear stresses through the sheared zone, and through the columns, showing the shear failure of columns.

The deviatoric stress and mean effective stress contours are shown in Figure 8-20 and Figure 8-21.

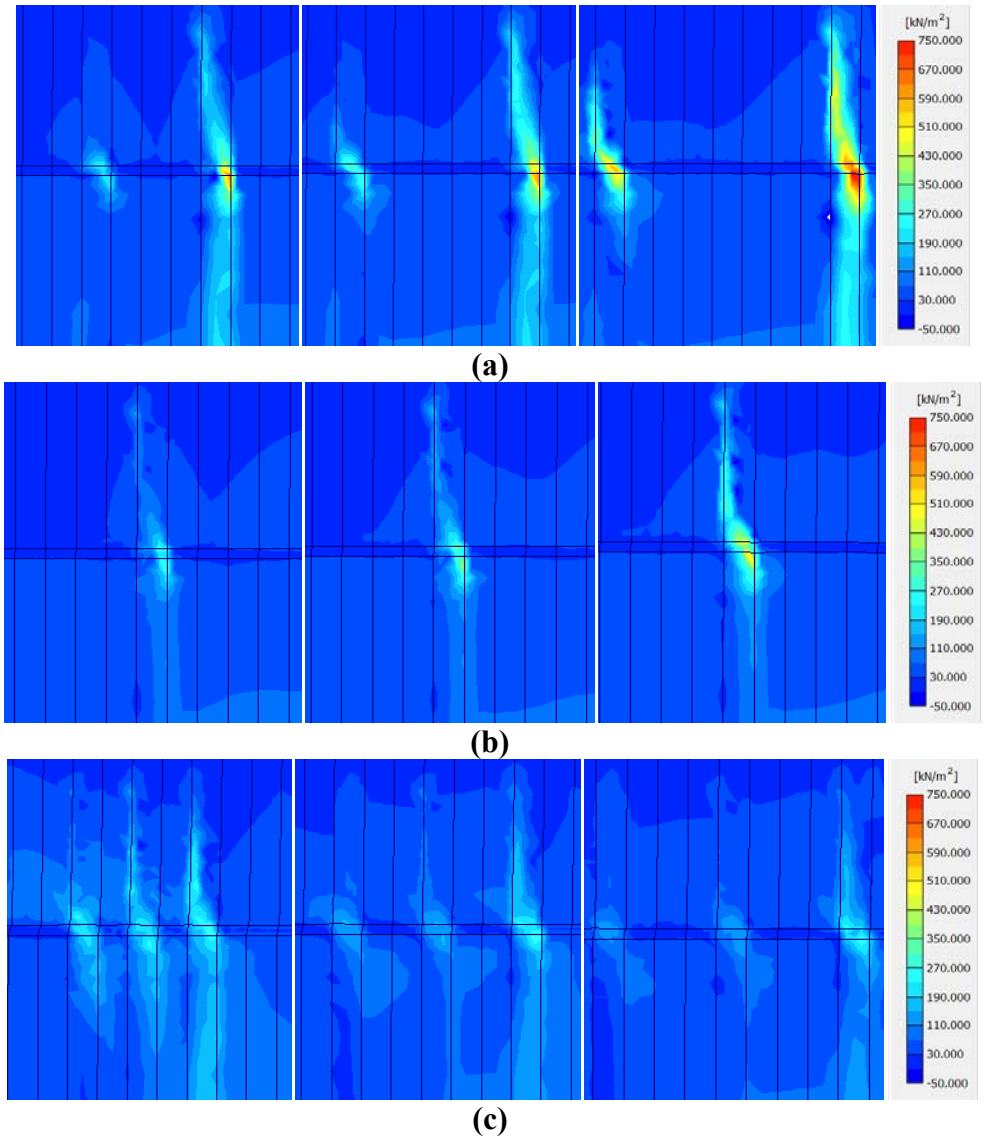

Figure 8-20: Deviatoric stress (*q*) contours at 2s, 3s and 4s (left to right) in (a) 3D plane 1, (b) 3D plane 2, and (c) in 2D.

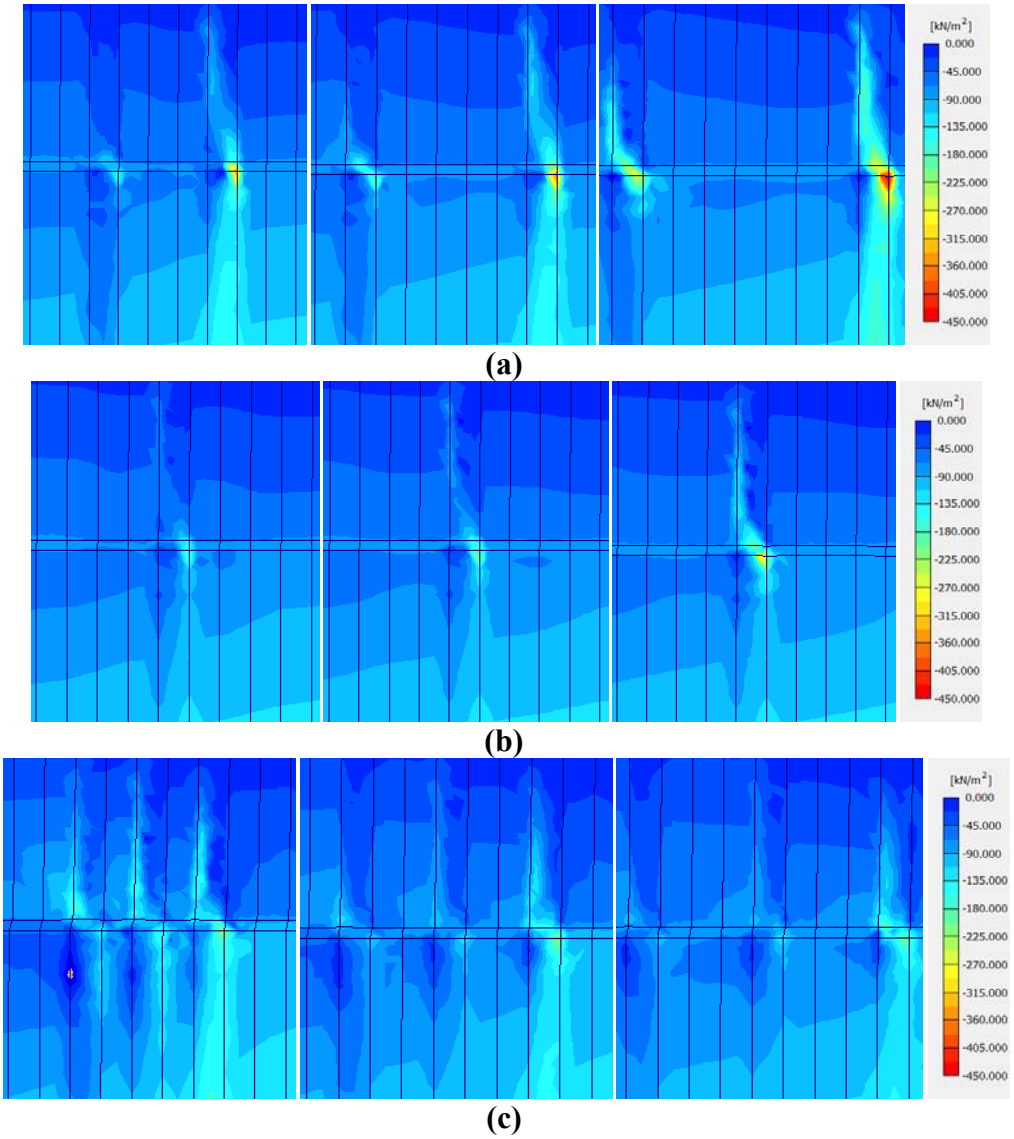

Figure 8-21: Mean effective stress (*p'*) contours at 2s, 3s and 4s (left to right) in (a) 3D plane 1, (b) 3D plane 2, and (c) in 2D.

Figure 8-20 and Figure 8-21 show that the deviatoric stress (q) and mean effective stress (p') are both higher in the columns in the 3D model at all spacings. In the 3D model, both q and p' increase in the columns in both plane 1 and plane 2 as the column spacing increases. This is due to the decrease in soil arching with an increase in spacing, causing an increased load on the columns. The 2D models do not show a significant change in the peak stresses with column spacing.

The stress paths of the soil were examined in the 2D and 3D models at points E and F, shown in Figure 8-22. Points E and F were selected to be just above the sheared zone so as not to be affected by failure in that zone, and on either side of the centre column (and in plane 2 in 3D) in order to be within the column group. It was anticipated that the soil at points E and F would have a lower mean effective stress with an increase in column spacing due to a decrease in group effects (confinement) from the other columns. Based on Figure 8-20 and Figure 8-21, it was also anticipated that in the 3D model, the stress paths of soil at these locations would be further from the failure envelope than in the 2D model. This is because in the 3D models, the partitioning of load between the columns and the soil due to the difference in their stiffness means that the columns attract more load at failure (as the columns do not deform as much as the soil). The results are shown in Figure 8-23 and Figure 8-24.

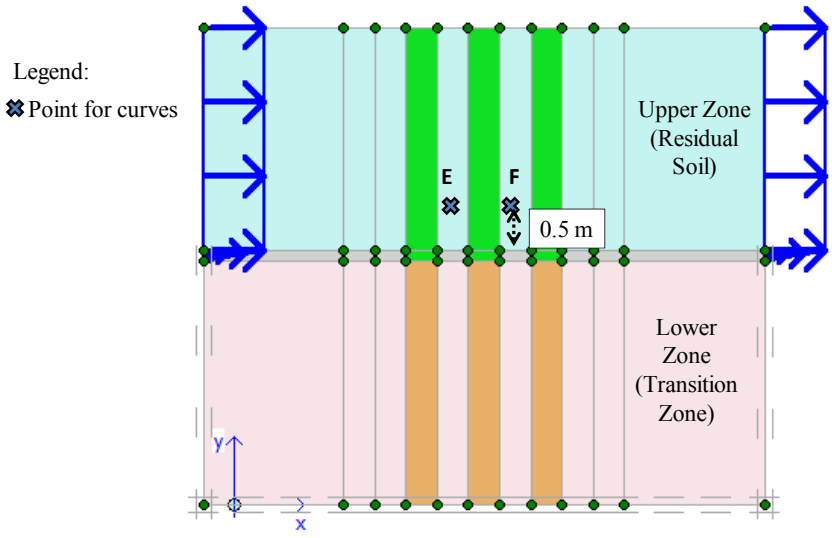

Figure 8-22: Location of stress points E and F (in plane 2).

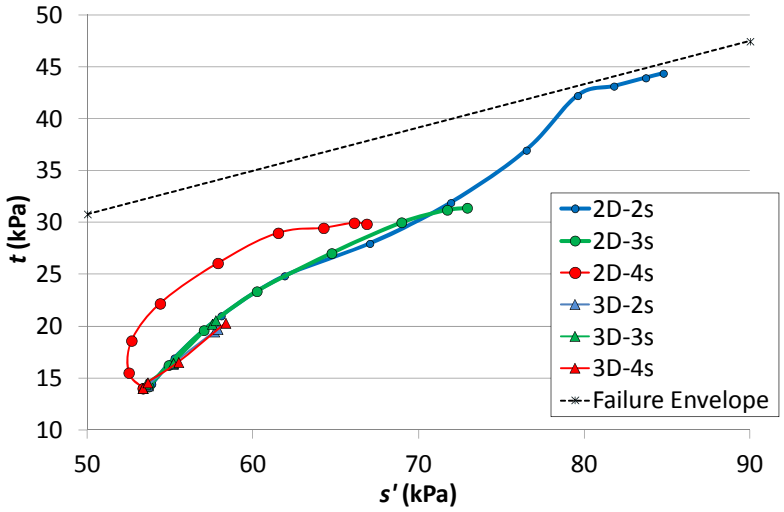

Figure 8-23: Stress paths at point E, plane 2 at 2s, 3s and 4s in 2D and 3D.

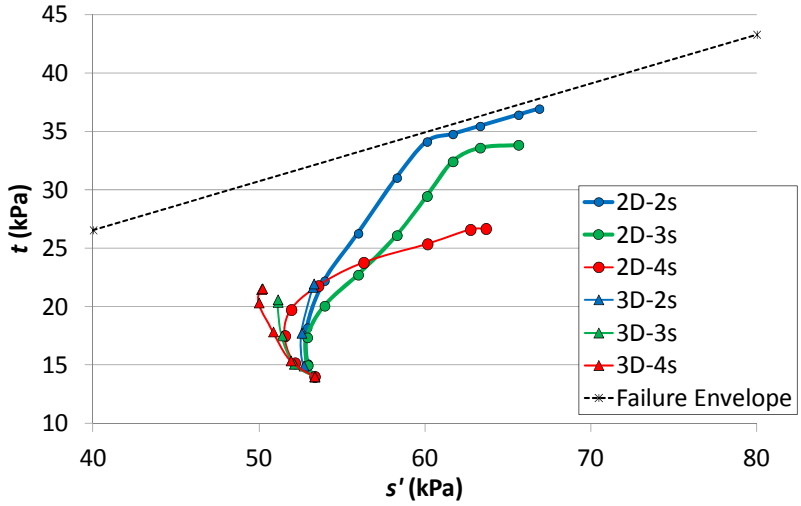

Figure 8-24: Stress paths at point F, plane 2 at 2s, 3s and 4s in 2D and 3D.

The stress paths show that for the 2D model, both points E and F reach close to the failure envelope at 2s spacing. The peak stress decreases at both points E and F with increasing column spacing for the 2D models. Points E and F in the 3D model (plane 2) are both well below the failure envelope and have lower peak stresses than the 2D model at all column

spacings. The mean effective stress reduces with an increase in column spacing at point F in the 3D model. This confirms that confinement due to the surrounding columns also decreases with an increase in column spacing at this point. It also confirms that more load is being taken by the columns rather than the soil as the column spacing increases in the 3D model (which is further demonstrated in Figure 8-20 and Figure 8-21).

8.5.4 Soil Arching

Following Kourkoulis et al. (2011), soil arching was investigated in the 3D models by examining the ratio of inter-column ground displacement (o_{ic}) to the displacement of the column (o_c) at failure. o_{ic} was measured in between the two columns in the out-of-plane direction, at both the leftmost and rightmost rows of columns as shown in Figure 8-25.

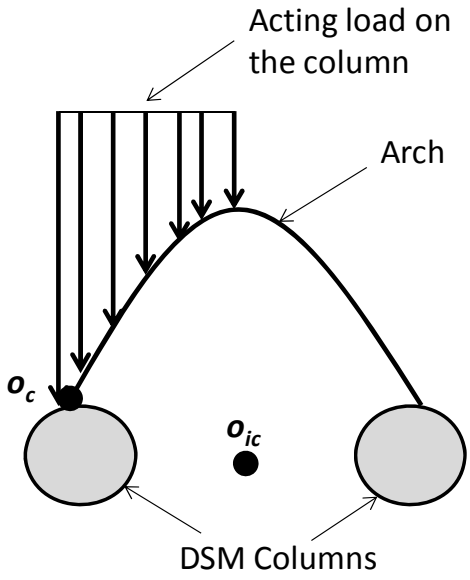

Figure 8-25: Arching and measurement of inter-column ground displacement (o_{ic}) and displacement at the front of the columns (o_c) (modified after Adachi et al., 1989).

If the ratio of o_{ic}/o_c is maintained at close to 1, the column and the inter-column soil displace by nearly the same amount and the columns can be considered to be effective in terms of arching (Kourkoulis et al., 2011). Arching is effective when movement between the columns

is close to that occurring at the columns, so the higher the o_{ic}/o_c ratio, the less the arching effect.

Figure 8-26 shows the o_{ic}/o_c ratio with depth for 2s, 3s and 4s column spacings at the left and right columns at failure in the 3D models. Less arching (higher o_{ic}/o_c ratio) is observed at higher column spacings. There is also more arching occurring at the rightmost column than the leftmost column at all column spacings. This may be due to the shadow effect (i.e. there is more displacement occurring within the left side of the model, and thus more displacement in the soil compared to the columns due to its lower stiffness). The o_{ic}/o_c ratio also increases significantly at the top of the sheared zone, where failure is occurring. Arching is effective in the top 3.5 m of the columns.

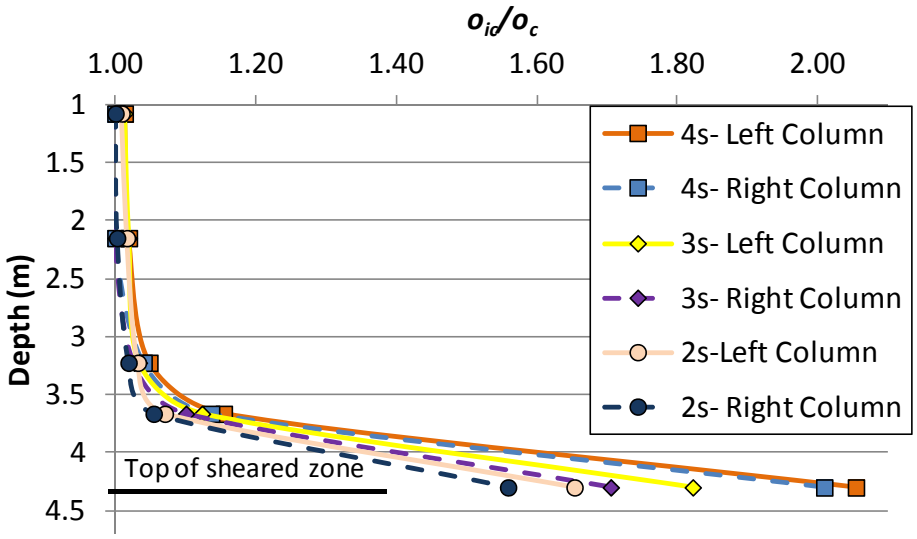

Figure 8-26: Ratio of inter-column displacement to column displacement with depth at different column spacings.

8.6 Alterations to the Replacement Ratio Method

It is evident from Figure 8-17 that the RF_{column} is overestimated by the 2D model as compared to the 3D model. This indicates that the strength of the columns using the RRM is too high. An increase in the replacement ratio of the soil (that is, the ratio of the soil material to the soil

and column material when computing the new strength parameters for the columns, as described in Section 6.5.2) would reduce these parameters to lower values which would reduce the RF in order to produce a better match to the 3D model.

The cohesion, angle of internal shearing resistance, and Young's modulus were reduced by altering the replacement ratio in order to reduce the resisting force provided by the columns in the 2D models and acquire an ultimate RF_{column} in the 2D model that coincided with that of the 3D model. This process was done through trial and error. It resulted in a modified replacement ratio (MRR) (i.e. the percentage of soil out of the total volume of soil and column material) of 0.8 in the 2s model, 0.924 in the 3s model and 0.984 in 4s model. The results of the RF_{column} are shown in Figure 8-27.

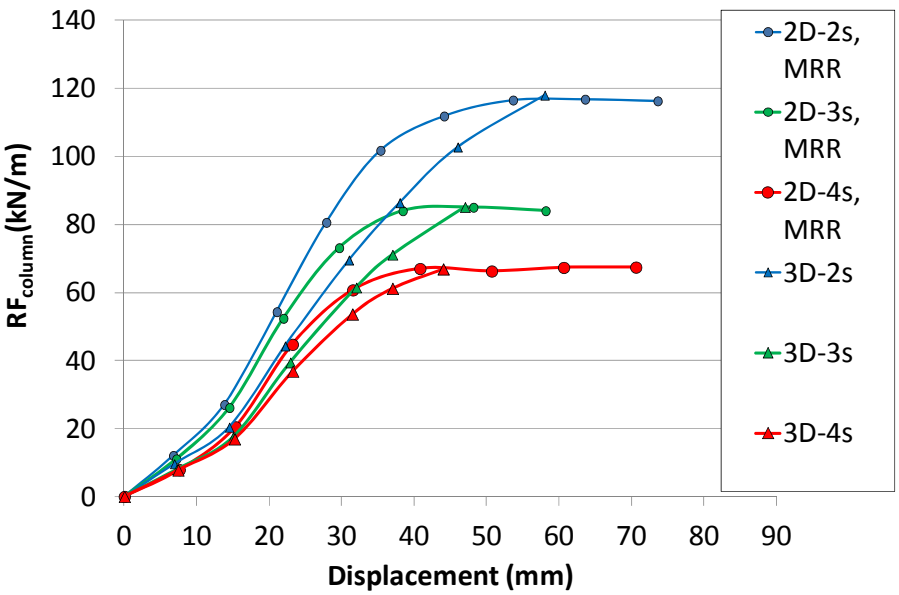

Figure 8-27: Ultimate RF_{column} of 2D model coinciding with 3D after modifying the replacement ratio.

The MRR method (MRRM) compared to the RR method (RRM) at 2s, 3s and 4s is shown in Table 8-4. The soil replacement ratio can be increased by 19.3% at 2s, 18.6% at 3s and 18% at 4s in order for the ultimate RF_{column} in the 2D model to match the 3D model results. This

change in the soil replacement ratio from RRM to the MRRM is approximately linear, as shown in Figure 8-28. Note that the MRRM is similar to increasing the column spacing while maintaining the column dimensions.

Table 8-4: Modified RRM soil replacement ratio compared to the standard RRM.

Column spacing	Soil- Percentage of Total Volume		
	RRM	Modified RRM	Change
2	0.607	0.8	0.193
3	0.738	0.924	0.186
4	0.804	0.984	0.18

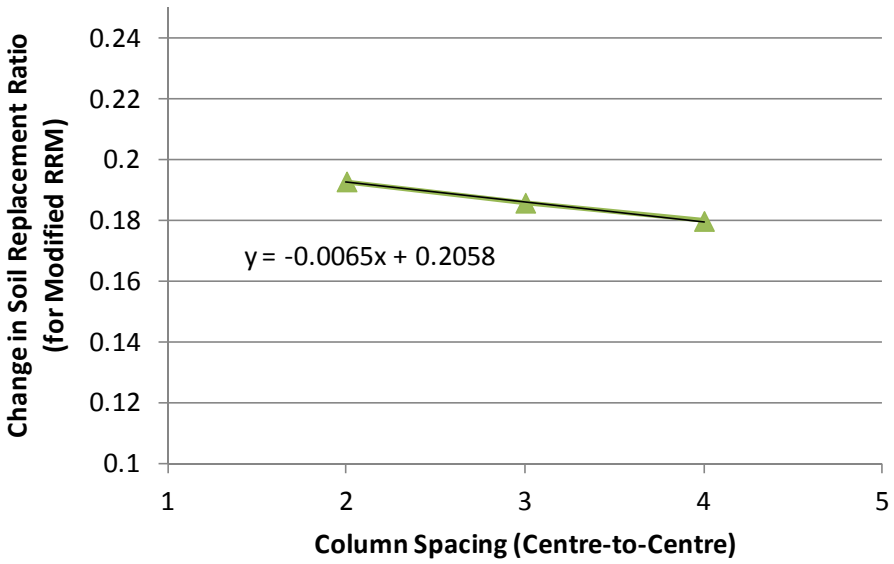

Figure 8-28: Change in soil replacement ratio from RRM to the MRRM at 2s, 3s and 4s.

The secant stiffness of the RF_{column} versus displacement curve at a displacement of 15 mm is shown in Table 8-5 for 2D (for both the RRM and MRRM) and 3D. The stiffness is higher in the 2D models than in the 3D model.

Table 8-5: Secant stiffness of RF_{column} versus displacement curve at 0.015 m displacement.

Model	Secant Stiffness at 0.015 m Displacement (kN)		
	2s	3s	4s
2D (RRM)	2333	2400	2600
2D (MRRM)	2067	1733	1267
3D	1467	1200	1133
Difference- 3D & RRM	867	1200	1467
Difference- 3D & MRRM	600	533	133

Table 8-5 shows that the MRRM results in a better match to the 3D results for the initial stiffness of the RF_{column} versus displacement curve compared to the original RRM.

This chapter has provided a comparison of the performance of laterally loaded DSM columns in 2D using the RRM to a more realistic 3D model, using a robust methodology to simplify the slope. The RRM is commonly used in practice, and the effectiveness of its performance has not been verified, making this a much needed analysis. The results have shown that the RRM overestimates the resisting force provided by the columns compared to the 3D model, both at failure and at pre-failure (working loads). This means that the RRM provides an overestimation when modelling the DSM columns in 2D because the strength and stiffness of the composite columns are too high to result in a lateral resistance that matches the more realistic 3D model. (Note that the DSM columns in the field are stronger than those in these models due to the reduced cohesion utilized, meaning that the computed values of the resisting forces provided by the columns are quite conservative). In 3D, differences in stiffness between the soil and the columns result in an increased load in the columns which is not accounted for in the RRM where the stiffness of the soil and columns is averaged.

The RRM has been modified to create a MRRM which results in a better match between the resisting force provided by the DSM columns in 2D to that provided in 3D. Under the conditions examined (i.e. using a column diameter of 0.6 m and the soil properties as shown in Table 8-1), the replacement ratio of the soil in the composite columns at 2s, for example, should be increased from 61% to 80% for a better match. (This means that the replacement

ratio for the column material should be reduced from 39% to 20%). This suggests that the current state of practice, which is to use a replacement ratio based on the volume of soil and column material in the out of plane direction, should be modified. The replacement ratio of the soil material should be increased, and that of the column material should be decreased. The required increase in the replacement ratio of the soil is slightly less with an increase in column spacing. The MRRM determined in this study can be used directly where the soil properties and column dimensions are the same as those used here. When the properties of the soil and dimensions of the column are different than those in this study, the MRRM determined here can provide an estimate of the modifications to the RRM that are required. Although it has been determined that the commonly used RRM provides an overestimation when modelling DSM columns in 2D (because the strength and stiffness of the composite columns need to be reduced in order to match the lateral resistance provided in the more realistic 3D model), this does not necessarily imply that the use of the RRM in an analysis will always result in a safe slope. The degree to which the overestimation of the resisting force provided by the columns from using the RRM will affect the results will depend on the specific details of the problem being analysed. The properties of DSM columns in a 2D slope model will certainly affect the deformation observed, but the column strength and stiffness may not have a significant impact on the factor of safety after the columns have been installed, especially if the slip surface being examined at that point is not through (or is only partially through) the DSM columns. Practitioners should consider performing a sensitivity analysis by increasing the replacement ratio of the soil by the amount suggested in this study to determine how much of an impact it will have on their results, as this will also vary depending on the location of the columns and the geometry of the slope. If the use of the MRRM is impacting their results, a 3D analysis should be considered.

The research in this chapter could be built upon by repeating this analysis with different soil and column properties and different column diameters. The results could then be tabulated to provide a reference for determining the MRRM for any soil type or DSM column diameter.

8.7 Conclusions

The RRM is a commonly used approach for representing laterally loaded DSM columns in 2D, and the need to compare this method to a more realistic 3D model to verify its

effectiveness has been identified. In order to do this, a simplified slope model of DSM columns with a representative region of soil surrounding them was developed based on a well-validated method by Kourkoulis et al. (2012). Three different column spacings were examined. Through the examination of the resisting force provided by the columns, displacements, and total stresses, the effectiveness of the RRM and how it varies from the 3D scenario was investigated.

It was found that both the resisting force provided by the DSM columns and horizontal stresses are overestimated in the 2D model. This implies that the current RRM overestimates the strength provided by the columns compared to the 3D scenario. Closer column spacing results in less deviation between 2D and 3D results. Soil arching was observed at all column spacings based on o_{ic}/o_c and was found to be most effective above the sheared zone in the top 3.5 m of the soil.

Over the spacings considered, it was found if the soil replacement ratio was increased by 19.3% at 2s, 18.6% at 3s and 18% at 4s, the ultimate RF_{column} in the 2D model would match that of the 3D model. This change in the replacement ratio is linear with column spacing. The increased soil replacement ratio also resulted in a better match between 2D and 3D results for the initial stiffness of the RF_{column} versus displacement curve. Note that this study has not included the effects of increased confinement and improved soil properties due to DSM column installation which have been discussed in Chapter 3 and Chapter 7. These effects may influence how well the RRM compares to the 3D model.

This analysis has revealed that the RRM provides an overestimation for modelling DSM columns in 2D because the strength and stiffness of the composite columns need to be reduced in order to match the lateral resistance provided in the more realistic 3D model. Therefore, the results of analyses that use the RRM may be affected. The degree to which the results are affected will depend on the details of the analysis being examined (i.e. the slope geometry, the location of the columns, and the location of the presumed slip surface). The RRM should be modified by increasing the replacement ratio of the soil material, and therefore decreasing that of the column material. For practical problems where the soil type and column size encountered are similar to those used in this study, the results of this study can assist in determining an estimate of the modifications to the RRM. When the soil

properties and column diameter are not similar those used in this study, it is recommended that practitioners consider performing a sensitivity analysis by increasing the replacement ratio of the soil (using the MRRM in this study as guidance), to determine the impact it will have on the results of their analysis. If their results are influenced by the use of the MRRM, the use of a 3D model should be considered.

9.0 Conclusions

The aims of this research were to investigate the properties and behaviour of Northland Allochthon residual clay soil, to investigate how laterally loaded DSM columns behave in this soil type, and how to better use numerical modelling as a tool to examine their behaviour and performance in a slope stabilization scenario. Three main field sites within the Mangakahia Complex of Northland Allochthon were examined: Mountain Road, Ogles No. 3, and Kaeo. All three of these sites have been subject to slope movement. Soil samples from Kaeo were used to acquire Atterberg limits, while soil from Mountain Road was subject to several different classification tests, in situ field testing, oedometer testing, and triaxial testing of intact and reconstituted specimens. Several laboratory tests were performed on soil from the Ogles No. 3 site in a previous study (O'Sullivan, 2009), and this site provides a basis for the numerical modelling of landslide stabilizing DSM columns.

Classification of clay soil from the field sites listed above using Atterberg limits show that the soil from these sites all fall on or slightly above or below the A-line. This confirms that the soils are all related but have undergone different degrees of weathering. The plasticity index (*PI*) of the residual soil from Mountain Road was found to be approximately 21.

During the field investigation portion of this research, sDMT testing was completed before and after DSM column installation in order to confirm that improvements to the soil around DSM columns occur. This had not previously been proven using an in situ testing method. The results demonstrate that increases to the soil "rigidity" and coefficient of lateral earth pressure at rest do take place. This is an important finding for practitioners for demonstrating that the improvements provided by the DSM columns are not limited to the columns themselves.

Field testing results show that the overconsolidation ratio (*OCR*) is substantially higher near the ground surface. This is likely due to frequent fluctuations in the groundwater table causing changes to the effective stress. The *OCR* is above one throughout the soil profile, though the history of the soil does not indicate that a preconsolidation pressure should exist. This suggests the existence of a pseudo-preconsolidation pressure, as proposed by Wesley

(1990). Undrained stress paths of intact specimens also show dilative (overconsolidated) behaviour at low stresses, further confirming this.

A λ value of 0.121 was acquired from oedometer testing on reconstituted soil from the Mountain Road site, which is typical of clay soils. The C_c value acquired was 0.278, which corresponds well with the C_c obtained from the relationship derived by Burland (1990) between C_c and the void ratio at *LL*.

The testing of reconstituted soil is fundamental in examining soil behaviour, and this study is the first to examine the triaxial behaviour of reconstituted specimens of Northland Allochthon soil. Triaxial testing results on reconstituted specimens from Mountain Road showed well defined critical states. The effective critical state angle of internal shearing resistance (φ'_{crit}) was found to be 33.7° to 34.6° which is high for a clay, and higher than the value acquired for the Ogles No. 3 site of 26° (O'Sullivan, 2009). A correlation made by Muir-Wood (1990) relating *M* (and therefore also φ'_{crit}) to the *PI* indicates that the higher φ'_{crit} is related to the low *PI*. Both the Ogles No. 3 site and Mountain Road site fall close to the trendline established from several clayey soils, which suggests that selecting a φ'_{crit} for Northland Allochthon residual clay soil can be based approximately on the *PI* of that soil. The slightly dilative behaviour seen near the end of the stress paths in the reconstituted state can also be explained by the low *PI* (less than 25%), which occurs as a result of turbulent shearing (Vaughan et al., 1978).

O'Sullivan (2009) hypothesized that the triaxial behaviour of Northland Allochthon residual clay soil may be affected by the natural structure of the soil. It was revealed through the careful comparison of reconstituted soil specimens to intact soil specimens from Mountain Road that the soil structure of the intact specimens results in an increased shear strength. The ratio of the Hvorslev cohesive intercept for the intact material to the reconstituted material (χ/χ^*) is 3.5. The ratio of the normalized strengths at intrinsic critical strength (T) is 1.2. The value of T, being greater than one, is evidence that the microstructure of the intact soil is stronger than that of the reconstituted soil, and bonding plays a role in the strength of the intact soil. The value of φ'_e was not affected, suggesting that the strength difference between the reconstituted and intact soil is related to the Hvorslev cohesive intercept only. The influence of microstructure on the strength of the Northland Allochthon residual clay soil

falls within the range of that determined for the four sedimentary clays examined by Burland et al. (1996).

The post-rupture strength of the intact specimens was estimated, and the near coincidence of this strength with the critical state angle of internal shearing resistance provides support for its use in examining first time slope failures in this soil type. This is an important finding for practitioners, as it demonstrates the value of testing reconstituted specimens which are much easier to obtain than high quality intact specimens.

Soil properties acquired in this study were tabulated along with those from other field sites in Northland Allochthon soil. It was found that there is significant variation between field sites, likely due to varying degrees of weathering, which is an important consideration for practitioners dealing with this soil type. The relationship between the behaviour of the soil and the *PI* is also seen in the strength parameters where there is a loose trend suggesting that a lower *PI* results in an increased φ'_{peak}. Findings on the behaviour of this soil type from this study and other studies have also been summarized.

Based on the comparison of a limited number of triaxial test results on Northland Allochthon clay soil to constitutive models using finite element numerical modelling, the Mohr-Coulomb (MC) and Hardening Soil models represent the behaviour of the intact soil from the Ogles No. 3 site well. The MC model was selected for use in the subsequent numerical models due to its simplicity. Reconstituted soil from Mountain Road was well represented by the Cam-clay model when λ/κ was reduced from 8 to 2. The MC model also provided a reasonable match to the laboratory results on reconstituted soil from Mountain Road. The dilatant nature of the intact soil from Mountain Road meant that although the MC model matched the laboratory deviatoric stress results, the pore pressure was overestimated by this constitutive model.

A case study of the road embankment failure at the Ogles No. 3 site demonstrated that the primary mechanism for ongoing movement could be due to the existence of a weakened shear failure plane after first-time failure. This type of failure mechanism has not been previously examined in this soil type, and this case study demonstrates it is a useful approach that should be considered when dealing with second time failure in Northland Allochthon slopes. This

case study also revealed that the MC model was able to reproduce small movements at the road shoulder due to groundwater fluctuations. The DSM columns failed in shear.

In conventional 2D analysis (i.e. the Ogles No. 3 case study mentioned above) soil movement around the columns could not be examined. Therefore, a plan view model of laterally loaded DSM columns was developed and fully validated against an analytical solution. The increased shear strength in the soil surrounding DSM columns seen by several researchers was implemented into the model, and led to an increase in the ultimate lateral pressure acting on the columns prior to failure of the soil in plastic flow around the columns. An increase/decrease in column spacing has a similar effect on the slope of the pressure-displacement curve as an increase/decrease in Young's modulus. Square columns with the same area as the circular columns have a slightly higher ultimate pressure acting on them prior to soil failure around the columns due to shape effects on arching mechanisms. The incorporation of lateral expansion induced by DSM columns into a slope stabilization scenario (i.e. laterally loaded) resulted in an increased ultimate pressure on the columns in both the drained and undrained conditions prior to failure of the soil in plastic flow around them. This analysis provides practitioners with evidence that improved soil property changes, found to occur in the soil surrounding DSM columns, lead to improved DSM column performance.

After examination of the DSM columns in conventional 2D analysis and in plan view, a 3D model was developed for comparison to 2D. A validated 3D method, developed by Kourkoulis et al. (2012) for simplifying a slope to facilitate the design of laterally loaded piles was applied to laterally loaded DSM columns for this different and new purpose which has not been previously performed. It was found that both the resisting force provided by the columns (RF_{column}) and horizontal stresses were overestimated in the 2D model as compared to the 3D model. This suggests that the RRM provides an overestimation when modelling the DSM columns because the strength and stiffness of the composite columns need to be reduced in order to match the lateral resistance provided in the more realistic 3D model. Closer column spacing resulted in less deviation between 2D and 3D results. The RRM was modified, and when the soil replacement ratio was increased by 19.3% at 2s, 18.6% at 3s and 18% at 4s, the ultimate RF_{column} in the 2D model was found to match that of the 3D model.

The required increase in the replacement ratio decreased linearly with an increase in column spacing. These findings do not necessarily imply that the use of the RRM in an analysis will always result in a safe slope. The degree to which it will influence the results will depend on several factors, such as the geometry of the slope, the location of the DSM columns, and the type of analysis (i.e. whether it is factor of safety analysis or deformation based analysis). It is recommended that when the soil properties and DSM column diameter are similar to those used in this study, the MRRM developed here be utilized. When they differ from this study, practitioners should perform a sensitivity analysis to assess the extent to which the overestimation provided by the RRM will affect their results. If their results are affected by the use of the MRRM, a 3D analysis should be considered.

This thesis covers several aspects of Northland Allochthon residual clay soil behaviour, and the use of DSM columns for road slips in this soil type. This study has shown that differences exist in soil strength between field sites within the Mangakahia Complex of Northland Allochthon soil, which have been found in this study to be related to differences in soil plasticity. Further investigation is required to explain the extent of these differences, and to verify that they occur as a result of different amounts of weathering. As soil structure has been found to play a role in soil strength at Mountain Road, investigation into how much of a role it plays at other field sites might give further insight into the differences between these sites.

During the field investigation portion of this study, it was identified that relationships developed by Marchetti (1980) and other researchers to determine OCR, K_0 and other soil parameters from the sDMT may not correspond to the actual soil parameters of a specific soil due to the need for site specific correlations. A detailed investigation into the used of the sDMT at specific field sites with corresponding laboratory testing and self-boring pressuremeter testing at various depths should be done to calibrate the relationships used to determine soil parameters from the sDMT.

The use of constitutive models for representing the behaviour of Northland Allochthon clay soil was only briefly investigated in this thesis, and was also investigated by O'Sullivan (2009). A more thorough investigation with a significant suite of intact and reconstituted

laboratory testing results could be done to compare the soil behaviour from a number of sites against several constitutive models, and possibly make modifications to them.

Thorough case studies of Northland Allochthon clay slope failures that would include borehole investigations, in situ testing, and the monitoring of slope movement and pore pressures over several years, throughout the soil profile, would be useful for characterizing the soil movement and creep behaviour, and relating it to rainfall events. This could also help to determine the effect of fissures, particularly with relation to movement in the transition zone and between soil layers. The effects of the shrink-swell behaviour of Northland Allochthon soil due to the high montmorillonite content could also be considered for future research as this has not yet been well investigated.

This research has shown that the changes to the soil around DSM columns exist, and that they influence the performance of the soil-column system. Much more research is possible into the property changes of the soil around the columns via in situ testing, laboratory testing, and numerical modelling. A thorough investigation using a combination of these could prove valuable for demonstrating the value of DSM for several different geotechnical applications.

This study has shown that modifications to the replacement ratio method were required in order to obtain a match between 2D and 3D results for laterally loaded DSM columns which fail in shear along a pre-defined slip surface. Further investigation into the differences between the performance of 2D and 3D models of DSM columns as used for slope failure mitigation would be useful for obtaining a more detailed methodology on how to model this three dimensional problem in 2D. Specifically, soil and column properties and the column diameter could be varied to determine the modifications required to the RRM under varying conditions. These results could be tabulated to provide a reference for determining the modified replacement ratio for any soil type or DSM column diameter.

10.0 References

Abbas, J., Chik, Z. H., & Taha, M. R. (2008). Single pile simulation and analysis subjected to lateral load. *Electronic Journal of Geotechnical Engineering, 13*(Bundle E), 15.

Adachi, T., Kimura, M., & Tada, S. (1989). Analysis on the preventative mechanism of landslide stabilizing piles. *Numerical models in geomechanics, Numlog III*, 691-698.

Ahmadi, M. M., & Ahmari, S. (2009). Finite-element modelling of laterally loaded piles in clay. *Proceedings of the Institution of Civil Engineers-Geotechnical Engineering, 162*(3), 151-163.

Al-Tabbaa, A., & Wood, D. M. (1987). Some measurements of the permeability of kaolin. *Geotechnique, 37*(4), 499-503.

Albert, C., Zdravkovic, L., & Jardine, R. J. (2003). *Behaviour of Bothkennar clay under rotation of principal stresses*. Paper presented at the International Workshop on the Geotechnics of Soft Soils- Theory and Practice, Noordwijkerhoud, Netherlands.

Allman, M. A., & Atkinson, J. H. (1992). Mechanical properties of reconstituted Bothkennar soil. *Geotechnique, 42*(2), 289-301.

Amsiejus, J., Dirgeliene, N., Norkus, A., & Zilioniene, D. (2009). Evaluation of soil shear strength parameters via triaxial testing by height versus diameter ratio of the sample. *Baltic Journal of Road and Bridge Engineering, 4*(2), 54-60.

Anderson, K. (2010). Carrs Road Bridge Geotechnical Design Report. In A. Holland (Ed.). Hamilton, New Zealand: AECOM.

Aniculaesi, M., Stanciu, A., & Lungu, I. (2013). Shrink-swell behaviour of expansive soils stabilized with eco-cement. In R. Q. Coutinho & P. W. Mayne (Eds.), *Geotechnical and Geophysical Site Characterization 4* (pp. 1677–1682). London, U.K.: Taylor and Francis Group.

ASTM. (2004). Standard Test Method for Consolidated Undrained Triaxial Compression Test for Cohesive Soils (Vol. D 4767-04, pp. 1-13). PA, USA: ASTM International.

ASTM. (2007). Standard Test Method for Unconsolidated Undrained Triaxial Compression Test on Cohesive Soils (Vol. D 2850 – 03a, pp. 1-6). PA, USA: ASTM International.

ASTM. (2010). Standard Test Methods for Specific Gravity of Soil Solids by Water Pycnometer (Vol. D854-10, pp. 1-7). PA, USA: ASTM International.

Atkinson, J. H. (1990). *Discussion of session 1.2*. Paper presented at the Proceedings of the Conference on Engineering Geology of Weak Rock, Leeds, U.K.

Atkinson, J. H. (1993). *The Mechanics of Soils and Foundations*. Abingdon, U.K.: McGraw-Hill

Atkinson, J. H., & Evans, J. S. (1985). The measurement of soil stiffness in the triaxial apparatus- Discussion. *Geotechnique, 35*(3), 378-382.

Baker, S., Leidberg, N. S. D., & Sallfors, F. (1997). *Deformation properties of lime cement stabilized soil in the working state*. Paper presented at the International Conference on Soil Mechanics and Foundation Engineering, Hamburg, Germany. 1667-1672.

Benmebarek, S., Khezzar, N., Kastner, R., & Dias, D. (2001). Improvement of the modified Cam-clay model for overconsolidated soils. In D. Billaux, X. Rachez, C. Detournay & R. Hart (Eds.), *FLAC and Numerical Modeling in Geomechanics* (pp. 3-6). Leiden, Netherlands: A. A. Balkema.

Bergado, D. T., Anderson, L. R., Miura, N., & Balasubramanian, A. S. (1996). *Soft ground improvement in lowlands and other environments*. ASCE Press. New York.

Berti, D. (2003). *Clay mineralogy and its effect on physical properties in the gulf of Mexico northwestern continental slope.* Master of Science, Texas A & M University.

Bhattarai, P., Marui, H., Tiwari, B., Watanabe, N., & Tuladhar, G. R. (2006). *Influence of weathering on physical and mechanical properties of mudstone*. Paper presented at the Proceedings of the Interpraevant International Symposium Disaster Mitigation of Debris Flows, Slope Failures and Landslides, Niigata, Japan. 467-479.

Bjerrum, L. (1954). Geotechnical properties of Norwegian marine clays. *Geotechnique, 4*(2), 46-69.

Bjerrum, L. (1967). Engineering geology of Norwegian normally consolidated marine clays as related to settlement of buildings. *Geotechnique, 17*(2), 81-118.

Bolton, M. (1991). *A Guide to Soil Mechanics*. Cambridge, U.K.: M. D. & K. Bolton.

Brandl, H. (1981). *Alteration of soil parameters by stabilization with lime*. Paper presented at the Proceedings of the 10th International Conference on Soil Mechanics and Foundation Engineering, Stockholm, Sweden. 587-594.

Bransby, M. F. (1996). Difference between load-transfer relationships for laterally loaded pile groups: Active p-y or passive p-delta. *Journal of Geotechnical Engineering, 122*(12), 1015-1018.

Bransby, M. F. (1999). Selection of p-y curves for the design of single laterally loaded piles. *International Journal for Numerical and Analytical Methods in Geomechanics, 23*(15), 1909-1926.

Bransby, M. F., & Springman, S. (1999). Selection of load-transfer functions for passive lateral loading of pile groups. *Computers and Geotechnics, 24*(3), 155-184.

BRANZ. (1987). *BRANZ Study Report: Assessment of Slope Stability at Building Sites*

BRE. (1993). *Low-rise buildings on shrinkable clay soil: Part 1*. London, U.K.: Construction Research Communications Ltd.

Brinkgreve, R. B. J., Broere, W., & Waterman, D. (2008). *Plaxis 2D Materials Models Manual Version 9.02*.

Broms, B. B. (2003). Deep soil stabilization: design and construction of lime and lime/cement columns. Stockholm, Sweden: Royal Institute of Technology.

Brooker, E. W., & Ireland, H. O. (1965). Earth pressure at rest related to stress history. *Canadian Geotechnical Journal, 2*(1), 1-15.

Bruce, D. A., & Bruce, M. C. (2003). *The practitioner's guide to deep mixing*. Paper presented at the Grouting and Ground Treatment, New Orleans, Louisiana, U.S.A. 474-488.

Burland, J. B. (1990). On the compressibility and shear strength of natural clays. *Geotechnique, 40*(3), 329-378.

Burland, J. B., Rampello, S., Georgiannou, V. N., & Calabresi, G. (1996). A laboratory study of the strength of four stiff clays. *Geotechnique, 47*(2), 390-390.

Calabresi, G. (1980). *The effect of sample size on strength parameters for intact and fissured stiff clays.* Paper presented at the Proceedings of Euromechanical Colloquium No. 134, Copenhagen, Denmark.

Callisto, L., & Calabresi, G. (1998). Mechanical behaviour of a natural soft clay. *Geotechnique, 48*(4), 495-513.

Campanella, R. G., & Robertson, P. K. (1991). Use and interpretation of a research dilatometer. *Canadian Geotechnical Journal, 28*(1), 113-126.

Carter, L. (1969). Mahurangi limestone from Puketotara peninsula, Northland, New Zealand. *New Zealand Journal of Geology and Geophysics, 12*(1), 104-118.

Casagrande, A. (1947). *Soil Mechanics Laboratory Notes*. Cambridge, U.S.A: Harvard University, Graduate School of Engineering.

Casagrande, A., Hirschfield, R. C., & Poulos, S. J. (1963). Harvard Soil Mechanics Series *Third Progress Report on Investigation of Stress-Deformation and Strength Characteristics of Compacted Clays* (Vol. 70, pp. 32). Cambridge, Massachusetts: Harvard University.

Chai, J. C., Miura, N., & Koga, H. (2005). Lateral displacement of ground caused by soil-cement column installation. *Journal of Geotechnical and Geoenvironmental Engineering, 131*(5), 623-632.

Chai, J. C., Miura, N., & Koga, H. (2007). Closure to "Lateral displacement of ground caused by soil-cement column installation" by Jin-Chun Chai, Norihiko Miura, and Hirofumi Koga. *Journal of Geotechnical and Geoenvironmental Engineering, 133*(1), 124-126.

Chandler, R. J. (1984). *Recent European experience of landslides in over-consolidated clays and soft rocks*. Paper presented at the Fouth International Symposium on Landslides, Toronto, Canada. 61-81.

Chandler, R. J. (2000). Clay sediments in depositional basins: The geotechnical cycle. *Quarterly Journal of Engineering Geology and Hydrogeology, 33*, 7-39.

Chandrasekaran, S. S., Boominathan, A., & Dodagoudar, G. R. (2010). Group interaction effects on laterally loaded piles in clay. *Journal of Geotechnical and Geoenvironmental Engineering, 136*(4), 573-582.

Chang, M. F. (1991). Interpretation of overconsolidation ratios from in situ tests in recent clay deposits in Singapore and Malaysia. *Canadian Geotechnical Journal, 28*(2), 210-225.

Chen, C. Y., & Martin, G. R. (2002). Soil-structure interaction for landslide stabilizing piles. *Computers and Geotechnics, 29*(5), 363-386.

Chen, L., & Poulos, H. G. (1993). Analysis of pile-soil interaction under lateral loading using infinite and finite elements. *Computers and Geotechnics, 15*(4), 189-220.

Coop, M. R., & Cotecchia, F. (1995). *The comparison of sediments at the achaelogical site of Sibari.* Paper presented at the 11th ECSMFE, Copenhagen, Denmark.

Cotecchia, F. (1996). *The effects of structure on an Italian Pleistogene clay.* University of London, London, U.K.

Cotecchia, F., & Chandler, R. J. (1997). The influence of structure on the pre-failure behaviour of a natural clay. *Geotechnique, 47*(3), 523-544.

Cotecchia, F., & Chandler, R. J. (2000). A general framework for the mechanical behaviour of clays. *Geotechnique, 50*(4), 431-447.

Craig, R. F. (2004). *Craig's Soil Mechanics, Seventh Edition*. London, U.K.: Spon Press.

Davisson, M. T., & Gill, H. L. (1963). Laterally loaded piles in a layered soil system. *Journal of Soil Mechanics and Foundations Division, 89*(3), 63-94.

Day, R. (2001). *Soil Testing Manual: Procedures, Classification Data, and Sampling Practice*: McGraw-Hill.

Duncan, J. M., & Dunlop, P. (1968). The significance of cap and base restraint. *Journal of the Soil Mechanics and Foundations Division, 94*(1), 271-290.

Edbrooke, S. W., & Brook, F. J. (Cartographer). (2009). Geology of the Whangarei Area.

EPA. (2011). *Recommended Practices Manual: A Guideline for Maintenance and Service of Unpaved Roads*. EPA (Choctawhatchee, Pea and Yellow Rivers Watershed Management Authority).

EuroSoilStab. (2002). Developement of design and construction methods to stabilise soft organic soils. Design guide soft soil stabilization.

Finlan, S., Quickfall, G., & Terzaghi, S. (2004). *Innovation in slip and settlement remedials: The soil mixing option*. Paper presented at the 9th Australia New Zealand Conference on Geomechanics, Auckland, New Zealand. 405-411.

Finno, R. J. (1993). Analytical interpretation of dilatometer penetration through saturated cohesive soils. *Geotechnique, 43*(2), 241-254.

Fletcher, L., Hungr, O., & Evans, S. G. (2002). Contrasting failure behaviour of two large landslides in clay and silt. *Canadian Geotechnical Journal, 39*(1), 46-62.

Fookes, P. G. (1997). Tropical Residual Soils. London, U.K.: Geological Society Engineering Group.

Fratta, D., Aguettant, J., & Roussel-Smith, L. (2007). *Soil Mechanics Laboratory Testing*. Boca Raton, Florida, U.S.A.: CRC Press, Taylor and Francis Group.

Gani, C. (2004). *Slope stabilisation- site investigation, design and application of deep soil mixing.* Paper presented at the 6th Australia-New Zealand Young Geotechnical Professional Conference, Auckland, New Zealand.

Gasparre, A. (2005). *Advanced laboratory characterisation of London Clay.* Doctor of Philosphy, Imperial College, London, U.K.

Georgiannou, V. N., & Burland, J. B. (2001). A laboratory study of post-rupture strength. *Geotechnique, 51*(8), 665-675.

Germaine, J. T., & Germaine, A. V. (2009). *Geotechnical Laboratory Measurements for Engineers*. Hoboken, New Jersey, U.S.A.: John Wiley & Sons.

Germaine, J. T., & Ladd, C. C. (1988). Triaxial testing of saturated cohesive soils. In R. T. Donaghe, R. C. Chaney & M. L. Silver (Eds.), *Advanced Triaxial Testing of Soil and Rock* (Vol. ASTM STP 977). Philadelphia, U.S.A.: American Society for Testing and Materials.

Goto, S., & Tatsuoka, F. (1988). Effects of end conditions on triaxial compressive strength for cohesionless soils. In R. T. Donaghe, R. C. Chaney & M. L. Silver (Eds.), *Advanced Triaxial Testing of Soil and Rock* (Vol. ASTM STP 977, pp. 13). Philadelphia, U.S.A.: American Society for Testing and Materials.

Goughnour, R. R., Sung, J. T., & Ramsey, J. S. (1991). *Slide correction by stone columns* (Vol. 1089): American Society for Testing and Materials.

Grammatikopoulou, A., Zdravkovic, L., & Potts, D. M. (2008). The influence of previous stress history and stress path direction on the surface settlement trough induced by tunnelling. *Geotechnique, 58*(4), 269-281.

Guetif, Z., Bouassida, M., & Debats, J. M. (2007). Improved soft clay characteristics due to stone column installation. *Computers and Geotechnics, 34*(2), 104-111.

Han, J., Oztoprak, S., Parsons, R. L., & Huang, J. (2007). Numerical analysis of foundation columns to support widening of embankments. *Computers and Geotechnics, 34*(6), 435-448.

Harada, K., Orense, R., Ishihara, K., & Mukai, J. (2010). Lateral stress effects on liquefaction resistance correlations. *Bulletin of the New Zealand Society for Earthquake Engineering, 43*(1), 13-23.

Harris, S. J. (2013). *The development of a site specific early warning system for rainfall induced landslides.* Doctor of Philosophy, University of Auckland, Auckland, New Zealand.

Hazelton, P., & Murphy, M. (2007). *Interpreting Soil Test Results: What Do All the Numbers Mean?* Sydney, Australia: CSIRO Publishing.

Head, K. H. (1998). *Manual of Soil Laboratory Testing, Volume 3: Effective Stress Tests* (Vol. 3). West Sussex, U.K.: John Wiley & Sons.

Head, K. H., & Epps, R. J. (2011). *Manual of Soil Laboratory Testing, Volume 2: Permeability, Shear Strength, and Compressibility Tests* (3 ed. Vol. 2). Dunbeath, U.K.: Whittles Publishing.

Hight, D. W. (2000). *Sampling methods: evaluation of disturbance and new practical techniques for high quality sampling of soil (Keynote Lecture)*. Paper presented at the Seventh National Congress of the Portuguese Geotechnical Society, Porto, Portugal.

Hight, D. W., Gasparre, A., Nishimura, S., Minh, N. A., Jardine, R. J., & Coop, M. R. (2007). Characteristics of the London Clay from the Terminal 5 site at Heathrow Airport. *Geotechnique, 57*(1), 3-18.

Hird, C. C., & Chan, C. M. (2005). *Correlation of shear wave velocity with unconfined compressive strength of cement stabilized clay*. Paper presented at the International Conference on Deep Mixing Best Practice and Recent Advances, Stockholm, Sweden. 79-85.

Holtrigter, M. (2010). *A comparison between the Flat Dilatometer and Cone Penetrometer Test with the aid of Artificial Neural Networks.* Master of Engineering, University of Auckland, Auckland, New Zealand.

Hosono, Y. (2011). [Personal Communiciation: Storage of soil specimens in a sealed container containing water as a measure to minimize moisture loss].

Hossain, A. T. M. S. (2001). *The engineering behaviour of the tropical clay soils of Dhaka, Bangladesh.* Doctor of Philosophy, Durham University Durham, U.K.

Houlsby, G. T. (1994). *How the dilatancy of soils affects their behaviour*. Paper presented at the 10th European Conference on Soil Mechanics and Foundation Engineering-Deformation of Soils and Displacements of Structures, Florence, Italy. 1189-1202.

Hryciw, R. D. (1990). Small strain shear modulus of soil by dilatometer. *Journal of Geotechnical Engineering, 116*(11), 1700-1716.

Hsiung, Y. M. (2003). Theoretical elastic-plastic solution for laterally loaded piles. *Journal of Geotechnical and Geoenvironmental Engineering, 129*(5), 475-480.

Huang, J., Han, J., & Oztoprak, S. (2009). Coupled mechanical and hydraulic modeling of geosynthetic-reinforced column-supported embankments. *Journal of Geotechnical and Geoenvironmental Engineering, 135*(8), 1011-1021.

Hvorslev, M. J. (1951). Time lag and soil permeability in ground-water observations. *Waterways Experiment Station, Corps of Engineers,* 1-50.

Imancli, G., Kahyaoglu, M. R., Ozden, G., & Kayalar, A. S. (2009). Performance functions for laterally loaded single concrete piles in homogeneous clays. *Structural Engineering and Mechanics, 33*(4), 529-537.

Insley, A. E., Chatterji, P. K., & Smith, L. B. (1977). Use of residual strength for stability analyses of embankment foundations containing pre-exisiting failure surfaces. *Canadian Geotechnical Journal, 14*(3), 408-428.

Irwin, M., & Rogers, N. (2006). *Land zonation mapping, stability hazard mapping/geotechnical assessment level, & effluent disposal potential for Kamo, Maunu, Onerahi, Otaika & Tikipunga*. (Job No: 22789). Whangarei, New Zealand: Tonkin & Taylor Ltd.

Isaac, M. J. (Cartographer). (1996). Geology of the Kaitaia Area.

Isaac, M. J., Herzer, R. H., Brook, F. J., & Hayward, B. W. (1994). *Cretaceous and Cenozoic Sedimentary Basins of Northland, New Zealand*. Institute of Geological and Nuclear Sciences monograph 8.

Itasca. (2008). *FLAC- Fast Langrangian Analysis of Coninua, Version 6.0 User's Manual*. Minneapolis, Minnesota, U.S.A.: Itasca Consulting Group.

Iwasaki, K., Tsuchiya, H., Sakai, Y., & Yamamoto, Y. (1991). *Applicability of the Marchetti dilatometer test to soft ground in Japan*: Coastal Development Institute of Technology.

Jardine, R. J., Gens, A., Hight, D. W., & Coop, M. R. (2004). *Developments in understanding soil behaviour*. Paper presented at the Advances in Geotechnical Engineering, London, U.K. 103-206.

Jardine, R. J., Symes, M. J., & Burland, J. B. (1984). The measurement of soil stiffness in the triaxial apparatus. *Geotechnique, 34*(3), 323-340.

Kaisaki, F. M. (1994). Assessing carbonates in the field with a dilute hydrochloric acid (HCl) solution. In N. R. C. S. United States Department of Agriculture (Ed.). Lincoln, U.S.A.: National Soil Survey Center.

Kamei, T., & Iwasaki, K. (1995). Evaluation of undrained shear strength of cohesive soils using a flat dilatometer. *Soils and Foundations, 35*(2), 111-116.

Kamon, M., & Bergado, D. T. (1991). *Ground improvement techniques- Theme Lecture.* Paper presented at the Proceedings of the 9th Asian Regional Conference Soil Mechanics & Foundation Engineering.

Karstunen, M. (1999). Alternative ways of modelling embankments on deep-stabilised soil. In H. Bredenberg, G. Holm & B. B. Broms (Eds.), *Dry Mix Methods for Deep Soil Stabilization* (pp. 221-228). Leiden, Netherlands: A. A. Balkema.

Karstunen, M., Krenn, H., & Aalto, A. (2005). *Recent advances in numerical modelling of deep-stabilized soil*. Paper presented at the Proceedings of the International Conference on Stabilisation/Solidification Treatment and Remediation. 303-312.

Kear, D., & Hay, R. F. (Cartographer). (1961). Sheet 1, North Cape.

Kitazume, M., & Maruyama, K. (2006). External stability of group column type deep mixing improved ground under embankment loading. *Soils and Foundations, 46*(3), 323-340.

Kitazume, M., & Maruyama, K. (2007). Internal stability of group column type deep mixing improved ground under embankment loading. *Soils and Foundations, 47*(3), 437-455.

Kitazume, M., Tabata, T., Ishiyama, S., & Karastanev, D. (1996). *Bearing capacity of improved ground with column type DDM*. Paper presented at the 2nd International Conference on Ground Improvement Geosystems, Tokyo, Japan. 503-508.

Kjekstad, O., Lunne, T., & Clausen, C. J. F. (1978). Comparison between in situ cone resistance and laboratory strength for overconsolidated North-Sea clays *Marine Geotechnology, 3*(1), 23-36.

Kok, Y. L. (2006). *Investigating the mechanical behaviour of two residual soils from Malaysia.* Doctor of Philosophy, University of Cambridge, Cambridge, U.K.

Kourkoulis, R. (2009). *Interplay of mat foundations and piles with a failing slope.* Doctor of Philosophy, National Technical University, Athens, Greece.

Kourkoulis, R., Gelagoti, F., Anastasopoulos, I., & Gazetas, G. (2011). Slope stabilizing piles and pile-groups: parametric study and design insights. *Journal of Geotechnical and Geoenvironmental Engineering, 137*(7), 663-677.

Kourkoulis, R., Gelagoti, F., Anastasopoulos, I., & Gazetas, G. (2012). Hybrid method for analysis and design of slope stabilizing piles. *Journal of Geotechnical and Geoenvironmental Engineering, 138*(1), 1-14.

Krenn, H., & Karstunen, M. (2009). *Numerical modelling of deep mixed columns below embankments constructed on soft soils*. Boca Raton: CRC Press-Taylor & Francis Group.

Kupka, M., Herle, I., & Arnold, M. (2009). Advanced calculations of safety factors for slope stability. *International Journal of Geotechnical Engineering, 3*(4), 509-515.

Lade, P. V., & Uzair, W. (1988). Effects of height-to-diameter ratio in triaxial specimens on the behavior of cross-anisotropic sand. In R. T. Donaghe, R. C. Chaney & M. L. Silver (Eds.), *Advanced Triaxial Testing of Soil and Rock* (Vol. ASTM STP 977, pp. 9). Philadelphia, U.S.A.: American Society of Testing and Materials.

Lambe, T. W., & Whitman, R. V. (1969). *Soil Mechanics*. New York, U.S.A.: John Wiley & Sons.

Larsson, S. (2005). *State of Practice Report- Execution, monitoring and quality control* Paper presented at the International Conference on Deep Mixing Best Practice and Recent Advances, Stockholm, Sweden. 732-786.

Larsson, S., & Kosche, M. (2005). *A laboratory study on the transition zone surrounding lime-cement columns*. Paper presented at the International Conference on Deep Mixing Best Practice and Recent Advances, Stockholm, Sweden. 111-118.

Larsson, S., Rothhamel, M., & Jacks, G. (2009). A laboratory study on the strength loss in kaolin surrounding lime-cement columns. *Applied Clay Science, 44*, 116-126.

Lee, K. L. (1978). End restraint effects on undrained static triaxial strength of sand. *Journal of Geotechnical Engineering, 104*(6), 687-704.

Lentfer, K. (2007). *Engineering geology of the Northland Allochthon, Silverdale, North Auckland, New Zealand.* Masters of Science, University of Auckland, Auckland.

Leroueil, S. (2001). Natural slopes and cuts: movement and failure mechanisms: 39th Rankine lecture. *Geotechnique, 51*(3), 197-243.

Leroueil, S., Tavenas, F., & Locat, J. (1984). Discussion on: Correlations between index tests and the properties of remoulded clays- Carrier W. D. and Beckman J. F. *Geotechnique, 35*(2), 223-226.

Leung, H., Gani, C., & Okada, W. (2006). Comparison of the effectiveness of deep soil mix columns using 2D and 3D Plaxis. *Plaxis Bulletin, 20,* 20-22.

Lin, H.-D., & Lin, S.-C. (2006). Discussion of "Lateral displacement of ground caused by soil-cement column installation" by Jin-Chun Chai , Norihiko Miura, and Hirofumi Koga. *Journal of Geotechnical and Geoenvironmental Engineering, 133*(1), 123-124.

Liyanapathirana, D. S., Carter, J. P., & Airey, D. W. (2005). Numerical modeling of nonhomogeneous behavior of structured soils during triaxial tests. *International Journal of Geomechanics, 5*, 10-23.

Lunne, T., Eide, O., & Deruiter, J. (1976). Correlations between cone resistance and vane shear-strength in some Scandinavian soft to medium stiff clays. *Canadian Geotechnical Journal, 13*(4), 430-441.

Lunne, T., Robertson, P. K., & Powell, J. J. M. (1997). *Cone Penetration Testing in Geotechnical Practice*. London, U.K.: Blackie Academic and Professional.

Lupini, J. F., Skinner, A. E., & Vaughan, P. R. (1981). The drained residual strength of cohesive soils. *Geotechnique, 31*(2), 181-213.

Malandraki, V., & Toll, D. (1994). *Yielding of a weakly bonded artifial soil* (Vol. 1). Rotterdam: A. A. Balkema.

Malandraki, V., & Toll, D. (1996). The definition of yield for bonded materials. *Geotechnical and Geological Engineering, 14*(1), 67-82.

Malandraki, V., & Toll, D. (2000). Drained probing triaxial tests on a weakly bonded artificial soil. *Geotechnique, 50*(2), 141-151.

Marchetti, S. (1980). In situ tests by flat dilatometer. *Journal of Geotechnical Engineering Division, ASCE, 106*(GT3), 299-321.

Marchetti, S., & Craps, D. K. (1981). Flat Dilatometer Manual: Internal report of GPE Inc.

Marchetti, S., Monaco, P., Totani, G., & Calabrese, M. (2001). *The flat dilatometer test (DMT) in soil investigations- A report by the ISSMGE committee TC16.* Paper presented at the Proceedings of the International Conference on In Situ Measurement of Soil Properties, Bali, Indonesia.

Martin, G. R., & Chen, C. Y. (2005). Response of piles due to lateral slope movement. *Computers & Structures, 83*(8-9), 588-598.

Masin, D., & Herle, I. (2005). *Numerical analysis of a tunnel in London clay using different constitutive models.* Paper presented at the Geotechnical Aspects of Underground Construction in Soft Ground, Amsterdam, Netherlands.

Massarsch, K. R. (2005). *Deformation properties of stabilized soil columns*. Paper presented at the International Conference on Deep Mixing Best Practice and Recent Advances, Stockholm, Sweden. 129-144.

Melrose, M. L., & Willis, M. L. (2010). *Slope stability analysis in Northland Allochthon Formation.* Honours, University of Auckland, Auckland, New Zealand.

Mesri, G., & Cepeda-Diaz, A. F. (1986). Residual shear strength of clays and shales. *Geotechnique, 36*(2), 269-274.

Messerklinger, S. (2006). *Non-linearity and small strain behaviour in lacustrine clay.* Doctor of Philosophy, ETH Zurich, Zurich, Austria.

Mills, J. J., Murphy, B. W., & Wickham, H. G. (1980). A study of three simple laboratory tests for the prediction of soil shrink-swell behaviour. *Journal of the Soil Conservation Service of New South Wales*(36), 77-82.

Mitchell, J. K. (1976). *Fundamentals of Soil Behaviour*. New York, N.Y., U.S.A.: John Wiley & Sons.

Mitchell, J. K., & Soga, K. (2005). *Fundamentals of Soil Behaviour* (Third ed.). Hoboken, New Jersey, U.S.A.: John Wiley & Sons Inc.

Monaco, P., & Marchetti, S. (2004). *Evaluation of the coefficient of subgrade reaction for design of multipropped diaphragm walls from DMT moduli* (Vol. 1 & 2). Rotterdam: Millpress Science Publishers.

Muir-Wood, D. (1990). *Soil Behaviour and Critical State Soil Mechanics*: Cambridge University Press.

Muir-Wood, D. (2004). *Geotechnical Modelling* (Vol. 1). Abingdon, U.K.: Spon Press.

Muntohar, A. S., & Hung, J. L. (2007). Strength distribution of soft clay surround lime-column. In D. Chan & K. T. Law (Eds.), *Soft Soil Engineering* (pp. 315-319). London, U.K.: Taylor & Francis Ltd.

MWH. (2002). PSMC002 Maintenance Contract, Preliminary Geotechnical Report, Mountain Road Slip, SH 1N RP 220/4.83. Whangarei, New Zealand: Transit New Zealand.

Nagaraj, T. S., Srinivasa Murthy, B. R., & Vatsala, A. (1994). *Analysis and Prediction of Soil Behaviour*. New Delhi, India: Wiley Eastern Ltd.

Navin, M. P. (2005). *Stability of embankments founded on soft soil improved with deep-mixing-method columns* Doctor of Philosophy, Virginia Polytechnic Institute and State University, Blacksburg, Virginia, U.S.A.

NIWA. (2011). Climate & Data Activities (Vol. 2011).

O'Sullivan, A. S. (2009). *Suitability of advanced soil models for stability analysis of slopes in Northland soils.* Masters of Engineering, University of Auckland, Auckland, New Zealand.

O'Sullivan, A. S. (2011a). [Personal Communication: Kaeo site investigation performed by Hiway Stabilizers Ltd.].

O'Sullivan, A. S. (2011b). [Personal Communication: Unconfined compressive strength of DSM columns in Northland Allochthon residual clay soil].

O'Sullivan, A. S. (2011c). [Personal Communication: Unit weight measurements of DSM columns in Northland Allochthon residual soil].

O'Sullivan, A. S., & Quickfall, G. (2011). [Personal Communication: Areas required for further research in DSM as a slope stabilization technique].

O'Sullivan, A. S., Quickfall, G., & Terzaghi, S. (2009). *Stabilisation of landslides using DSM columns in New Zealand* Paper presented at the International Symposium on Deep Mixing and Admixture Stabilization, Okinawa, Japan.

Oliveira, P. J. V., Pinheiro, J. L. P., & Correia, A. A. S. (2011). Numerical analysis of an embankment built on soft soil reinforced with deep mixing columns: Parametric study. *Computers and Geotechnics, 38*(4), 566-576.

Pender, M. J., Wesley, L. D., & Ni, B. (2003). *Laboratory stiffness and other properties of Auckland residual soil.* Paper presented at the Geotechnics and the Volcanic Edge – NZ Geotechnical Society Symposium, Tauranga, New Zealand.

Peng, J. R., Rouainia, M., & Clarke, B. G. (2010). Finite element analysis of laterally loaded fin piles. *Computers & Structures, 88*(21-22), 1239-1247.

Plaxis. (2004). *Plaxis 3D Tunnel Manual, Version 2.0*. Delft, Netherlands: Plaxis.

Plaxis. (2008). *Plaxis 2D Manual, Version 9.0*. Delft, Netherlands: Plaxis.

Porhaba, A. (2000). State of the art in deep mixing technology: Part IV design considerations. *Ground Improvement, 3*, 111-125.

Poulos, & Davis, E. H. (1980). Pile Foundation Analysis and Design (pp. 397). New York, NY, U.S.A.: John Wiley & Sons.

Poulos, H. G. (1999). *Design of Slope Stabilizing Piles* (Vol. 1 & 2). Leiden, Netherlands: A. A. Balkema.

Powell, J. M. M., & Uglow, I. M. (1988, July 1988). *The interpretation of the Marchetti dilatometer test in U.K. clays.* Paper presented at the Institution of Civil Engineers, Penetration Testing in the U.K., Birmingham, U.K.

Powrie, W. (2004). *Soil Mechanics Concepts and Applications* (2nd ed.). London, U.K. and New York, U.S.A.: Spon Press

Rahardjo, H., Aung, K. K., Leong, E. C., & Rezaur, R. B. (2004). Characteristics of residual soils in Singapore as formed by weathering. *Engineering Geology, 73*, 157-159.

Rampello, S., & Vigianni, G. M. B. (2001). *Prefailure Deformation Characteristics of Geomaterials.* Paper presented at the Prefailure Deformation Characteristics of Geomaterials, Torino, Italy.

Randolph, M. F., & Houlsby, G. T. (1984). The limiting pressure on a circular pile loaded laterally in cohesive soil. *Geotechnique, 34*(4), 613-623.

Rao, K. M., Prasad, K. N., & Pullaiah, M. (1999). *Influence of shape of pile on lateral response of pile foundations*.

Rao, S. M., Sridharan, A., & Chandrakaran, S. (1989). Influence of drying on the liquid limit behaviour of a marine clay. *Geotechnique, 39*(4), 715-719.

Rees, S. (2012). Part 1: Introduction to Triaxial Testing *What is Triaxial Testing?* (pp. 1-3). Hampshire, U.K.: GDS Instruments.

Reese, L. C., & Hudson, M. (1956). *Non-dimensional solutions for laterally loaded piles with soil modulus assumed proportional to depth.* Paper presented at the Proceedings of the 8th Texas Conference on Soil Mechanics and Foundation Engineering, Austin, Texas, U.S.A.

Reese, L. C., Wang, S.-T., & Fouse, J. L. (1992). Use of drilled shafts in stabilizing a slope. *ASCE Geotechnical Special Publication, No. 31, Stability and performance of slopes and embankments, 2*, 1318-1332.

Rogers, C. D. F., & Glendinning, S. (1996). The role of lime migration in lime pile stabilization of slopes. *Quarterly Journal of Engineering Geology, 29*, 273-284.

Roscoe, K. H., & Burland, J. B. (1968). On the generalised stress-strain behaviour of 'wet' clay. In J. Heyman & F. A. Leckie (Eds.), *Engineering plasticity* (pp. 535-609). Cambridge: Cambridge University Press.

Scarpelli, G., Sakellariadi, E., & Fruzzetti, V. M. E. (2003). *The dilatant behaviour of overconsolidated clays*. Paper presented at the Deformation Characteristics of Geomaterials, Lyon, France. 451-458.

Schofield, A. N. (1980). Cambridge geotechnical centrifuge operations: 20th Rankine lecture. *Geotechnique, 20*(2), 129-170.

Schofield, A. N., & Wroth, C. P. (1968). *Critical State Soil Mechanics*: McGraw-Hill.

Shave, J., Christie, T., Denton, S., & Kidd, A. (2010). *Development of traffic surcharge models for highway structures.* Paper presented at the Bridge Design to Eurocodes – U.K. Implementation, London, U.K.

Shen, S.-L., Han, J., & Du, Y. J. (2008). Deep mixing induced property changes in surrounding sensitive marine clays. *Journal of Geotechnical and Geoenvironmental Engineering, 134*(6), 845-854.

Shen, S.-L., Huang, X. C., Du, S. J., & Han, J. (2003a). Laboratory studies on property changes in surrounding clays due to installation of deep mixing columns. *Marine Georesources & Geotechnology, 21*(1), 15-35.

Shen, S.-L., Miura, N., Han, J., & Koga, H. (2003b). *Evaluation of property changes in surrounding clays due to installation of deep mixing columns.* Paper presented at the 3rd International Conference on Grouting and Ground Treatment, New Orleans, Louisiana, U.S.A.

Shen, S.-L., Miura, N., & Koga, H. (2003c). Interaction mechanism between deep mixing column and surrounding clay during installation. *Canadian Geotechnical Journal, 40*(2), 293-308.

Shen, W. Y., & Teh, C. I. (2004). Analysis of laterally loaded piles in soil with stiffness increasing with depth. *Journal of Geotechnical and Geoenvironmental Engineering, 130*(8), 878-882.

Sivadass, T., Lee, C. Y., & Karim, M. S. A. (2003). *Behaviour of tropical residual soil.* Paper presented at the Deformation Characteristics of Geomaterials, Lyon, France.

Skempton, A. W. (1964). Long-term stability of clay slopes. *Geotechnique, 14*(2), 77-101.

Skempton, A. W. (1970). The consolidation of clays by gravitational compaction. *Quarterly Journal of the Geological Society of London, 125*, 373-412.

Skempton, A. W. (1977). *Slope stability of cuttings in brown London Clay*. Paper presented at the Proceedings of the 9th International Conference on Soil Mechanics and Foundation Engineering, Tokyo, Japan. 261-270.

Skempton, A. W., & Northey, R. D. (1952). The sensitivity of clays. *Geotechnique, 3*(1), 30-53.

Smith, P. R., Jardine, R. J., & Hight, D. W. (1992). The yielding of Bothkennar clay. *Geotechnique, 42*(2), 257-274.

Spira, Y., Lackner, R., Pichler, C., & Mang, H. A. (2005). Viscoplastic material models for soil: new insight into the soil-support interaction in NATM tunnel excavation. *Archives of Mechanics, 57*, 209-240.

Stark, T. D., Choi, H., & McCone, S. (2005). Drained shear strength parameters for analysis of landslides. *Journal of Geotechnical and Geoenvironmental Engineering, 131*(5), 575-588.

Take, W. A., & Bolton, M. D. (2011). Seasonal ratcheting and softening in clay slopes, leading to first time failure. *Geotechnique, 61*(9), 757-769.

Takenaka, D., & Takenaka, K. (1995). Deep chemical mixing method- using cement as a hardening agent. Tokyo, Japan: Takenaka Corporation.

Tatarniuk, C. M., & Bowman, E. T. (2012a). *Case study of a road embankment failure mitigated using deep soil mixing*. Paper presented at the 4th International Conference on Grouting and Deep Mixing, New Orleans, Louisiana, U.S.A. 471-482.

Tatarniuk, C. M., & Bowman, E. T. (2012b). *Two dimensional numerical modelling of landslide stabilizing deep soil mixed columns*. Paper presented at the 11th International & 2nd North American Symposium on Landslides, Banff, Alberta, Canada. 1753-1758.

Tatarniuk, C. M., & Bowman, E. T. (2013). *A simplified numerical model of deep soil mixed columns used for road slip mitigation in 2D versus 3D*. Paper presented at the 19th New Zealand Geotechnical Society Symposium, Queenstown, New Zealand. 731-738.

Terashi, M. (2005). *Keynote Lecture: Design of deep mixing in infrastucture application*. Paper presented at the International Conference on Deep Mixing Best Practice and Recent Advances, Stockholm, Sweden. 25-44.

Terashi, M., Tanaka, H., Mitsumoto, T., Niidome, Y., & Honma, S. (1980). Fundamental properties of lime and cement treated soils (2nd report) *Report of the Port and Harbour Research Institute* (Vol. 9, pp. 33-62).

Terzaghi, K., Peck, R. B., & Mesri, G. (1996). *Soil Mechanics in Engineering Practice*. New York, U.S.A.: John Wiley & Sons.

Terzaghi, S. (2014). [Personal Communication: Stress relaxation around DSM columns].

Terzaghi, S., Okada, W., Houghton, L. D., & Quickfall, G. (2005). *Deep soil mixing in New Zealand- an update.* Paper presented at the International Conference on Deep Mixing Best Practice and Recent Advances, Stockholm, Sweden.

Terzhagi, S., Wataru, O., & Houghton, L. (2004). *Deep soil mixing In New Zealand- role in slope stabilisation.* Paper presented at the ASEP-GI International Symposium, Paris, France.

Thompson, B. N. (Cartographer). (1961). Sheet 2A, Whangarei.

Tilsley, S. C. (1998). PA 1651 Investigation, Design & Supervision for State Highway 1 - Albany to Puhoi Realignment (ALPURT) Sector B1 - Silverdale to Orewa: Beca Carter Hollings & Ferner Ltd.

Tong, S. Y., Tang, S. K., & Sugawara, S. (2004). *Characterization of marine clay soil for a mass rail transit system in Singapore*. Rotterdam, Netherlands: Millpress Science Publishers.

Totani, G., Calabrese, M., Marchetti, S., & Monaco, P. (1997). *Use of in situ flat plate dilatometer (DMT) for ground characterization in the stability analysis of slopes.* Paper presented at the 15th International Conference on Soil Mechanics and Foundation Engineering, Hambourg, Germany.

Vardanega, P. J., & Bolton, M. D. (2013). Stiffness of clays and silts: normalizing shear modulus and shear strain. *Journal of Geotechnical and Geoenvironmental Engineering, 139*(9), 1575-1589.

Vaughan, P. R. (1988). *Characterising the mechanical properties of in situ residual soil*. Paper presented at the Proceedings of the 2nd international conference on Geomechanics in Tropical Soils, Singapore. 469-487.

Vaughan, P. R., Hight, D. W., Sodha, V. G., & Walbancke, H. J. (1978). *Factors controlling the stability of clay fills in Britain.* Paper presented at the Clay Fills, London, U.K.

Vesic, A. S. (1972). Expansion of cavities in infinite soil mass. *American Society of Civil Engineers Soil Mechanics and Foundations Division, 98*(SM3), 26.

Vogler, U., & Karstunen, M. (2009). *Application of volume averaging technique in numerical modelling of deep mixing*. Boca Raton, U.S.A.: CRC Press-Taylor & Francis Group.

Wang, W. L., & Yen, B. C. (1974). Soil arching in slopes. *Journal of the Geotechnical Engineering Division, 100*(1).

Wesley, L. D. (1988). *Engineering classification of residual soils.* Paper presented at the Proceedings of the 2nd International Conference on Geomechanics in Tropical Soils, Singapore.

Wesley, L. D. (1990). Influence of structure and composition on residual soils. *Journal of Geotechnical Engineering, 116*(4), 589-601.

Wesley, L. D. (2010a). *Fundamentals of Soil Mechanics for Sedimentary and Residual Soils*. Hoboken, New Jersey, U.S.A.: John Wiley & Sons.

Wesley, L. D. (2010b). *Geotechnical Engineering in Residual Soils*. Hoboken, New Jersey, U.S.A.: John Wiley & Sons.

Wierzbicki, J. (2009). Analysis in changes in overconsolidation ratio in selected profiles of non-lithified deposits. *Architechture, Civil Engineering, and Environment*(3), 77-84.

Williams, P. (2009). Limestone country - Limestone, dolomite and marble, Te Ara-Encyclopedia of New Zealand (Publication no. http://www.TeAra.govt.nz/en/limestone-country/1). from Government of New Zealand

Winkler, G. E. (2003). *Geotechnical engineering of the Northland Allochthon.* Paper presented at the New Zealand Geotechnical Society 2003 Symposium.

Wong, J. T. F., Wong, M. F., & Kassim, K. (1993). *Comparison between dilatometer and other in situ and laboratory tests in Malaysian alluvial clay.* Paper presented at the Proceedings of the 11th Southeast Asian Geotechnical Conference, Singapore.

Xing-Cheng, L. (2014a). [Personal Communication: Dimensions of specimen in triaxial test simulations in Plaxis do no affect the results].

Xing-Cheng, L. (2014b). [Personal Communication: Explanation of tau max].

Yang, K., & Liang, R. (2006). Numerical solution for laterally loaded piles in a two-layer soil profile. *Journal of Geotechnical and Geoenvironmental Engineering, 132*(11), 1436-1443.

Yang, L. (2002). Geotechnical Report- Mountain Road Slip. In J. Chisnall (Ed.). Whangarei, New Zealand: Montgomery Watson Harza (MWH).

Ye, S. L., Han, J., & Ye, G. B. (1994). Soil Improvement and Underpinning Techniques. *China Architecture and Building Press*.

Zhou, Y. (2006). *Soil Mechanics: Laboratory Testing*. Tuscon, Arizona, U.S.A.: National Highway Institute.

Zienkiewicz, O. C., Humpheson, C., & Lewis, R. W. (1975). Associated and non-associated visco-plasticity and plasticity in soil mechanics. *Geotechnique, 25*(4), 671-689.

APPENDIX A

K_D results at sDMT5, 6 and 7; I_D results at sDMT 3, 4, 5, 6 and 7

Table A1: K_D, p_0 and p_1 results at sDMT 7, 6 and 5.

sDMT7				sDMT6				sDMT5			
Depth below ground level (m)	p_0 (kPa)	p_1 (kPa)	K_D	Depth below ground level (m)	p_0 (kPa)	p_1 (kPa)	K_D	Depth below ground level (m)	p_0 (kPa)	p_1 (kPa)	K_D
0.25	158	427	37.2	0.25	177	352	41.6	0.25	176	447	41.4
0.50	227	528	26.9	0.50	241	376	28.6	0.50	244	450	29.0
0.75	149	241	11.8	0.75	179	240	14.2	0.75	227	429	18.1
1.00	182	198	11.0	1.00	156	220	9.4	1.00	172	239	10.3
1.25	406	779	20.4	1.25	266	321	13.0	1.25	197	223	9.5
1.50	149	147	6.1	1.50	440	762	18.0	1.50	340	700	14.0
1.75	205	210	7.4	1.75	177	184	6.1	1.75	225	294	7.8
2.00	230	259	7.4	2.00	207	327	6.4	2.00	257	391	7.8
2.25	204	249	5.8	2.25	198	369	5.4	2.25	158	227	4.3
2.50	163	262	4.2	2.50	245	355	6.0	2.50	225	239	5.5
2.75	237	266	5.5	2.75	215	227	4.8	2.75	379	854	8.6
3.00	101	315	2.2	3.00	135	189	2.8	3.00	189	225	3.9
3.25	247	290	5.1	3.25	203	242	4.0	3.25	192	205	3.8
3.50	231	297	4.6	3.50	194	266	3.7	3.50	194	285	3.7
3.75	360	597	6.9	3.75	328	482	6.1	3.75	267	408	4.9
4.00	358	537	6.6	4.00	377	578	6.8	4.00	343	598	6.1
4.25	374	596	6.6	4.25	346	509	6.0	4.25	334	536	5.7
4.50	340	629	5.7	4.50	333	558	5.5	4.50	379	601	6.3
4.75	424	735	6.9	4.75	464	759	7.5	4.75	411	787	6.6
5.00	536	861	8.5	5.00	529	834	8.3	5.00	515	799	8.0
5.25	513	891	7.8	5.25	528	944	8.0	5.25	478	820	7.1
5.50	471	771	6.9	5.50	440	733	6.4	5.50	406	641	5.8
5.75	335	553	4.6	5.75	344	474	4.7	5.75	346	465	4.7
6.00	346	543	4.6	6.00	312	463	4.1	6.00	351	465	4.6
6.25	250	289	3.1	6.25	254	321	3.1	6.25	335	436	4.3
6.50	268	360	3.3	6.50	285	334	3.5	6.50	314	384	3.8
6.75	265	431	3.1	6.75	293	512	3.5	6.75	252	349	2.9
7.00	197	578	2.1	7.00	314	815	3.6	7.00	259	422	2.9
7.25	262	495	2.9	7.25	231	537	2.4	7.25	200	456	2.0
7.50	305	599	3.3	7.50	269	410	2.8	7.50	231	398	2.3
7.75	301	455	3.2	7.75	221	392	2.2	7.75	266	564	2.7
8.00	286	443	2.9	8.00	273	307	2.7	8.00	225	369	2.1
8.25	576	1386	6.3	8.25	205	343	1.8	8.25	219	300	2.0
8.50	291	1248	2.8	8.50	235	809	2.1	8.50	242	281	2.2
8.75	290	781	2.6	8.75	387	911	3.8	8.75	216	256	1.8
9.00	344	1219	3.2	9.00	712	1662	7.3	9.00	294	745	2.6
9.25	833	2735	8.3	9.25	692	1879	6.9	9.25	497	1521	4.8
9.50	672	1720	6.4	9.50	882	2116	8.7	9.50	658	1903	6.3
9.75	808	2047	7.6	9.75	907	2553	8.7	9.75	951	2120	9.2
10.00	885	2559	8.2	10.00	826	2885	7.7	10.00	680	1852	6.2
10.25	1875	3709	17.6	10.25	1236	3186	11.5	10.25	909	2136	8.3
10.50	1789	3246	16.3	10.50	1310	3893	11.9	10.50	772	2335	6.8
10.75	1742	3062	15.5	10.75	1842	3287	16.5	10.75	914	2554	7.9
11.00	1671	3092	14.4	11.00	1760	3213	15.3	11.00	842	2337	7.1
11.25	946	2492	7.7	11.25	1469	2721	12.4				
11.50	1029	4049	8.2	11.50	1204	3754	9.7				
11.75	2932	5547	24.1	11.75	2700	5036	22.2				

Table A2: I_D results and soil descriptions at sDMT 3, 4, 5, 6, and 7

Depth below ground level (m)	sDMT3		sDMT4		sDMT5		sDMT6		sDMT7	
	I_D	Soil Description	I_D	Soil Description	I_D	Soil Description	I_D	Soil Description	I_D	Soil Description
0.25	0.56	SILTY CLAY	0.81	SILT	1.54	SANDY SILT	0.99	SILT	1.70	SANDY SILT
0.50	0.38	SILTY CLAY	0.83	SILT	0.84	SILT	0.56	SILTY CLAY	1.33	SANDY SILT
0.75	0.34	SILTY CLAY	0.52	SILTY CLAY	0.89	SILT	0.34	SILTY CLAY	0.62	CLAYEY SILT
1.00	0.50	SILTY CLAY	0.65	CLAYEY SILT	0.39	SILTY CLAY	0.41	SILTY CLAY	0.09	MUD AND/OR PEAT
1.25	0.66	CLAYEY SILT	0.61	CLAYEY SILT	0.13	MUD	0.20	CLAY	0.92	SILT
1.50	1.40	SANDY SILT	0.83	SILT	1.06	SILT	0.73	CLAYEY SILT		MUD AND/OR PEAT
1.75	1.30	SANDY SILT	0.63	CLAYEY SILT	0.31	CLAY	0.04	MUD AND/OR PEAT	0.03	MUD AND/OR PEAT
2.00	1.03	SILT	0.81	SILT	0.52	SILTY CLAY	0.58	SILTY CLAY	0.13	MUD
2.25	1.18	SILT	0.80	SILT	0.44	SILTY CLAY	0.87	SILT	0.22	CLAY
2.50	1.24	SANDY SILT	1.09	SILT	0.06	MUD AND/OR PEAT	0.45	SILTY CLAY	0.60	CLAYEY SILT
2.75	1.61	SANDY SILT	0.92	SILT	1.25	SANDY SILT	0.05	MUD AND/OR PEAT	0.12	MUD
3.00	0.89	SILT	1.01	SILT	0.19	CLAY	0.40	SILTY CLAY	2.13	SILTY SAND
3.25	0.84	SILT	0.66	CLAYEY SILT	0.07	MUD AND/OR PEAT	0.19	CLAY	0.18	CLAY
3.50	0.46	SILTY CLAY	0.32	CLAY	0.48	SILTY CLAY	0.38	SILTY CLAY	0.29	CLAY
3.75	0.78	CLAYEY SILT	0.44	SILTY CLAY	0.54	SILTY CLAY	0.48	SILTY CLAY	0.67	CLAYEY SILT
4.00	0.46	SILTY CLAY	0.72	CLAYEY SILT	0.77	CLAYEY SILT	0.55	SILTY CLAY	0.51	SILTY CLAY
4.25	0.48	SILTY CLAY	1.08	SILT	0.63	CLAYEY SILT	0.49	SILTY CLAY	0.61	CLAYEY SILT
4.50	2.12	SILTY SAND	1.12	SILT	0.61	CLAYEY SILT	0.71	CLAYEY SILT	0.89	SILT
4.75	0.83	SILT	1.14	SILT	0.95	SILT	0.66	CLAYEY SILT	0.76	CLAYEY SILT
5.00	0.99	SILT	0.86	SILT	0.57	SILTY CLAY	0.60	SILTY CLAY	0.63	CLAYEY SILT
5.25	0.97	SILT	0.62	CLAYEY SILT	0.75	CLAYEY SILT	0.82	SILT	0.77	CLAYEY SILT
5.50	1.06	SILT	1.27	SANDY SILT	0.62	CLAYEY SILT	0.71	CLAYEY SILT	0.67	CLAYEY SILT
5.75	0.94	SILT	0.96	SILT	0.37	SILTY CLAY	0.41	SILTY CLAY	0.71	CLAYEY SILT
6.00	1.34	SANDY SILT	1.23	SANDY SILT	0.36	SILTY CLAY	0.54	SILTY CLAY	0.62	CLAYEY SILT
6.25	0.91	SILT	1.12	SILT	0.33	SILTY CLAY	0.30	CLAY	0.18	CLAY
6.50	0.46	SILTY CLAY	0.99	SILT	0.25	CLAY	0.20	CLAY	0.40	SILTY CLAY
6.75	0.20	CLAY	0.77	CLAYEY SILT	0.45	SILTY CLAY	0.86	SILT	0.73	CLAYEY SILT
7.00	0.36	SILTY CLAY	0.99	SILT	0.74	CLAYEY SILT	1.82	SILTY SAND	2.42	SILTY SAND
7.25	1.39	SANDY SILT	1.15	SILT	1.62	SANDY SILT	1.61	SANDY SILT	1.06	SILT
7.50	1.49	SANDY SILT	0.80	CLAYEY SILT	0.89	SILT	0.62	CLAYEY SILT	1.13	SILT
7.75	1.53	SANDY SILT	0.84	SILT	1.36	SANDY SILT	0.98	SILT	0.61	CLAYEY SILT
8.00	0.86	SILT	1.62	SANDY SILT	0.82	SILT	0.15	MUD	0.67	CLAYEY SILT
8.25	1.39	SANDY SILT	1.43	SANDY SILT	0.48	SILTY CLAY	0.89	SILT	1.54	SANDY SILT
8.50	1.37	SANDY SILT	2.54	SILTY SAND	0.21	CLAY	3.18	SILTY SAND	4.03	SAND
8.75	1.10	SILT	1.28	SANDY SILT	0.25	CLAY	1.58	SANDY SILT	2.11	SILTY SAND
9.00	1.20	SILT	1.27	SANDY SILT	1.92	SILTY SAND	1.46	SANDY SILT	3.06	SILTY SAND
9.25	0.62	CLAYEY SILT	0.92	SILT	2.35	SILTY SAND	1.88	SILTY SAND	2.46	SILTY SAND
9.50	1.17	SILT	1.89	SILTY SAND	2.10	SILTY SAND	1.51	SANDY SILT	1.72	SANDY SILT
9.75	0.95	SILT	1.11	SILT	1.32	SANDY SILT	1.96	SILTY SAND	1.67	SANDY SILT
10.00	0.83	SILT	0.83	SILT	1.92	SILTY SAND	2.72	SILTY SAND	2.05	SILTY SAND
10.25	0.92	SILT	0.99	SILT	1.47	SANDY SILT	1.67	SANDY SILT	1.02	SILT
10.50	0.68	CLAYEY SILT	0.43	SILTY CLAY	2.24	SILTY SAND	2.09	SILTY SAND	0.85	SILT
10.75	0.92	SILT	1.35	SANDY SILT	1.96	SILTY SAND	0.82	SILT	0.79	CLAYEY SILT
11.00	0.85	SILT	1.46	SANDY SILT	1.96	SILTY SAND	0.86	SILT	0.89	SILT
11.25	0.71	CLAYEY SILT	1.29	SANDY SILT			0.90	SILT	1.79	SANDY SILT
11.50	1.33	SANDY SILT	1.33	SANDY SILT			2.28	SILTY SAND	3.19	SILTY SAND
11.75	1.05	SILT	1.05	SILT			0.89	SILT	0.92	SILT

APPENDIX B

Load cell and pore pressure versus strain to 4% for comparison of top cap types

Figure B1 shows a comparison of change in pore pressure versus axial strain between the knob-and-dimple top cap and the top cap with the vylastic sleeve at three different confining pressures. Figure B2 shows a comparison of load cell readings versus axial strain between the knob-and-dimple top cap and the top cap with the vylastic sleeve at the same three confining pressures.

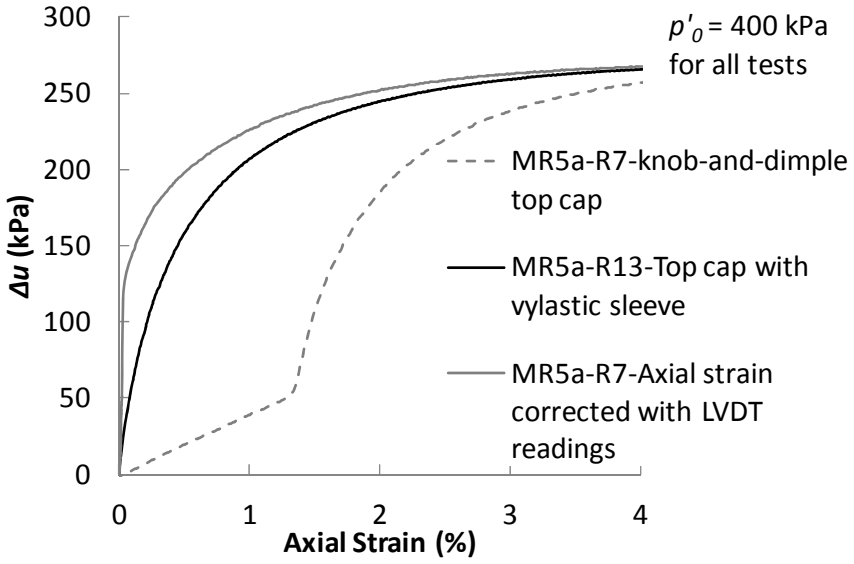

(a)

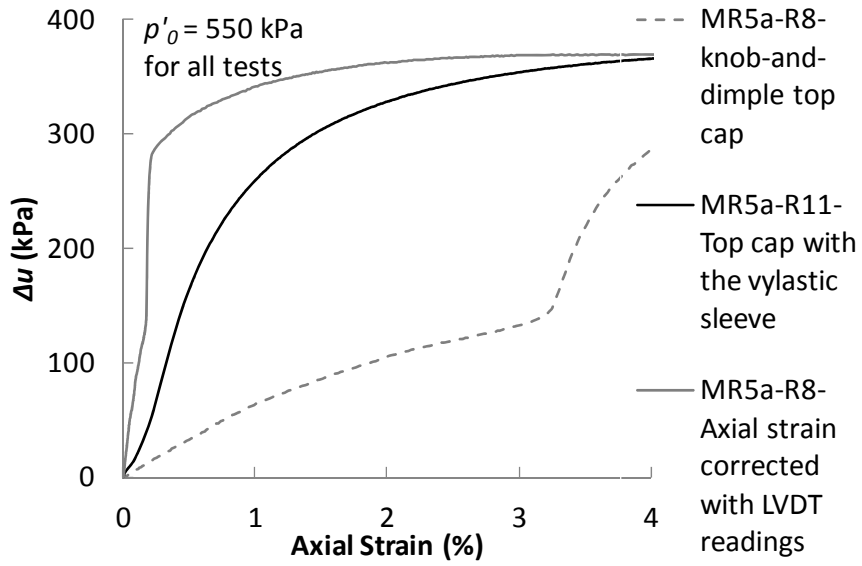

(b)

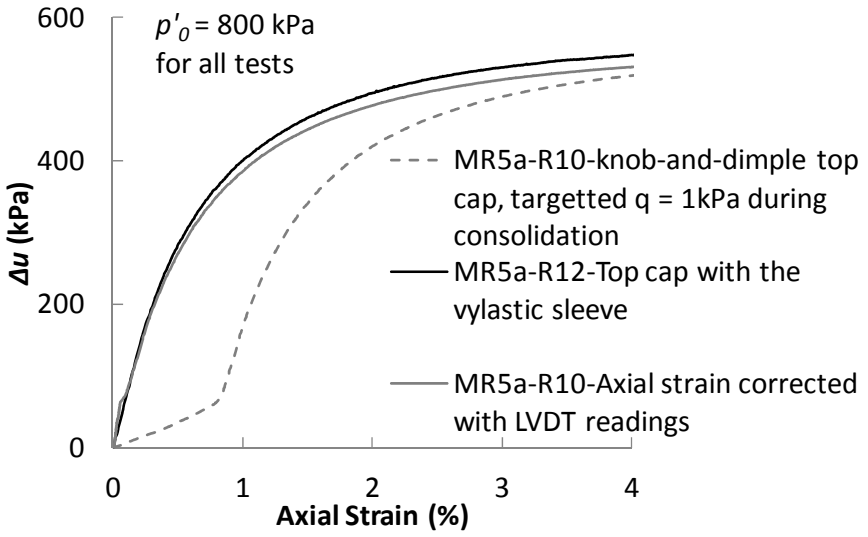

(c)

Figure B1: Comparison of change in pore pressure versus axial strain between the knob-and-dimple top cap and the top cap with the vylastic sleeve at (a) p'_0 = 400 kPa, (b) p'_0 = 550 kPa and (c) p'_0 = 800 kPa.

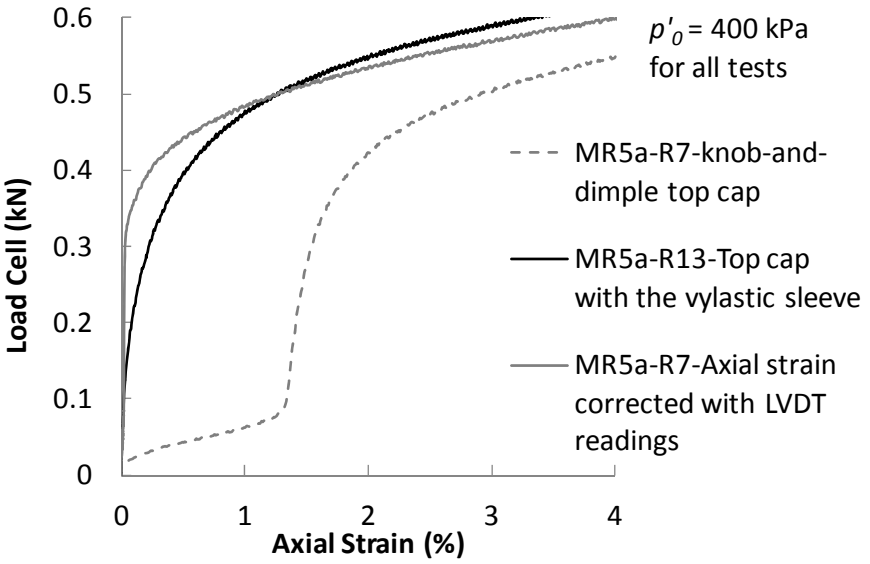
0.6
0.5
0.4
0.3
0.2
0.1
0
Load Cell (kN)
0
1
2
3
4
Axial Strain (%)
p'_0 = 400 kPa for all tests
MR5a-R7-knob-and-dimple top cap
MR5a-R13-Top cap with the vylastic sleeve
MR5a-R7-Axial strain corrected with LVDT readings

(a)

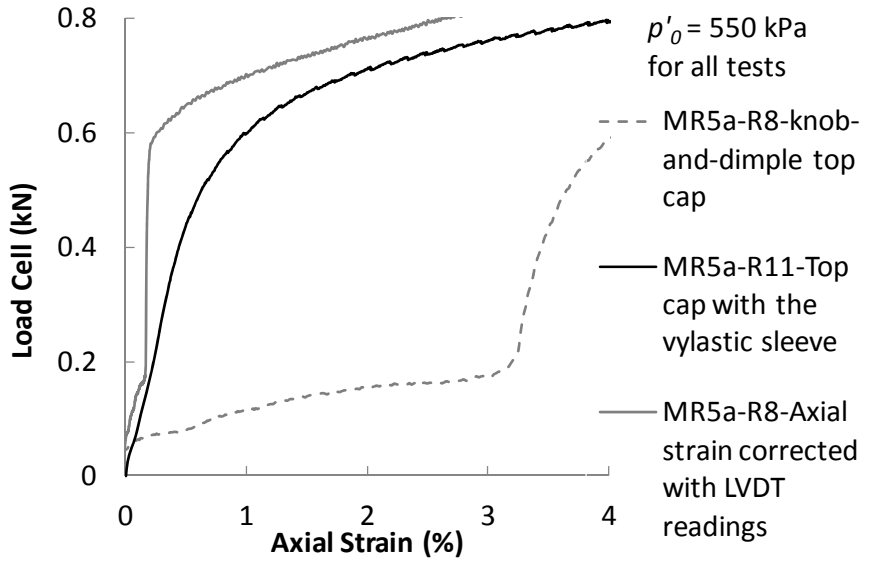
0.8
0.6
0.4
0.2
0
Load Cell (kN)
0
1
2
3
4
Axial Strain (%)
p'_0 = 550 kPa for all tests
MR5a-R8-knob-and-dimple top cap
MR5a-R11-Top cap with the vylastic sleeve
MR5a-R8-Axial strain corrected with LVDT readings

(b)

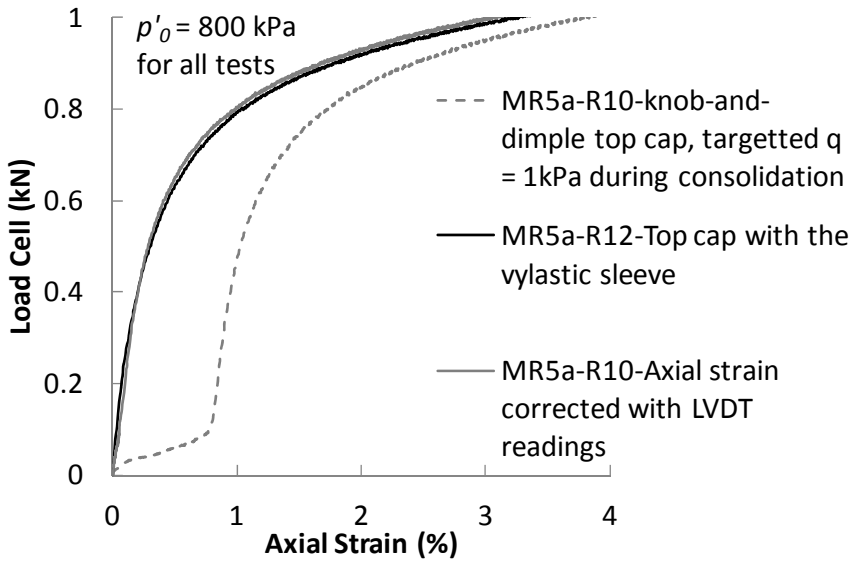

(c)

Figure B2: Comparison of load cell readings versus axial strain between the knob-and-dimple top cap and the top cap with the vylastic sleeve at (a) p'_0 = 400 kPa, (b) p'_0 = 550 kPa and (c) p'_0 = 800 kPa.

APPENDIX C

Photographs of soil specimens at failure

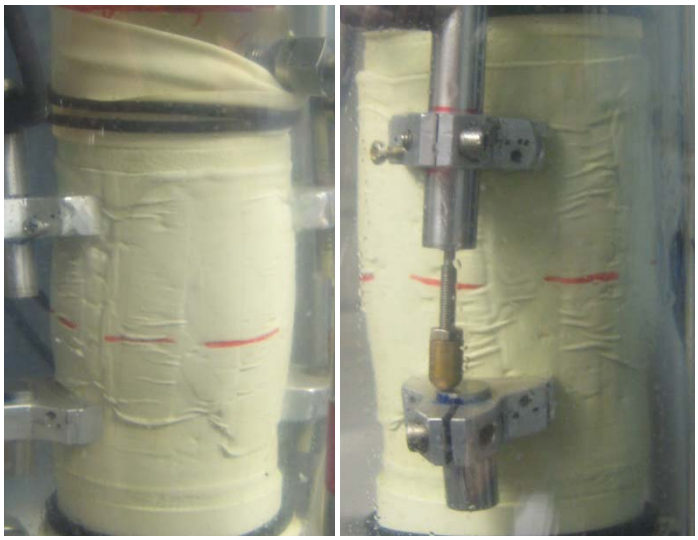

Figure C1: MR5a-R1

Figure C2: MR5a-R2

Figure C3: MR5a-R3

Figure C4: MR5a-R4

Figure C5: MR5a-R5

Figure C6: MR5a-R6

Figure C7: MR5a-R7

Figure C8: MR5a-R8

Figure C9: MR5a-R9

Figure C10: MR5a-R10

Figure C11: MR5a-R11

Figure C12: MR5a-R12

Figure C13: MR5a-R13

Figure C14: MR5c

Figure C15: MR5b

Figure C16: MR5d

APPENDIX D

Comparison of stress paths to other clays

The shape of the stress paths for the reconstituted Northland Allochthon residual clay is similar to that of Indonesian residual red clay (Figure D3) and Bangladeshi residual clay (Figure D4) in that they show a slight bend to the left (contractive) followed by a sharp bend to the right when close to failure (dilative). The stress paths of the intact Indonesian residual red clay and Bangladeshi residual clay are very similar in shape to their destructured counterparts. For the Northland Allochthon residual clay, the stress paths of the reconstituted and intact specimens are somewhat different. Due to the fact that they were tested at lower confining pressures, the intact specimens are less dilative prior to failure. Their stress paths barely bend to the left prior to taking a slow turn to the right.

Comparing Figures D2 to D4 to Figures D5 to D8, there is a clear similarity in the stress paths of the three residual clay soils which does not exist between the four stiff clays examined by Burland et al. (1996). The Atterberg limits shown in Table D1 (plotted on a conventional plasticity chart in Figure D1) demonstrate that the residual clays also all have fairly similar plastic limits and plasticity indices. The Vallericca clay is also closest to these clays on the plasticity chart, and shows the most similar behaviour. This confirms the influence of plasticity on the stress path behaviour. However, the Valerricca clay does not exhibit the same dilatant behaviour (i.e. curve to the right in the stress path) just before failure seen in the reconstituted normally consolidated specimens. The Indonesian red clay is derived from the weathering of volcanic deposits (mainly tuff and ash), and has large inter-void ratios, contributing to turbulent shearing (and dilative behaviour). The Bangladeshi residual clay is intensively weathered soil derived from underlying sand deposits. Illite is the most common clay mineral present wtih high amounts of kaolinite also present. Quartz is the most abundant non-clay mineral. The organic content (although it was not measured) is not suspected to be high. Thus, there is nothing in the composition of the Dhaka clay to suggest that it has a high inter-void ratio and would undergo turbulent shearing. However, the plasticity index at 29 and 34 is relatively close to the value of 25 suggested by Vaughan et al. (1978) as the point below which turbulent shearing tends to occur.

Figure D9 shows the stress paths for the undrained tests on Ogles No. 3 soil, plotted with the undrained tests on intact Mountain Road soil. The first three tests from Ogles No. 3 were estimated from the graph in O'Sullivan (2009). Raw data was available for the fourth test from this site. Figure D9 shows that the undrained stress paths from the Ogles No. 3, like those from the Mountain Road site have dilative behaviour. The in situ effective stress of the samples was no more than 80 kPa, indicating overconsolidated behaviour for the 100 kPa and 110 kPa tests.

Table D1: Atterberg limits for several residual and sedimentary clays.

Soil Type	Northland Allochthon Residual Clay (Mountain Road)	Indonesian Residual Red Clay^^	Bangladeshi Residual Clay (Borehole 1 & 2)^	Bangladeshi Residual Clay (Borehole 3)^	Pietrafitta Clay*	Corinth Marl*	Todi Clay*	Vallericca Clay*
Plastic Limit (%)	29	36	22	19	53	6	28	33
Liquid Limit (%)	50	76	51	53	87	27	67	60
Plasticity Index	21	40	29	34	34	21	39	27

*Burland et al. (1996)
^Hossain (2001)
^^Wesley (1990)

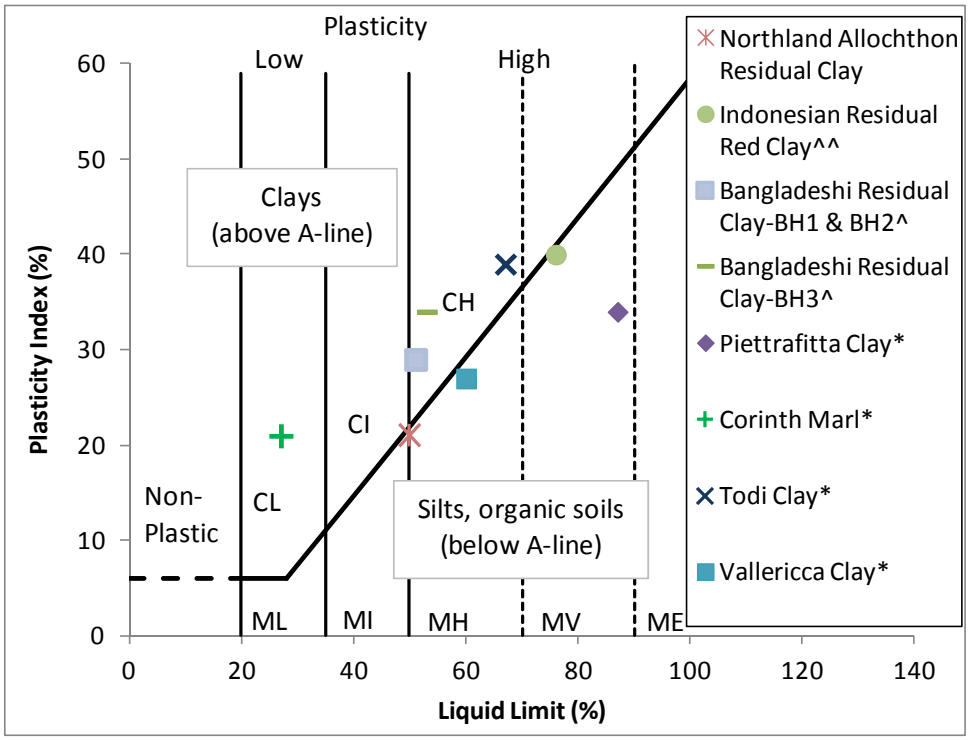

C = Clay	L = Low Plasticity	LL< 35%
M = Silt	I = Intermediate Placticity	35% < LL< 50%
O = Organic	H = High Plasticity	50% < LL < 90%
Pt = Peat	V = Very High Plasticity	70% < LL< 90%
	E = Extremely High Plasticity	LL> 90%

*Burland et al. (1996)
^Hossain (2001)
^^Wesley (1990)

Figure D1: Plasticity index versus liquid limit for several residual and sedimentary clays.

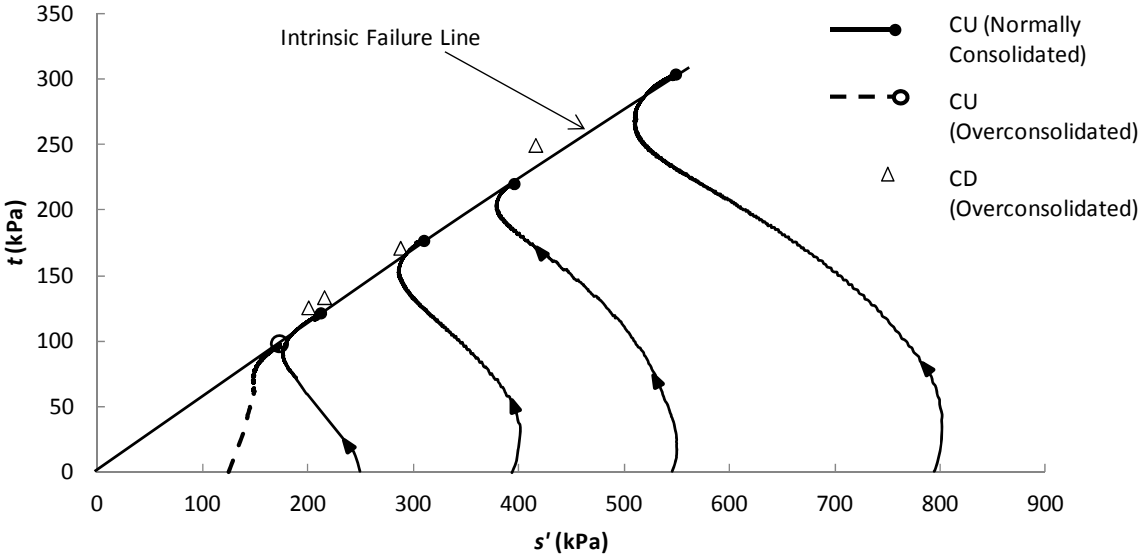

(a)

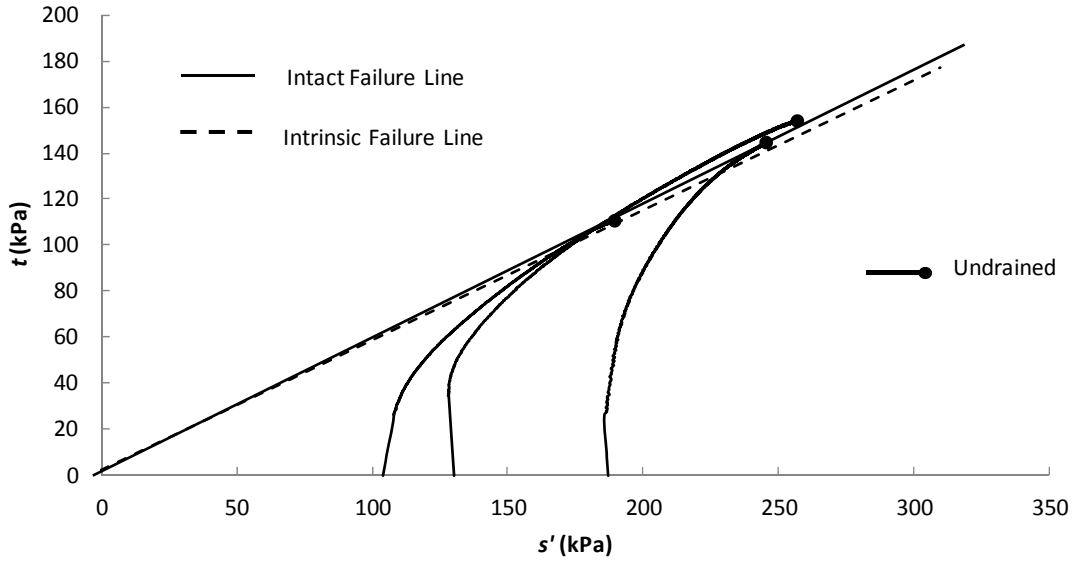

(b)

Figure D2: Peak strengths and undrained stress paths for (a) reconstituted and (b) intact (natural) specimens of Northland Allochthon residual clay.

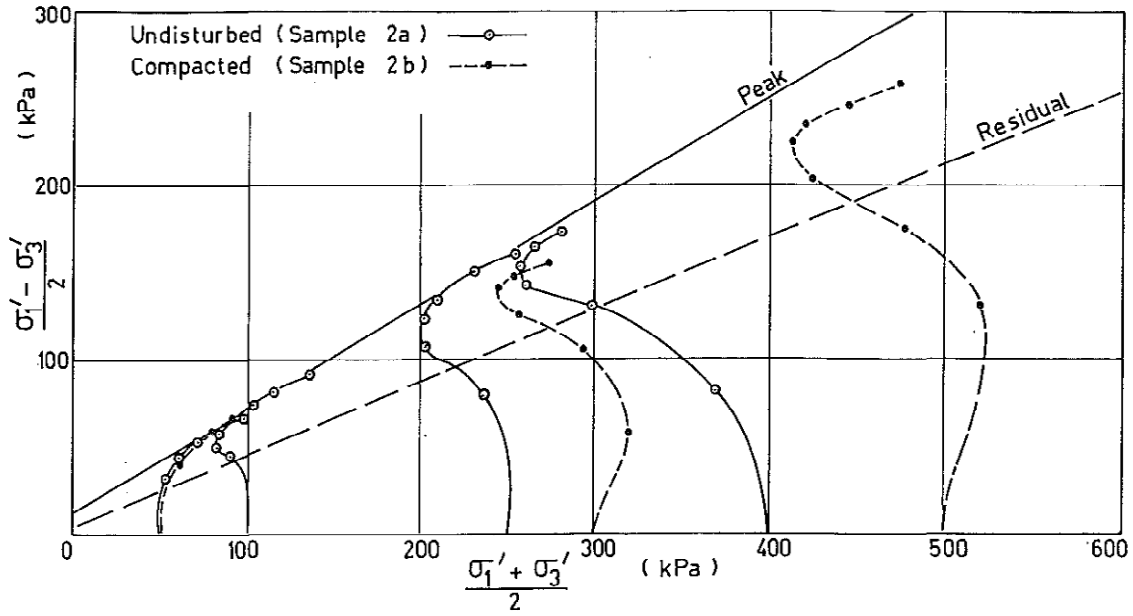

Figure D3: Stress paths for undisturbed (natural) and compacted Indonesian residual red clay (Wesley, 1990).

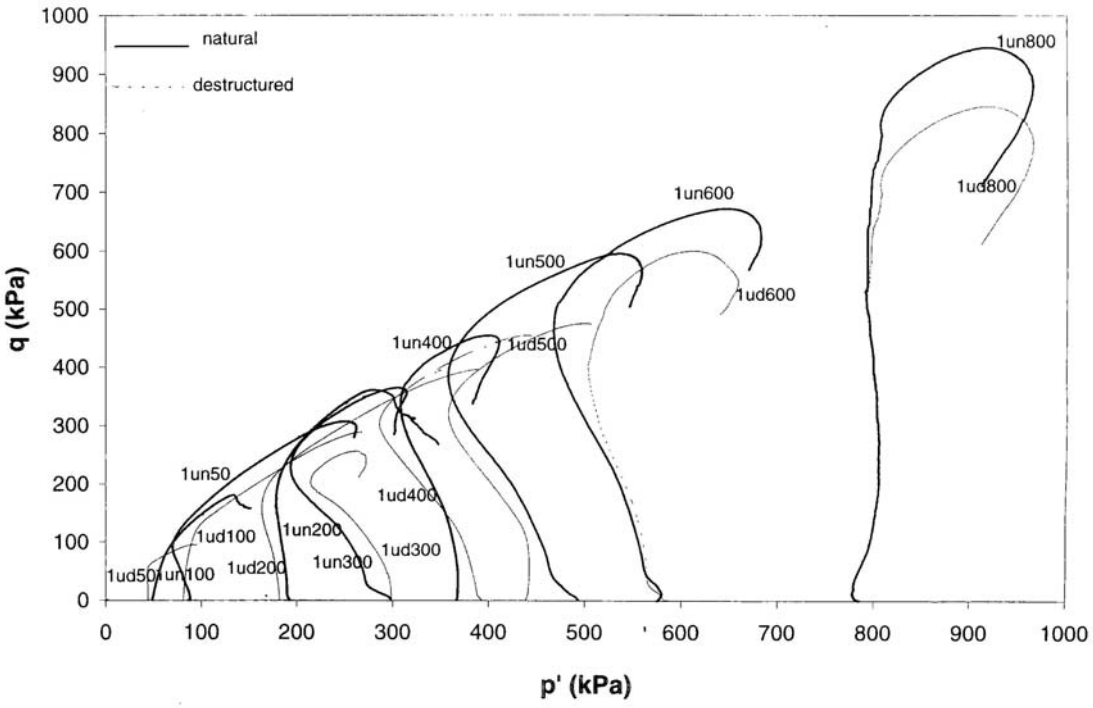

Figure D4: Stress paths for natural and destructured Bangladeshi residual clay (Hossain, 2001).

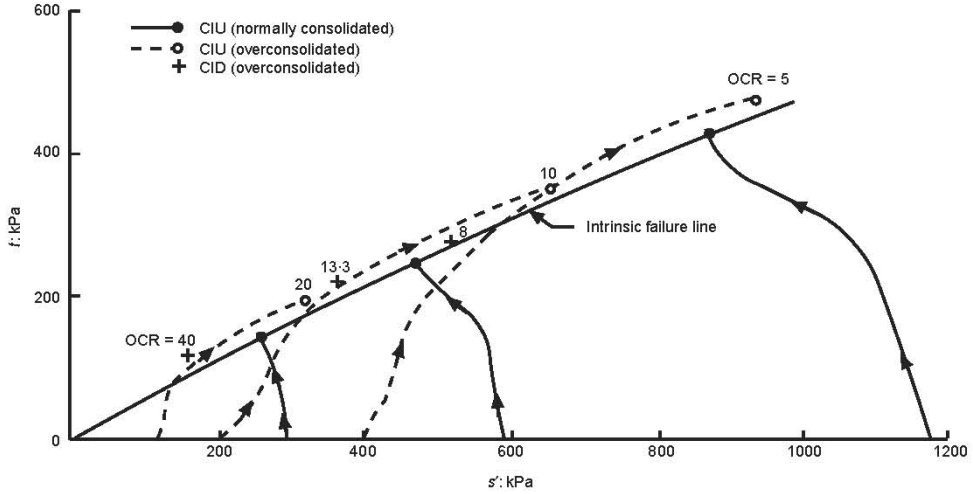

(a)

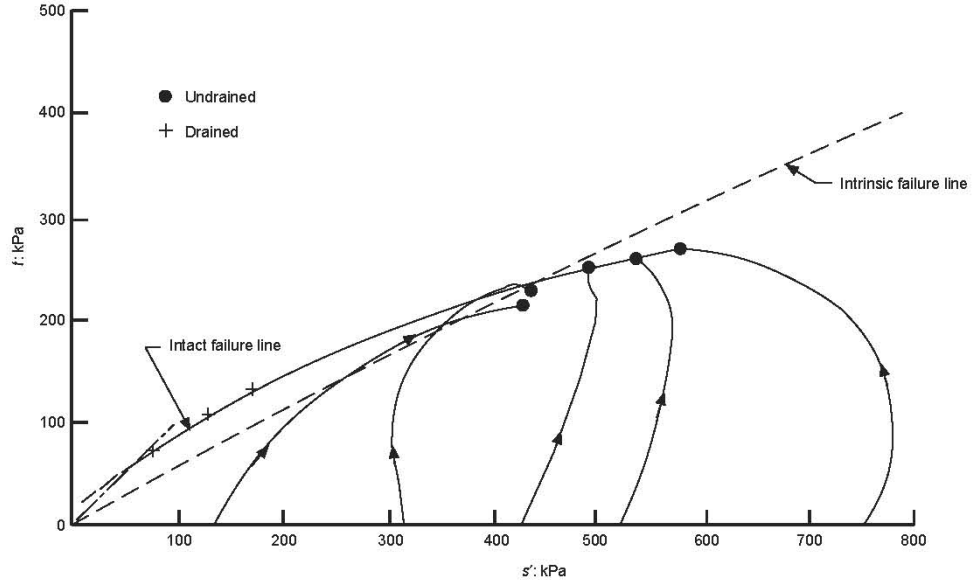

(b)

Figure D5: Stress paths for (a) reconstituted Pietrafitta clay (b) and intact Pietrafitta clay (Burland et al., 1996).

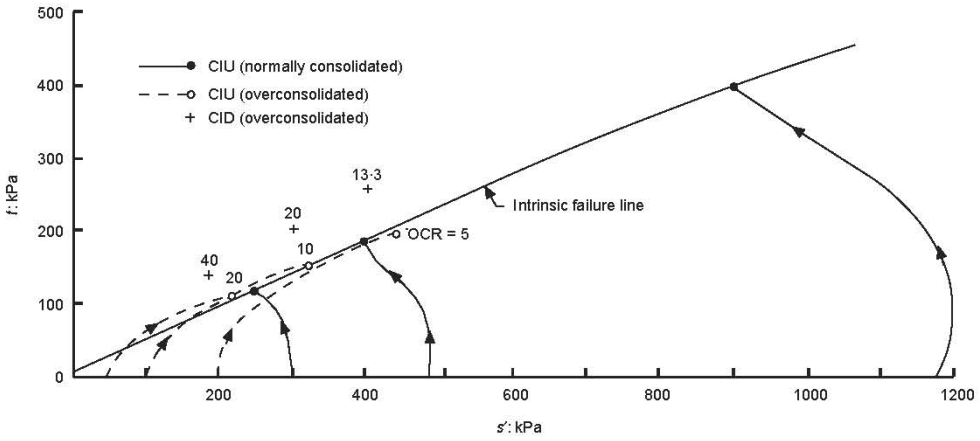

(a)

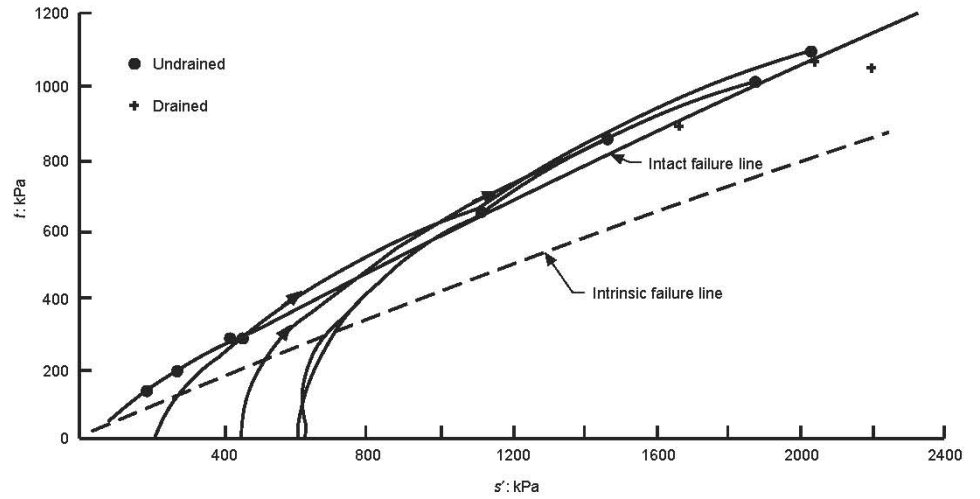

(b)

Figure D6: Stress paths for (a) reconstituted Todi clay (b) and intact Todi clay (Burland et al., 1996).

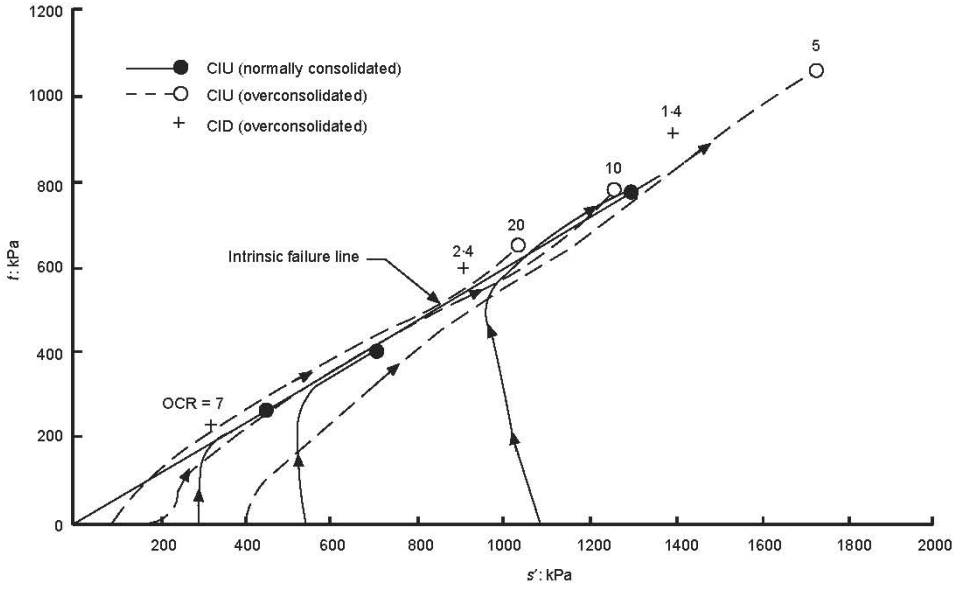

(a)

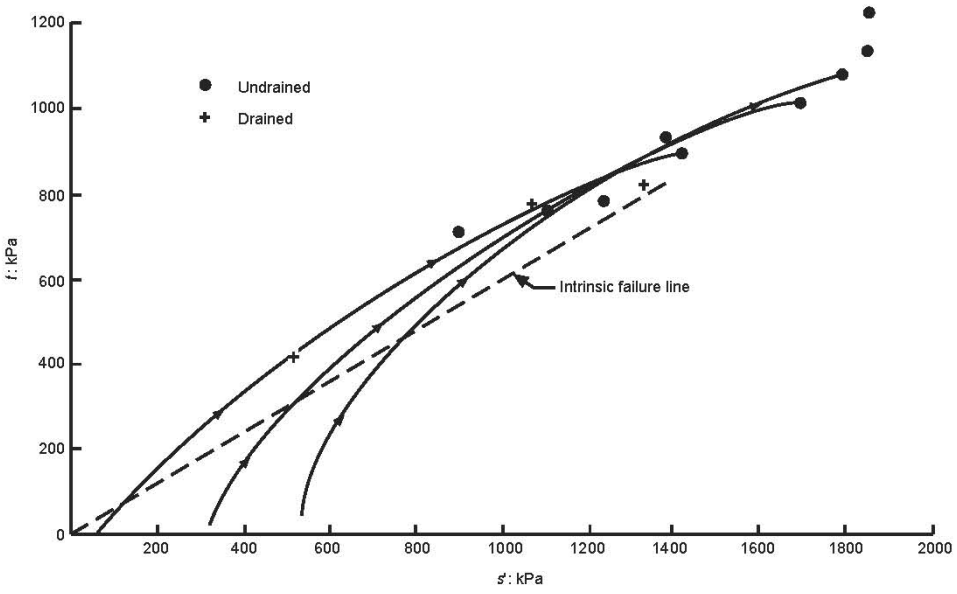

(b)

Figure D7: Stress paths for (a) reconstituted Corinth marl and (b) intact Corinth marl (Burland et al., 1996).

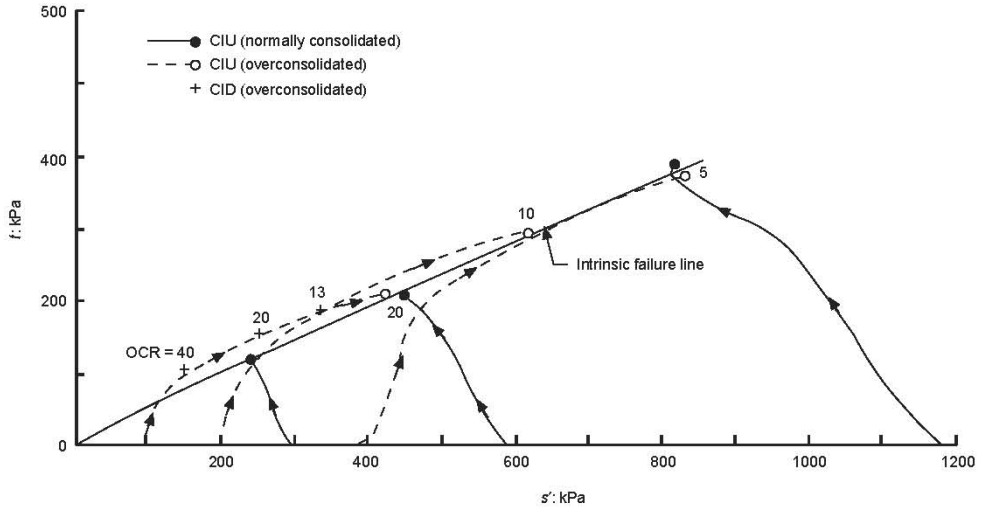

(a)

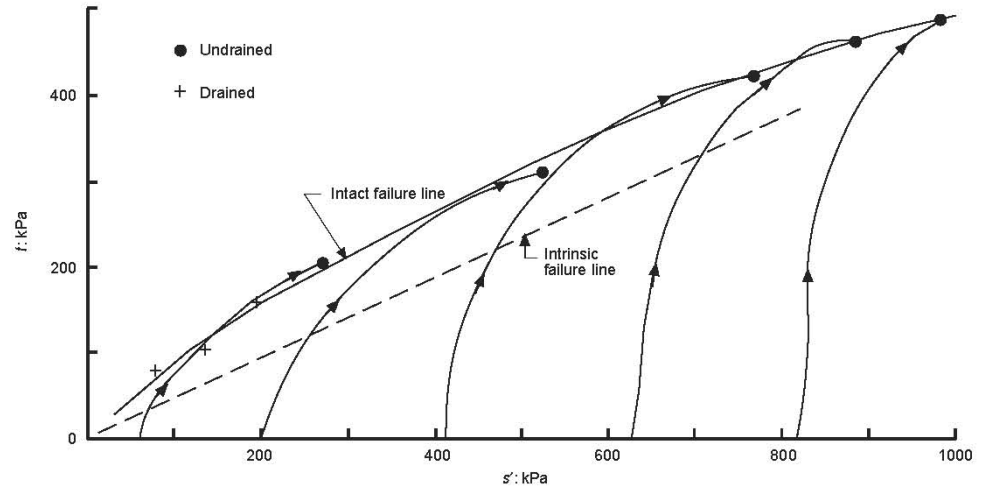

(b)

Figure D8: Stress paths for (a) reconstituted Vallericca clay and (b) intact Vallericca clay (Burland et al., 1996).

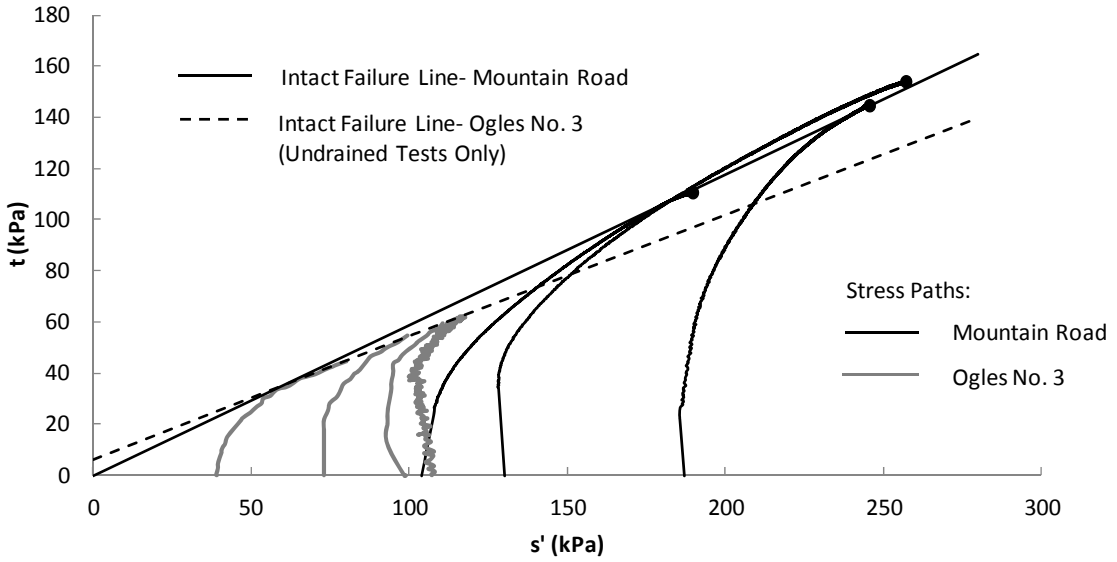

Figure D9: Undrained stress paths for intact (natural) specimens of Northland Allochthon residual clay from Ogles No. 3 and Mountain Road.

APPENDIX E

UCS test results from Kahoe Hill

UNCONFINED COMPRESSIVE STRESS WITH YOUNG'S MODULUS

Project :	Kahoe Hill SH10
Location :	Col. 58
Client :	Hiway Stabilizers
Client ref :	O/No. HS 62977
Contractor :	Hiway Stabilizers
Sampled by :	-
Date sampled :	14/02/2010
Sampling method :	Not Stated
Sample condition :	As Received
Sample description	Turbojet

7 Day Test

OPUS

Project No:	1-L0100.01
Lab ref No:	F2/015/10

Sample ID	F2/015/10						
Bulk Density t/m³	1.88						
Water Content %	25.9						
Dry Density t/m³	1.49						
Max Stress kPa	2755.39		Young's Modulus		402.0		Mpa
Strain at Failure %	0.7		for Strain		0.20 -0.4		%

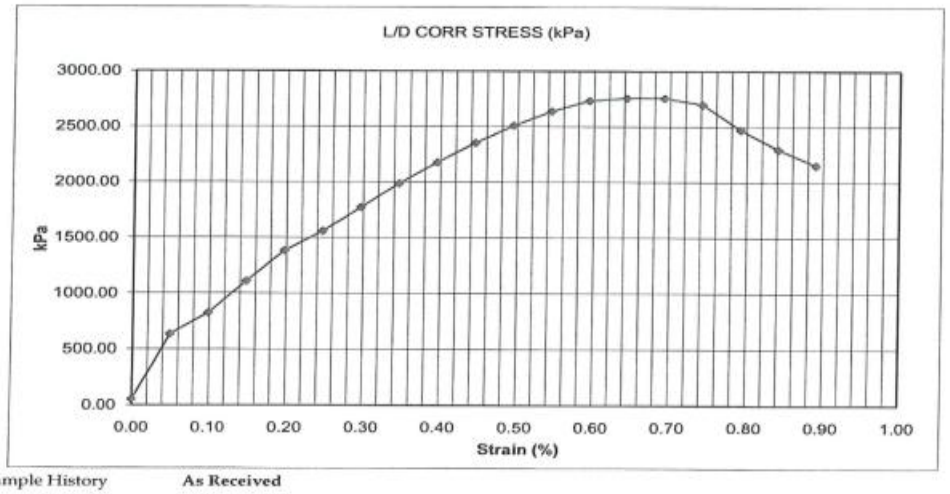

Sample History **As Received**

Test Methods

Unconfined Compression Test NZS 4402;1986 Tests 6.3.1

Tested By Dave Hotham 3/03/2010

19 laboratory

All tests reported herein have been performed in accordance with the laboratory's scope of accreditation

IANZ Approved Signatory Date : 4/03/2010

D Hotham
Senior Civil Engineering Technician

Opus International Consultants Limited
Auckland Laboratory
Quality Management Systems Certified to ISO 9001

Unit A, 7 Ride Way, Nth Harbour Industrial Estate
Private Bag 10-1982, N.S.M.C., North Shore City
Auckland, New Zealand

Telephone +64 9 415 4660
Facsimile +64 9 415 4661
Website www.opus.co.nz

UNCONFINED COMPRESSIVE STRESS WITH YOUNG'S MODULUS

Project :	**Kahoe Hill SH10**
Location :	**Col. 58**
Client :	**Hiway Stabilizers**
Client ref :	**O/No. HS 62977**
Contractor :	**Hiway Stabilizers**
Sampled by :	**-**
Date sampled :	**24/02/10**
Sampling method :	**Not Stated**
Sample condition :	**As Received**
Sample description	**Turbojet**

28 Day Test

Project No:	**1-L0100.01**
Lab ref No:	**F2/017/10**

Sample ID	**F2/017/10**						
Bulk Density t/m³	**1.84**						
Water Content %	**26.0**						
Dry Density t/m³	**1.46**						
Max Stress kPa	**3634.84**		**Young's Modulus**		**456.6**		**Mpa**
Strain at Failure %	**0.9**		**for Strain**		**0.31 -0.82**		**%**

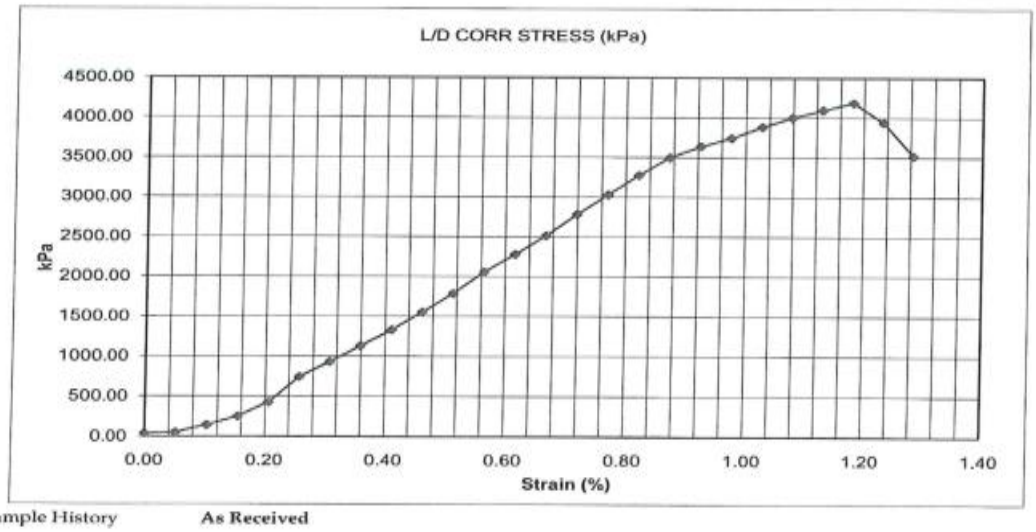

Sample History **As Received**

Test Methods

Unconfined Compression Test NZS 4402;1986 Tests 6.3.1

Tested By C Johnston 24/02/10

All tests reported herein have been performed in accordance with the laboratory's scope of accreditation

IANZ Approved Signatory **Date :** 25/02/10

D Hotham
Senior Civil Engineering Technician

s International Consultants Limited
kland Laboratory
lity Management Systems Certified to ISO 9001

Unit A, 7 Ride Way, Nth Harbour Industrial Estate
Private Bag 10-1982, N.S.M.C., North Shore City
Auckland, New Zealand

Telephone +64 9 415 4660
Facsimile +64 9 415 4661
Website www.opus.co.nz

APPENDIX F

Ogles No. 3 Borehole Logs 1 and 2

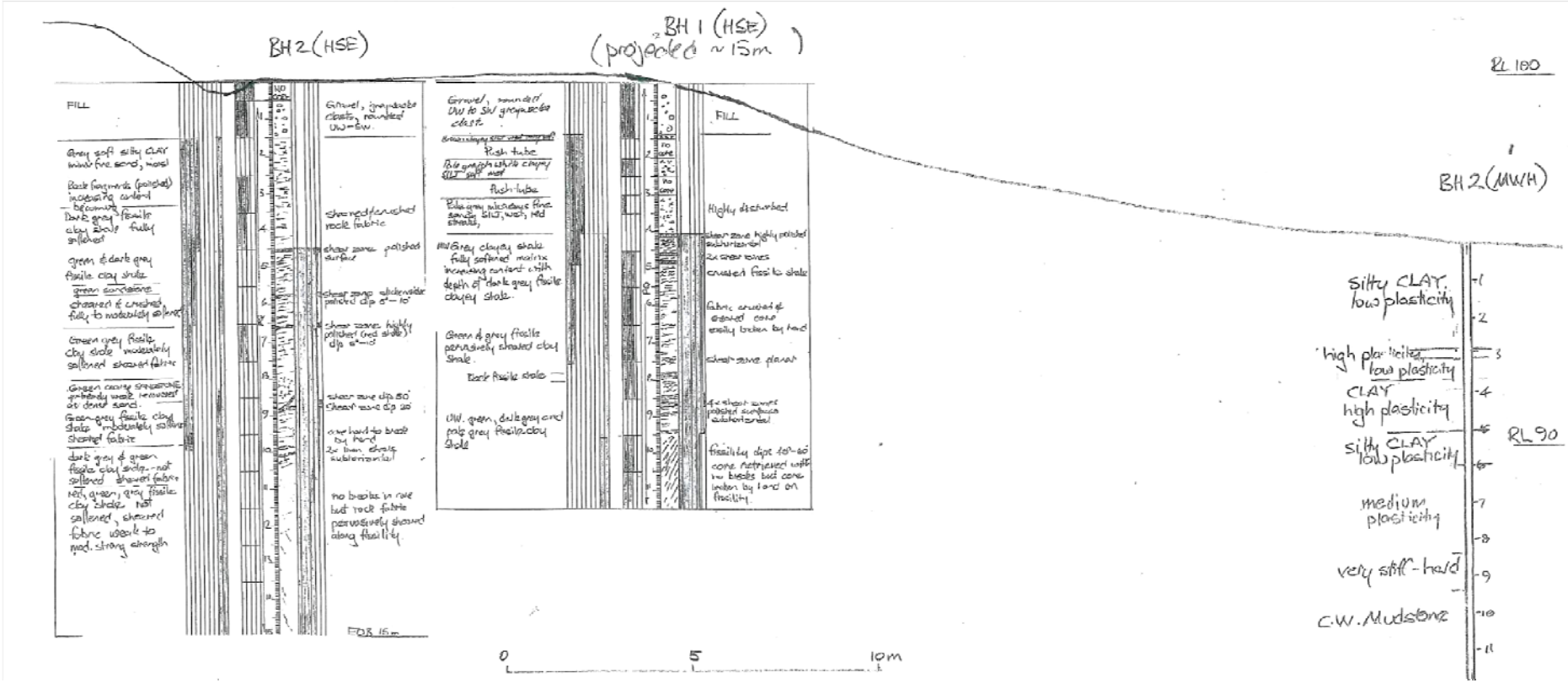

Figure E1: BH1 and BH2- Ogles No. 3 site (acquired from O'Sullivan (2009), courtesy of Tonkin & Taylor Ltd.)

APPENDIX G

Verification of Stress Calculations in Plaxis

Table G1: Hand calculations versus Plaxis outputs at two different stages in the Ogles No. 3 case study at point A.

Stage	Calculation Type	σ_{yy}	σ_{yy}'	σ_{xx}	σ_{xx}'	σ_1	σ_1'	σ_3	σ_3'	τ^*
After high groundwater (following road construction)	Hand Calculation	66.2	64.2	40.6	38.6	71.4	61.4	33.4	23.4	19
	Plaxis	64.5	62.3	31.7	29.5	65.7	63.4	28.7	26.5	17.7
After butress construction	Hand Calculation	66.2	66.2	38.6	38.6	72	72	32.8	32.8	19.6
	Plaxis	51.1	51.1	32.1	32.1	51.7	51.7	31.4	31.4	10.16

Sample calculations:

$\gamma_{soil} = 20$ kN/m^3

$\gamma_{road\ fill} = 18$ kN/m^3

$\varphi'_{soil} = 24.6°$

$\gamma_{water} = 10$ kN/m^3

After high groundwater, following road construction:

$\sigma_{yy} = (18\ \text{kN/m}^3)(0.9\text{m}) + (0.2\text{m})(20\text{kN/m}^3) + (2.3\text{m})(20\ \text{kN/m}^3)$

$\underline{\sigma_{yy} = 66.2\ \text{kPa}}$

$\sigma'_{yy} = 66.2\ \text{kPa} - (10\text{m})(0.2\text{m})$

$\underline{\sigma'_{yy} = 64.2\ \text{kPa}}$

σ'_{xx} = (1-sin(24.6°))(66.2 kPa)

$\underline{\sigma'_{xx} = 38.6 \text{ kPa}}$

σ_{xx} = 38.6 kPa + (0.2m)(10m)

$\underline{\sigma_{xx} = 40.6 \text{ kPa}}$

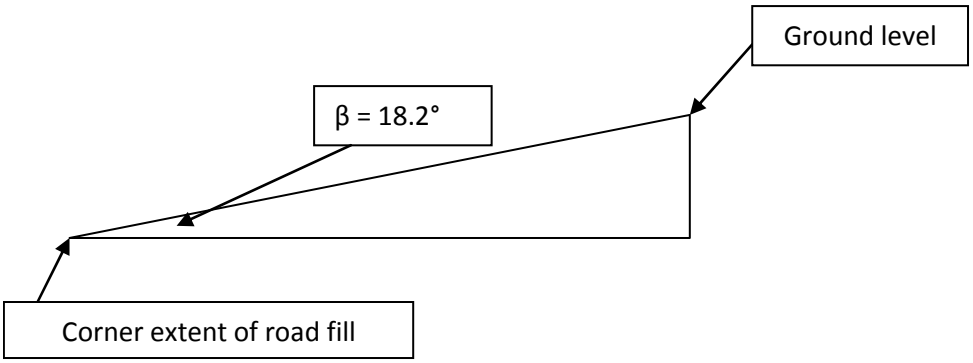

$\tau^* = \sigma'_{yy}(\cos\beta)(\sin\beta)$

$\tau^* = 64.2(\cos(18.2°))(\sin(18.2°))$

$\underline{\tau^* = 19 \text{ kPa}}$

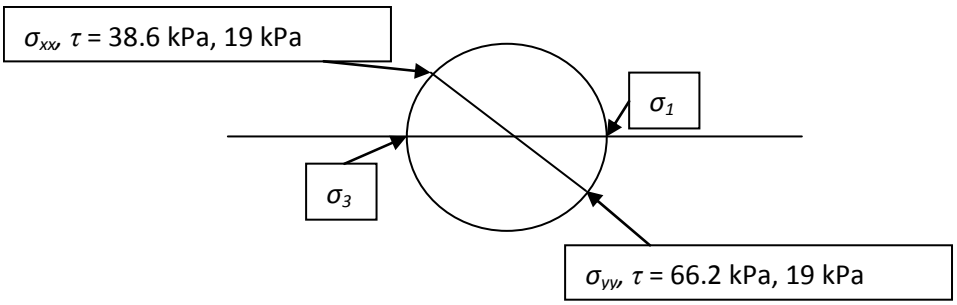

(σ_{xx}, τ) = (38.6 kPa, 19 kPa)

(σ_{yy}, τ) = (66.2 kPa, 19 kPa)

$s = (38.6 \text{ kPa} + 66.2 \text{ kPa})/2$

$\underline{s = 52.4 \text{ kPa}}$

$t^2 = ((66.2 \text{ kPa} + 38.6 \text{ kPa})/2)^2 + (19 \text{ kPa})^2$

$\underline{t = 23.5 \text{ kPa}}$

$\sigma_1 = s + \tau = 52.4 \text{ kPa} + 19 \text{ kPa}$

$\underline{\sigma_1 = 71.4 \text{ kPa}}$

$\sigma_3 = s - \tau = 52.4 \text{ kPa} - 19 \text{ kPa}$

$\underline{\sigma_3 = 33.4 \text{ kPa}}$

$\sigma'_1 = 71.4 \text{ kPa} - 10 \text{ kPa}$

$\underline{\sigma'_1 = 61.4 \text{ kPa}}$

$\sigma'_3 = 33.4 \text{ kPa} - 10 \text{ kPa}$

$\underline{\sigma'_3 = 23.4 \text{ kPa}}$